INAUGURAL DISSERTATION

zur

Erlangung der Doktorwürde

der

Naturwissenschaftlich-Mathematischen Gesamtfakultät

der

Ruprecht-Karls-Universität Heidelberg

vorgelegt von

M.Sc. Christiane H. Antoni

geboren in Bensheim

Tag der mündlichen Prüfung: 24. Juli 2017

Chemically Modified Substrates to Probe Cell Behaviour in Wound Healing

„Ich bin immer noch verwirrt, aber auf einem höheren Niveau.“

Enrico Fermi, Physiker

Contents

Abstract

Cell migration plays a major role in processes like wound healing, including lymphangiogenesis. It is especially influenced by the extracellular matrix. In this thesis chemical synthesis and material science are combined to address biological questions in a biological chemistry approach. This enables the analysis of the influence of different extracellular matrix modules on cell behaviour. On the one hand a concentration and density dependent effect of short hyaluronan is analysed. On the other hand a novel specific and unspecific binding model for the extracellular matrix is developed.

Several chemical modification strategies are tested to immobilise hyaluronan on a surface. Therefore modifications at the reducing-end are introduced using cysteamine hydrochloride, propargylamine and dibenzocyclooctyne-amine and at the carboxy groups within the chain using again propargylamine. In case of the end-thiolated hyaluronan a degree of thiolation of 4.0 ± 0.5 % is achieved, and for the functionalisation within the chain a degree of alkynation of 16 % is determined. All desired molecules could be synthesised and enable immobilisation of the hyaluronan species.

After the chemical modification, the bioactivity is verified via the analysis of the interaction between the hyaluronan species and the hyaladherine aggrecan as well as LYVE-1. Especially the interaction between aggrecan and hyaluronan proves the conservation of the bioactivity during the modification.

To determine the influence of short hyaluronan on lymphendothelial cells the AlamarBlue® and CyQuant® assay are established. A cell density of 131 /mm^2, an incubation time of $2\,\mathrm{h}$ (AlamarBlue® assay) and $5\,\mathrm{min}$ (CyQuant® assay) are determined. Compared are the influences of an enzymatically digested (10 kDa) and short hyaluronan (20 kDa) species which are applied to lymphendothelial cells in different concentrations and densities. To analyse the density related effect, the hyaluronan is immobilised on gold nanostructured surfaces. Between the two employed species no difference in cell behaviour is found. In the case of the application of hyaluronan in solution no difference in the relative metabolic activity is found. For the immobilised hyaluronan species a reduced ability to adhere to the surface is observed for the increasing nanoparticle density. Here, for both hyaluronan species a biphasic effect in relative metabolic activity is detected with maxima for a particle density of 540 /μm^2.

To investigate collective cell migration two novel photocleavable ligands are developed. Synthesised are an unspecific ligand 1-(4,5-dimethoxy-2-nitrophenyl)ethyl 11-mercaptoundecanoate and the specific, caged antagonist of the

integrin $\alpha_5\beta_1$ 1-(4,5-dimethoxy-2-nitrophenyl)-ethyl $(3(S))$-3-(4-(3-(6-(3-mer-captopropanamido)-hexanamido)-propoxy)-benzamido)-4-(4-(3-((4-methoxy-pyridin-2-yl)-amino)-propoxy)phenyl)butanoate.

1-(4,5-dimethoxy-2-nitrophenyl)ethyl 11-mercaptoundecanoate can be synthesised with a yield of 18 %. In QCM-D experiments, the adsorption happens with a specific decay time of (1899.0 ± 776.3) min at 21 °C, while the cleavage after UV irradiation takes (2.52 ± 0.64) min at 21 °C. The absorption spectrum of the molecule shows a band at 345 nm, which is blue shifted to 322 nm upon irradiation with UV light. Also, an isobestic point can be observed at 370 nm. An analysis of the toxicity of 4,5-dimethoxy-2-nitrophenyl ethanol shows an increasing metabolic activity of the used MDCK II cells for 4,5-dimethoxy-2-nitrophenyl ethanol, but no effect for 1-(4,5-dimethoxy-2-nitrophenyl)ethyl 11-mercaptoundecanoate is observed.

In summary, well-controlled chemical variations of surfaces enable novel approaches to study biological systems. Here a method is demonstrated to immobilise HA on a surface which allows the evaluation of the influence of HA on the basal side of lymphendothelial cells. Furthermore a novel intergrin-specific photocleavable ligand is developed to study collective cell migration.

Zusammenfassung

Herstellung chemisch modifizierter Substrate zur Analyse von Zellverhalten

Zellmigration ist ein wichtiger Prozess bei der Wundheilung und der Lymphangiogenese. Diese wird im Besonderen durch die extrazelluläre Matrix beeinflusst. In dieser Arbeit werden chemische Synthese und Materialentwicklung zu einem neuen Konzept der biologischen Chemie vereint, um biologische Fragestellungen zu untersuchen. Auf diese Weise ist es möglich, den Einfluss verschiedener Modelle für die extrazelluläre Matrix und ihren Einfluss auf das Zellverhalten zu analysieren. Auf der einen Seite wird ein konzentrations- und dichteabhängiger Effekt von kurzkettiger Hyaluronsäure untersucht. Auf der anderen Seite wird ein neuartiges Modell der extrazellularen Matrix für unspezifische und spezifische Zellinteraktion vorgestellt.

Verschiedene Strategien zur chemischen Modifikation werden getestet, um die Immobilisierung von Hyaluronsäure auf Oberflächen zu ermöglichen. Dazu werden Modifikationen am reduzierenden Ende der Hyaluronsäure mittels Cysteaminhydrochlorid, Propargylamin und Dibenzocyclooctin-amin durchgeführt. Außerdem wird die Carboxygruppe in der Kette mit Propargylamin modifiziert. Im Fall der endständigen Thiolierung kann ein Thiolierungsgrad von (4.0 ± 0.5) % und im Fall der Alkinierung innerhalb des Moleküls ein Alkinierungsgrad von 16 % erreicht werden. Alle angestrebten Modifikationen konnten erfolgreich durchgeführt werden und ermöglichen die Immobilisierung der Hyaluronsäurevarianten.

Nach der chemischen Modifikation, die nötig ist, um die Hyaluronsäure zu immobilisieren, wird die biologische Aktivität der Spezies überprüft. Dazu wird die Interaktion der immobilisierten Hyaluronsäure mit dem Hyaladherin Aggrecan sowie dem Rezeptor LYVE-1 analysiert. Besonders die Interaktion zwischen Aggrecan und Hyaluronsäure zeigt, dass die Bioaktivität durch die chemische Modifikation nicht beeinträchtigt wird.

Um den Einfluss kurzkettiger Hyaluronsäure auf Lymphendothelzellen zu untersuchen wird sowohl der AlamarBlue[®] als auch der CyQuant[®] Assay eingesetzt. Für die Verwendung der Assays wird eine optimale Zelldichte von $131\,/\mathrm{mm}^2$ und eine Inkubationszeit von 2 h für den AlamarBlue[®] und 5 min für den CyQuant[®] Assay ermittelt.

Anschließend wird der konzentrations- und dichteabhängige Einfluss einer enzymatisch verdauten (10 kDa) und einer kurzen (20 kDa) Hyaluronsäurespezies auf Lymphendothelzellen untersucht. Um den Einfluss der Dichte zu un-

tersuchen, wird endthiolierte HA auf Gold-nanostrukturierten Oberflächen im-mobilisiert. Der Vergleich der beiden verschiedenen Spezies zeigt keine Verän-derung im Zellverhalten. Im Fall der Inkubation der Zellen mit Hyaluronsäure in Lösung konnte ebenfalls kein Einfluss auf die metabolische Aktivität ermit-telt werden. Für die immobilisierte Hyaluronsäure hingegen wird ein Rückgang in der Zelladhäsion mit zunehmender Nanopartikeldichte verzeichnet. Sowohl für die enzymatisch verdaute als auch die kurzkettige Hyaluronsäure wird ein biphasischer Effekt für die relative metabolische Aktivität festgestellt, mit einem Maximum bei einer Partikeldichte von $540\,/\mu m^2$.

Um kollektive Zellmigration zu untersuchen werden im zweiten Teil zwei neuartige photospaltbare Liganden vorgestellt. Zum einen ein Ligand für ein unspezifisches Bindungsmodell (1-(4,5-Dimethoxy-2-nitrophenyl)ethyl 11-mer-captoundecansäure) und zum anderen für ein selektives Bindungsmodell, der spezifische, maskierte Antagonist des Integrins $\alpha_5\beta_1$ 1-(4,5-Dimethoxy-2-nitro-phenyl)-ethyl-(3(S))-3-(4-(3-(6-(3-mercaptopropanamido)-hexanamido)-prop-oxy)-benzamido)-4-(4-(3-((4-methoxypyridin-2-yl)-amino)-propoxy)-phenyl)-butansäure. 1-(4,5-Dimethoxy-2-nitrophenyl)ethyl 11-mercaptoundecansäure kann mit einer Ausbeute von $18\,\%$ hergestellt werden. Mittels QCM-D wird die Adsorption und Spaltung des Liganden untersucht und eine spezifische Halb-wertszeit von (1899.0 ± 776.3) min für die Adsorption und (2.52 ± 0.64) min für die Spaltung jeweils bei $21\,°C$ ermittelt. Das Absorptionsspektrum des Lig-anden weist eine Bande bei $345\,nm$ auf, die eine Blauverschiebung zu $322\,nm$ aufgrund einer Bestrahlung mit UV-Licht aufweist. Außerdem zeigt das Spek-trum einen isobestischen Punkt bei $370\,nm$. Die Analyse der Toxizität von 4,5-Dimethoxy-2-nitrophenylethanol und 1-(4,5-Dimethoxy-2-nitrophenyl)ethyl-11-mercapto-undecansäure zeigt einen Anstieg der metabolischen Aktivität der genutzten MDCK II Zellen mit zunehmender Ligandenkonzentration für 4,5-Dimethoxy-2-nitrophenylethanol, jedoch keinen Effekt für die Thiolspezies.

Kurzum, durch die kontrollierte chemische Veränderung von Oberflächen ist es möglich, neue Strategien zur Untersuchung biologischer Fragestellun-gen zu entwickeln. In dieser Arbeit werden chemische Methoden vorgestellt, um Hyaluronsäure zu immobilisieren und so deren Auswirkung auf Lymphen-dothelzellen zu untersuchen. Dabei erfolgt die Wechselwirkung von Zellen und Hyaluronsäure an der basalen Seite. Darüberhinaus wird ein neuer photospalt-bar maskierter Ligand vorgestellt, der zur Untersuchung kollegtiver Migration verwendet werden kann.

Part I.

Introduction and Aim

Chapter 1.

Introduction

The migration of cells is of great importance in many processes like morphogenesis, wound healing and metastatic spreading of cancer. During wound healing cells migrate in a coordinated sheet-like structure to close wounds and reform blood and lymph vessels. The migration of the cells is triggered by extraneous influences like an increased level of several growth factors and the composition of the extracellular matrix.[1–3]

1.1. Structure of the Human Skin
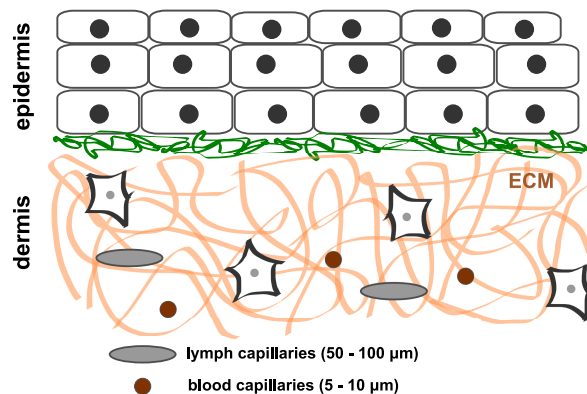
Figure 1.1.: Scheme of a healthy skin tissue with the epidermis consisting of keratinocytes and the dermis formed by the ECM with fibroblasts and the embedded blood and lymph capillaries (adapted from [4]). Epidermis and dermis are separated by the basement membran (green).[4, 5]

The largest organ in the human body is the skin. The two outer layers are formed by the dermis and the epidermis (fig. 1.1). In the epidermis, layers of keratinocytes protect the body against the environment and mechanical force. The dermis, which is separated from the epidermis by the basement membrane, consists of the extracellular matrix (ECM) with fibroblasts and endothelial cells. Here the fibroblasts produce and organise the ECM, whereas the endothelial cells form blood and lymph capillaries in the dermis.[4, 6, 7] The ECM itself is formed by three major groups of macromolecules which are also

3

responsible for the water binding in the tissue due to their large hygroscopic properties. The macromolecules include structural proteins like collagen, fibronectin and laminin, which are embedded in the so-called ground substance made of gycosaminoglycans and proteoglycans, and the connective tissue glycoproteins. In a healthy tissue, the basement membrane consists mainly of the structural proteins collagen and laminin.[3,8] Glycosaminoglycans (GAG) are unbranched polysaccharide chains like heparan sulfate, chondroitin sulfate, keratan sulfate and hyaluronan (hyaluronic acid, HA). Hyaluronan is a special case of these macromolecules, because it is the only polysaccharide without any sulfate groups, whereas the other members of this group are found with different sulfate densities within the chains.
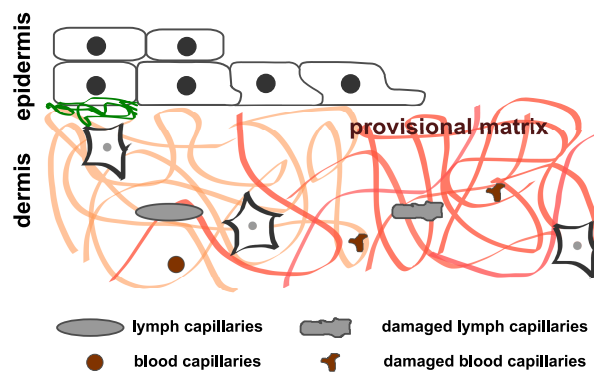
Figure 1.2.: Scheme of a wounded skin tissue with migrating keratinocytes, which start closing the epidermis and the dermis with the provisional matrix (dark red) and damaged capillaries (adapted from [4]).

After an injury fibroblasts synthesise the provisional matrix (fig. 1.2). To assist the re-epithelialisation, lymph- and angiogenesis, the composition of the ECM changes. In the healthy skin the ECM is mainly formed by laminin and collagen (type IV and VII).[7] During wound healing more collagen type I, fibronectin and vitronectin are present.[7] Because of the change in the ECM, different integrins are addressed to promote wound healing and angiogenisis. During re-epithelisation the fibrin clot is formed within minutes and several cytokines and chemokines are released. In the following 1 to 3 days migration of the keratinocytes is promoted to close the wound. In the upcoming weeks and month the fibroblasts within the dermis start to remodel the ECM.[6,7]

1.2. The Lymphatic System and Lymphangiogenesis

The mechanism of formation of new blood vessels (angiogenesis) during wound healing is a well studied phenomenon, while not much is known about lymphangiogenesis.[9–11] The objective of the lymph system is the uptake of the interstitial fluid, which contains immune cells and various macromolecules,
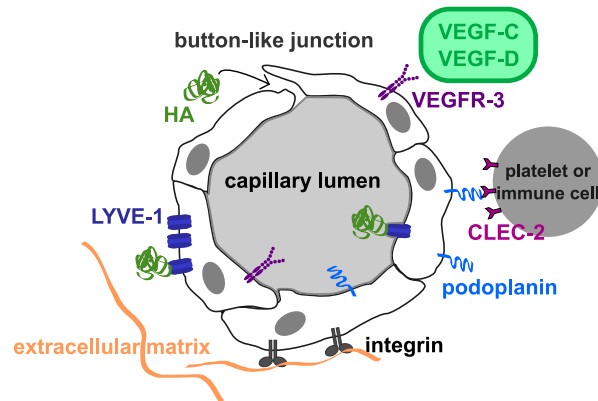
Figure 1.3.: The lymph capillaries are formed by partly-overlapping endothelial cells. They are connected via button-like junctions which enable the uptake of macromolecules like HA into the lumen. Cell migration during wound healing is promoted by the interaction of HA with LYVE-1, the growth factors VEGF-C and -D with their receptor VEGFR-2 and the integrins with the ECM. Podoplanin enable the interaction of immune cells or platelets with lymphatic cells via CLEC-2.[4, 5, 12, 13]

and its transport to the lymph nodes, were the fluid is cleaned and drained back in the blood circulation.[12] The lymph vessels end in the dermis in small blind ended capillaries. Compared to the blood capillaries found in the dermis, these lymph capillaries are much larger (diameter of 50 to 100 µm) to enable the transport function.[5] The lymph capillaries are formed by endothelial cells which are partly-overlapping connected by button-like junctions (fig. 1.3). These junctions work as microvalves and enable the uptake of the interstitial fluid.[5, 14, 15] The microvalves have a size of 500 to 800 nm in diameter.[15] During inflammation, infection and tissue injury the flux in the vessels is increased dramatically to remove degraded ECM and other compounds in the wound which need to be removed.[15] Thus, an intact lymph system is very important for wound healing. In case of an injury of lymph capillaries, a highly organised migration of the cells through the ECM starts. During this process the button-like junctions change into zipper-like junctions, so that the vessel stays intact during the migration. A key player in the regulation of this permeability of the lymphatic vessels is podoplanin.[9] Podoplanin binds to galactin-8 and CLEC-2 (C-type lectin-like receptor), which is expressed on platelets and immune cells. The binding to immune cells increases their motility and protrusion, whereas the binding to platelets promotes their aggregation and activation. On the intracellular side, it binds to ezrin, which is known to promote cell migration and interacts with CD44, a receptor for HA.[13, 16–18] The migration itself is influenced by the growth factors VEGF-C and -D and their receptor VEGFR-3, which is important in the regulation of lymphangiogenesis, and the HA recep-

tor LYVE-1, which is the main HA receptor in lymphendothelial cells.[9, 15] Because the composition of the ECM changes during wounding and due to the signaling of growth factors and short hyaluronan the expression of integrins, which promote the migration, is increased.[5, 12, 15] Signaling of HA and its fragments occur here in different ways. So the HA can interact with the HA receptors on the ECM side of the capillary and on its luminal side. The role in signaling of the uptake of the HA through the microvalves is not clear yet.[19]

1.3. Interaction Between Extracellular Matrix and Cells

To enable the migration of cells in wound healing or lymphangiogenesis the cells interact with the ECM via integrins. Integrins are heterodimeric transmembrane proteins which are formed by an α and a β subunit. Both units are non-covalently connected to each other. There are 18 different α and 8 different β subunits known which can form 24 different integrins. The combination of both subunits enable the adhesion to different structural proteins in the ECM. Thus, the $\alpha_5\beta_1$ integrin binds to fibronectin whereas the $\alpha_v\beta_1$ intergrin typically binds to vitronectin and the $\alpha_2\beta_1$ integrin to collagen.[6, 7, 20]
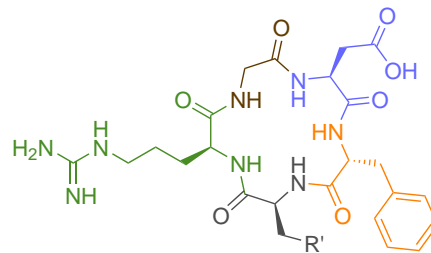
Figure 1.4.: The artificial peptide cyclic RGD mimics a binding domain of fibronectin. It consists of arginine (R, green), glycine (G, brown) and aspartic acid (D, blue). To enable the cyclisation phenylalanine (orange) and a modified glycine (grey) with a functional group (R'), which enables the immobilisation on a substrate, is added.

One common binding sequence in fibronectin and vitronectin is the amino acid sequence arginine-glycine-aspartic acid (RGD, fig. 1.4). Thus, it is possible to use only a small peptide with this sequence in cell experiments instead of the whole protein. New developments are directing the specific adhesion of chosen integrins to a surface. Published are for example antagonists to the $\alpha_5\beta_1$ or the $\alpha_v\beta_3$ integrin (fig. 1.5).[21–23] This enables the analysis of migration and adhesion depending on the addressed integrins. Due to the usage of small peptides instead of whole proteins it is possible to analyse the influence of the density of adhesive molecules on a surface. Therefore surfaces decorated with gold nanoparticles can be used (fig. 1.6). To create a defined particle pattern on
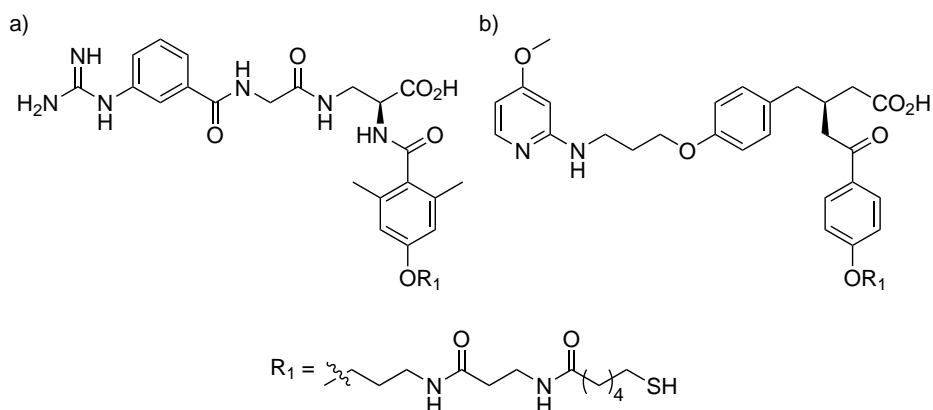
Figure 1.5.: These peptides are artificial, highly selective antagonists to the a) $\alpha_5\beta_1$ and b) $\alpha_v\beta_3$ integrins.[21]

the surface the block copolymer nanolithography (BCML) technique is used. Via thiol functions the peptides can be immobilised on the gold nanoparticles in a well-controlled manner. To ensure that cells only adhere to the peptides, the glass surface itself is functionalised with a silane bearing polyethylenglycol (PEG) to passivate the surface against any unspecific interactions.[24–27] To
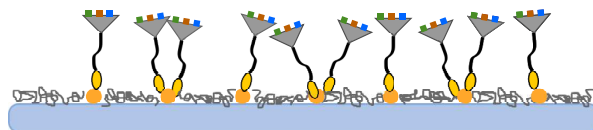
Figure 1.6.: Via block copolymer nanolithography (BCML) glass surfaces are decorated with gold nanoparticles. Afterwards the surface is passivated with PEG_{2000}−silane and the nanoparticles functionalised with cRGD to enable the use in cell experiments.

form the adhesion, two different ways are possible. On the one hand, anchor proteins like talin, paxillin and vinculin bind to the intracellular part of the integrin. This leads to a conformational change of the integrin. Due to this the binding affinity of the extracellular domain to the binding sequence is increased (inside-out signaling). On the other hand the ECM protein binds to the integrin first. This induces clustering of the integrins and the binding of intracellular anchor proteins (outside-in signaling).[28] Via the anchor proteins like talin the cytoskeleton is connected to the focal complexes which form the focal adhesions (fig. 1.7). During migration the focal adhesions are important to transfer the force of the moving cell to the substrate. The formation of the focal adhesions is regulated during the process via different kinases like focal adhesion kinase (FAK) and tyrosine-protein kinase (Src), which co-localise with the focal complex. These proteins are also important for signaling in cell
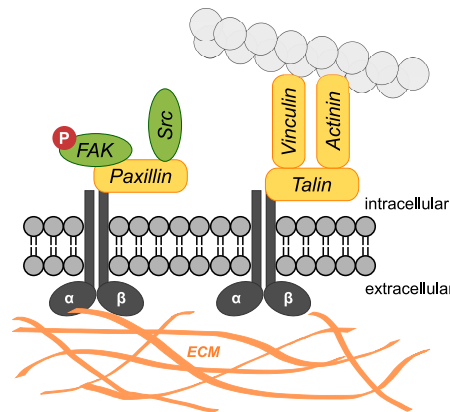
Figure 1.7.: Cells interact via integrins with the ECM. The anchor protein
talin associated with vinculin connects the cytoskeleton (actin) to integrins.
Proteins like paxillin and the kinases Src and FAK (P: phoshporylated),
which are important for the signaling in cell migration, actin organisation,
survival and proliferation are members of the focal complex.[8, 12, 20, 28]

migration, actin organisation, survival of the cell and proliferation.[8, 20]

To promote the ability of cells to migrate during wound healing the expression level of different integrins is changed during injury. Additionally, the composition of the ECM changes and thus the integrins which enable migration can be addressed. During wound healing an up regulation of $\alpha_5\beta_1$ intergrins are found in the first days.[12] After day three also the number of integrins with the subunit α_v are increased, especially the integrins $\alpha_v\beta_5$ and $\alpha_v\beta_6$.[6, 7] In contrast, the key player in lymphangiogenesis is the integrin $\alpha_9\beta_1$ which promotes the cell migration.[12]

1.4. Hyaluronan - **A Polysaccharide**

In the skin the HA is synthesised by fibroblasts which are located in the dermis. The dermis contains about 200 to 500 µg/g and the epidermis 100 µg/g of hyaluronan. Overall, the human body (70 kg) contains about 15 g HA, of which about one third is renewed every day.[15, 29] The half-live of HA within the dermis is below 24 h and within the epidermis even in the range of 2 to 3 h.[30, 31]

HA consist of repeating disaccharide units of *N*-acetyl-D-glucosamine and D-glucuronic acid, which are linked via β-(1→4) and β-(1→3) glycosidic bonds (fig. 1.8). Native HA has a weight of 10^3 - 10^4 kDa corresponding to 2000 to 25 000 disaccharide units and a total contour length of 2 to 25 mm.[15, 34, 35] In literature a secondary and tertiary structure of HA in aqueous solutions is reported comparable to the structure of proteins.[32, 34, 35] Depending on the counter ion, helical structures of 2 to 4 HA chains are found. In case of
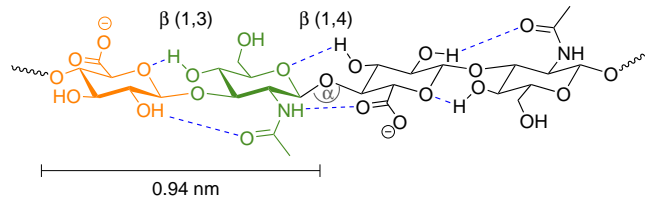
Figure 1.8.: Hyaluronan consists of repeating disaccharide units of D-glucuronic acid (orange) and *N*-acetyl-D-glucosamine (green). For each unit a rotation of about 90° (α) is found due to the hydrogen bonds (blue).[32, 33]

Ca^{II} for example, three HA chains form with additional six water molecules per Ca^{II} one large complex. In this complex each cation complexes only two HA chains. In the crystallised species a length of 0.94 nm/unit is discovered. Due to hydrogen bonds within each chain a rotation of 90° per unit is determined. As tertiary structure a coiling of the HA chain is found with a radius of gyration of 150 to 500 nm.[32] In the ECM tissue specific proteoglycans
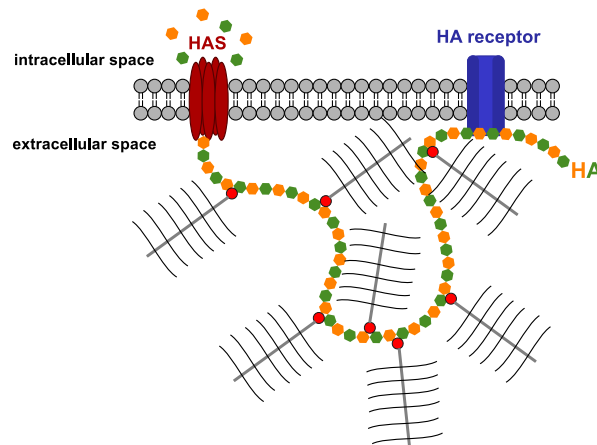
Figure 1.9.: HA is synthesised by hyaluronan synthase (HAS) at the non-reducing end, while the HA is released in the extracellular space. Aggrecan (grey) binds with the link protein (red dot) to the HA chain, which binds to its receptor in the membrane. Additionally other GAGs like chondroitin bind to the aggrecan.[30, 36]

like aggrecan, versican and the link protein bind to HA (fig. 1.9). Aggrecan itself binds other GAGs like chondroitin for example.[37] The HA is synthesised via the transmembrane proteins hyaluronan synthase (HAS 1-3) in the inner leaflet of the plasma membrane of fibroblasts. They synthesise the HA from the non-reducing end on, while the chain is released in the extracellular space.[15, 36, 38] The cells can interact with HA via different receptors. The main receptors are RHAMM, CD44 and its analogous LYVE-1.[39, 40] CD44 is

expressed in fibroblasts, keratinocytes, lymphocytes and endothelial cells.[30] RHAMM is also expressed in fibroblasts and endothelial cells with a limited level in healthy skin but increases in cancer.[30, 39, 41] LYVE-1 is expressed in lymphatic endothelial cells. The interaction between HA and the different receptors enables the stimulation of different processes. So it is shown that small fragments of HA (10 kDa) interacting with endothelial cells promote proliferation, migration and tube formation.[2, 10, 41, 42] Thus, short HA also influences the angiogenesis which is important in tumor progression. In case of the receptor LYVE-1 the lymphangiogenesis is promoted.[39] To recognise the HA and to enable different processes a minimal number of repeating disaccharide units is necessary. In case of LYVE-1 8 to 10 repeating units are required, whereas for its analogous CD44 6 to 8 repeating units are sufficient.[15, 39]

1.4.1. Hyaluronan in Wound Healing and Lymphangiogenesis

During wound healing, HA with a high molecular weight is found to inhibit proliferation, migration and has an anti-angiogenic and anti-inflammatory effect on blood vessel cells.[2, 30, 41, 43] HA with a medium molecular weight (100 to 300 kDa) promotes wound closure in experiments with human keratinocytes, whereas low molecular weight HA stimulates proliferation, motility and tube formation in endothelial cells and promotes inflammation and angiogenesis. [2, 41] Besides the different length depending effect, also a concentration depending effect is described. The application of an oligo HA (4 to 20 repeating units) on blood vessel cells stimulate proliferation in a concentration range of 3 to 20 µg/mL showing a maximum response at 10 µg/mL.[41] This biphasic effect is also found for the application of a low molecular weight HA species on mouse lymphendothelial cells. Here a maximal effect on proliferation for a concentration of 3.13 µg/mL is found.[44]

1.4.2. Chemical Modification of Hyaluronan
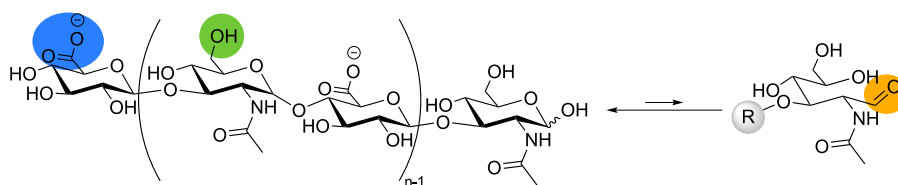
Scheme 1.1.: Functional groups of hyaluronan: carboxy group in blue, primary hydroxy group in green and carbonyl group in orange. The carbonyl-function appears only during the anomerisation between the α- and β-species of the N-acetyl-D-glucosamine-motif at the reducing-end of hyaluronan. The equilibrium is on the side of the closed ring-form.

To enable a well-controlled method to analyse the interaction of HA with

cells or receptors at the basal side (bottom side of cells) in different ECM models, it is necessary to modify HA in a chemical fashion to immobilise the HA. The modification of HA is straight-forward due to its various, accessible functional groups as shown in scheme 1.1. Via the primary and secondary hydroxy groups as well as the carboxy function the short HA can be statistically modified within the chain. To create only a single modification per chain, the carbonyl group at the reducing end is used, which occurs during anomerisation.

One possibility to immobilise HA on a surface is to use a host/guest interaction between ferrocen and cyclodextrine. The cyclodextrine is randomly attached to the hyaluronan chain using the carboxy groups. The cyclodextrine can interact with immobilised ferrocen and bind so the HA.[45–47] Disadvantage of this approach is the large construct which is needed to immobilise the HA on the surface which might also interfere with the bioactivity of the HA. Other
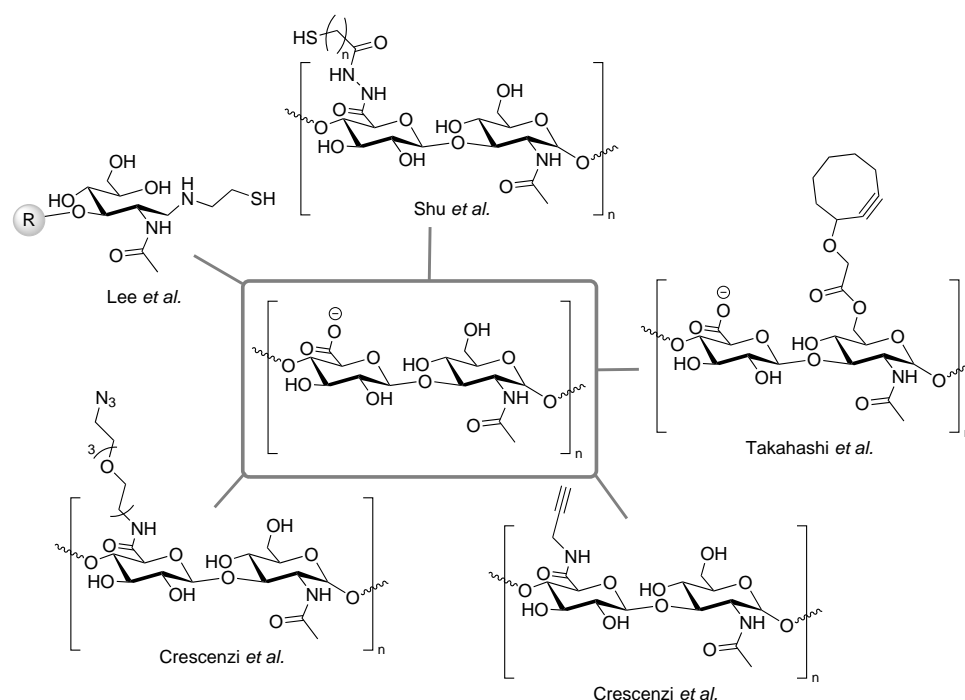
Figure 1.10.: Overview of chemical modifications of HA which can be easily transferred to immobilise HA on a surface.[48–51]

chemical modifications of the HA are mainly used to form hydrogels.[48,51,52] Here also the carboxy group within the chain is functionalised to enable the cross linking between several HA molecules (fig. 1.10). On the one hand thiol groups are introduced which lead to a cross linking via dithiol bonds or more complex systems.[51,52] This allows also the direct immobilisation of the HA to a gold surface or a gold nanostructured surface. On the other hand, the functionalisation with azide and alkyne groups within the HA chain is found.

[48] Here the copper catalysed azide alkyne cycloaddition (CuAAC) is used to form the gels.

To immobilise HA via CuAAC on a surface, the approach used in the host/guest approach can be used. In this case different thiol terminated oligoethylenglycol (OEG) molecules are added to a gold coated surface. They form a dense SAM on a gold surface, which passivates the surface against unspecific interactions. A second functionality allows the immobilisation of the HA to the SAM.[45, 53, 54] Alternatively the cooper-free strain-promoted azide-alkyne cycloaddition (SPAAC) can be performed to immobilise the HA. In this case a strained cyclooctenyl-ring is used instead of the smaller alkyne function. Because the driving force is the strained ring no copper is necessary, which is better in a biological context.[50, 55–57]

1.5. Photolabile Protecting Groups

Since the 1960's photolabile protecting groups are found in organic chemistry. They are used especially in cases where many different functional groups are available like in peptide, nucleotide and carbohydrate synthesis, among other things.[58, 59] Photolabile groups which are successfully used are derivatives of benzoin esters (a),[58–61] $o-$nitrobenzyl (b),[58–61] coumarin (c)[60, 61] and indol derivatives (d),[60, 61] ruthenium complexes (e)[60, 61] or dinitrobenzene-sulphenyl (f),[58] antraquinon (g)[58, 60] and phenacyl derivatives (h, fig. 1.11). [58–61] These groups are stable against most chemicals and can be cleaved off with a good yield. Because no strong acids or bases are necessary for deprotection, it is a rather mild method in synthesis, even though irradiation with UV light is necessary. The applied wavelength for the cleavage ranges from 245 to 420 nm depending on the functionality (fig. 1.11). Besides their application in synthesis, photolabile groups are also used in a more technical context like for example for creating matrices in MALDI MS,[63] in single molecule force microscopy,[64] to facilitate a controlled polymerisation[65] and to create defined patterns or films on a surface.[66] More and more the approach of photolabile protection is found as approach in biological chemistry to prepare surfaces for cell experiments.[62] Here, photocleavable systems are used to release amino acids,[67–69] proteins[70] or growth factors to study their influence as a drug delivery system especially in cancer therapy.[71] This approach is also used to create well-controlled patterns on a surface with for example proteins[72, 73] or to tune the adhesion of cells to a surface.[74, 75] A further development is to use a photocleavable molecule not only to create a pattern on the surface but to use the system as a chemical barrier to investigate cell migration.

1.5.1. Development in Wound Healing Assays

To observe collective cell migration as a wound healing model several techniques are established (fig. 1.12). Therefore methods are used where a cell
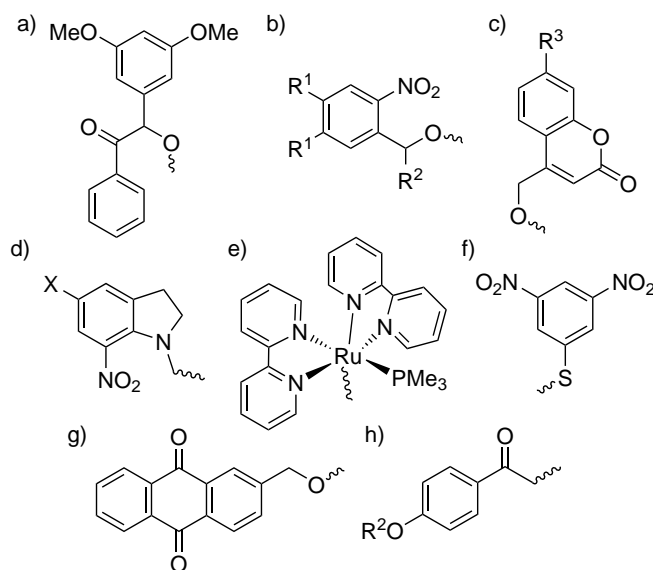
Figure 1.11.: Overview of photolabile protecting groups and their cleavage wavelength: a) benzoin ester (245 nm), b) *o*-nitrobenzyl derivatives (250 to 360 nm), c) coumarin derivatives (360 to 420 nm), d) indol derivatives (350 to 370 nm), e) ruthenium complexes (800 nm), f) dinitrobenzenesulphenyl derivatives (245 nm), g) anthraquinon derivatives (245 nm) and h) phenacyl derivatives (245 nm).[58–62]

sheet is damaged using a sharp object like a tip or scalpel, a laser beam or electricity.[76–78, 81] The removed cells leave a gap in which the remaining cells can start to migrate into. Disadvantage of all these methods is, that during the process cells get damaged and so all intracellular components are released and can induce a uncontrolled signaling, which influences the migration process in an unknown manner. Additionally, the surface coating used in the assay can be removed so that the cell-surfaces interaction remains unclear. Much more defined systems can be created using a physical barrier like custom made PDMS masks[79, 80, 82] or commercially available masks.[83] Advantage of this system is, that the migration is started by removing the barrier and thus no cells get damaged and no unknown signaling occurs. Also the surfaces stay intact and the influence of the coating can be analysed. Disadvantage of this method is, that it is difficult to use on surfaces with a rough structure or a high water content like PEG- or HA-hydrogels, or even PEG-passivated, nanostructured surfaces. Here, it is very difficult to form a defined cell sheet, because the physical barrier does not stick to the surface or due to the roughness gaps are found between the surface and the barrier so that cells can crawl underneath it (fig. 1.13). To overcome this problem a chemical barrier can be used (fig. 1.12 e).
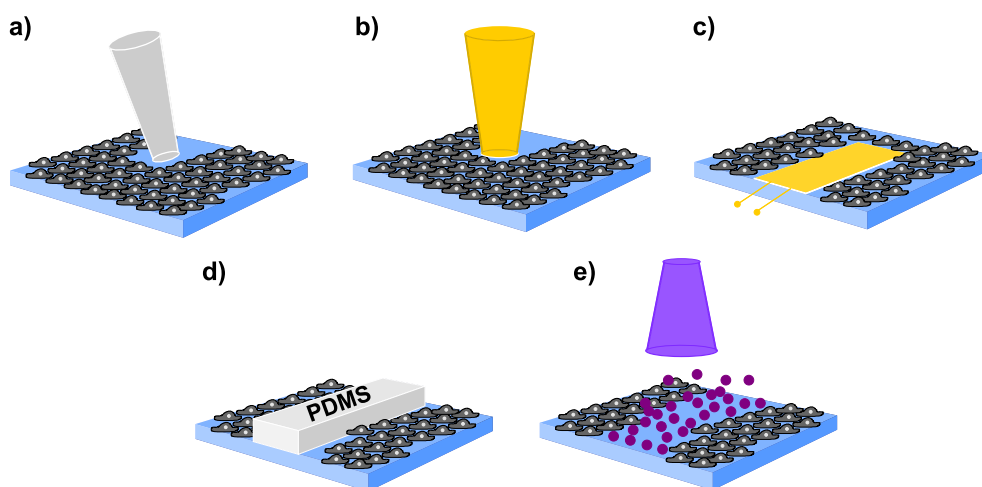
Figure 1.12.: Several methods to study cell migration in a wound healing assay are reported in literature. The wound can be created with a scratch assay where the cells are removed with a sharp object (a), with a laser beam (b) or with electricity (c). Alternatively a physical barrier out of PDMS can be used to create a gap between two collectives (d).[76–80] An alternative is the use of a chemical barrier where a photocleavable protection layer is used on the surface (e).[60]
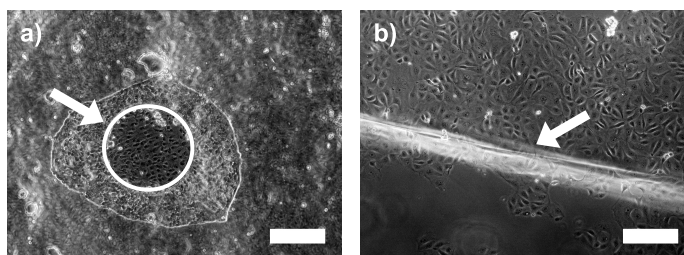
Figure 1.13.: It proves to be difficult to use a PDMS mask to create a cell sheet on a rough surfaces, because the cells crawl underneath the barrier if there is a gap. The pictures shows a physical barrier with a circular (a) and rectangular shape (b). The edges of the barriers are markt with an arrow (scale bar: 300 µm).

1.5.2. Triggering Cell Adhesion and Migration with Photoactivatable Surfaces

To create a chemically modified biointerface two approaches are available. On the one hand, it is possible to functionalise the surface with a photocleavable protected (caged) ligand which allows an unspecific adhesion of the cells on the substrate.[84–86] On the other hand, it is possible to functionalise the surface with a caged ligand which enables a specific adhesion of the cells.

A possible candidate for the specific interaction is the amino acid sequence arginine-glycine-aspartic acid (RGD).[87–89] This RGD sequence matches to the binding domain of many proteins of the extracellular matrix (ECM) and enables so a wide application. The commonly used protecting group used in this method are derivatives of $o-$nitrobenzyl. To use this approach a surface is functionalised with the photocleavable ligand (fig. 1.14). The formed layer
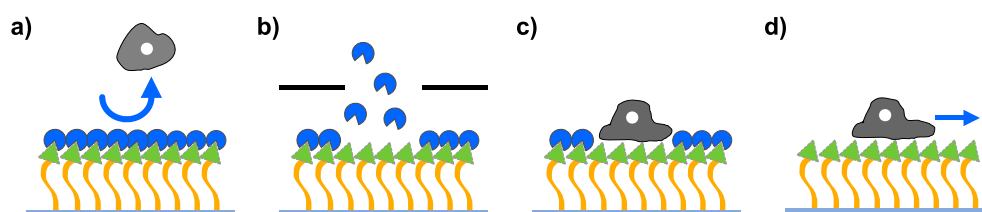
Figure 1.14.: Scheme of the pattering of a surface decorated with a caged adhesion molecule to analyse cell migration. In a) the surface is covered with the $o-$nitrobenzyl-caged ligand, which prevents cell adhesion. After irradiation of the surface through a mask with defined pattering (b), the photolabile protecting groups are removed in this areas. This enables the adhesion of cells in defined regions on the surface (c). After a second irradiation the cells can start to migrate (d).

passivates the surface against unspecific interactions between cells and the surface (a). In a second step the surface is irradiated through a photomask to create a defined pattern on the surface (b). The irradiated areas, the o-nitrobenyl-protecting group is cleaved off. Thus this area is now adhesive and controlled cell sheets can only form here (c), because the passivation in the non-irradiated area stays intact. In a second irradiation step of the surface the remaining protecting groups are removed and the cells can begin to migrate into the open space (d).

The wavelength which is necessary to cleave different $o-$nitrobenzyl derivatives depends strongly on the substitution of the aromatic ring of the protecting group (tab. 1.1). To use photocleavable layers in this biological chemistry approach the applied wavelength is very important as well as the yield of the cleavage in a preferably short irradiation time, because the UV light itself can damage cells.[90] In general, higher wavelengths are (as close to the visible range of light as possible, 390 to 700 nm) better suitable in cell experiments. So substituents are chosen which lead to a high cleavage wavelength. To reduce the irradiation time a substitution pattern is applied with a high attenuation coefficient (ϵ) so that the irradiation time can be kept low. The overview of different substituents shows the highest attenuation coefficient for the case of o-nitrobenzyl (tab. 1.1 # 2) with the specific wavelength of 260 nm. Because of this a compromise between attenuation coefficient and wavelength needs to be found. A very common applied version is the dimethoxy-substitution (#5).

Table 1.1.: Overview of different pattern in substituents and their specific cleavage wavelength and molar attenuation coefficient. X represents the molecule which is protected with the *o*-nitrobenzyl derivativ.[60]
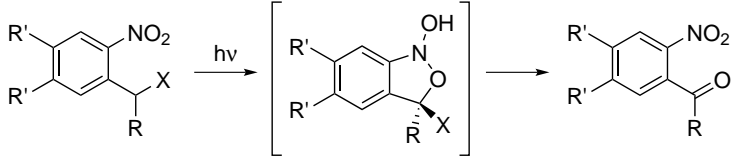
#	substitution	λ_{max} [nm]	$\varepsilon_{\lambda max}$ [1/(mol cm)]
1	R' = R = H	346	7159
2	R' = H; R = Me	260	19600
3	R' = H; R = COOH	266	5200
4	R' = OMe; R = H	360	5000
5	R' = OMe; R = Me	355	5340

1.6. Aim of the Study

The overview of the migration processes in epidermis and dermis after an injury raises four major questions which will be addressed in this study:

1. Which role do different ECM compounds and especially short HA species play during lymphangiogenesis and wound healing?

2. Which strategies can be employed to immobilise HA on a surface in a well-controlled manner to probe cell behaviour in a lymphangiogenesis model?

3. What is needed to develop a migration assay on structurally advanced surfaces?

4. How is wound healing influenced by the density of a specific or unspecific binding model of the ECM?

In the first part of this thesis, human primary lymphendothelial cells are chosen as a minimal model for this process to analyse the influence of short HA on lymphangiogenesis. The cells are incubated with different concentrations of HA in the absence and presence of cRGD. Two different molecular weights of HA are compared (10 kDa, 20 kDa), to study the effect of chain length on cell behaviour. The determined parameters are toxicity of the HA species and concentration as well as metabolic activity of the cells.

Because cells can interact with HA both at the basal (outside of lumen) and apical side (inside the lumen) a method needs to be developed to immobilise HA on a surface to mimic the ECM. Therefore several strategies are tested. Possible methods to immobilise HA are via thiol-groups to gold surfaces like

nanostructured surfaces or gold coated quartz crystals, or via alkyne groups to azide bearing surfaces via CuAAC or SPAAC. Before using the modified HA species their bioactivity is verified. Afterwards, the HA can be immobilised on a gold nanostructured surface whose HA density can be tuned in presence of cRGD by chaning the particle density.

In the second part the strategy of using a chemical barrier method to analyse cell migration is established. Here two novel, photocleavable ligands with a 4,5-dimethoxy-2-nitrophenyl ethanol protecting group are applied to analyse cell migration. The ligands can be immobilised on gold nanostructured surfaces which enables variation of the density of the adhesive background. Chosen are an unspecific (11-mercaptoundecanoic acid) and specific antagonist to integrin $\alpha_5\beta_1$ $(((S))$-3-(4-(3-(6-(3-mercaptopropanamido)hexanamido)propoxy)-benzamido)-4-(4-(3-((4-methoxypyridin-2-yl)amino)propoxy)phenyl)butanoic acid).

Part II.

Materials, Methods and Synthesis

Chapter 2.

Materials and Methods

2.1. Materials

Table 2.1.: Overview of the used consumables

Compound	Supplier
12-well plate	Greiner-bio-one
96-microwell plate µClear	Greiner-bio-one
96-well plate	Greiner-bio-one
dialysis membrane (3.5 kDa)	Carl Roth
glass surface 20 x 20 mm	Carl Roth
glass surface 24 x 24 mm	Carl Roth
glass surface d = 22 mm	Menzel Glaeser
gold coated quartz crystal (QSX301)	QSense AB
petridish (6 cm)	Greiner-bio-one
TLC plate	Merck
TwinSil 22	picodent

Table 2.2.: Overview of the used chemicals. All chemicals were used as received from the suppliers unless stated otherwise. All reactions were carried out under atmospheric conditions unless stated otherwise.

Chemical Compound	Supplier
acetone	Carl Roth
$up\alpha lpha$-amino-ω-alkyne PEG$_{3000}$	Rapp Polymere
ascorbic acid	Sigma Aldrich
5-(3-Carboxy-4-nitrophenyl)disulfanyl-2-nitro-benzoic acid	Sigma Aldrich

Chemical Compound	Supplier
chloroform	Carl Roth
copper sulfate	Sigma Aldrich
cRGD-azide	PSL
cysteamine hydrochloride	Sigma Aldrich
d-chloroform	Sigma Aldrich
d_6-DMSO	Carl Roth
DBCO-amine	Sigma Aldrich
DCC	Sigma Aldrich
DCM	Carl Roth
deuterium oxide	Sigma Aldrich
3,4-dimethoxyacetophenone	Sigma Aldrich
4-dimethylaminopyridine	Sigma Aldrich
DIPEA	Sigma Aldrich
ethanol	Carl Roth
ethyl acetate	Merck
glacial acetic acid	Fluka
hyaluronan (20 kDa, batch: 024505)	lifecore
hydrochloric acid	Sigma Aldrich
hydrogen peroxide	AppliChem
magnesium sulfate	Gruessing
11-mercaptoundecanoic acid	Sigma Aldrich
methanol	Carl Roth
α-methoxy-ω-amino PEG$_{2000}$	Rapp Polymere
moleculare sieve (4 Å)	Carl Roth
nitric acid	Sigma Aldrich
2-propanol	Carl Roth
propargylamine	Sigma Aldrich
SDS	Carl Roth
silica gel	Carl Roth
sodium acetate	Sigma Aldrich
sodium borhydrid	Sigma Aldrich
sodium chloride	Sigma Aldrich
sodium cyanoborhydrid	Sigma Aldrich
sodium tetraborate	Sigma Aldrich

Chemical Compound	Supplier
sulfuric acid	Sigma Aldrich
THF	Carl Roth
toluen	Merck
triethylamine	Sigma Aldrich
trifluoroacetic acid	Sigma Aldrich
triisopropylsilyl ether	Sigma Aldrich
tris(hydroxymethyl)-aminomethane	Carl Roth
tris(3-hydroxypropyltriazolylmethyl)amine	Sigma Aldrich
Tritylchloride	Sigma Aldrich

Table 2.3.: Overview of the used cell culture consumables.

Compound	Supplier
AlamarBlue® kit	ThermoFischer
cellculture flask ($75\,\mathrm{cm}^2$)	Greiner-bio-one
cellculture flask ($25\,\mathrm{cm}^2$)	Greiner-bio-one
CyQuant® kit	ThermoFischer
EGM-2 MV	Lonza
FBS	Gibco, Life Technology
fibronectin (bovine)	Sigma Aldrich
Ibidi-chamber	ibidi
L-glutamine	Gibco, Life Technology
LEC (Batch 3061003.3)	Promocell
MEM	Sigma Aldrich
MDCK II	Sigma Aldrich
PBS tablets	Gibco, Life Technology
Penicillin/Strepomycin	Gibco, Life Technology
Pluronic F-127	Sigma Aldrich
Trypsin-EDTA	Gibco, Life Technology

Table 2.4.: Overview of the used antibodies for cell stainings.

Compound	Supplier
primary antibodies	
DAPI	Sigma Aldrich
mouse anti-Paxillin (IgG)	BD (610620)

Compound	Supplier
mouse anti-Talin (monoclonal)	Sigma Aldrich
mouse anti-Vinculin (monoclonal)	Sigma Aldrich
Phalloidin/FITC	Sigma Aldrich (P1951)
Phalloidin-647	Lifetechnologies
rabbit anti-LYVE-1 (polyclonal)	abcam
rabbit anti-human LYVE-1 (polyclonal)	Reliatech (102-PA50S)
rabbit anti-Paxillin (monoclonal)	abcam
secondary antibodies	
goat anti-mouse Alexa 488 (2 mg/mL)	Invitrogen
goat anti-rabbit Alexa 594 (2 mg/mL)	Invitrogen
goat anti-rabbit Alexa 647 (2 mg/mL)	Invitrogen

2.2. Analytical Methods

2.2.1. NMR-Spectroscopy

All NMR-analyses were performed at the NMR-department of the inorganic-chemical institute at Heidelberg University. The spectra were all measured at room temperature using the "Avance III 400" (^{1}H: 400 MHz; ^{13}C: 100 MHz) or "Avance III 600" (^{1}H: 600 MHz; ^{13}C: 150 MHz) NMR of the company *Bruker*. The chemical shift (δ) was specified in part per million (ppm) and the J-coupling accordingly in Hertz (Hz). The spectra were calibrated to the solvent residual signal of the used solvent (^{1}H: D_2O = 4.79 ppm, $CDCl_3$ = 7.26 ppm, $(CD_3)_2SO$ = 2.50 ppm; ^{13}C: $CDCl_3$ = 77.16 ppm, $(CD_3)_2SO$ = 39.52 ppm)[91] To analyse the NMR-spectra the software "Topspin" (version 3.5pl4; *Bruker*) was utilised and following abbreviations were used: s = singlet, d = doublet, t = triplet, q = quartet, m = multiplet, b = broad.

To identify the signals the 2D-spectra COSY (^{1}H^{1}H) and HSQC (^{1}H^{13}C) were performed as well.

2.2.2. Mass-Spectrometry

The MS-analyses were performed at the mass spectrometry facility of the organic-chemical institute at Heidelberg University. The measurements are performed with the ionisation methods ESI and DART using the "ICR Apex-Qe" from *Bruker*.

2.2.3. Absorption Spectroscopy

Experiments Using a UVVIS Spectrometer

For analysing the interaction of light with the photocleavable molecules the UVVIS-spectrometer "Cary 500 Scan" (*Varian/ Agilent Technologies*) from the

group of Prof. Herten (institute of physical chemistry at Heidelberg University) was used. The measurement was performed in quartz cuvettes from *Hellman Analytics* against air and corrected to the absorption of the cuvette containing the pure solvent (acetonitril) and to the offset coming from the change of the ligth source at 350 nm. For irradiation of the compounds a pulsed diode laser source ("pdl375", *PicoQuant*) with a wavelength of 375 nm and 800 µW is applied. 100 µL of a 100 µM solution of DMNPE-thiol (**1**) respectively DMNPE (**2**) are irradiated. The measurement is started before the irradiation up to 70 min between 250 to 500 nm. To prevent evaporation of the solvent the cuvette is closed with a Teflon stopper and parafilm. The resulting spectra are corrected and plotted using "OriginPro 2016G" (version b9.3.226; *OriginLab Corporation*).

Experiments Using a Plate Reader

For the performance of the Ellman's, AlamarBlue® and CyQuant®assay the plate reader "Infinite 200 Pro" from *Tecan* was used with a 96- or 12-well plate from *greiner-bio-one* respectively 96-well microplate "µClear" (*greiner-bio-one*). The measurements are corrected to the well plate containing the utilised media. The different used wavelength are summerised in table 2.5. The evaluation of the data is performed using "Excel for Mac" (2011, version 14.7.1, *Microsoft*). The results for the AlamarBlue® and CyQuant®assay are plotted and the Kruskal-Wallis test followed by Dunn's multiple comparison test was performed using "GraphPad Prism6" (for Mac, version 6.0e, *GraphPad Software Inc., USA*).

Table 2.5.: Summary of the used wavelength in the Ellmans's, AlamarBlue® and CyQuant®assay.

#	assay	fluorescence [nm]		absorption [nm]
		λ_{ex}	λ_{em}	
1	Ellman			420
2	AlamarBlue®	540	585	570 and 600
3	CyQuant®	480	520	

2.3. Microscopy

2.3.1. Zeiss Oberserver Z1

To perform the migration assay the inverted, partially motorised "Observer Z1" (*Zeiss*) is used. It is equipped with an "Orca ER" camera (*Hamamatsu*), a "definite focus" module as well as a small incubation chamber for 12-well plates (*Peacon*), which enabled the control of temperature, CO_2 ("TempModulS",

"CO$_2$ModulS", all *Zeiss*) and humidity. For imaging the software Zen2pro (*Zeiss*) was applied. For illumination in phase contrast images a "HAL 100" halogen lamp was used. For the irradiation of the surfaces functionalised with a photocleavable linker the UV-lamp "X-cite" (Series 120 PC, *EXFO*) and the BFP-filter set (Excitation 377 ± 28 nm; Beamsplitter 403 nm; Emission 464 ± 100 nm, *Zeiss*) are used. Before phase contrast images were taken the light path was always adjusted according to the Koehler method.[92, 93] For imaging a 20x objective ("EC-Plan Neofluar", num0.5 NA, PH2, *Zeiss*) was used. Irradiation was performed via a 5x objective ("Plan Apochrom", 0.16 NA, *Zeiss*).

2.3.2. Zeiss Axiovert

For imaging the glass surfaces within a well-plate and the overview images a "Axiovert 40 C" (*Zeiss*) using a 10x objective ("A-Plan", 0.25, PH1, *Zeiss*) was used. The microscope was equipped with a "DS-2Mν" camera system (*Nikon*).

2.3.3. Leica DM 6000B

To analyse the fluorescence staining an upright microscope from *Leica Microsystems CMS GmbH* ("DM6000B"; "CT3 HS controller") equipped with a motorised stage is used. The microscope is equipped with a 1.4 MPixel CCD camera ("DFC 365 FX", *Leica*) and the external light source "EL 6000" (*Leica*). For taking images a 10x mgnification objective ("HCX PL APO", 0.4, *Leica*) and the software "LAS AF" (Version 3.2.0.9652; *Leica*) is used.

2.4. QCM-D

The quartz crystal microbalance (QCM) is a nanogram sensitive technique based on the inverse piezoelectric effect.[94] Therefore a silicon single crystal is cut using the AT-cut. This cut enables a standing transversal wave in the crystal and shows a low influence of temperature to the resonance frequency. The crystal is sandwiched between two electrodes. An external electric potential is applied to the crystal, which leads to an internal mechanical stress and thus to an oscillation. Because the oscillation is induced through an electric field, which leads to a charge separation at the crystal edge with the electrodes attached, only odd harmonics can be excited. The resonance frequency of the oscillation of the crystal depends on the thickness of the wafer, its chemical structure, its shape as well as its mass. Because of this correlation any adsorption on top of the crystal leads to a change of the resonance frequency and its harmonics.[94–96] Sauerbrey describes the direct correlation between the absorbed mass (Δ m), the density of the crystal (c_Q) and the change in frequency (equation 2.1 and 2.2).

$$\Delta m = \frac{c_Q}{n} \cdot \Delta f \qquad (2.1)$$

$$c_Q = \frac{t_Q \cdot \rho_Q}{f_0} \tag{2.2}$$

Often crystals with a thickness t_Q of $330\,\mu m$ and thus a fundamental frequency f_0 of about $5\,MHz$ are used. This leads to a density c_Q of approximately $-17.7\,Hz\,ng/cm$. This equation is only valid, if the adsorbed mass is small relative to the mass of the crystal, the mass is evenly distributed and a rigid film is formed on the surface.[94, 96] To increase the response of adsorbed mass on the crystal, which enables QCM as analysis method, a ring electrode is placed on top of the crystal around the adsorption area, which achieves the function of an acoustic lens. In a QCM-D experiment the resonance frequency with harmonics are determined in air. Afterwards, the crystal is equilibrated in buffer (B) used in the experiment. This equilibrium is set to zero before adding the compounds of interest (fig. 2.1 a, step 1). The adsorption leads to a decrease in frequency. After the system is equilibrated again the pure buffer (B) is added on top of the crystal to remove unbound compounds. To determine the change in frequency ($\Delta\Delta\,f_n$, fig. 2.1 a grey) due to the adsorbed mass the plateau values in buffer are compared. This is repeated for every compound respectively layer on the surface. Additional to the change in frequency the adsorbed substances influence the damping of the sinusoidal frequency (equation 2.3).

$$A(t) = A_0 \cdot exp[t/\tau] \cdot \sin(2\pi f t + \alpha) \tag{2.3}$$

This is observed in the dissipation, which is described with $D = 1/(\pi f t)$. If a rigid film is adsorbed on top of the crystal only a small decay of the oscillation is determined and thus a small change in dissipation (fig. 2.1 a, step 1). If a large molecule with many numbers of degrees of freedom is adsorbed, a high loss of energy occurs and thus a large change in dissipation is observed (fig. 2.1 a, step 2). In the case shown in figure 2.1 a) the adsorption of the compound in step 2 is reversible and it can be washed away again.

The QCM-D technique is applied to analyse the adsorption and bioactivity of various functionalsied HA and to analyse the adsorption and cleavage properties of 1-(4,5-dimethoxy-2-nitrophenyl)ethyl 11-mercaptoundecanoate. The experiments are either performed in the fully automated "Omega Auto" (bioactivity assays) or the manual "E4 modul" (both *Q-Sense AB*) with the so called "open modul" (*machine workshop* at Heidelberg University; fig. 2.1 b; photocleavable assay, adsorption of HA). For the experiment gold coated quartz crystals ("QSX301", *Q-Sense AB*) are used, which were activated using a UV-ozone cleaner ("OzoneProCleaner™", *BioForce Nanoscience*) with an irradiation time of 10 min. After installing the sensor in the instrument the fundamental frequency and its overtones (n = 3, 5, 7, 9, 11 and 13) are determined in air. Then the system is equilibrated in the applied buffer and the change in frequency as well as the dissipation are observed. The equilibrium is indicated by a plateau in $\Delta f_n/n$. Then the different compounds are added in the buffer, the system
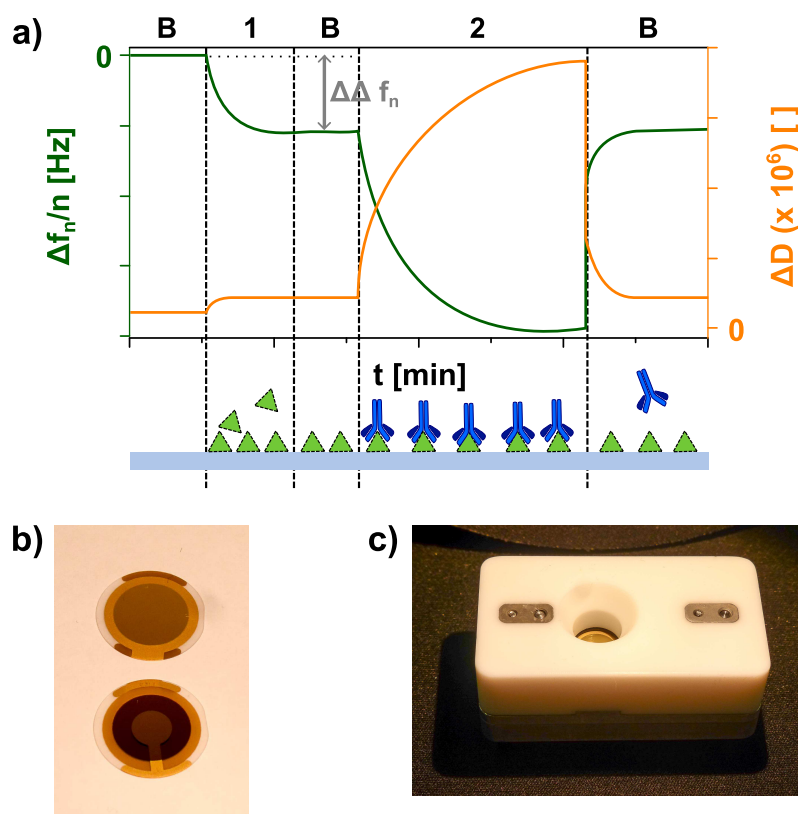
Figure 2.1.: Overview of a QCM-D experiment. An exemplary change in frequency (Δf, green) and dissipation (ΔD, orange) progress of a QCM-D experiment is shown in a) (adapted from Dixon[94]). After equilibrating the crystal in buffer (B), a rigid layer is formed at the surface (step 1), followed by the reversible adsorption of a molecule, which forms a viscoelastic layer (step 2). In b) a QCM-D sensor with gold coating in top and bottom view is shown and and a scheme of the open module c).

is equilibrated in, followed by a washing step with buffer each time. To analyse the data the average of the last 5 min of each buffer plateau were calculated including the standard deviation using "Excel for Mac2011" (Version 14.7.1, *Microsoft*) or "Open Office" (version 4.1.2, *Appache*). The change in frequency and dissipation for n = 7 is plotted using "Origin" (OriginPro2016G, version b9.3.226, *Origin Lab Corporation*).

Cleaning Procedure

To clean the system the sensors as well as the chamber itself is rinsed with 2 wt% SDS in water in the ultrasonic bath for 10 min. Afterwards the sensors were rinsed with ddH$_2$O and dried under a stream of nitrogen before adding them to a mixture of ddH$_2$O:NH$_3$ (23 %): H$_2$O$_2$ (30 %) 5:1:1 at 80 °C for 5 min

Table 2.6.: Summary of all compounds used in the QCM-D experiments with their concentrations.

#	compound	amount
1	HA	0.4 g/L
2	HA-end-thiol (**3**)	0.4 g/L
3	HA-end-alkyne (**4**)	0.4 g/L
4	HA-end-DBCO (**5**)	1.0 g/L
6	HA-side-alkyne (**6**)	1.0 g/L
7	DMNPE−thiol (**1**)	100 μM
8	11-mercaptoundecanoic acid (**7**)	100 μM
9	DMNPE (**2**)	100 μM
10	BSA	0.4 %
11	EDTA	1 mM
12	THPTA	500 μM
13	aggrecan	100 μg/mL
14	LYVE-1[a]	20 μg/mL

a) recombinant humna LYVE-1 with a C-terminal 6-His tag (*R&D Systems*)

Table 2.7.: Overview of the used buffers with their concentrations and pH values used in the QCM-D experiments.

#	buffer	concentration	pH
1	PBS		7.5
2	TRIS	100 mM	8.5

according to the cleaning protocol form *Q-Sense*. Afterwards the crystal is rinsed with ddH$_2$O and dried under a stream of nitrogen.

E4-Module

In the QCM-D experiment 200 μL solution are added to the middle of the crystal. To change the solution the complete 200 μL are removed at the edge of the chamber. For experiments with the photocleavable linker the open moduls were covered with a quartz glass slide and the sensor irradiated with UV light (365 nm, "VL-6L", *Vilbert Lourmat*) until a plateau is reached.

Omega Auto[1]

The gold-coated sensors were activated by a O_2-plasma treatment for 45 min with 150 W and 0.4 mbar ("360M", *PVA Tepla*). The Omega Auto is used with a flow rate of 20.0 μL/min. Each channel was running independently with a seperate Hamilton syringe pumpe. The crystals were cleaned with a 2 % hellmanex solution (*Hellmanex*), rinsed with ddH$_2$O and dried under a nitrogen stream.

2.5. Water Contact Angle

Surfaces show different properties respective their surface energy, which can be changed by functionalisation for example with a SAM. This change can be used to characterise the surface and its surface energy via its wetting behaviour. To analyse this, the so called contact angle (Θ) is measured. For this a solvent-droplet is introduced to the sample and its geometric properties are determined. [97,98] The change of geometry of the drop is due to the difference in surface tension between the liquid and the surface. The liquid molecules interact with their neighbours within the droplet resulting in a balance net force of zero. The molecules at the interfaces have no direct neighbour (or of a different kind), which leads to an inward-looking force, manifesting in the drop shape with the lowest surface free energy (fig. 2.2). These unbalanced forces contract the droplet and correlate with the surface tension. Additional external forces like gravity, influence the droplet as well, so due to that only amounts of liquid of 1 to 5 μL were used.[98]
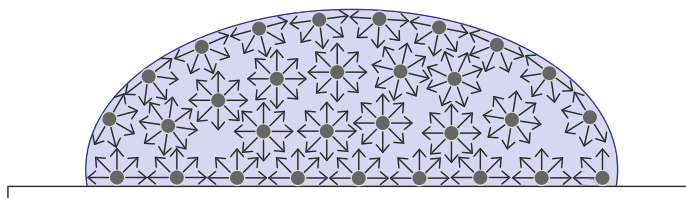
Figure 2.2.: The surface tension is due to unbalanced forces between liquid molecules and their environment, which is manifested in the shape of the droplet.(adapted from [98])

In the case where the substrate surface energy is higher than the liquid surface tension, the resulting contact angle will be in the range of $0° < \Theta_Y < 90°$. This corresponds to a high wetting ability (fig. 2.3), which means for using water a very hydrophilic surface (for example HA coated surfaces). Contrarily, for a lower surface tension in compared to the substrate surface tension the

---

[1]The experiments with the Omega Auto were performed by Dr. Burcu B. Minsky and were published in Scientific Reports.[54]

liquid undergoes poorly wetting ($90° < \Theta_Y < 150°$), which relates for water to a hydrophobic surface. This culminates in the case of a so called superhydrophobic surface, which corresponds to a contact angle Θ_Y larger than 150° with almost no wetting (lotus effect).[97–99]

0° < Θ < 90°   Θ = 90°   90° < Θ < 150°   Θ > 150°
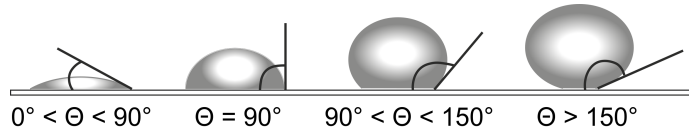
Figure 2.3.: Scheme of different water contact angles on an homogeneous, solid surface with $\Theta_Y < 90°$ for hydrophilic surfaces up to $\Theta_Y > 150°$ for superhydrophobic surfaces (lotus effect).(adapted from [98])

The correlation between the surface tension and the measurable contact angle in an equilibrated system is described by the three interfacial tensions, describing the three different interfaces of the system: surface and liquid interface (γ_{sl}), surface and vapour interface (γ_{sv}) and liquid and vapour interface (γ_{lv}).[98–100] This is expressed through the Young-Dupre equation (2.4) with Θ_Y as Young's contact angle:

$$cos(\Theta_Y) = \frac{\gamma_{sv} - \gamma_{sl}}{\gamma_{lv}} \qquad (2.4)$$

The Young-Dupre equation is only valid for ideal surfaces. This implies homogeneous, inert and smooth surfaces, which can be produced with the following techniques accoring to Lamour *et al.* and Kwok *et al.*: heat pressing, solvent castig, SAM formation, dip coating, vapour deposition and surface polishing.[99, 100] Cassie and Baxter postulated a possibility to analyse the contact angle of rough and porous surfaces as well in 1944. They expanded the Young-Dupre equation with a geometrical model to describe the rough surface. [101]

Measurement of the Contact Angle

The contact angle measurements were performed with the "OCAH 230" devices (*DataPhysics Instruments GmbH*) applying the sessile drop method. Therefore 1.0 μL water is pipetted to the surface and an image was captured by a CCD camera. The contact angles of the left and the right side of the drop were evaluated by the software "SCA20" (*DataPhysics Instruments GmbH*). Five spots were measured per surface and multiple measurements were done.

Surface Preparation for Contact Angle of HA Functionalised Surfaces[2]

The used silicon wafer (*Silicon Materials*, 2" wafer, Typ P/ Boron <100>, R = 5 - 10 Ω, d = 256 to 306 µm) is cleaned with freshly prepared Caro's acid (H$_2$SO$_4$: H$_2$O$_2$ (30 %) 3:1) for 1 h and is coated with gold (100 nm) using a thermal evaporation method (1 Å/s; p = 10^{-6} millibar, *Pfeiffer* "Vacuum Classic 500"). The surfaces are incubated with either a 0.004 % solution of the end-thiolated HA species or a 100 mM solution of HS$-$(CH$_2$)$_{11}$$-EG_3$$-$OH and HS$-$(CH$_2$)$_{11}$$-EG_6$$-$HA in a ratio of 2:1. Here the HA is clicked to the azid with the CuAAC before the adsorption on the surface. The solutions are incubated for 1 h, the surfaces rinsed with water and dried under a stream of nitrogen.

Surface Preparation for Contact Angles of Photocleavable Functionalised Surfaces

The used glass slide (*Carl Roth*, 24 x 24 mm) is coated with titanium (3 nm) and gold (30 nm) using the sputter coater from *Bal-Tec* (tab. 2.8; Bal-Tec Med 020 Coating System with Bal-Tec MCS 010 Multi Control System). Before using the surface, they were rinsed with EtOH and then incubated with a 100 µM solution of DMNPE-thiol (**1**) (1 % EtOH in PBS) over night using a humidifying chamber. After incubation the surfaces were again rinsed with ddH$_2$O and dried under a stream of nitrogen. The surfaces were irradiated with a UV hand lamp ("VL-6 L", *Vilber*) at 365 nm for 60 min and washed with ddH$_2$O before measuring the contact angle again. The measured contact angles are plotted and a Kruskal-Wallis test followed by Dunn's multiple comparison test are performed using "GraphPad Prism6" (for Mac, version 7.0c, *GraphPad Software Inc., USA*).

Table 2.8.: Parameter used for sputtering of glass slides and silicon wafers.

metal	thickness [nm]	I [mA]	t [s]	p [mbar]
Ti	3	60	40	$1.3 \cdot 10^{-2}$
Au	30	60	35	$5.0 \cdot 10^{-2}$

2.6. BCML

2.6.1. Preparation of Micellar Solution

Poly(styrene(x)-block-(2-vinylpyridine)(y))(PS(x)-b -P2VP(y)) was dissolved in toluene to a final concentration of 2-8 mg/mL in a pre-cleaned glass tube.

---

[2]The contact angles were measured by Dr. Burcu B. Minsky and were published in Scientific Reports.[54]
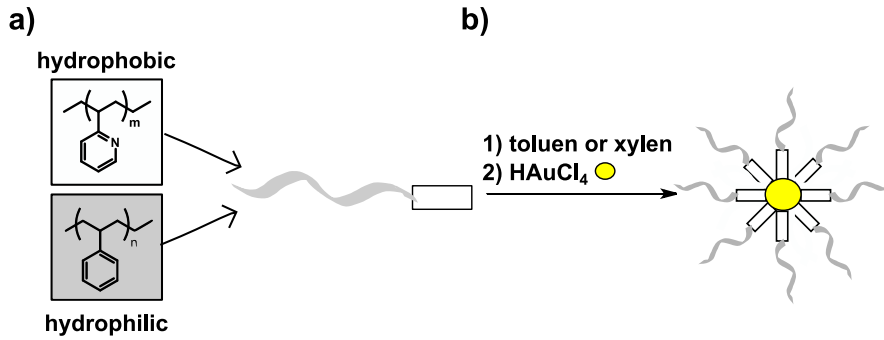
Figure 2.4.: Scheme of the preparation of micellular solution. a) A coblock-polymer consisting of polystyrene (PS, grey) and polyvinylpyridine (P2VP, white) is suspended in toluene or xylene (b). After the formation of the micells HAuCl$_4$ is added to load the micells with gold.

The utilised ratio between PS- and P2VP-units depends on the target inter-particle spacing (tab. 2.9). The solution was stirred for 24 h to obtain the formation of micelles. The tetrachloroaureate(III)trihydrate (HAuCl$_4 \cdot$ 3 H$_2$O) was added and the solution stirred for another 24 h while being protected from light (fig. 2.4). The amount of required salt is calulated applying equation 2.5 and should be in a range of 0.2 to 0.5 depending on the used polymer.

$$m_{\text{HAuCl}_4 \cdot 3\,\text{H}_2\text{O}} = \frac{m_{polymer}}{M_{polymer}} \cdot (2 - VP_{units} \cdot L) \cdot M_{\text{HAuCl}_4 \cdot 3\,\text{H}_2\text{O}} \qquad (2.5)$$

Table 2.9.: Overview of the ratio of styrene- (PS) to vinylpyridine-units (P2VP) and the possible resulting interparticle spacing.

#	PS units (x)	P2VP units (y)	particle spacing [nm]
1	154	33	18 to 32
2	227	99	24 to 30
3	451	228	42 to 83
4	1057	495	55 to 110
5	1776	694	46 to 102
6	3120	875	53 to 112
7	5348	713	180 to 300

2.6.2. Nanostructuring of Glass Slides by Dip-coating

Before using, the glass surfaces were cleaned with freshly prepared Caro's acid (H$_2$SO$_4$: H$_2$O$_2$ (30 %) 3:1) over night. Afterwards they were rinsed with

ddH$_2$O and dried under a nitrogen stream. The glass slides were dipped into the prepared micellular solution with a defined immersion and retraction speed (table 2.10) at a $\Theta = 90°$ angle towards the solution surface using a home-build dipping-machine (*machine shop University of Heidelberg*, fig. 2.5, tab. 2.10).The surfaces were dried on a lint free paper. The metal salt (Au$^{III} \rightarrow$ Au^0) was reduced and the polymer shell removed by using hydrogen plasma (W10, 350 W, 0.4 mbar, 45 min, "Plasma System 100-E", *TePLa*).
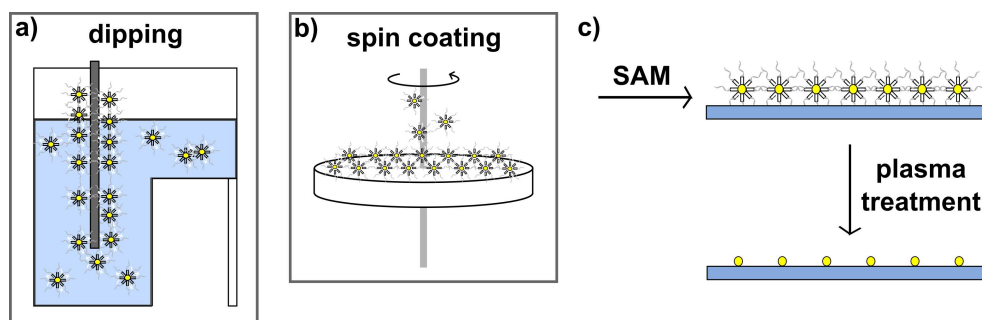
Figure 2.5.: Overview of the preparation of nanostructured glass surfaces. The micellular solutions is either distributed on the surface via a) dipping or b) spin coating. The resulting SAM of gold loaded micells c) is plasma treated to remove the polymer coat and to reduce the Au^{III} to Au^0.

Table 2.10.: Overview of used loading of the micelles in $o-$xylen and applied speed/ voltage for creating nanostructured surfaces and the resulting interparticle spacing.

#	spacing [nm]	c [mg/mL]	loading	voltage [V]
1	40	5	0.5	7 to 12
2	60	5	0.3	12 to 15
3	100	3	0.3	12 to 15

2.6.3. Nanostructuring of Glass Slides by Spin-coating

Before the modification, the glass surfaces were cleaned with freshly prepared Caro's acid (H$_2$SO$_4$: H$_2$O$_2$ (30 %) 3:1) over night. Afterwards they were rinsed with ddH$_2$O and dried under a nitrogen stream. The slides were fixed in the spin-coater applying a slight vacuum. 20.0 μL of the micellular solution were quickly added on top of the rotating glass slide in the spin coater (fig. 2.5 b). Each surface was spin coated for 30 s and a speed between 5000 and 12 000 rpm (tab. 2.11). The metal salt (Au$^{III} \rightarrow$ Au^0) was reduced and the polymer shell removed by using hydrogen plasma (W10, 350 W, 0.4 mbar, 45 min, "Plasma System 100-E", *TePLa*).

Table 2.11.: Overview of used loading of the micelles in o−xylen and applied speed for creating nanostructured surfaces and the resulting interparticle spacing.

#	spacing [nm]	c [mg/mL]	loading	speed [rpm]
1	35	5	0.5	12 000
2	61	8	0.3	4000
3	102	3	0.4	3000

2.7. General Protocol for the Passivation of Surfaces

Protocol for the passivation of 10 cover glasses, which were labelled with numbers using a diamond writer:

component	m [mg]	V
PEG	5.0	
Toluene (dry)		20 mL
Triethyl amine		3 drop

The surfaces were treated with oxygen-plasma (10 min, 0.4 mbar, 150 W, either "Plasma System 100-E", *TePLa* or "360M", *PVA Tepla*) to activate the surface. A Schlenk flask was flushed with nitrogen. then the toluene, NEt_3 and PEG (section 3.2) were filled in the flask. The surfaces were inserted into a glass holder and added to the flask. If the humidity is very low ($\leq 20\%$) 1 μL ddH_2O per 10.0 mL toluene were added. The reaction solution was heated up to 80 °C over night. After the reaction the glass slides were rinsed twice with ethyl acetate and sonicated for 1 min in ethyl acetate. then they were rinsed with methanol, ddH_2O and dried under a nitrogen stream.

2.7.1. Passivation of Pure Glass Surfaces with PEG

The glass cover slides were pre-cleaned with freshly prepared Caro's acid ($H_2SO_4 : H_2O_2$ (30 %) 3:1) over night. The glass slides were rinsed with ddH_2O and dried under a nitrogen stream. For this passivation PEG_{2000}−silane (**8**, $(EtO)_3Si−(CH_2)_3−NH−C(O)−NH−PEG_{2000}$) was used following the general protocol.

2.7.2. Passivation of Nanostructured Surfaces with PEG

For the passivation of nanostructured surfaces PEG_{2000}−silane (**8**) was utilised following the general protocol.

2.7.3. Passivation of Pure Glass Surfaces with Click-PEG

The glasses were pre-cleaned with freshly prepared Caro's acid ($H_2SO_4 : H_2O_2$ (30 %) 3:1) over night. The glass slides were rinsed with ddH_2O and dried under a nitrogen stream. The further procedure follows the general protocol using a mixture of PEG_{2000}−silane (**8**) and PEG_{3000}−alkyne (**9**, $(EtO)_3Si$-$(CH_2)_3$−NH−C(O)−NH−PEG_{3000}−NH−C(O)−$(CH_2)_2$−C≡CH) in a ratio of 100:1.

2.7.4. Passivation of Nanostructured Surfaces with Click-PEG

The cover glasses were treated according to the passivation protocol using a mixture of PEG_{3000}−alkyne (**9**) and PEG_{2000}−silane (**8**) in a ratio of 1:100.

2.8. MDCK II migration experiments

MDCK II (Madine-Darby Canine Kidney Strain II, *Sigma Aldrich*) cells were grown in $75\,cm^2$ cellculture flasks in $10\,mL$ Minimum Essential Medium Eagle with phenolred (MEM) containing 5.0% Fetal Bovine Serum (FBS), 1.0% L-glutamine, and 0.1% Penicillin/Streptomycin (PenStrep) at $37\,°C$ with 5.0% CO_2. The cells were splitted at 80% confluence. The cells were washed 3 times with $10.0\,mL$ warm PBS ($37\,°C$), once with $2.5\,mL$ trypsin-EDTA and incubated with $2.5\,mL$ trypsin-EDTA at $37\,°C$ for 8 to $10\,min$. The cells were re-suspended in $7.5\,mL$ pre-warmed MEM complete to deactivate the trypsin enzyme. $10.0\,µL$ were taken to count the cells using a Neubauer counting chamber. The cells were centrifuged at 1200 rpm (220 g) for $3\,min$ in a $15.0\,mL$ falcon. The cells were diluted as desired for the experiment or splitting (tab. 2.12).

Table 2.12.: Number of cells seeded to different used surfaces

type	# seeded cells
splitting	1.0 to 1.5 $\cdot 10^6$
photocleavable surface	$2 \cdot 10^5$
96 well plate	5000

Functionalisation of Nanostructured Surfaces with 1-(4,5-dimethoxy-2-nitrophenyl)ethyl 11-(tritylthio)undecanoate (1)

The 24 x 24 mm PEG-passivated, nanostructured surface was incubated with $70.0\,µL$ of a $100\,µM$ solution of **1** in 1.0% EtOH and PBS over night using a humidifying chamber. The surface was washed with ddH_2O three times for

10 min and glued to a custom-made Teflon-ring using "PicoDent Twinsil" (*Pi-coDent*). Before irradiating the surface with UV light, the surfaces are washed with PBS. For irradiating for the first time the microscope "Observer Z1" with a 5x magnification and the UV-lamp "X-cite" (Series 120 PC, *EXFO*) are utilized. The used pattern is created with a rectangular aperture in an imaging plan conjugated to the sample surface. The surface is irradiated under PBS and after washing with PBS the surfaces are prepared for the cell experiment. For the second irradiation step the surfaces with the Teflon-rings are added to a 12 well incubation chamber (*Peacon*) at the microscope (37 °C, 5 % CO_2). Several positions along the edge of the collective are chosen, the positions saved with the software Zen (*Zeiss*) and irradiated with UV light for 60 s. Afterwards the same positions are observed for 2 h and a phase contrast image is taken every 20 min.

2.9. Influence of sHA on Lymphatic Endothelial Cells

The "human dermal lymphatic endothelial cells" (LEC, *PromoCell*) used in the following experiments were always taken from Batch 3 061 003.3 (order no. C12 216) unless stated otherwise.

The LECs were thawed and 10 000 to 20 000 cells were seeded in a 25 cm^2 flask in 5.0 mL "EGM-2 MV" medium (endothelial basal medium-2, *Lonza*). The media contains 0.1 % epidermal growth factor ("hEGF"), 0.1 % vascular endothelial growth factor ("VEGF"), 0.1 % R3-Insulin like growth factor ("R3-IGF-1"), 0.1 % ascorbic acid, 0.04 % hydrocortisone, 0.4 % human fibroblast growth factor-beta ("hFGF-β") 5.0 % fetal bovine serum ("FBS") and 0.1 % Gentamicin/ Amphotericin-B ("GA", all *Lonza*). After one day the medium was changed completely. When the cells reached 80 % confluence, they were washed twice with 5.0 mL warm PBS (37 °C) and incubated with 2.0 mL trypsin-EDTA for approximately 3 min. 8.0 mL medium were added to the flask to deactivate the trypsin enzyme. The cells were centrifuged for 5 min at 1200 rpm (0.2 g). The cells were re-suspended and after counting the cells 10 000 to 20 000 were seeded in a 25 cm^2 flask in 5.0 mL medium. When the cells reached again 80 % confluence, they were used for further experiments.

2.9.1. Functionalised and Unfunctionalised HA in Solution on Cell Culture Plastic

Stock solutions of the utilised HA-species of 40 μg/mL in media were prepared and further diluted in the ratios of 1:20, 1:8; 1:4 and 1:2. 100 μL of these dilutions were added to each well before 4210 cells were seeded per surface suspended in 100 μL medium. This results in a final concentration of the HA-species of 0.0, 1.0, 2.5, 5.0 and 20.0 μg/mL. After 46 h the AlamarBlue® assay was performed according to the protocol in section 2.10.1 followed by the CyQuant® assay (section 2.10.2).

2.9.2. Functionalised and Unfunctionalised HA in Solution on Click-PEG Surfaces

Round glass cover slide (d = 22 mm) were passivated with click-PEG according to the protocol for the passivation of glass slides with click-PEG (section 2.7). Afterwards the surfaces were incubated with 75 µL of the click-reaction-buffer (table 2.13) on parafilm in a humidifying chamber for 1.5 h at room temperature. The surfaces were washed three times with ddH$_2$O for 10 min each and dried under a stream of nitrogen. then the surfaces were added under sterile conditions to a 12-well plate and washed with sterile PBS. A stock solution of the HA-species of 40 µg/mL was diluted in the ratios of 1:20, 1:8; 1:4 and 1:2. 500 µL medium containing the different dilutions were added to each well before 50 000 cells per surfaces were seeded in additional 500 µL medium. This results in the final concentrations of HA of 1.0, 2.5, 5.0 and 20.0 µg/mL. After 46 h the AlamarBlue® assay was performed according to the protocol in section 2.10.1 followed by the CyQuant® assay (section 2.10.2).

2.9.3. Immobilised, End-thiolated HA on Nanostructured Surfaces

Round, nanostructured glass cover slides (d = 22 mm) were passivated with click-PEG according to the protocol for nanostructured glass slides (section 2.7). Afterwards the surfaces were incubated with 75 µL of the click-reaction-buffer (table 2.13) on parafilm in a humidifying chamber for 1.5 h at room temperature. The surfaces were washed three times with ddH$_2$O for 10 min and dried under a stream of nitrogen. To functionalise the Au-nanoparticles the surfaces were incubated with 75 µL of a solution of HA or end-thiolated HA (1 wt%/v% in PBS [pH = 7.4]) on parafilm in a humidifying chamber for 1 h at room temperature. The surfaces were washed twice with PBS and added to a 12-well plate under sterile conditions. The surfaces were again washed with sterile PBS before 50 000 cells per surface were seeded in 1.0 mL medium. After 46 h the AlamarBlue® assay was performed according to the protocol in section 2.10.1 followed by the CyQuant® assay (section 2.10.2).

Table 2.13.: Composition of click-reaction buffer to create an adhesive background on nanostructured, passivated glass surfaces with HA in ddH$_2$O.

#	substance	concentration [mM]
1	TRIS (pH 8.5)	100.00
2	ascorbic acid	100.00
3	R^3-Azide	0.15
4	CuSO$_4$	1.00

2.9.4. Influence of Immobilised Hyaluronan on the Clustering and Adhesion of LECs

To analyse the clustering of LECs, glass surfaces as well as nanostructured surfaces are prepared as described above. In a first step the surfaces are passivated with click-PEG (section 2.7), followed by the functionalisation with cRGD via CuAAC. The nanostructured surfaces were incubated with 75 µL of a solution of HA or end-thiolated HA ($1\,wt\%/v\%$ in PBS, pH = 7.4) on parafilm in a humidifying chamber for 1 h at room temperature. After the functionalisation with cRGD and end-thiolated HA the surfaces are glued to a Teflon ring using Twinsil and washed sterile with PBS. Then 50 000 cells are seeded per surface and the cells incubated for 48 h at 37 °C and $5\,\%$ CO_2. Afterwards the cells are fixed with a solution of $4\,\%$ PFA in PBS and an ICC staining is performed (section 2.11).

2.10. Assays

2.10.1. AlamarBlue® Assay

To analyse the influence of environmental factors like the surface, the proliferation and metabolic activity of the cells are measured. This is possible because stressed cells will show a different metabolism and proliferation rate than resting cells. One well established method for testing the metabolic activity of organisms is the MTT-assay.[102] This is a colorimetric assay based on the cleavage of the tetrazolium salt 3-(4,5-dimethylthiazol-2-yl)-2,5-diphenyltetrazolium bromide to (E,Z)-5-(4,5-dimethylthiazol-2-yl)-1,3-diphenylformazan. The transformation through Mitochondrial Reductase leads to a colorimetric change from yellow to purple, which can be spectroscopically observed.[102–104]

An alternative to the MTT-assay is the AlamarBlue® assay. In comparison to the MTT-assay, the AlamarBlue® assay is more sensitive to smaller numbers of cells, which is important especially for studies of cell toxicity of chemicals. [105] Since components of the AlamarBlue® kit are not toxic for cells, they can be used for further analysis (no end-point assay), which is a huge advantage of this assay.[106–108] Disadvantage of this assay is the missing linear correlation between reduced dye and cell number. This is due to the interaction of BSA or FBS with resazurin, which leads to a reduced uptake of the chromophore by the cell and also quenches the fluorescence of resorufin. To overcome this, the assay can be combined with an assay like the CyQuant® assay.[107–109] The AlamarBlue® assay is as well based on a colorimetric change of a dye by reduction induced through a product of the metabolic pathway, for example ROS, NAD(P)H or FADH.[105–107, 110]

The AlamarBlue® assay was developed in the 1940's to measure the contamination of fresh milk. This assay is based on the pH and oxidative state depending properties of resazurin (fig. 2.1).[110] During metabolism, products
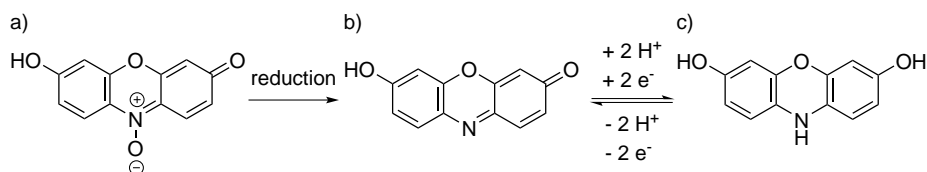
Scheme 2.1.: Active species of the AlamarBlue®kit: a) Resazurin (blue in alkali, pink acid, non-fluorescent), b) Resorufin (pink, fluorescent, colourless in acid) and c) Dihydroresorufin (colourless, nonfluorescent)

appear, which can reduce resazurin (blue) to resorufin (pink) and to dihydroresorufin (colourless), which leads to a detectable change in colour. Later, an additional change in the fluorescence was observed, making it easy to analyse the metabolic activity of different species.[106, 111]

Although it is not fully understood where the reduction of the resazurin takes place, it is known, that the cells need to take up the chromophore. It was shown that resazurin is very stable in cell culture media ($t_{1/2} = 10$ d) and the analysis based on confocal microscopy did not show any reduction of resazurin on the cell surface as on the mitochondrial surface.[106, 108] Analysing the redox-potential of AlamarBlue® ($E_0 = +380$ mV, pH 7.0, 25 °C) NAD(P), FADH, FMNH and Cytochrome could be identified as key players.[107] Proof for this is, that blocking Cytochrome C, which is correlated to the production of reactive oxygen species needed for the reduction, with NaN_3 inhibits the AlamarBlue® assay.[112]

To analyse the metabolic activity either the change in fluorescence of resorufin ($\lambda_{ex} = 540$ nm; $\lambda_{em} = 585$ nm) or the change in adsorption at the two different wavelength 570 and 600 nm are measured. Using equation 2.6 the relative metabolic activity can be calculated.

$$\%reduction = \frac{\epsilon_{ox,600nm} \cdot A_{570nm} - \epsilon_{ox,570nm} \cdot A_{600nm}}{\epsilon_{red,570nm} \cdot A_{C,600nm} - \epsilon_{red,600nm} \cdot A_{C,570nm}} \cdot 100 \qquad (2.6)$$

Table 2.14.: Molar attenuation coefficient ϵ of reduced and oxidised resazurin at 570 and 600 nm used for the calculation of the relative amount of reduced resazurin.[113]

#	λ [nm]	state	ϵ [L/(mol cm)]
1	570	oxidised	80586
2		reduced	155677
3	600	oxidised	117216
4		reduced	14652

The measurement at two different wavelength helps to reduce systematic errors. Therefore the molar attenuation coefficient ϵ for the oxidised form of AlamarBlue® (table 2.14) is multiplied with the value for the absorption (A). The result is normalised to the absorption of the negative controls (A_C) multiplied with the according molar attenuation coefficient of the reduced AlamarBlue®. The adsorption of the used media with AlamarBlue® and without cells is used as negative control in this case.

Toxicity Assay

The assay is performed in a "μ-Clear" 96 well plate (*greiner-bio-one*). The cells are incubated for 18 h with the substance of interest in different concentrations in 200 μL media. Afterwards 100 μL media are removed and 10 μL of the AlamarBlue® kit are added. The cells are incubated for either 1 h or in case of the UV toxicity 1, 2 and 3 h. Then the adsorption at 570 and 600 nm is measured. For each condition three surfaces are prepared. The data are evaluated using "Excel for Mac 2011" (version 14.7.1, *Microsoft*), plotted and a Kruskal-Wallis test followed by Dunn's multiple comparison test was performed using "GraphPad Prism6" (for Mac, version 6.0e, *GraphPad Software Inc., USA*).

Metabolic Activity Assay

The cells are incubated with HA either in solution or immobilised on the surface for 46 h. Afterwards 100 μL (96 well plate) respectively 450 μL (12 well plate) are removed and 10 μL/ 55 μL of the AlamarBlue® kit are added. After 2 h incubation the fluorescence is measured (table 2.5). For each condition in each experiment three surfaces are prepared and normalised to the mean value of the background. The data is evaluated using "Excel for Mac 2011" (version 14.7.1, *Microsoft*), plotted and a Kruskal-Wallis test followed by Dunn's multiple comparison test performed using "GraphPad Prism6" (for Mac, version 6.0e, *GraphPad Software Inc., USA*).

2.10.2. CyQuant® Assay

The CyQuant® assay is based on an unsymmetrical cyanine dye, which is more sensitive to low cell numbers compared to "Neutral Red" or "Methylene Blue" even below 1000 cells per sample.[114] Unlike the MTT assay, this assay is not based on the conversion of a dye via cellular metabolic activity, thus it is a rapid method. The fluorescence of the used dye increases when it is bound to cellular nucleic acids.[114, 115] Even though the dye binds to DNA and RNA, no high fluorescence signal for the binding to RNA is found. The assay can only be used for non-synchronised cell lines to eliminate the error due to the variation in amount of DNA during the cell cycle.[114]

In this study the CyQuant® assay is combined with the AlamarBlue® assay to determine the relative metabolic activity. Therefore, the surfaces are washed twice with warm PBS after the AlamarBlue® assay. Then the cells with the surfaces are frozen at $-80\,°C$. For the assay the CyQuant-dye (400 x solution) and cell-lysis buffer (20 x solution) are diluted in ddH_2O to their final concentrations. Either $600\,\mu L$ (12-well) or $200\,\mu L$ (96-well) of this solution are added to the surfaces. After $5\,min$ the fluorescence is measured with an excitation wavelength (λ_{ex}) of $480\,nm$ and an emission wavelength (λ_{em}) of $520\,nm$. The evaluation of the data is performed using "Excel for Mac 2011" (version 14.7.1, *Microsoft*). For each condition in each experiment three surfaces are prepared and normalised to the mean value of the background. The results are evaluated and a Kruskal-Wallis test followed by Dunn's multiple comparison test performed using "GraphPad Prism6" (for Mac, version 6.0e, *GraphPad Software Inc., USA*).

2.10.3. Relative Metabolic Activity

To calculate the relative metabolic activity of the LECs the normalised results of the AlamarBlue® assay are divided by the corresponding normalised results of the CyQuant® assay (equation 2.7).

$$rel.\ metab.\ activity = \frac{AlamarBlue_x/\overline{AlamarBlue_C}}{CyQuant_x/\overline{CyQuant_C}} \cdot 100 \qquad (2.7)$$

The values of each surface were normalised to the mean value of the surfaces without applied HA. The results were plotted in a box plot and a Kruskal-Wallis test followed by Dunn's multiple comparison test was performed using "GraphPad Prism6" (for Mac, version 6.0e, *GraphPad Software Inc., USA*).

2.10.4. Ellman's Assay

The degree of thiolation was determined with the Ellman's assay. It is based on the quantitative reaction of 5,5′-dithiobis-2-nitrobenzoic acid (DTNB) with a thiol-group (scheme 2.2). The reaction releases 2-nitro-5-thiobenzoate (TNB^{2-}), which shows a detectable yellow colour ($\varepsilon = 13\,600/cm$ at $412\,nm$).[116–118] Due to the direct correlation between the absorbance and the concentration (equation 2.8[116]) it can be used in a wide range of applications, for example to determine an enzymatic activity and blood testing.[118, 119]

$$c(-SH) = \frac{absorbance}{13600}\frac{mol}{L} \qquad (2.8)$$

To create a calibration curve, samples of $850.0\,\mu L$ containing different concentrations of cysteamine hydrochloride (0, 5, 10, 15, 20, 30, 40, 50, 60, 80 and $100\,\mu M$) were prepared by diluting a $2\,mM$ stock solution in ddH_2O. To every sample $100.0\,\mu L$ $1\,M$ Tris-HCl buffer (pH 8.0) and $50.0\,\mu L$ of a $2\,mM$ DTNB
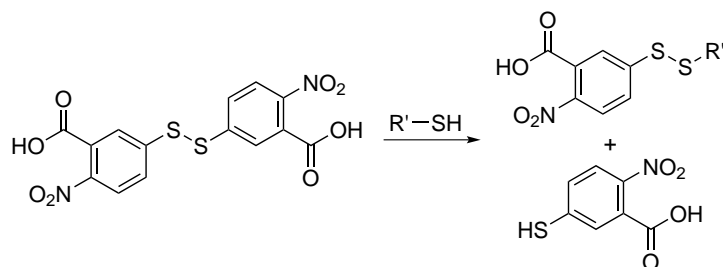
Scheme 2.2.: The reaction of 5,5′-dithiobis-2-nitrobenzoic acid (DTNB) with thiol-groups causes in the release of the detectable, yellow 2-nitro-5-thiobenzoate (TNB^{2-}), which is used for the Ellman's assay.

solution in ddH$_2$O containing 50 mM sodium acetate were added. Three different dilutions (1: 41.5; 1:16; 1:9.6) of a stock solution with 1.0 mg/mL of the end-thiolated HA were prepared and 100.0 μL of a 1 M Tris-HCl buffer (pH 8.0) and 50.0 μL of a 2 mM DTNB solution were added. The absorbance at $\lambda = 420$ nm of 300.0 μL of each sample were measured using a plate reader.

$$amount\ of\ thiols\ =\ \frac{c_f}{c_{HA}} = \frac{A_{420} \cdot M \cdot V_{Stock} \cdot V_{end}}{a \cdot m} = \frac{A_{420}}{a \cdot c_{Stock} \cdot V_{end}} \quad (2.9)$$

The data of the concentration range is plotted for creating the calibration curve and a linear fit obtained using "GraphPad Prism6" (for Mac, version 6.0e, *GraphPad Software Inc., USA*). The linear equation $A_{420} = a \cdot c_f$ (A_{420}: absorbance at 420 nm; a: gradient; c_f concentration of thiols), the concentration of HA (c_{HA}) and the volume of the measured sample (V_{end}) is used to calculate the amount of thiols for each sample via equation 2.9. The concentration of the HA can be calculated via the mass of HA (m), the molecular weight of HA (M) and the volume of the used stock solution (V_{stock}). The degree of thiolation is the mean of the three samples with different concentrations.

2.11. Protocol for ICC Staining

2.11.1. ICC Staining

To label compounds of the cells with a fluorescent dye the media is removed from the cells and the cells washed with warm PBS. Afterwards, the cells are incubated with a solution of 4 % PFA in PBS for 10 min to fix the cells to the surface. The cells are washed again with PBS for 2 min. To permeabilise the cell membrane, the cells are incubated with a solution of 0.1 % Triton X-100 in PBS for 3 min, followed by washing with PBS for 2 min twice. To block unspecific labelling, the cells are incubated with a 5 % solution of goat-serum in PBS for 60 min. To incubate the cells with the primary antibody a

solution of 5 % goat-serum, 0.1 % Triton X-100 and the primary antibody in the appropriate dilution (tab. 2.15) in PBS is prepared and the surface placed up side down on a drop of this solution on parafilm for 60 min. If only the nuclei are labelled the cells are incubated with DAPI instead of an antibody and can be evaluated after washing for two times 10 min with PBS. If a secondary antibody is necessary the cells are washed with PBS and again incubated with a solution of 0.1 % Triton X-100 in PBS for 5 min. After two times washing with PBS for 10 min and 10 min incubation with a 5 % solution of goat-serum in PBS, the cells are incubated with a solution of 5 % goat-serum, 0.1 % Triton X-100 and the secondary antibody in the appropriate dilution (tab. 2.15). The surfaces are washed twice for 10 min with PBS and stored in PBS at 4 °C.

Table 2.15.: Summary of the dilution of primary and secondary antibodies used for the ICC staining.

#	antibody	dilution
primary antibodies		
1	DAPI[a]	1:1000
2	mouse anti-Paxillin	1:100; 1:200
3	mouse anti-Talin	1:500; 1:1000
4	mouse anti-Vinculin	1:100; 1:200
5	Phalloidin/FITC[a]	1:100
6	Phalloidin-647[a]	1:100
7	rabbit anti-LYVE-1	1:140; 1:300; 1:500
8	rabbit anti-human LYVE-1	1:200; 1:50
9	rabbit anti-Paxillin	1:100; 1:200; 1:500
secondary antibodies		
10	goat anti-mouse Alexa 488	1:1000
11	goat anti-rabbit Alexa 594	1:1000
12	goat anti-rabbit Alexa 647	1:1000

a) incubated with the secondary antibody

2.11.2. Evaluation of MDCK II Cells on Surfaces

To determine the number of cells on a PEG-passivated surface with and without UV irradiation the staining of the nuclei with DAPI is used. Therefore, five positions arranged like on a die are measured using the "Observer Z1". To determine the number of cells on a surface Fiji (ImageJ 1.51h) is used. Each picture is set to a saturation of 0.35. Via "Find Maxima" with a noise of 125 and the output "count" the number of nuclei is determined. The results are plotted in a result frame. The data is plotted using "GraphPad Prism7" (for

Mac, version 7.0c, *GraphPad Software Inc., USA*).

2.11.3. Evaluation of LECs on Surfaces

To determine the number of cells on a surface with immobilised HA and without HA the staining of the nuclei with DAPI is used. In the middle of each surface an area of 8.5 x 6.2 mm is measured. To determine the number of cells on a surface Fiji (ImageJ 1.51h) is used. Each picture is set to a saturation of 0.35. Via "Find Maxima" with a noise of 125 and the output "count" the number of nuclei is determined. The results are plotted in a result frame. The data is plotted using "Excel for Mac 2011" (version 14.7.1, *Microsoft*).

Chapter 3.

Synthesis

3.1. Functionalisation of Short Hyaluronan

3.1.1. General Procedure of the Functionalisation at the Reducing End

component	M [g/mol]	n [mmol]	c [mM]	m [mg]	ρ [g/mL]	V [mL]
short HA	n·361.31			100.0		
sodium chloride[b]	58.44	8.0	400.0	468.0		
NaBH$_3$CN	62.84	4.0	200.0	251.0		
borate buffer			100.0			20.0
DMSO[c]						10.0
cysteamine · HCl	113.61	1.1	52.8	120.0		
propargylamine	55.08	1.0	52.3	57.6	0.86	0.067
DBCO-amine[a]	276.33	0.04	4.0	10.0		
BCN-amine[a]	207.27	0.02	25.0	40.0		

a) only 50.0 mg HA are used
b) not added if the solvent is DMSO
c) solvent amount for half approach

To functionalise the *N*-acetyl-D-glucosamine unit at the reducing end of HA a protocol by Lee *et al.* is adapted.[49] Therefore, HA is diluted in borate buffer (100 mM, pH 8.5) containing 4.7 wt% NaCl and then the amine species is added. The solution is stirred for 2 h at room temperature. 2.5 wt% sodium cyanoborohydrid is added and the reaction solution stirred for 5 d at 40 °C. Afterwards the solution is dialysed (MWCO: 2000 Da) against 4.5 L ddH$_2$O containing 10 mL 2 M HCl and 5 g NaCl for 2 h followed by the dialysis against 4.5 L ddH$_2$O containing 10 mL 2 M HCl for 2 d, while the water is exchanged six times. The functionalised HA is recovered by freeze-drying ("Benchtop Freeze Dry System", *Latconco*, USA) and stored at −80 °C.

3.1.2. End-thiolated Hyaluronan (3)[49]
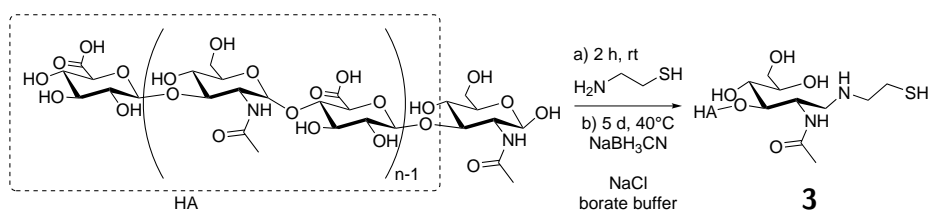
The reaction is performed according to the general protocol 3.1 using cysteamine hydrochloride as the amine species. Before the dialysis, an excess of DTT is added and the solution stirred for 2 h at 40 °C.

3.1.3. End-alkynated Hyaluronan (4)
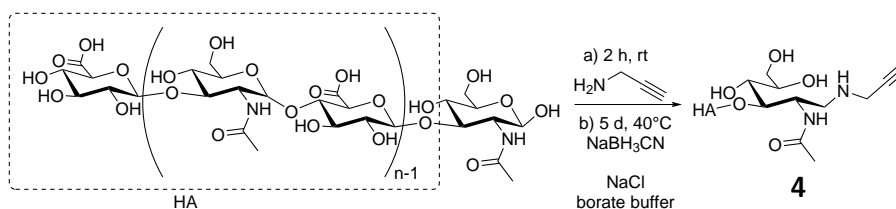
The reaction is performed according to the general protocol 3.1 applying propargylamine as amine species.

3.1.4. sHA-end DBCO-amine (5)
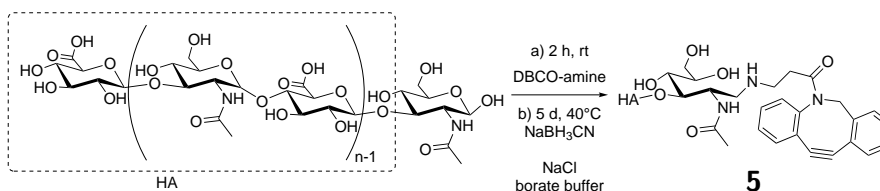
The reaction is performed according to the general protocol 3.1 to functionalise HA at the reducing end applying DBCO–amine as amine species and DMSO as a solvent. The sodium cyanoborohydride is added in 5 mL borate buffer.

3.1.5. Internal Alkynation of Hyaluronan (6)[48]

To functionalise the HA within the chain, HA was dissolved in MES buffer. 1.4 wt/wt EDC/HCl, 1.4 wt/wt NHS and 1.1 wt/wt propargylamine were added to the solution. The reaction mixture was stirred at room temperature

6
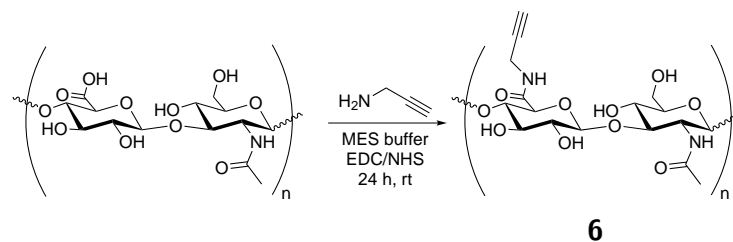
for 24 h before it was dialysed (MWCO: 3500 Da) against ddH$_2$O containing 5 g NaCl solution for 1 d and against ddH$_2$O for 5 d. The solution was lyophilised and the product stored at $-80\,°C$.

^{1}H-NMR (600 MHz, D$_2$O): δ (ppm) = 4.68 to 4.29 (m, 2 H, H$_2$, H$_3$, H$_{14}$), 4.00 to 3.14 (m, 11 H, H$_1$, H$_4$, H$_5$, H$_7$, H$_{10}$, H$_{11}$, H$_{12}$, H$_{13}$, H$_{15}$), 2.69 to 2.53 (m, 0.4 H, H$_9$), 1.99 (s, 3 H, H$_{17}$).
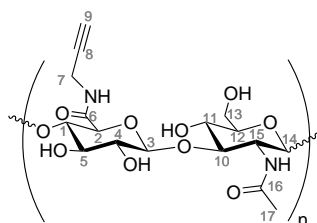
3.2. Synthesis of PEG-derivative for Surface Functionalisation

3.2.1. Synthesis of PEG$_{2000}$−silane (8)[25]

8
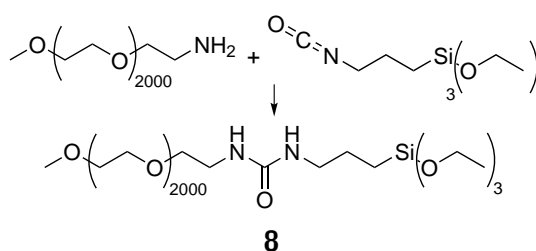
component	m [mg]	ρ [g/mL]	V [µL]	eq
H$_2$N−PEG$_{2000}$	500.0			1.0
DMF			5000.0	
3-(triethoxysilyl)propyl isocyanate	43.0	0.999	43.0	1.1

α-Methoxy-ω-amino PEG (H_2N-PEG_{2000}) was washed three times with toluene in a brown glass flask and dried in vacuum. Afterwards, dry DMF and 1.1 eq 3-(triethoxysilyl)propyl isocyanate were added under nitrogen atmosphere. The reaction mixture was stirred for 24 h at room temperature. The solution was cooled to 0 °C and 10.0 mL cold diethyl ether were added. The mixture was gently stirred for 1.5 h. The white precipitate was filtered off by using a ceramic frit and washed with cold diethyl ether. The product was dried over night under reduced pressure.
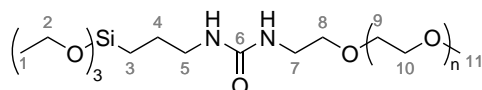
^{1}H-NMR (600 MHz, CDCl$_3$): δ (ppm) = 3.75 (t, ^3J(H) = 4.7 Hz, 2 H, H$_5$), 3.71 (q, ^3J(H) = 7.0 Hz, 5 H, H$_2$), 3.69 to 3.59 (m, 182 H, H$_9$,H$_{10}$), 3.56 to 3.53 (m, 2 H, H$_7$), 3.53 to 3.50 (m, 1 H, H$_8$), 3.37 (s, 3 H, H$_{11}$), 1.40 to 1.36 (m, 1 H, H$_4$), 1.24 (t, ^3J(H) = 7.0 Hz, 5 H, H$_1$), 0.7 (bs, 2 H, H$_3$).

3.2.2. Synthesis of Silane$-$PEG$_{3000}$$-$alkyne (9)[120]

9
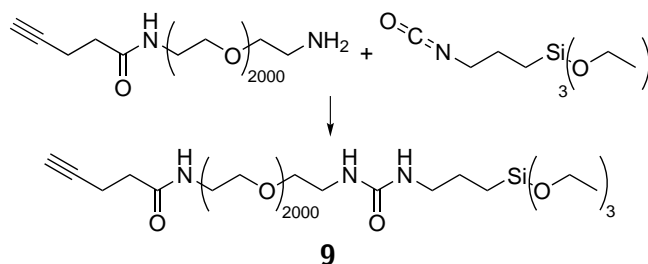
component	m [mg]	ρ [g/mL]	V [μL]	eq
H_2N-PEG_{3000}-alkyne	500.0			1.0
DMF			5000.0	
3-(triethoxysilyl)propyl isocyanate	43.0	0.999	43.0	1.1

After α-amino-ω-alkyne PEG ($H_2N-PEG_{3000}-$alkyne) was washed three times with toluene in a brown glass flask, dry DMF and 1.1 eq 3-(triethoxysilyl)propyl isocyanate were added. The reaction mixture was stirred for 24 h at room temperature under nitrogen atmosphere. To precipitate the product, the solution was cooled to 0 °C and 10.0 mL diethyl ether were added. The mixture was gently stirred for 1.5 h, the white solid was filtered off by using a suction filter and washed with cold diethyl ether. The product was dried over night under reduced pressure.
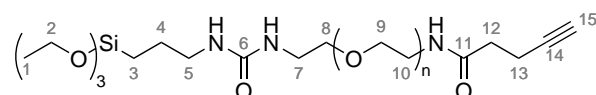
^{1}H-NMR (600 MHz, CDCl$_3$): δ (ppm) = 5.97 (s, 1 H, HNH), 3.76 to 3.73 (m, 7 H, H$_8$), 3.73 to 3.56 (m, 874 H, H$_2$, H$_9$, H$_{10}$), 3.55 to 3.45 (m, 6 H, H$_5$, H$_7$), 2.96 (s, 2 H, H$_{13}$), 2.88 (s, 2 H, H$_{12}$), 1.37 (t, ^3J(H) = 7.2 Hz, 1 H, H$_4$), 1.23 (t, ^3J(H) = 7.0 Hz, 9 H, H$_1$).

3.3. Synthesis of 1-(4,5-dimethoxy-2-nitrophenyl)ethyl 11-mercaptoundecanoate (1)

3.3.1. Nitration of 3,4-Dimethoxyacetophenone
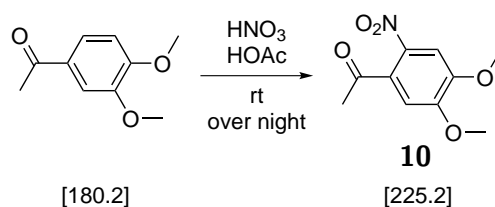
component	M	n	m	ρ	V	eq
	[g/mol]	[mmol]	[g]	[g/mL]	[mL]	
3,4-dimethoxy-acetophenone	180.20	11.1	2.0	-	-	1.0
nitric acid	63.01	83.25	5.2	1.51	3.5	7.5
acetic acid	60.05	832.50	49.9	1.05	47.6	75.0

3,4-Dimethoxyacetophenone was dissolved in acetic acid. While stirring the solution at 0 °C, 7.5 eq nitric acid was added dropwise. Afterwards, the reaction solution was stirred for 24 h at room temperature. The yellowish solution was poured onto ice, the yellowish solid was filtered off using a ceramic frit (# 4) and washed with cold ddH$_2$O. The filtrate was stored at 4 °C over night and filtered again. The combined solid fractions were dried under vacuum. The raw product was dissolved in acetone and filtered over silica gel (h = 0.5 cm) using a ceramic frit (# 4). The acetone was removed under reduced pressure. The yellowish product was obtained with a yield of 67 % (7.4 mmol, 1.67 g).

R$_f$ (n-hexane : acetone 2:1) = 0.23.
HR-MS (EI+): for C$_{10}$H$_{11}$NO$_5$ calcd 225.0632, found 225.0645.
^{1}H-NMR (600 MHz, CDCl$_3$): δ (ppm) = 7.62 (s, 1 H, H$_5$), 6.76 (s, 1 H, H$_8$), 3.99 (s, 6 H, H$_9$,H$_{10}$), 2.50 (s, 3 H, H$_1$).

^{13}C-NMR (150 MHz, **CDCl$_3$**): δ (ppm) = 200.1 (C$_2$), 154.0 (C$_6$, C$_7$), 149.6 (C$_4$), 132.9 (C$_3$), 108.6 (C$_8$), 106.8 (C$_5$), 56.7 (C$_9$, C$_{10}$), 56.6 (C$_9$, C$_{10}$), 30.5 (C$_1$).
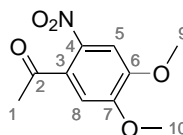
3.3.2. Hydration of 4,5-Dimethoxy-2-nitroacetophenone (10)
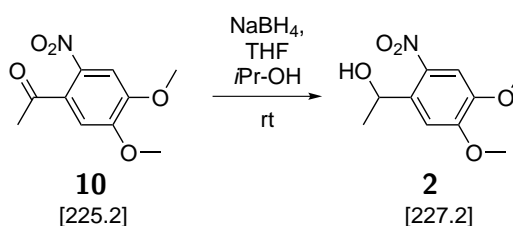
component	M	n	m	V	eq
	[g/mol]	[mmol]	[g]	[mL]	
3,4-dimethoxy-2-nitroacetophenone	225.22	7.4	1.67		1.0
NaBH$_4$	37.83	10.4	0.39		1.4
THF				8.0	
isopropanol				16.0	

    4,5-Dimethoxy-2-nitroacetophenone was dissolved in a mixture of THF and isopropanol at room temperature. To the dark yellow solution 1.4 eq NaBH$_4$ were added and the reaction solution stirred for 6 h at room temperature. The now reddish solution was quenched with 3.3 mL 2 M HCl and 16.0 mL ddH$_2$O. The product was extracted three times with CHCl$_3$. The combined organic layers were washed once with ddH$_2$O and dried over MgSO$_4$. The solvent was removed in vacuo. The product was purified via column chromatography (SiO$_2$, n-hexane:acetone 2:1) and the yellow 4,5-dimethoxy-2-nitrophenyl ethanol (DMNPE, **2**) was obtained with a yield of 93 % (1.56 g, 6.9 mmol).

HR-MS (DART-): for C$_{10}$H$_{13}$NO$_5$ calcd 227.0799, found 227.0800,
for C$_{20}$H$_{25}$N$_2$O$_{10}$ calcd 453.1515, found 453.1516.
^{1}H-NMR (600 MHz, **CDCl$_3$**): δ (ppm) = 7.58 (s, 1 H, H$_5$), 7.31 (s, 1 H, H$_8$), 5.58 (q, ^3J(H) = 6.3 Hz, 1 H, H$_2$), 4.01 (s, 3 H, H$_{10}$), 3.95 (s, 3 H, H$_9$), 1.56 (d, ^3J(H) = 6.3 Hz, 3 H, H$_1$).

^{13}C-NMR (150 MHz, CDCl$_3$): δ (ppm) = 153.8 (C$_6$, C$_7$), 147.8 (C$_8$), 108.5 (C$_3$, C$_4$), 107.7 (C$_5$), 65.8 (C$_2$), 56.4 (C$_9$, C$_{10}$), 24.3 (C$_1$).
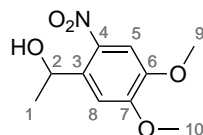
3.3.3. Protection of Thiol-group of 11-mercaptoundecanoic acid (7)

component	M	n	m	V	eq
	[g/mol]	[mmol]	[g]	[mL]	
7	218.35	13.7	3.0		1.0
trityl chloride	278.78	16.5	4.6		1.2
triethylamine				0.5	
DCM				10+10+5	

Trityl chloride was dissolved in DCM containing a catalytic amount of NEt$_3$. 11-mercaptoundecanoic acid was dissolved in DCM as well and added drop wise to the reaction solution over a period of 20 min. The solution was stirred for 2.5 h at room temperature, before washing with ddH$_2$O three times. The combined aqueous layers were washed once with DCM. The combined organic layers were dried over MgSO$_4$. The solvent was removed under reduced pressure. The product (white solid, NMR yield: 52 %) was used without further purification because no complete purification could be obtained.

R$_f$ (hexane/ EtOAc 3:1) = 0.15.
HR-MS (DART-): for C$_{30}$H$_{35}$O$_2$S calcd 459.2363, found 459.2364, for C$_{60}$H$_{71}$O$_4$S$_2$ calcd 919.4799, found 919.4802.
^{1}H-NMR (600 MHz, CDCl$_3$): δ (ppm) = 7.42 to 7.40 (m, 6 H, H$_{15}$, H$_{17}$), 7.33 to 7.27 (m, 12 H, H$_{14}$, H$_{18}$), 7.20 (tt, ^3J(H) = 7.3 Hz, ^4J(H) = 1.5 Hz, 3 H, H$_{16}$), 2.34 (t, ^3J(H) = 7.5 Hz, 2 H, H$_{11}$), 2.13 (t, ^3J(H) = 7.4 Hz, 2 H, H$_2$), 1.62 (quint, ^3J(H) = 7.5 Hz, 3 H, H$_{10}$), 1.38 (quint, ^3J(H) = 7.5 Hz, 3 H, H$_3$), 1.33 to 1.28 (m, 5 H, H$_9$), 1.28 to 1.11 (m, 11 H, H$_4$, H$_8$).

^{13}C-NMR (150 MHz, CDCl$_3$): δ (ppm) = 147.0 (C$_1$), 145.2 (C$_{13}$), 129.8 (C$_{15}$, C$_{17}$), 127.9 (C$_{14}$, C$_{18}$), 126.6 (C$_{16}$), 66.5 (C$_{12}$), 33.9 (C$_{11}$), 32.2 (C$_{12}$), 29.5 to 29.2 (5 C, C$_4$, C$_5$, C$_6$, C$_7$, C$_8$), 29.1 (C$_9$), 28.7 (C$_3$), 24.8 (C$_{10}$).
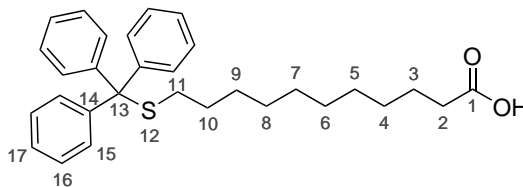
3.3.4. Coupling of 4,5-dimethoxy-2-nitrophenyl ethanol (2) and 11-(tritylthio)undecanoic acid (11)

11
[227.22]

2
[460.68]

12
[669.88]
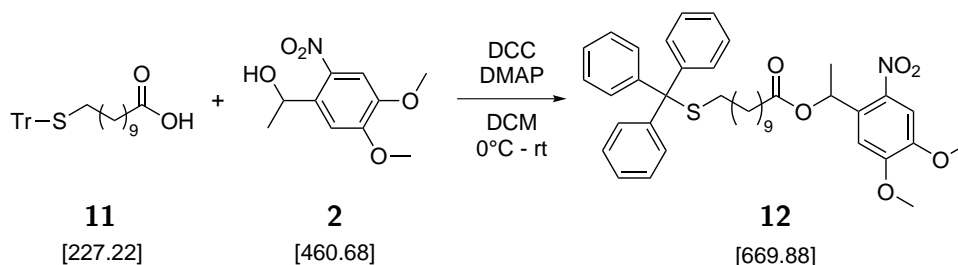
component	M [g/mol]	n [mmol]	m [g]	V [mL]	eq
2	227.22	4.4	1.0		1.0
11	460.68	6.7	3.1		1.5
DCC	206.33	6.7	1.36		1.5
DMAP	122.17	0.3	0.03		0.06
DCM				75	

DMNPE (**2**) was dissolved in DCM at 0 °C. Then 1.5 eq DCC and a catalytic amount of DMAP were added to the reaction solution as well as 1.5 eq 11-(tritylthio)undecanoic acid (**11**). The reaction solution was stirred for 3 h at room temperature before the reaction was quenched with 30.0 mL aqueous, saturated sodium carbonate solution. The organic layer was removed and washed three times with aqueous, saturated sodium carbonate solution. The combined aqueous phases were extracted with CHCl$_3$ three times. The combined organic layers were dried over MgSO$_4$. The solvent was removed under reduced pressure. The product was purified via column chromatography (SiO$_2$, n-hexane:acetone 4:1) and the yellow 1-(4,5-dimethoxy-2-nitrophenyl)ethyl 11-(tritylthio)undecanoate (**12**) was obtained with a yield of 33 % (239 mg, 0.4 mmol).

R$_f$ (hexane/ acetone 4:1) = 0.2.
^{1}H-NMR (600 MHz, CDCl$_3$): δ (ppm) = 7.58 (s, 1 H, H$_{21}$), 7.41 (d, ^3J(H) = 7.5 Hz, 6 H, H$_2$), 7.33 to 7.27 (m, 12 H, H$_1$, H$_3$), 7.20 (t, ^3J(H) = 7.3 Hz, 3 H, H$_1$), 7.00 (s, 1 H, H$_{26}$), 6.48 (quint, ^3J(H) = 6.9 Hz, 1 H, H$_{17}$), 3.96 (s, 3 H, H$_{25}$), 3.93 (s, 3 H, H$_{23}$), 2.39 to 2.27 (m, 2 H, H$_6$), 2.13 (t, ^3J(H) = 7.4 Hz, 2 H, H$_{15}$), 1.64 to 1.59 (m, 5 H, H$_7$), 1.38 (quint, ^3J(H) = 7.4 Hz, 2 H, H$_{14}$), 1.33 to 1.10 (m, 11 H, H$_8$, H$_9$, H$_{10}$, H$_{11}$, H$_{12}$, H$_{13}$, H$_{18}$).
^{13}C-NMR (150 MHz, CDCl$_3$): δ (ppm) = 172.5 (C$_{16}$), 153.7 (C$_{22}$, C$_{24}$), 148.2 (C$_{20}$), 145.4 (C$_4$), 129.8 (C$_2$), 128.1 (C$_3$), 127.9 (C$_1$), 126.6 (C$_{19}$), 108.2 (C$_{26}$), 107.9 (C$_{21}$), 68.2 (C$_{17}$), 66.6 (C$_5$), 56.5 (C$_{23}$, C$_{25}$), 34.6 (C$_6$), 32.2 (C$_{15}$), 31.7 to 29.1 (C$_8$, C$_9$, C$_{10}$, C$_{11}$, C$_{12}$, C$_{13}$), 28.8 (C$_{14}$), 22.8 (C$_7$), 14.2 (C$_{18}$).
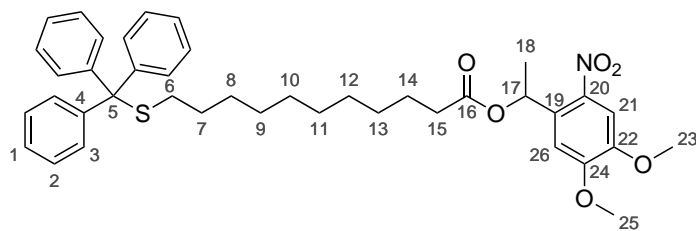
3.3.5. Deprotection of Thiolgroup of 1-(4,5-dimethoxy-2-nitro-phenyl)ethyl 11-(tritylthio)undecanoate (12)
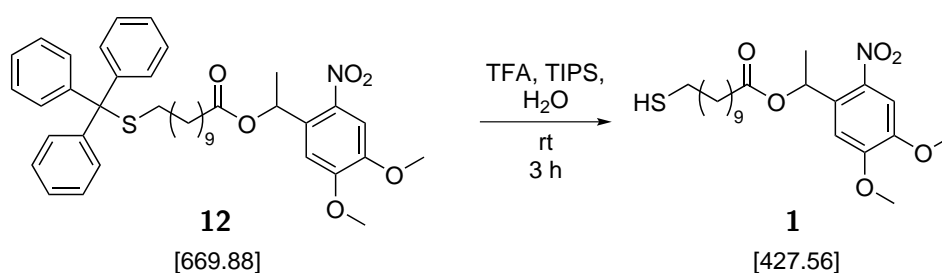
component	M	n	m	ρ	V	eq
	[g/mol]	[mmol]	[g]	[g/mL]	[mL]	
12	657.87	0.6	0.40			1.0
TFA	114.02	120.0	13.68	1.48	9.24	200.0
TIPS	158.36			0.773	0.19	
ddH$_2$O					0.19	

To deprotect the thiol function, TFA, TIPS and ddH$_2$O (95.0:2.5:2.5 v%) were mixed and 1-(4,5-dimethoxy-2-nitrophenyl)ethyl 11-(tritylthio)undecanoate (**12**) added. The reaction solution was stirred for 2 h at room temperature. Afterwards, the reaction was quenched by adding 5 mL ddH$_2$O and the solution was extracted with CHCl$_3$ for three times and the combined organic layers dried over MgSO$_4$. The solvent was removed under reduced pressure. The raw producte was dissolved in acetone and filtered over silica gel using a ceramic frit (#4). To obtain the product the solvent was removed under reduced pressure. with CHCl$_3$ three times. The combined organic layers were dried over MgSO$_4$. The solvent was removed under reduced pressure. The product was purified via column chromatography (SiO$_2$, n-hexane:ethyl acetate 5:1) and the yellow 1-(4,5-dimethoxy-2-nitrophenyl)ethyl 11-mercaptoundecanoate (DMNPE-thiol, **1**) was obtained with a yield of 89 % (228 mg, 0.53 mmol).

R$_f$ (hexane/ EtOAc 5:1) = 0.09.
HR-MS (DART-): for C$_{21}$H$_{30}$NO$_6$S calcd 424.1800, found 424.1799,

for $C_{21}H_{32}NO_6S$ calcd 426.1956, found 426.1956.

^{1}H-NMR (600 MHz, CDCl$_3$): δ (ppm) = 7.58 (s, 1 H, H$_2$), 7.01 (s, 1 H, H$_7$), 6.47 (quint, ^3J(H) = 6.4 Hz, 1 H, H$_9$), 3.97 (s, 3 H, H$_6$), 3.94 (s, 3 H, H$_4$), 2.54 to 2.49 (m, 3 H, H$_{21}$), 2.40 (t, ^3J(H) = 7.5 Hz, 1 H, H$_{12}$), 2.38 to 2.27 (m, 2 H, H$_{10}$), 1.95 to 1.55 (m, H$_{20}$), 1.43 to 1.12 (m, 27 H, H$_{13}$, H$_{14}$, H$_{15}$, H$_{16}$, H$_{17}$, H$_{18}$, H$_{19}$).

^{13}C-NMR (150 MHz, CDCl$_3$): δ (ppm) = 172.6 (C$_{11}$), 153.7 (C$_3$, C$_5$), 148.0 (C$_3$), 140.0 (C$_7$), 133.5 (C$_1$), 108.0 (C$_2$), 107.8 (C$_7$), 68.2 (C$_9$), 56.5 (C$_4$, C$_6$), 34.2 (C$_{20}$), 34.1 (C$_{12}$), 29.5 to 28.5 (C$_{14}$, C$_{15}$, C$_{16}$, C$_{17}$, C$_{18}$, C$_{19}$), 25.1 (C$_{13}$), 24.8 (C$_{21}$), 22.2 (C$_{10}$).
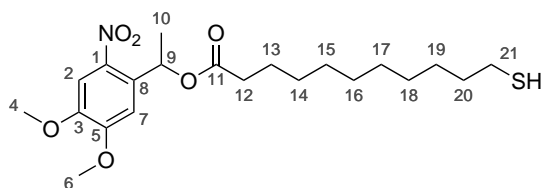
3.4. Modification of $\alpha_5\beta_1$-specific Antagonist

component	M	n	m	V	eq
	[g/mol]	[mmol]	[g]	[mL]	
13					
2	227.22	6.6	1.5		2.1
DCC	206.33	4.6	1.0		1.5
DMAP			cat.		
DCM				0.3	

(S)-3-(4-(3-(6-(3-mercaptopropanamido)hexanamido)propoxy)benzamido)-4-(4-(3-((4-methoxypyridin-2-yl)amino)propoxy)phenyl)butanoic acid (**13**) and DMNPE (**2**) are dissolved in DCM. Then, DCC and DMAP were added under stirring at room temperature. The reaction solution is stirred for 3 h at room temperature, before the reaction is quenched with 200 µL of a saturated sodium hydrogen carbonate solution. The organic phase is removed and the aqueous phase extracted three times with 200 µL CHCl$_3$. The combined organic phases are dried over MgSO$_4$ and the solvent removed under reduced pressure. The raw product is purified using an HPLC. As solvents are used 0.1 M TEAA in ddH$_2$O (buffer A) and 0.1 M TEAA in 75 % acetonitrile and 25 % ddH$_2$O (buffer B). A flow rate of 3 mL/min is applied with a linear gradient of 13 % buffer B in buffer A up to 100 % buffer B over 30 min. The used conditions are appropriate to deprotect the thiol-function during the purification.

13

[980.23]

DMNPE
2
DCC
DMAP

DCM
3h, rt

14

[947.11]
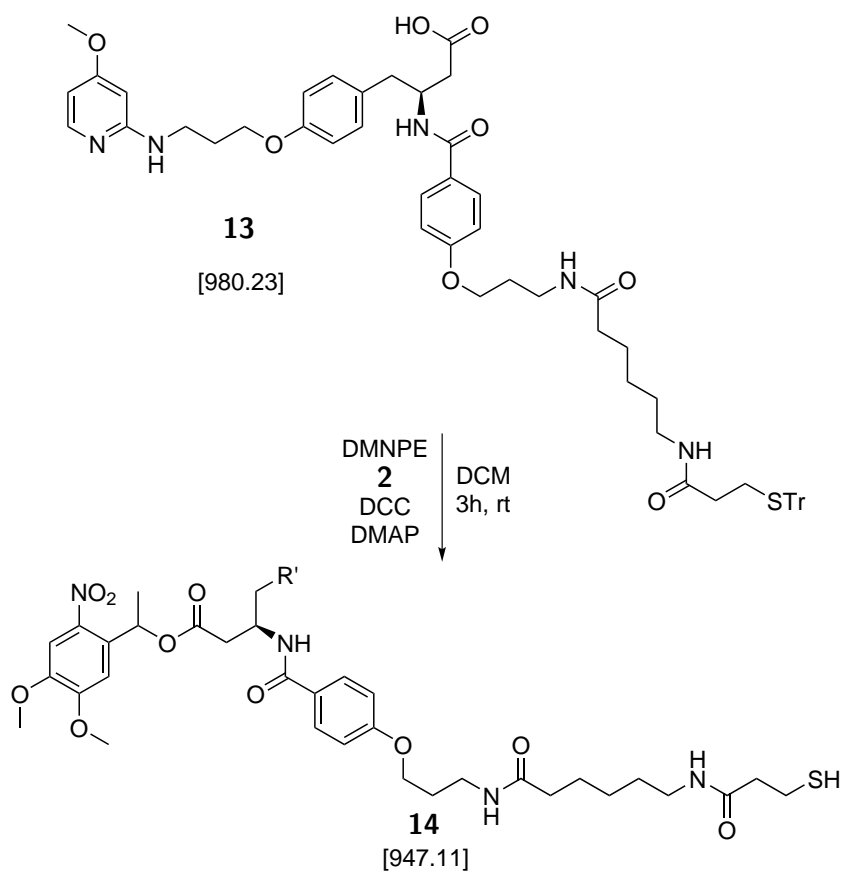
retention time (min) = 37.4 to 38.3.

¹H-NMR (600 MHz, CDCl₃): δ (ppm) = 7.56 (s, 1 H, H$_{26}$), 7.43 (s, 1 H, H$_{30}$), 7.32 (s, 1 H, H$_{11}$), 7.23 (s, 1 H, H$_6$), 7.08 (s, 1 H, H$_{27}$), 5.57 (quint, ^3J(H) = 6.2 Hz, 1 H, H$_{18}$), 3.99 (s, 3 H, H$_{23}$), 3.93 (s, 3 H, H$_{25}$), 3.71 (q, ^3J(H) = 7.1 Hz, 7 H, H$_{36}$), 3.13 to 3.07 (m, 1 H1, H$_{41}$), 2.97 (s, 1 H, H$_{14}$), 2.72 (s, 1 H, H$_{14}$), 2.65 (s, 1 H, H$_{16}$), 2.26 (s, 1 H, H$_{16}$), 2.12 (s, 4 H, H$_8$), 2.08 (s, 1 H1, H$_7$), 2.05 (s, 5 H, H$_6$), 1.55 (d, ^3J(H) = 6.2 Hz, 3 H, H$_{19}$), 1.41 (t, ^3J(H) = 7.2 Hz, 16 H, H$_{40}$), 1.23 (t, ^3J(H) = 7.2 Hz, 12 H, H$_{38}$).
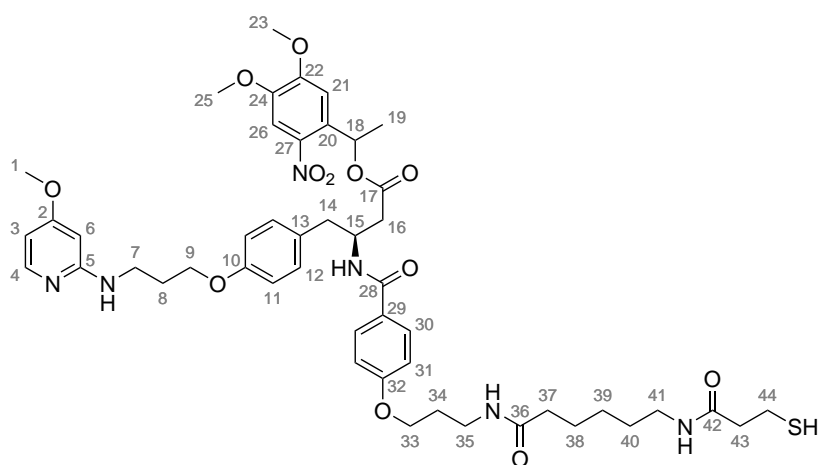
Part III.

Experiments

Chapter 4.

Experiments

The following section deals with the modification of HA to enable its immobilisation on surfaces. Nanostructured surfaces with immobilised HA can be used to probe the influence of HA in a defined density. In this study the immobilised (basal) and diluted (apikal) application of HA is compared. Additionally a concentration dependency is tested. In the second part a novel photocleavable ligand is introduced and characterised, which enables cell adhesion without addressing specific integrins. In the end also a novel photocleavable ligand to the integrin $\alpha_5\beta_1$ is introduced.

4.1. Chemical Modification Strategies to Immobilise Short Hyaluronan

To create an interface with a well-controlled amount of short HA, it is necessary to enable the immobilisation of short HA on the surface. Two different strategies are followed to achieve the immobilisation of the HA chain. On the one hand an alkyne function is introduced to the HA chain. So it is possible to attach the HA to an azide bearing surface using a [3+2]-cycloaddition. On the other hand a thiol function is introduced to enable the immobilisation on a gold coated surface.
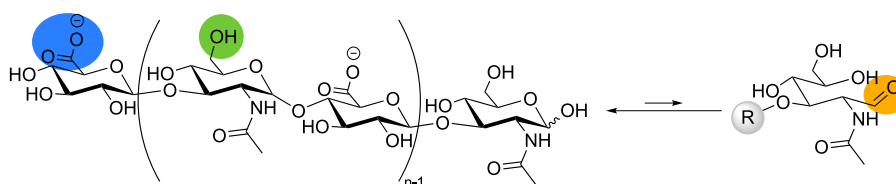
Scheme 4.1.: Functional groups of hyaluronan enable different chemical modification strategies: carboxy group in blue, primary hydroxy group in green and carbonyl group in orange. The Carbonyl-function appears only during the anomerisation between the α- and β-species of the *N*-acetylglucosamine-motif at the reducing-end of hyaluronan. The equilibrium is on the side of the closed ring-form.

The modification of HA is straight-forward due to its various, accessible

functional groups as shown in scheme 4.1. Via the primary and secondary hydroxy groups as well as the carboxy function the short HA can be statistically modified within the chain. To create only a single modification per chain, the carbonyl group at the reducing end is used, which occurs during anomerisation. To investigate the biocompatibility and bioactivity of the modification strategies, the HA species are characterised using QCM-D.

4.1.1. Introducing a Terminal Thiol Function to Short Hyaluronan

For the decoration of a gold coated quartz crystal in the QCM-D with short hyaluronan, the HA is functionalised with a thiol group at its reducing end. Therefore the carbonyl-group, which appears during the anomerisation between α- and β-*N*-acetylglucosamine (scheme 4.1), is modified according to a protocol of Lee *et al.*.[49]
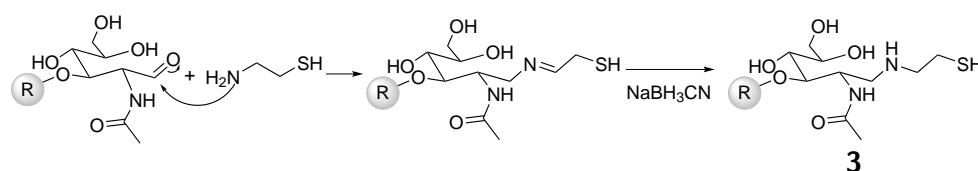
Scheme 4.2.: Reaction scheme for the coupling of HA with cysteamine. In the first step the amine attacks the carbonyl C-atom and forms a imine which is selectively hydrogenated with sodium cyanoborohydrid.

The amine group of cysteamine hydrochloride substitutes the carbonyl-group at the reducing-end of the HA in a nucleophilic substitution reaction (scheme 4.2). The formed imine is selectively hydrogenated using $NaBH_3CN$. Due to the statistically rare open-form of the terminal *N*-acetylglucosamine, the reaction time is rather long. To prevent the development of dithiol bonds within two HA molecules or to break already formed dithiol bonds, dithiothreitol is added as reducing agent after 5 days.

Purification of the reaction mixture is carried out via dialysis. Here, modified and unmodified HA cannot be separated because of the small difference in size, so only the amine and the reducing agent could be removed. Analysis of the HA derivative with NMR and MS is challenging due to the large difference in size between the HA (10 -20 kDa) and the cysteamine linker (M = 77.15 g/mol). A good alternative method to characterise the HA species is QCM-D, which is very sensitive to the binding of the thiol modified HA to a gold-coated quartz crystal.[121] This enables also further analysis of the HA and different interactions. Figure 4.1 compares the interaction between thiolated and non-functionalised HA with a gold surface, as well as the adsorption of the cysteamine hydrochloride. For the measurement, the sensor is equilibrated in PBS before the endthiolated short HA (**3**, 0.4 g/L), short HA (0.4 g/L) and the cysteamine (100 μM) are added to the different gold

coated crystal surfaces in PBS. After reaching the equilibrium the crystals are washed three times with PBS. The difference in frequency between the two plateaus in PBS is correlated to the amount of immobilised substance. The large change in frequency for **3** ($\Delta(\Delta f_7) = 65\,\mathrm{Hz}$) shows the specific adsorption of the HA species and thus that the synthesis was performed successfully. In comparison, the change in frequency due to uncoupled cysteamine amounts only to $\Delta(\Delta f_7) = 17\,\mathrm{Hz}$. Furthermore, after the dialysis almost no impurities of the cysteamine should remain. The unfunctionalised HA does also interact with the activated surfaces ($\Delta(\Delta f_7) = 22\,\mathrm{Hz}$, dark green), but in a reversible manner. Using the so-called open module for the QCM-D experiments, no permanent flow is applied, which leads to sedimentation of the HA. While the solution is changed on top of the crystal the sedimented HA or other unbound compounds are removed again. This can be seen in the increase of frequency due to the change of PBS (step 1 $\Delta(\Delta f_7) = 26\,\mathrm{Hz}$, step 2 $\Delta(\Delta f_7) = 24\,\mathrm{Hz}$). In the case of the immobilised short HA the change in frequency stays constant when the PBS is exchanged. This is also true for the change in dissipation for the different, analysed surfaces.
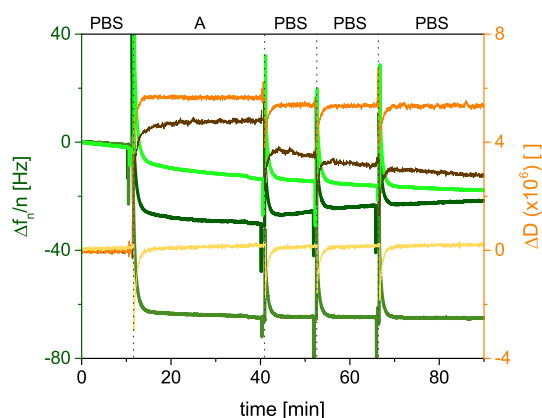
Figure 4.1.: Successful adsorption of end-thiolated HA (**3**) on a gold coated quartz crystal which verifies the modification. Comparison of the adsorption of **3** (0.4 g/L, Δf_7: green, D: orange), unfunctionalised short HA (0.4 g/L, Δf_7:dark green, D: dark brown) and cysteaminehydrochloride (100 μM, Δf_7: light green, D: light brown) for the 7th overtone on a gold surface: The system is equilibrated in PBS, then the three compounds (step A) are added in PBS. Afterwards, the crystal is washed three times with PBS.

Additionally the water contact angle (Θ_W) of the pure gold surface as well as with the short HA-layer on top are measured to verify the adsorption. The activated, pure gold surface shows an angle of 69° and for the short HA-layer of below 20°, which indicates the presence of a highly hydrophilic surface.[54]

Another possibility to determine the presence of the thiol group is the Ell-

man's assay. This is performed for each batch of **3** to determine the thiolation degree (section 2.10.4). This assay is well established in literature to analyse the amount of thiol groups in a sample. The assay is based on the conversion of 5,5′-dithiobis-2-nitrobenzoic acid to 2-nitro-5-thiobenzoate, which is utilised for detection at $\lambda = 412\,\mathrm{nm}$. A thiolation degree below $5\,\%$ was identified as successful synthesis (Appendix B).

The combination of QCM-D experiment, which shows the binding of the thiolated short HA (**3**), and the performance of an Ellmann's assay, to directly detect the chemical modification of the HA, proves the successful thiolation of short HA at the reducing end.

4.1.2. Introducing a Terminal Alkyne Function to Short Hyaluronan

To enable the variation of the density of immobilised HA on a surface as well as to create the possibility of the co-representation of HA with an adhesive background, an alkyne-group is introduced to the reducing end of short hyaluronan via propargylamine (fig. 4.3). As passivating background OEG $(\mathrm{HS-(CH_2)_{11}-EG_3-OH})$ is chosen, because it prevents unspecific interactions of proteins and cells with the surface and can be used in QCM-D studies. [53,122,123] Additional, it is a simplified model for PEG, which is used in cell culture experiments to prevent unspecific interactions. The synthesis is per-
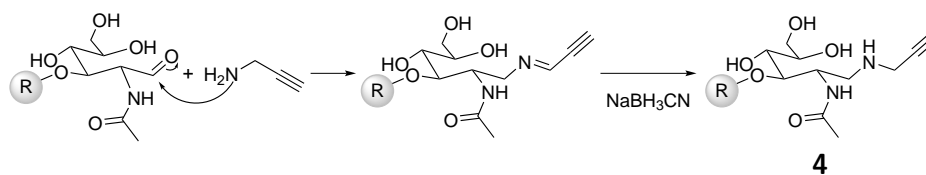
Scheme 4.3.: Reaction scheme for the coupling of HA with propargylamine. In the first step the amine attacks the carbonyl C-atom and forms a imine which is selectively hydrogenated with sodium cyanoborohydrid.

formed adapting the protocol from Lee *et al.* for creating end-thiolation of HA.[49] Therefor, propargylamine is used instead of cysteamine hydrochloride. The amine function of propargylamine undertakes the nucleophilic attack to the carbonyl group (scheme 4.2).[54] The following step is the hydrogenation of the occuring imin-function. According to Likhar *et al.*, it is possible to perform a selective hydrogenation of a N=C double bond orthogonal to an alkyne group.[124]

To analyse the functionalisation and to enable further characterisation of the HA species, again QCM-D experiments are performed. Therefore a click-reaction is performed with the modified HA and an OEG-SAM with statistically distributed azide groups (ratio of terminal hydroxy to azide groups 3:2, Appendix C) in the QCM-D. In a first step the mixture of thiol bearing OEGs

a)

b)
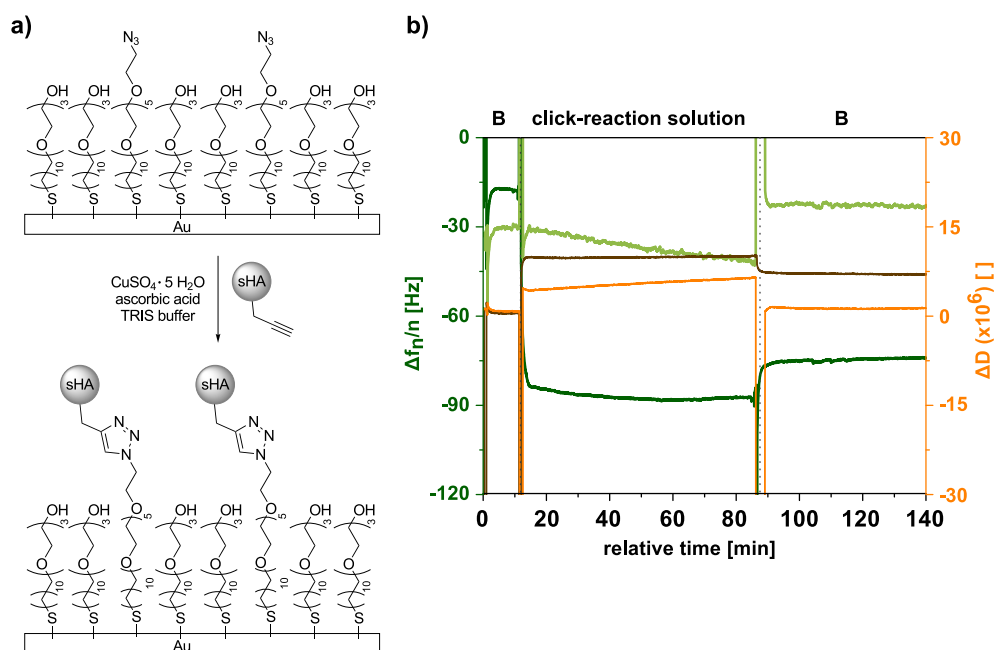
Figure 4.2.: To characterise the short HA with an alkyne group at the reducing end, the HA is coupled to an azide bearing OEG-SAM as published in [54]. a) The surface is decorated with $HS-(CH_2)_{11}EG_3-OH$ and $HS-(CH_2)_{11}EG_6-N_3$ in a ratio of 3:2. The CuAAC is performed in TRIS buffer (100 M TRIS-buffer, pH 8.5), 100 mM ascorbic acid and 1 mM $CuSO_4$. The reaction is observed via QCM-D (b). Shown is the 7th overtone of the performed reaction with (Δf_7: dark green, D: brown) and without (Δf_7: light green, D: orange) adding $CuSO_4$. To simplify the diagram the preparation of the OEG-SAM is not shown. B corresponds to the used TRIS buffer (100 M, pH 8.5).[54]

($HS-(CH_2)_{11}EG_3-OH$ and $HS-(CH_2)_{11}EG_6-N_3$) is added at a total concentration of 100 µM in TRIS-buffer (100 mM, pH 8.5) to the gold-coated crystal (fig. 4.2 a). A dense SAM is formed. In a next step the end-alkyne, short HA species (**4**, 100 µM) is added in TRIS-buffer containing 100 mM ascorbic acid and 1 mM $CuSO_4$. After the system is equilibrated, the crystals are washed with buffer again and the change in frequency was determined (fig. 4.2). The performance of the click-reaction leads to an irreversible drop in frequency ($\Delta(\Delta f_7) = 57$ Hz), which proves the covalent binding of the short HA species to the OEG coated surface. Without adding $CuSO_4$ to the click-buffer, no change in frequency is observed. The kinetic of the side reaction, the uncatalysed click-reaction between alkyne and azide is to small to be detectable.[125] Due to the steric hindrance of the large HA molecule the contact of alkyne and azide-group is a rare event, which decreases the kinetic of the side as well as the main reaction.[54]

The water contact angles for these surfaces are measured as well. For pure gold surfaces a water contact angle of 69°, 48° for the OEG-SAM before adding HA and an angle below 20° for the surfaces with HA is measured.[54]
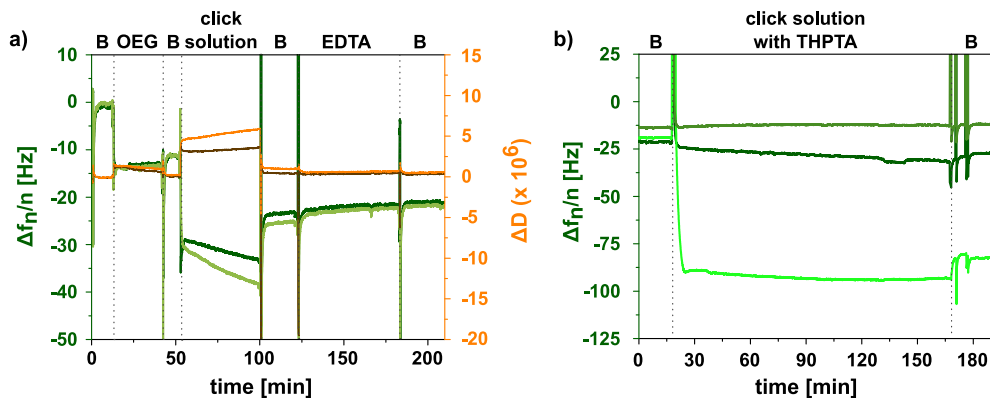
Figure 4.3.: Because the incorporation of Cu-ions into the OEG-layer is found, the usage of a Cu-THPTA-complex is tested unsecessful. a) The surface is passivated with a 100 % HS$-$(CH$_2$)$_{11}$EG$_3$$-$OH layer, formed in TRIS buffer (100 mM, pH 8.5, B), incubated with the click reaction solution (TRIS buffer with ascorbic acid and CuSO$_4$) with (light green, orange) or without short HA-end-alkyne (dark green, dark brown). Afterwards, the surface is washed with EDTA-solution (1 mM) to remove the copper. b) An OEG-layer with a 1:1 ratio of azide terminus to hydroxy terminus is rinsed with the click reaction mixtures with CuSO$_4$ and HA-end-alkyne (positive control, lime green) and with additional tris(3-hydroxypropyltriazolylmethyl)amine (THPTA) with (dark green) and without short HA (green).

However, a more detailed analysis of the data revealed that the usage of the Cu^I-species as catalyst has some disadvantages. The analysis indicates that the Cu^I-species, which is necessary to catalyse the click-reaction, is incorporated into the OEG-layer. In a control experiment, an OEG-coated surface is prepared only consisting of HS$-$(CH$_2$)$_{11}$EG$_3$$-$OH (fig. 4.3 a). After the formation of the SAM, the click solution, containing 100 mM ascorbic acid and 1 mM CuSO$_4$ in TRIS-buffer (100 mM, pH 8.5), is added to the surfaces either with 0.4 g/L HA-end-alkyne or without HA. In both cases no click reaction can be performed due to the absence of an azide-function. Because of this no change in frequency should be observed. After washing with TRIS buffer (100 mM, pH 8.5), a $\Delta(\Delta f_7)=$ of 14 Hz (with HA-end-alkyne) and 12 Hz (without HA-end-alkyne) are observed. To remove copper ions, the layer is washed with a 1 mM EDTA-solution in TRIS buffer. This will preferably remove the Cu^{II} ions. The observed change in frequency decreases with the washing from 14 Hz to 10 Hz respectively from 12 Hz to 11 Hz. So it is observed that washing with EDTA can not remove all copper from the SAM. Another possible explanation is an unspecific interaction of one other compound of the system, which is not

influenced by EDTA.

To exclude unspecific binding of copper or ascorbic acid, the potential of a Cu^I specific chelater is investigated.[126–128] Therefore CuSO$_4$ is mixed with ascorbic acid and tris(3-hydroxypropyltriazolylmethyl)amine (THPTA) in a ratio of 1:50:5. So the Cu^{II} species is reduced by the ascorbic acid and Cu^I ions are chelated by THPTA. The reaction solution is added to the surface with (fig. 4.3 b) and without HA-end-alkyne (fig. 4.3), respectively. As positive control the classical click reaction is performed (fig. 4.3). While a $\Delta(\Delta f_7)$ of 62 Hz is observed for the positive control, no click reaction can be detected in the presence of the copper-THPTA complex. A possible explanation for this is the steric hindrance due to the THPTA ligand and mainly the large HA, which prevents the reaction. These results show that neither the application of the Cu^I-THPTA complex nor washing with EDTA lead to a successful reaction without the incorporation of copper ions. To solve this problem a different approach without catalyst is examined. This is presented in the following section.

4.1.3. Introducing Dibenzocyclooctyne-amine to Short Hyaluronan

For the application in a biological relevant context an alternative to the Cu^I-catalysed [3+2]-cycloaddition is needed. Therefor, this work will focus on the strain-promoted alkyne-azide cycloaddition (SPAAC). The reactivity of the alkyne depends on the strain of the cyclooctyne-species.
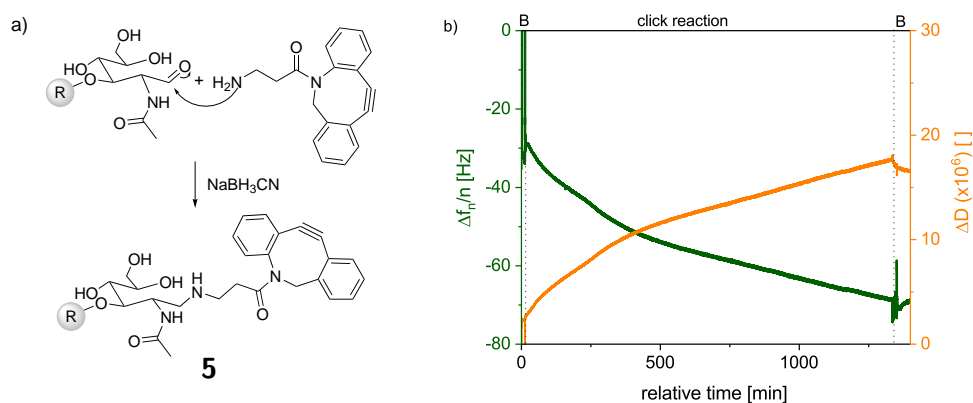
Figure 4.4.: Successful introduction of a dipenzocyclooctyne-amine to the reducing-end of HA adapting the protocoll of Lee *et al.*.[49] a) shows the reaction scheme of this modification. b) The click reaction of this HA species with an azide bearing surface (7.5 % azide) is observed using QCM-D in TRIS-buffer (100 mM; pH 8.5) over night. Shown is the 7th overtone, in green the change in frequency and in orange the dissipation is plotted. To simplify the figure the formation step of the azide-bearing layer is not shown.

To introduce a dibenzocyclooctyne-amine (DBCO-amine) to short HA (fig. 4.4 a) a variation of the protocol of Lee *et al.* is applied.[49] Again, the amine substitutes the carbonyl-function (fig. 4.4) at the reducing end of the short HA, followed by the hydrogenation of the occurring imine. Due to the solubility of the reactants, the reaction is performed in DMSO. The sodium cyanoborhydride for the hydrogenation is added in borate buffer (30 v%). After the purification via dialysis, the functionalised HA is characterised using QCM-D. The ring strained alkyne is added to an azide bearing surface on the quartz-crystal. After the system is equilibrated in TRIS-buffer (100 mM; pH 8.5), the short HA with DBCO (2.5 mg/mL) is added to the surface. An example of the change in frequency for the 7th overtone due to the SPAAC is shown in figure 4.4 b). Comparing the needed time until a plateau is reached for the CuAAC and SPAAC a large decrease in reaction time is seen. The SPAAC takes about 24 h until the reaction is complete whereas the CuAAC needs less then 1 h. This discrepancy is due to the different mechanisms behind the reactions. The driving force in this case is the strain of the dibenzocyclooctyne. Due to the sp-hybridisation of the alkyne carbon-atoms the resulting angle between those atoms would be 180°. The cycle in which the triple bond is incorporated enforces a angle of approximately 160°.[55] So the high energetic triple bond reacts spontaneously with the azide on the surface. This takes much longer than the copper catalysed reaction. Additionally a sterical hindrance due to the large HA molecule decreases the reaction speed. As a result of the rather slow reaction kinetic of the SPAAC compared to the CuAAC, the reaction was performed over night. The QCM-D experiments show a frequency change for $\Delta(\Delta f_7)$ of 42 Hz respectively of 58 Hz.

Although the SPAAC with the DBCO bearing short HA and azide is slow, it could be proven that the SPAAC is an appropriate alternative to the CuAAC to immobilise hyaluronan to a surface.

4.1.4. Introducing an Alkyne Function within the Chain of Short HA (6)

To enable the analysis of the influence of the position of the introduced modification, an alkyne group is presented within the HA chain via functionalisation of carboxy groups. To keep the amount of alkyne-groups within a single chain low, the disaccharide units are used in high excess. The synthesis is performed according to Crescenzi *et al.*.[48] In a first step the carboxy group is activated using *N*-(3-dimethylaminopropyl)-*N'*-ethylcarbodiimide (EDC) (scheme 4.4). The formed intermediate can either react with the primary amine-group of propargylamine or further with *N*-hydroxysuccinimide (NHS) to form an active ester, which enables the coupling to amine-groups as well.

The characterisation of the HA with alkyne groups within the chain is obtained using QCM-D again. The CuAAC is performed outside the QCM-D in TRIS buffer (100 mM, pH 8.5) in the presence of 100 mM ascorbic acid,
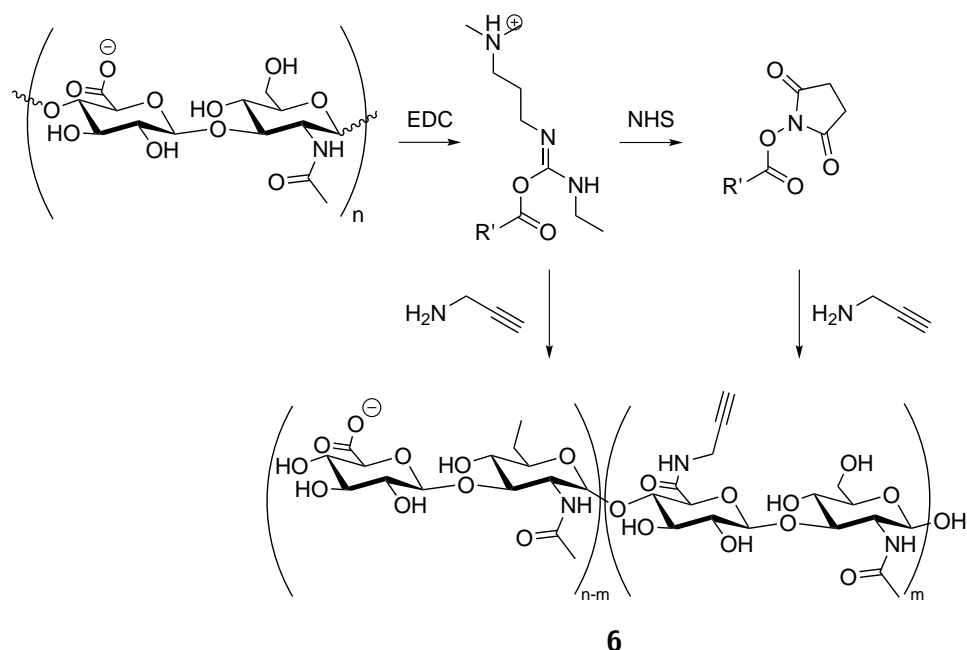
Scheme 4.4.: Reaction scheme of the functionalisation of HA within the chain using active ester chemistry applying EDC and NHS (R' = HA).

1 mM $CuSO_4$, 100 µM $HS-(CH_2)_{11}EG_6-N_3$ and 100 µM functionalised HA. After the reaction, 1 mM EDTA is added to chelate the remaining metal ions. The $HS-(CH_2)_{11}EG_6-sHA$ is mixed with the $HS-(CH_2)_{11}EG_3-OH$ to a molar ratio of 2:1 and added to the QCM-D sensor using the flow module.[54] Figure 4.5 shows a change in frequency for the HA-modified layer of $\Delta(\Delta f_7)$ of 53 Hz. Disadvantage of the pre-clicking of the short HA in this case is that the short HA has more alkyne-groups per chain and thus can bind to several $HS-(CH_2)_{11}EG_6-N_3$-molecules. This influences the formation of the SAM on the surfaces. Although the density of alkyne-functionalities is kept low, the groups are statistically distributed in the chain without control of their location.

The degree of alkynation is determined via NMR analysis. The integral of the alkyne-proton signal (δ = 2.67 - 2.54 ppm) is compared to the integral of the methyl-group signal of the *N*-acetylglycosamine-unit (δ = 1.98 ppm; Appendix F). Considering the stoichiometric ratio of the integrals, normalised to the number of represented protons, a degree of alkynation of 16 % is calculated.

The results in the previous section show several strategies to chemical modify HA to immobilise HA on a surface. One the one hand modifications at the reducing-end are performed using cysteamine hydrochloride, propargylamine and dibenzocyclooctyne-amine. On the other hand the propargylamine is introduced at the carboxy groups within the chain. In case of the end-thiolated HA
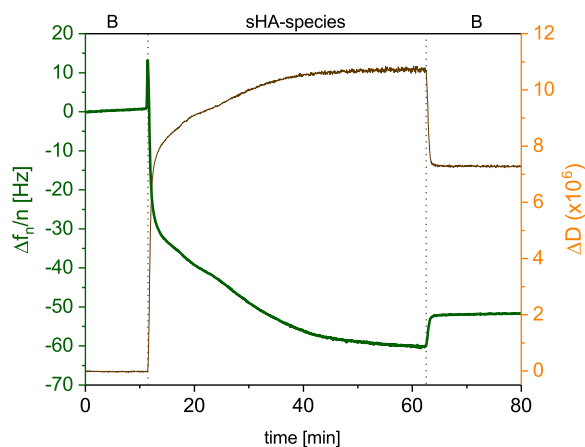
Figure 4.5.: Successful immobilisation of HA with alkyne groups within the chain on an OEG-SAM in the QCM-D. The OEG-SAM consists of $HS-(CH_2)_{11}EG_3-OH$ and $HS-(CH_2)_{11}EG_6-side-HA$ (ratio 3:2). Beforehand **6** is coupled to $HS-(CH_2)_{11}EG_6-N_3$ using the CuACC reaction. The 7th overtone is shown for an experiment on a gold surface with the change in frequency in green and the dissipation in brown. The system is equilibrated in PBS.[54]

a degree of thiolation of below 5 % (Appendix B) and of the functionalisation within the chain a degree of alkynation of 16 % is determined. All synthesis are possible and enable the immobilisation of the HA-species.

4.2. Bioactivity of Chemical Modified Short Hyaluronan

The possibility to immobilise short hyaluronan and to create surfaces with well-controlled HA patterns enables the analysis of specific and unspecific interactions between HA and biological samples. Therefore, it needs to be tested, if the modified short HA is still bioactive. Due to the chemical modifications, there is the risk that the short HA is not recognisable by some HA-binding receptors, respectively other hyaladerins, if the reducing end is important for these interactions. Therefore modifications at the reducing end are compared with the modification within the chain. In case of the modification within the chain, it is necessary to keep the modification degree low because typical HA receptors need a defined number of disaccharide units to recognise HA (chapter 1). To ensure the bioactivity, the interaction of the differently immobilised HA species with aggrecan, a HA binding protein, and LYVE-1, a HA receptor, as well as the passivation properties of HA are determined in QCM-D experiments.[54]

4.2.1. Passivation Properties of Immobilised sHA

HA can be used to prevent unspecific interactions between proteins and a surface. To analyse the passivation properties of the different modified HA species, the different prepared surfaces are incubated with a 4 % solution of BSA as a model protein. Compared are coated gold surfaces decorated with the end-thiolated HA species (**3**) and the two different alkyne functionalised surfaces with an additional passivating OEG background (fig. 4.6). The first
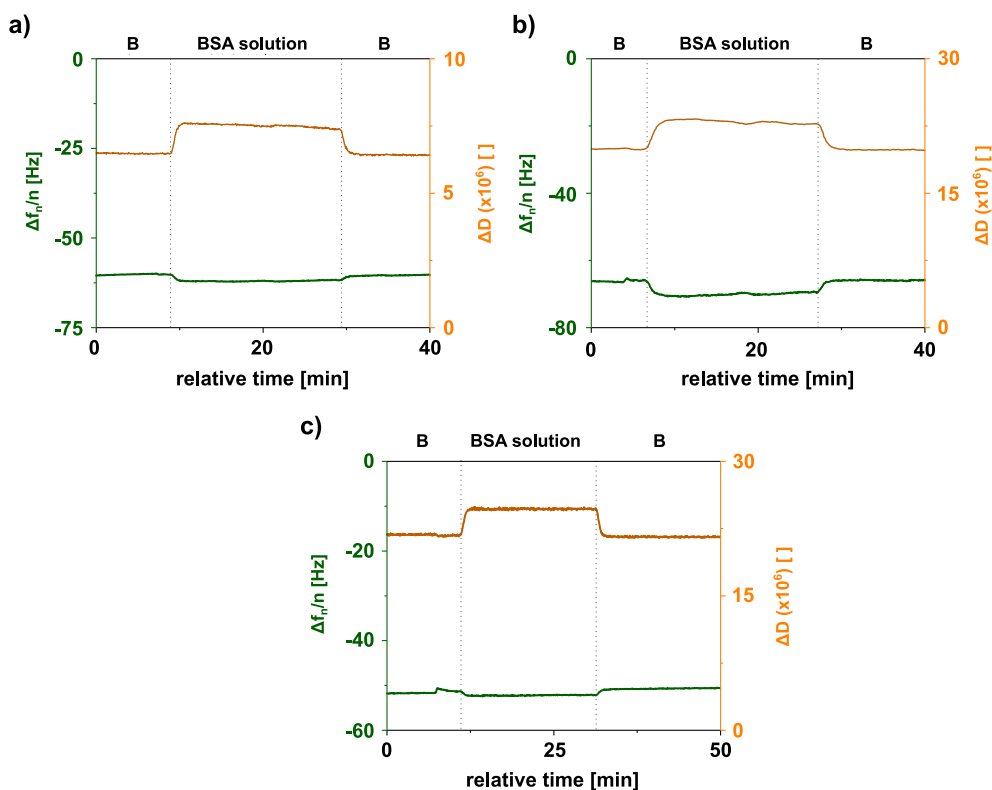
Figure 4.6.: Intact passivation properties of different chemical modified, immobilised HA layers. For testing the passivation properties of a) a layer of thiolated HA (**3**) (in PBS) and the two HA species with alkyne groups (in TRIS buffer) b) at the reducing end (**4**) and c) within the chain (**6**, Δf green, ΔD: orange) the surfaces are rinsed with a 4 % solution of BSA in the corresponding buffer. The 7th overtone is shown with the change in frequency in green and the dissipation in orange.[54]

analysed surface is decorated with the end-thiolated HA species (**3**) (a). After the incubation with a 4 % BSA solution, the system is again equilibrated in buffer, which removes all BSA. So no change in frequency due to BSA can be obtained. The modification at the reducing end with a thiol has no influence on the passivation properties of the HA. In the cases of the OEG-SAM

decorated with alkynated HA, neither an interaction between the BSA and the functionalisation at the reducing end nor the functionalisation within the chain is observed. The comparison of the three different surfaces shows, that the position of the functionalisation of the HA does not influences the passivation properties of the HA. Furthermore, the homogeneous immobilisation of HA on a gold surface via a thiol group is sufficient to protect a surface against unspecific interactions.

4.2.2. Specific Interaction of Immobilised sHA and Aggrecan

For this analysis on the one hand the OEG-SAM, consisting of 67% of the azide bearing $HS-(CH_2)-EG_6-N_3$ and 33% $HS-(CH_2)-EG_3-OH$, which was modified with both propargylated species before it is applied to the surface, and on the other hand the homogeneous short HA-end-thiol modified surfaces are compared. This enables the determination of the influence of the position of the modification as well as the testing, if a very dense HA surface has a major effect on the activity. Therefore a solution of aggrecan $(100\,\mu g/mL)$ is applied to the different surfaces and the change in frequency as well as the change in dissipation in a QCM-D experiment is determined. The summary of the relative changes in frequency and dissipation are shown in figure 4.7 a. As expected, no interaction between aggrecan and the OEG control can be observed (A). Furthermore, no interaction between aggrecan and the HA-side-alkyne can be found (D). Possibly, the HA structure is disturbed due to the binding of the OEG-molecules. Because of this it is possible that the aggrecan can not recognise the HA and thus prevent the binding of aggrecan to the HA. For both end-modified HA-species a change in frequency is observed in a similar range. The larger change in frequency and dissipation might be due to the different amount of immobilised HA in the two systems. Because the aggrecan binds to and thus recognises the HA, it is still bioactive after the chemical modification.

4.2.3. Specific Interaction of Immobilised sHA and LYVE-1

Complementary, the interaction of HA with LYVE-1, a HA-receptor, is investigated. Therefore, HA-modified surfaces are rinsed with a $20\,\mu g/mL$ solution of LYVE-1. In this case only the OEG-HA-samples are compared, because it is very important to have a passivated background to prevent unspecific interactions between LYVE-1 and the pure gold surface. The low molecular weight of LYVE-1 $(30\,kDa)$[39] makes it difficult to measure binding to the HA with QCM-D. To increase the weight, a LYVE-1-his tag is bound to a monoclonal anti-polyhistidine-alkaline phosphatase antibody. A solution of this species $(39.9\,ng/mL)$ is rinsed over the different surfaces. The results are summarised in figure 4.7 b. For the interaction between LYVE-1 and the OEG-SAM surface no change in frequency and dissipation is observed (A). In case of **4** a small de-
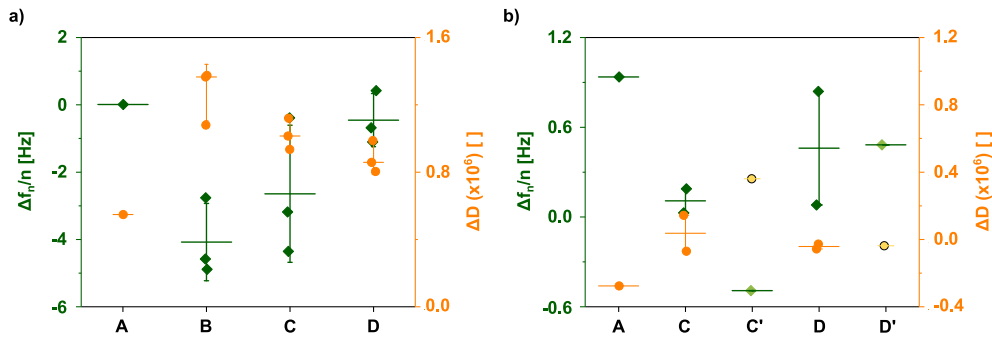
Figure 4.7.: Verification of the specific interaction between chemical modified HA and hyaladherin or HA receptor. Compared is the interaction of a HA modified surface with a) aggrecan and b) LYVE-1 and a LYVE-1-antibody construct to increase the weigth (C', D'). Shown are the changes in frequency and dissipation for A the negative control without HA, B the end-thiolated HA (**3**), C the end-alkynated HA (**4**) and D the HA with the alkyne group within the chain (**6**).

crease in frequency and dissipation can be observed (C), which can be slightly increase by using the LYVE-1-antibody construct (C'). So it is still difficult to prove a strong binding of LYVE-1 to the HA. For the HA modified within the chain less binding is observed (D), which can not be increased be using the LYVE-1-antibody construct (D'). The antibody itself is not able to bind to the surfaces. So a interaction of LYVE-1 and the terminal functionalised HA can be proven, even though the small change in frequency and dissipation indicates only a weak interaction. In case of **6** the interaction seems more difficult than in the other case because the found change in frequency and dissipation is even smaller. An extensive discussion about the binding of LYVE-1 to the immobilised HA is published in Minsky *et al.*.[54]

After the chemical modification to immobilise HA, the bioactivity is verified via the analysis of the interaction between the HA species and the hyaladerine aggrecan as well as LYVE-1. Especially the interaction between aggrecan and HA proves the conservation of the bioactivity during the modification.

4.3. Establishment of Different Cell Assays

In this section the concentration depended influence of hyaluronan on cell behaviour in a lymphangiogenisis model is analysed. After enabling the immobilisation of HA and the verification of the bioactivity of chemical modified HA species, the influence of immobilised HA is compared to HA, which is diluted to different concentrations. To generate a surface with a well-defined HA pattern, nanostructured surface are used (fig. 4.8). To vary the HA concentration, the density of gold nanoparticles is varied. This will be compared to the
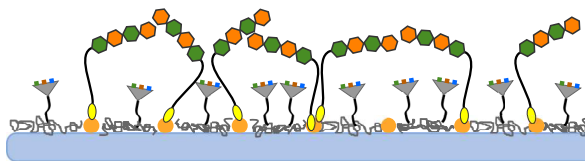
Figure 4.8.: Scheme of the surface applied in the study to investigate the influence of HA on the behaviour of LECs. The glass surface is decorated with gold nanoparticles (yellow dots) with different particle densities and passivated with click-PEG (grey). The click-PEG is functionalised with cRGD (triangles) as adhesive background and the nanoparticles with the end-functionalised HA (green/orange).

variation of HA, diluted in different concentration. Analysed is the metabolic activity of human primary lymphendothelial cells (HUPLEC) based on the AlmarBlue® assay, the adhesion of the cells via the CyQuant® assay and the toxicity of HA using the AlamarBlue® assay. The CyQuant® assay analyses the amount of DNA, which is directly correlated to the number of cells on the surface. To compare different samples, the determined metabolic activity is normalised to the amount of DNA.

4.3.1. Establishment of the CyQuant® Assay

On different surfaces cells might adhere and behave in a different manner. To compare the metabolic activity of cells on different surfaces, the amount of cells on each surface is determined using the CyQuant® assay, which analysed the amount of DNA in a sample. The CyQuant® assay is based on a colorimetric change of the kit due to the binding of the dye to the DNA. The fluorescence is measured at λ_{ex} of 480 nm and λ_{em} of 520 nm. For the CyQuant® assay the surface is washed twice with PBS to remove the complete media. After freezing the cells at -80 °C 200 µL of the CyQuant® kit are added containing 49.8 % lysis buffer. Different numbers of cells are incubated for several minutes before the fluorescence is measured at different time points. For an optimal usage of this assay the responding fluorescence signal after the incubation of the dye with cells needs to be within the linear range for the concentration depended fluorescence signal. For this optimisation experiment 1000, 5000, 10 000, 20 000, 30 000, 40 000 and 50 000 cells are seeded in a 96 well plate in 200 µL media. To access the DNA after 48 h, the cells are frozen at -80 °C so that the membrane is permeabilised. After freezing the cells with the surfaces 200 µL of the CyQuant® kit are added. Additional, the dye is added in a lysis buffer according to the protocol in section 2.10.2. The fluorescence is measured with an excitation wavelength $\lambda_{ex} = 480$ nm and an emission wavelength $\lambda_{em} = 520$ nm after 5, 15, 25 and 35 min in each well (fig. 4.9). For a cell number below 12 500 a linear increase of the fluorescence signal is deter-

mined for all incubation times (fig. 4.9 a). The determination of the incubation time leads to an optimal time of 5 min for this number of cells. Analysing the correlation between fluorescence and incubation time, a linear increase of the signal is found up to an incubation time of 15 min.
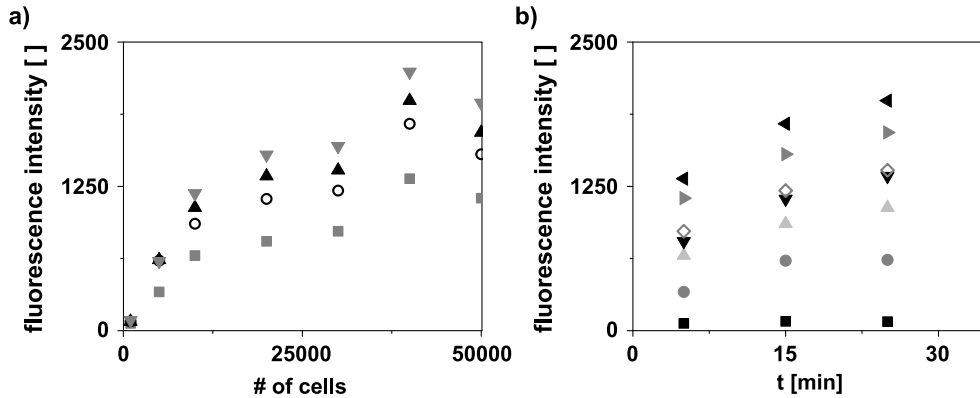
Figure 4.9.: Determination of optimal incubation time and cell number for using the CyQuant® assay. The measured absorbance at excitation 480 nm and emission 520 nm a) Incubation time □ 5 min ○ 15 min △ 25 min ▽ 35 min b) □ 1000 ○ 5000 △ 10000 ▽ 20000 ◇ 30000 ◁ 40000 ▷ 50000

So an incubation time of 5 min is chosen which is in the middle of the linear range. Since the CyQuant® assay is performed right after the AlmarBlue® assay (section 4.3.2), the cell number depends also on that assay.

4.3.2. Applicability of AlamarBlue

The system is checked for any interaction between resazurin, the dye used in this assay, and the used HA species before it is used for further experiments. For the cell experiments HA concentrations of 1.0, 2.5, 5.0 and 20.0 µg/mL are used. This different concentrations are tested in growth media with 10 % AlamarBlue® kit. The absorption of the solution is measured in a 96-well plate at a wavelength of 570 and 600 nm after mixing and again after the incubation for 1 and 2 h at 37 °C in the presence of 5 % CO_2 (fig. 4.10). The relative amount of reduced resazurin is calculated according to equation 2.6 in section 2.10.1. The performed Kruskal-Wallis test with Dunn's comparison (non-parametric statistical analysis; Appendix E) shows neither a significant difference between the different applied HA-concentrations nor the different time-points of the measurement. This indicates no interaction between the resazurin or resorfurin with HA.

In a second step, the system is checked for any interference between the media with the supplements and the resazurin, which might falsify the fluorescence measurement. Therefore the fluorescence of resazurin, respectively the AlamarBlue® kit, is measured of a mixture of media with 10 % of the kit at
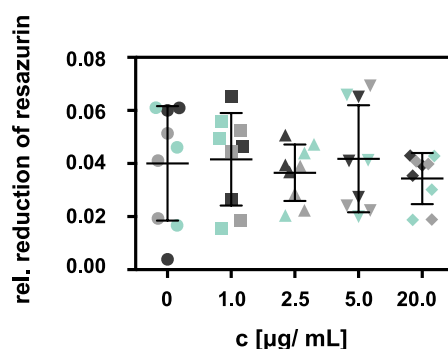
Figure 4.10.: The analysis of the interaction of growth media for LECs, resazurin and different concentrations of end-tiolated, short HA-end-thiol shows no interference of the compounds. The absorption is measured at 570 nm and 600 nm after 0 h (dark grey), 1 h (light grey) and 2 h (light blue) and the relative amount of resazurin calculated applying equation 2.6. The Kruskal-Wallis test followed by Dunn's multiple comparison showed no significant difference between the samples ($p > 0.05$).

a excitation wavelength of 540 nm and an emission range of 550 to 700 nm. For the measurement 0 to 50 000 cells are incubated at 37 °C for 0 to 27 h (fig. 4.11). The comparison shows an increase of the fluorescence at 585 nm with increasing cell number (a) and increasing time frame (b), which correlates with a raising amount of metabolic products. Because no disturbing interactions
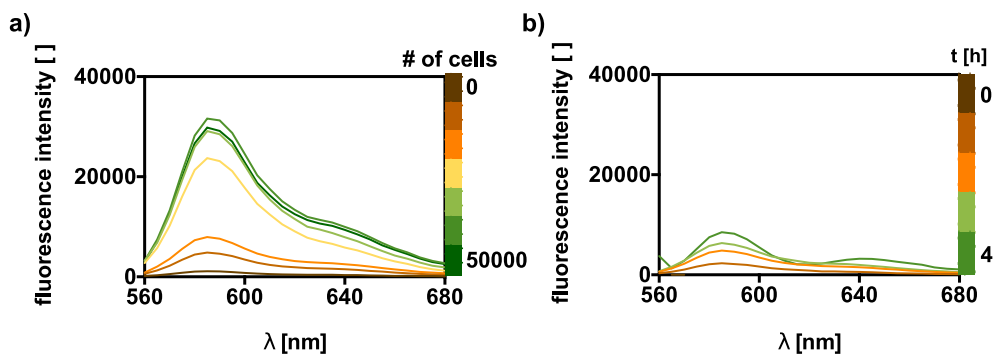
Figure 4.11.: No interference of the used compound with resazurin is found in the fluorescence spectra. The fluorescence intensity is measured of media with 10 % AlamarBlue®kit and 0 to 500 000 cells after 0 to 27 h. The results are normalised to the background. a) shows the example of the measurement after 2 h with the full range of cells and b) the example of 5000 cells from 0 to 4 h.

of the utilised components with the AlamarBlue® kit could be observed, the assay is adaptable for the ongoing experiments.

4.3.3. Establishment of the AlamarBlue® Assay

After exclusion of disturbing interference between resazurin, growth media and HA, the optimal incubation time and cell number needs to be determined. As described in section 2.10.1, the arising fluorescence is determined and it needs to be ensured that only a small amount of dye is converted according the scheme 4.5 to resofurin. If the number of cells is to high, the formation of dihydroresorufin will falsify the result.
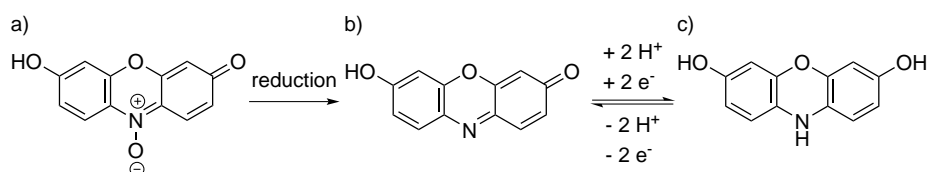
Scheme 4.5.: Active species of the AlamarBlue®kit: Resazurin (blue in alkali, pink acid, non-fluorescent), Resorufin (pink, fluorescent, colourless in acid), Dihydroresorufin (colourless, nonfluorescent)

To identify this linear range, 0 to 50 000 cells were seeded in 200 µL media in a 96-well plate. After 48 h 100 µL media are removed and 10 µL of the AlamarBlue®kit are added. The absorption is measured after 1, 2, 3, 4 and 27 h incubation. The last value is needed to determine the maximal concentration of reduced resazurin. The results are normalised to the mean of the pure media and the relative fluorescence intensity is plotted against the number of cells or the incubation time (fig. 4.12).
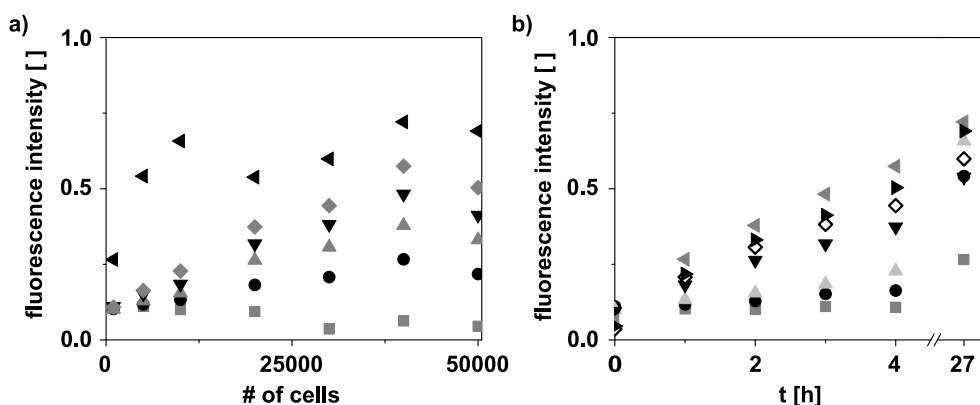
Figure 4.12.: Determination of optimal incubation time and cell number for using the AlamarBlue®assay in LECs in a 96-well plate. The fluorescence is measured with an excitation wavelength of $\lambda = 540$ nm and an emission wavelength of $\lambda = 585$ nm. a) Incubation time □ 0 h ○ 1 h △ 2 h ▽ 3 h ◇ 4 h ◁ 27 h b) □ 1000 ○ 5000 △ 10000 ▽ 20000 ◇ 30000 ◁ 40000 ▷ 50000

Figure 4.12 a) indicates a linear range for a cell number lower than 20 000 cells for 1 to 4 h, which is confirmed through b). In a) a linear range for an incubation time of 1 to 3 h can be observed. In b) the curve for 1000 to 10 000 show a wide linear range within a good observable time frame (1 to 4 h). For further experiments a cell number, in the middle of the linear range, of 4210 cells respectively $131/mm^2$ for a 96 well (tab. 4.1) and a incubation time of 2 h is chosen. The chosen number of cells is also suitable for the CyQuant® assay, where a number of cells below 12 500 is needed for a useful application.

4.3.4. Summary of the Established Assays

The establishment of the CyQuant® and AlmarBlue® assays showed a suitable number of cells of $131/mm^2$ on the used surface and an incubation time of 5 min and 2 h. Also the performance of both assays right after each other shows no further challenges. Because in the upcoming experiments surfaces with different sizes are used and the recommended amount of kit were confirmed for the use in a 96 well plate with LECs, the required amount of dye for the glass surface (d = 22 mm in 12 well) is calculated (table 4.1).

Table 4.1.: Summary of the used amount of liquid for the AlamarBlue® and CyQuant® assay depending on the used surface areas and number of cells. Additionally the quantity of the dye solution is noted.

#	surface area [mm]	cell number	AB [μL][a]	CQ [μL][b]
1	34.0 (96 well)	4210	110	200
2	380.1 (12 well)	50000	605	600

a) containing 10 % AlamarBlue® kit
b) containing 5 % CyQuant® kit

To determine the influence of hyaluronan on LECs the performance of the AlamarBlue® and CyQuant® assay are established. A cell density of $131/mm^2$, an incubation time of 2 h (AlamarBlue® assay) and 5 min (CyQuant® assay) are established.

4.3.5. Toxicity of Different HA Species

Finally it is analysed if the different HA species and applications have a toxic effect on the cells. Therefore the adsorption of the AlamarBlue® kit is measured at 570 nm and 600 nm after 2 h of incubation to enable the calculation of reduction of resazurin according to equation 2.6. Compared are the effect of the digested and short HA (a) with each other and the two end-thiolated species in solution (fig. 4.13 b). Also the effect of both immobilised species are compared (c). Shown is also the passivation control, which has no cells

on top, to analyse effects of the surface without HA and cells on resazurin. For the statistical analysis all samples are compared to the positive control and the different species at the same concentration with each other. In case
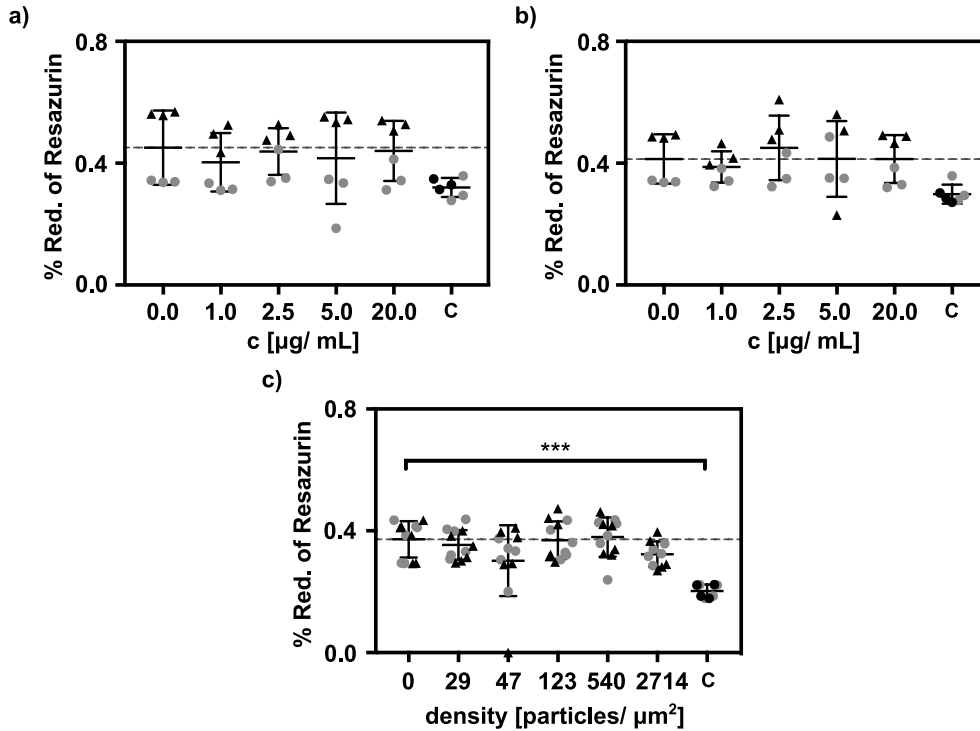
Figure 4.13.: The comparison of the toxic effect of the different HA species on LECs shows similar influences in all cases. The analysis is performed using the AlamarBlue® assay (section 2.10.1). In a) the unfunctionalised short (grey circles) and digested (black triangles) HA are compared. Their end-thiolated analogues are presented in b) in solution and immobilised on a nanostructured surface in c). C corresponds to the passivation control without cells. The significant difference between the concentrations and the species is analysed applying a Kruskal-Wallis test followed by the Dunn's multiple comparison (p > 0.05; Appendix E).

of the unfunctionalised HA species a splitting up between both species are observed. Although the positive control (0 μg/mL) has no HA incorporated. The performed statistical analysis (Kruskal-Wallis test followed by the Dunn's multiple comparison, Appendix E) shows no significant difference between the surfaces as well as between the applied species. Because no splitting up effect is found for the negative control (C) the impact is not due to the surface itself or the used equipment, but due to the cells used at different days, although it is the same cell passage. In case of the end-thiolated HA the distribution of the data points is less pronounced compared to the unfunctionalised HA species. Again the statistical analysis (Kruskal-Wallis test followed by the Dunn's mul-

tiple comparison, Appendix E) shows no significant difference neither between the different applied concentrations nor the different species. For the immobilised HA species no separation in the data is observed due to the different species. The performed Kruskal-Wallis test followed by the Dunn's multiple comparison (Appendix E) shows no significant difference between the different species or different particle densities compared to the positive control. Whereas a significant difference is found between positive and negative control. This is expected, because no cells can contribute to the reduction of resazurin in case of the negative control.

The determination of the toxic impact of digested and short HA species applied in different concentrations or different densities shows no negative effect to the metabolic activity.

4.4. Concentration Dependent Influence of Short Hyaluronan on Human Primary Lymphendothelial Cells

In this section the effect of short hyaluronan, a digested HA and their end-thiolated analogues incubated with LECs are tested. Therefore experiments are performed either on cell culture plastic (96 well-plate) or cRGD functionalised click-PEG surfaces (cover slide, $d = 22\,mm$) with HA in solution or immobilised on nanostructured surfaces with cRGD functionalised click-PEG (cover slide, $d = 22\,mm$). The used short HA has a weight distribution of $10\,000$ to $20\,000$ Da. The enzymatically digested HA[1], based on a HA with an averaged weight of $4\,000\,000$ Da, has a final weight distribution of 1000 to $10\,000$ Da.

4.4.1. Comparison of the Impact of sHA on Cell Culture Plastic

In a 96-well plate 4210 cells were seeded in growth medium containing 0, 1.0, 2.5, 5.0 and $20.0\,\mu g/mL$ of either short HA and digested HA (fig. 4.15) and incubated for $46\,h$ at $37\,°C$ and $5\,\%$ CO_2. Afterwards the AlamarBlue® and the CyQuant® assay performed.

Do cells adhere differently when applying different concentrations of HA?

The permeabilised cells are incubated for $5\,min$ with the CyQuant® kit and the fluorescence is measured ($\lambda_{ex} = 540\,nm$; $\lambda_{em} = 585\,nm$). The results are corrected to the background (well plate) and normalised to the average of the control sample without HA. The comparison of the impact on the cell attachment of the digested HA species (fig. 4.14 a) shows no significant difference.

---

[1]The digested HA-species was produced by Melanie Rothley (ITG, KIT) based on "Healon 5" (*Abbott Medical Optics*)

Also no significant difference is determined for the short HA species according
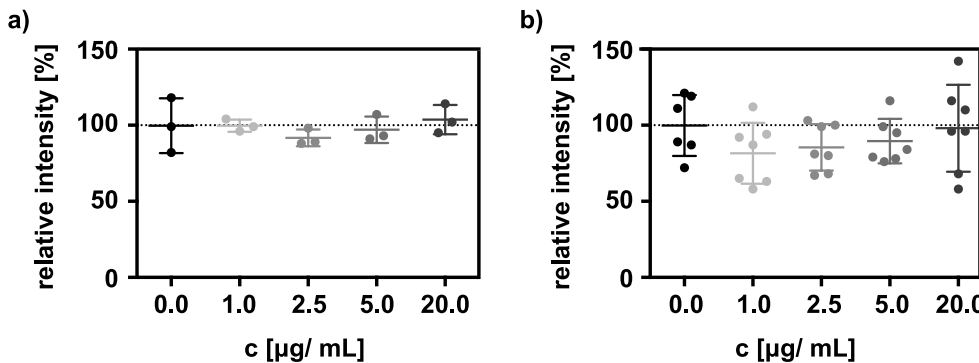
Figure 4.14.: Results of CyQuant®assay of unfunctionalised HA in solution
with LECs in a 96-well plate: a) for enzymatically digested HA and b) short
HA. The performed Kruskal-Wallis test followed by a Dunn's multiple com-
parison shows no significant difference between the different surfaces. The
results are baseline corrected and normalised to the average of the surfaces
without short HA.

to the performed Kruskal-Wallis test followed by the Dunn's comparison ($p <$
0.05). Only a small decrease of DNA becomes apparent for the smallest short
HA concentration. The statistical analysis of the samples between the two
types of HA also showed no significant difference of the same concentration of
the different species ($p < 0.05$, Appendix E). No difference in the amount of
DNA on the surfaces, which were incubated with different concentrations of
HA as well as the different species is observed. So no evidence of a reduced
cell adhesion due to the HA is found.

Do the different HA species influence the metabolic activity of LECs?

After 46 h the cells are incubated for 2 h with the AlamarBlue® kit and the
fluorescence is measured ($\lambda_{ex} = 540$ nm; $\lambda_{em} = 585$ nm) using a plate reader.
The results are corrected to the background (well plate) and normalised to the
average value of the control.

For the digested HA three data points are measured per concentration and
plotted in a scatter plot (fig. 4.15 a). Adding the HA leads to a small decrease
in the intensity compared to the control. The activity is slightly increasing
again, but stays below the control-level. The performed Kruskal-Wallis test
followed by Dunn's comparison ($p < 0.05$, Appendix E) shows no significant
difference. As well in case of the short HA no significant difference according to
the results of the Kruskal-Wallis test followed by Dunn's multiple comparison
(fig. 4.15 b) is found, although the same trend for the activity like for the
digested HA is visible.
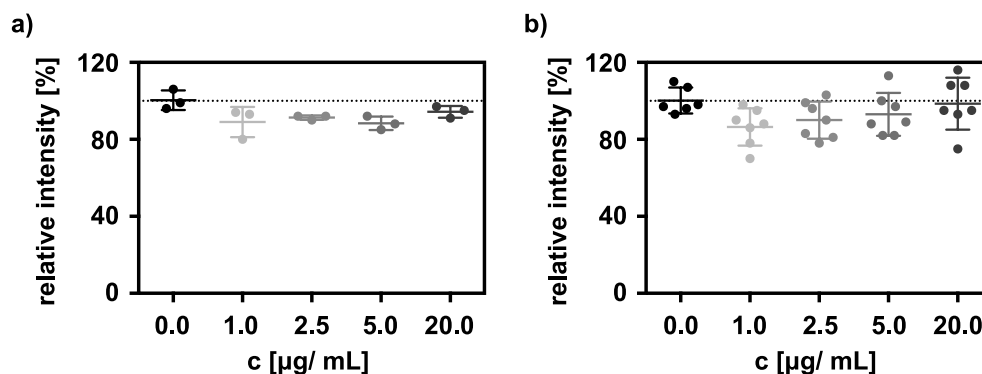
Figure 4.15.: Results of AlamarBlue®assay of unfunctionalised short HA in solution with LECs in a 96-well plate: a) for enzymatically digested HA and b) short HA. The performed Kruskal-Wallis test followed by Dunn's comparison shows no significant difference between the different surfaces (p < 0.05, Appendix E). The results are baseline corrected and normalised to the average of the surfaces without short HA.

Additionally, the influence of the two species are compared. For both the same trend in activity is observed, which is not significant (fig. 4.16). The performed Kruskal-Wallis test followed by the Dunn's multiple comparison indicated no significant difference between the same concentrations of the two corresponding HA-species (p < 0.05, Appendix E). Due to this, no differentiation in digested HA and short HA is necessary in this case.

The performed Kruskal-Wallis test followed by the Dunn's multiple comparison shows no significant difference comparing the different applied concentrations of HA. This is found for both species. The comparison between both species also shows no significant difference according to the performed analysis.

Determination of the Relative Metabolic Activity

To enable the comparison between the different surfaces and concentrations, the detected relative metabolic activity, based on the AlamarBlue® assay, is normalised to the relative amount of DNA, based on the CyQuant® assay. The results are shown in fig. 4.17. Neither for the digested HA (a) nor the short HA (b) a significant difference can be obtained. Furthermore, no significant difference between the two HA species can be detected at all so the results can be pooled and analysed as a whole (fig. 4.17).
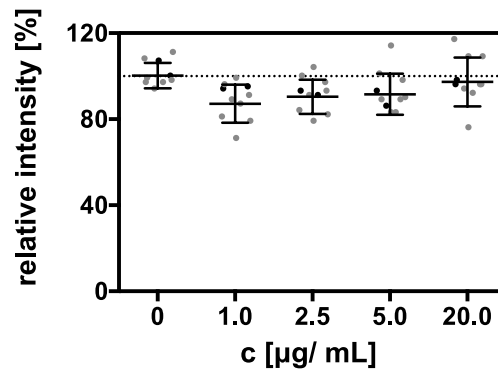
Figure 4.16.: To compare the used HA species all data is plotted in one figure, where black represents the digested HA and light grey the short HA. The performance of the Kruskal-Wallis test followed by the Dunn's multiple comparison shows no significant difference between the species (Appendix E).
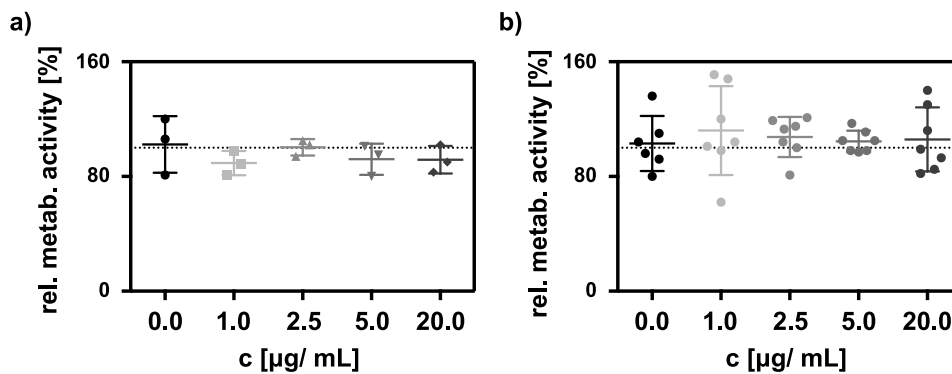
Figure 4.17.: Presentation of the metabolic activity of LECs (based on AlamarBlue®assay) normalised to the amount of DNA on the surface (based on CyQuant®assay) for a) using digested HA and b) an short HA. The performance of the Kruskal-Wallis test followed by the Dunn's multiple comparison shows no significant difference between the control and the different concentrations of the HA species ($p < 0.05$, Appendix E).

4.4.2. Comparison of the Impact of sHA in the Presence of cRGD

In a second step, the analysed system is transferred from cell culture plastic to glass surfaces with click-PEG, which is statistically modified with cRGD to enable cell adhesion. To prepare the surface, a glass slide is passivated

with a mixture of PEG_{2000}–silane (**8**) and PEG_{3000}–alkyne (**9**) in a ratio of 1:100 (click-PEG). Afterwards the click-PEG is functionalised with cRGD via CuAAC according to the protocol 2.9. 50 000 cells are seeded per glass surface, which is added to a 12 well-plate, with 600 µL media. The cells are incubated with 1.0, 2.5, 5.0 and 20.0 mg/L of the HA for 46 h at 37 °C and 5 %. In this case the short HA, the digested HA and their end-thiolated analogous are compared. To determine the HA influence the AlamarBlue® and CyQuant® assays are performed.

Do cells adhere differently when applying different concentrations and species of HA?

To determine the adhesion of the cells the amount of DNA per surface is detected via the CyQuant® assay. Therefore the permeabilised cells are incubated for 5 min with the kit and the fluorescence ($\lambda_{ex} = 540$ nm; $\lambda_{em} = 585$ nm) measured, corrected to the background and normalised to the control surface without HA.

In a first step the influence of the functionalised, digested HA in solution is determined (fig. 4.18 a). Here no significant difference between the control and the applied concentrations is observed. Although a small increased fluorescence signal is detected for a concentration of 5.0 µg/mL. Figure 4.18 b) shows the results of the measurements for the unfunctionalised, short HA. Here no significant change is observed as well. Nevertheless, a decrease in fluorescence intensity for a concentration of 2.5 µg/mL and an increase in fluorescence for 5.0 µg/mL compared to the mean value of the control is found. The mean values for the concentrations of 1.0 and 20.0 µg/L are comparable to the control level.

In a second step the terminal thiolated HA analogous are incubated with the cells and the CyQuant® assay is performed. Figure c) shows the fluorescence values for the application of the end-thiolated, digested HA. For the digested HA species no significant difference can be observed. For a concentration of 5.0 µg/mL a large distribution of the values is found. A possible explanation for this might be a damaged surface due to the freezing-process at −80 °C in the 12 well-plate to permeabilise the cells. If media or PBS, which was used for washing, remains under the glass slide it can break it during freezing. If the damage is clearly visible, the surface is not evaluated. Small damages, which can not be seen, falsify the result. Nevertheless, no significant difference between the concentrations is observed. For 20.0 mg/mL only one surfaces could be evaluated.

Do the different HA species influence the metabolic activity of LECs?

After incubating the cells with HA-containing medium for 46 h, 450 µL are removed and 55 µL AlamarBlue® kit are added. After 2 h the fluorescence of
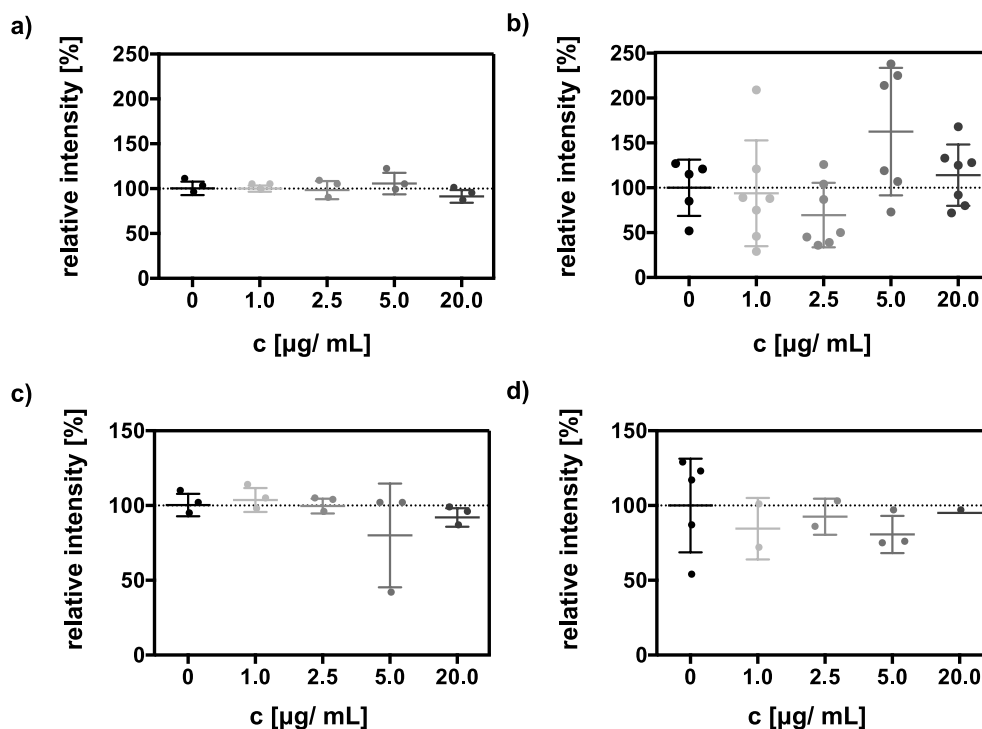
Figure 4.18.: Results of CyQuant®assay of unfunctionalised and end-thiolated HA in solution with LECs in a 12-well plate on glass surfaces, functionalised with click-PEG: a) for enzymatically digested HA, b) short HA, c) end-thiolated, digested HA and d) end-thiolated, short HA. The performed Kruskal-Wallis test followed by the Dunn's multiple comparison shows no significant difference between the used concentrations and the control (Appendix E). The results are baseline corrected and normalised to the average of the surfaces without HA.

the different solutions is measured. The comparison of the different applied concentrations of digested HA on click-PEG surfaces shows no significant difference ($p < 0.05$, Appendix E). The mean value of the treated samples shows a small decrease compared to the control (fig. 4.19 a). The lowest activity can be found for the sample treated with 2.5 mg/mL HA. In the cases of a higher as well as a lower concentrations of HA, the relative intensity is increasing. The same result is found for the cells, which are treated with the short HA species (fig. 4.19 b). Between the different concentrations no significant difference can be observed ($p < 0.05$, Appendix E), but a biphasic trend with its minimum for the sample with 2.5 mg/mL HA.

In the following the influence of the end-thiolated analogous are determined and compared to the results of the unfunctionalised HA species. Applying the end-thiolated, digested HA to the cells again no significant difference between the added amounts of HA are observed (fig. 4.19 c; Kruskal-Wallis test followed
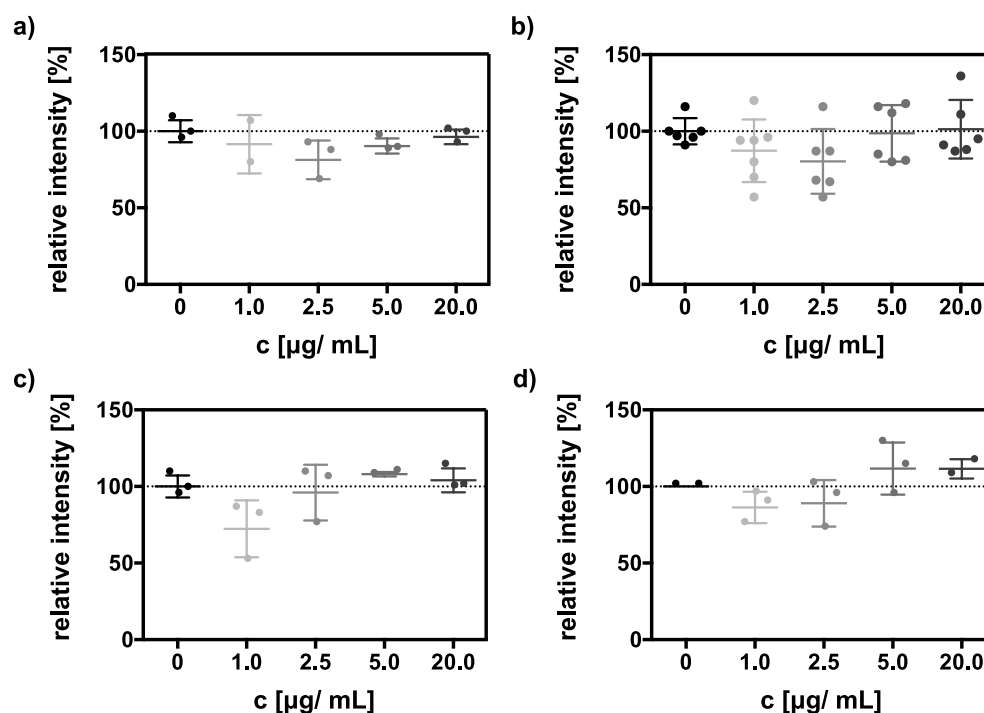
Figure 4.19.: Results of AlamarBlue®assay of unfunctionalised and end-thiolated HA species in solution with LECs in a 12-well plate on glass surfaces, functionalised with click-PEG: a) for enzymatically digested HA, b) short HA, c) terminal functionalised, digested HA and c) end-thiolated, short HA. The performed Kruskal-Wallis test followed by the Dunn's multiple comparison shows no significant difference between the different surfaces ($p < 0.05$, Appendix E). The results are baseline corrected and normalised to the average of the surfaces without HA.

by the Dunn's multiple comparison, $p < 0.05$, Appendix E). Compared to the unfunctionalised, digested HA a different trend can be seen. Here, the lowest mean intensity is found for 1.0 mg/mL. The value increases with increasing HA-concentration up to the level of the control. A similar trend is found for the end-thiolated, short HA (fig. 4.19 d). A decrease in the mean relative intensity for 1.0 and 2.5 mg/mL is observed, but the change is not significant. The mean value for 5.0 and 20.0 mg/mL is even higher than in the level of the control.

Finally, the four different HA-species are compared with each other. Therefore, the data is analysed sorted by concentration independent of the species (fig. 4.20). Here again the mean value for 1.0 and 2.5 mg/mL are below the control level whereas 5.0 and 20.0 mg/mL are at the comparable level. The performed Kruskal-Wallis test followed by the Dunn's multiple comparison ($p < 0.05$, Appendix E) shows no significant difference between the species as well

as between the different applied concentrations. This enables the summary of the data.
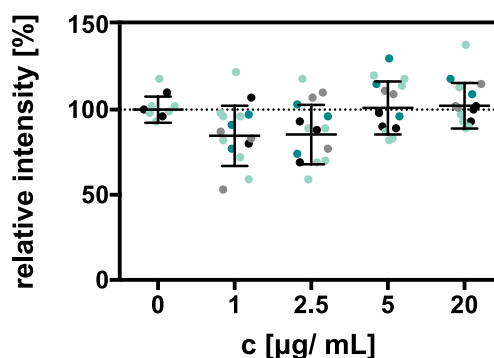
Figure 4.20.: The comparison of both used HA species show no difference in their impact. To compare the used HA-species all data is summarised in one plot, where black represents the digested HA without a thiol-function and light grey with the thiol-function, light blue the short HA without and turquoise with thiol-function. The performance of the Kruskal-Wallis test followed by the Dunn's multiple comparison shows no significant difference between the species (Appendix E)

Determination of the Relative Metabolic Activity

On click-PEG the same result as for the cell culture plastic is found. No significant difference in the CyQuant® and AlamarBlue® assay is found neither for the digested HA, the short HA nor their thiolated analogous. To reach a better comparability between the different samples the metabolic activity of different surfaces, the results of the AlamarBlue® assay, are normalised to the relative amount of DNA, which was measured via the CyQuant® assay. The performed Kruskal-Wallis test followed by the Dunn's multiple comparison shows no significant difference in the relative metabolic activity of the cells due to the different concentrations and functionalisation of HA (fig. 4.21). Although no significant difference between the applied concentrations can be observed, a biphasic trend is identifiable. The lowest mean for the relative metabolic intensity is found for adding 1.0 mg/mL.

4.4.3. Comparison of the Impact of Immobilised sHA in the Presence of cRGD

Finally, the two end-thiolated HA species are immobilised on gold nanostructured glass slides. Five different particle densities are used in this experiments: 29, 47, 123, 540 and 2714 particles/μm^2. The surfaces are compared to a surface without nanoparticles respectively without HA. The glass slides are
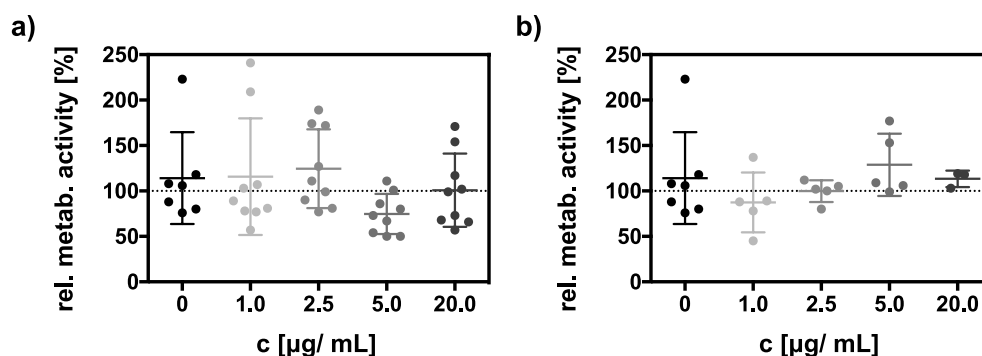
Figure 4.21.: Presentation of the metabolic activity of LECs (based on AlamarBlue®assay) normalised to the amount of DNA on the surface (based on CyQuant®assay) on click-PEG for a) using digested HA and b) a different short HA. The performance of the Kruskal-Wallis test followed by the Dunn's multiple comparison shows no significant difference between the control and the different concentrations of the HA species (Appendix E).

passivated against unspecific cell adhesion utilizing click-PEG, a mixture of PEG_{3000}−azide (**9**) and PEG_{2000}−silane (**8**) with a ration of 1:100, according the protocol in section 2.7. Afterwards cRGD-alkyne is attached to the azide via CuACC. The nanoparticles are functionalised with the thiolated HA-species by incubating the surface with a 0.004 % (w/v) solution of thiol for 1 h. After washing the surface with sterile PBS the surfaces are inserted in a 12 well plate and 50 000 cells are seeded in 1 mL media. The cells are incubated on the surface for 46 h at 37 °C and 5 % CO_2 before the assys are performed.

Do cells adhere differently when applying different concentrations and species of HA?

After washing and freezing of the cells on the surfaces 600 μL of the diluted CyQuant® kit are added. After the incubation for 5 min the fluorescence is measured ($\lambda_{ex} = 480$ nm; $\lambda_{em} = 520$ nm). The results are normalised to the mean value of the control surface without nanoparticles. This surface represent 100 % of DNA. In case of the digested HA-species no significant difference due to the various particle density can be determined (fig. 4.22). Although, a drop in the relative DNA amount with increasing particle density becomes apparent. This observed trend manifest in case of the short HA. A significant decrease in the relative DNA amount can be detected for 540 particles/μm^2 and even larger for 2710 particles/μm^2 compared to the control surfaces.

The decrease in the amount of DNA indicates a decrease in the number of cells on the surfaces. Because all surfaces statistically present the same amount of cRGD on the surface, the decrease in adhesion must be due to
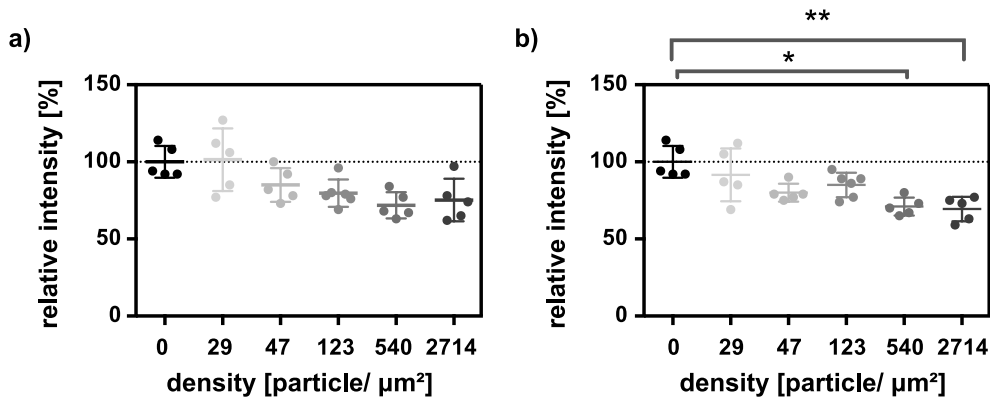
Figure 4.22.: Results of CyQuant®assay of immobilised, end-thiolated short HA with LECs in a 12-well plate on nanostructured glass surfaces, functionalised with click-PEG: a) for enzymatically digested HA and b) short HA. The performed Kruskal-Wallis test followed by the Dunn's multiple comparison shows a significant difference between the control surface without HA and the particle density of 540 and 2714 particle/cm^2. The results are baseline corrected and normalised to the average of the surfaces without HA.

the nanoparticles decorated with HA. The large HA molecule on the surface might cover some cRGD-groups respectively reduces the accessibility of it. As a consequence less cells can adhere to the surface.

Do the different HA species influence the metabolic activity of LECs?

For the AlamarBlue® assay 450 µL media are removed per well after 46 h and 55 µL of the kit are added. After an incubation time of 2 h the fluorescence (λ_{ex} =540 nm; λ_{em} =585 nm) is measured. The results are normalised to the mean value of the control surfaces as described before (fig. 4.23). In case of the digested HA species a significant drop in the relative intensity between control and the surface with the highest particle respectively HA density is observed. The same result is found for the short HA species. The significant decrease in the relative intensity is larger in case of the digested HA than for the short HA. Both cases show the lowest metabolic activity for the highest particle density. In case of the short HA species the comparison between the mean values of the relative intensity show almost no difference between the surface without and the lowest concentration of short HA. Then the intensity decreases for 47 particles/µm^2, normalises to the control level and drops to its lowest value for 2714 particles/µm^2. The direct comparison between the two HA-species shows no significant difference between the two species (fig. 4.24). Because no significant difference between the species can be found, the results can be combined.
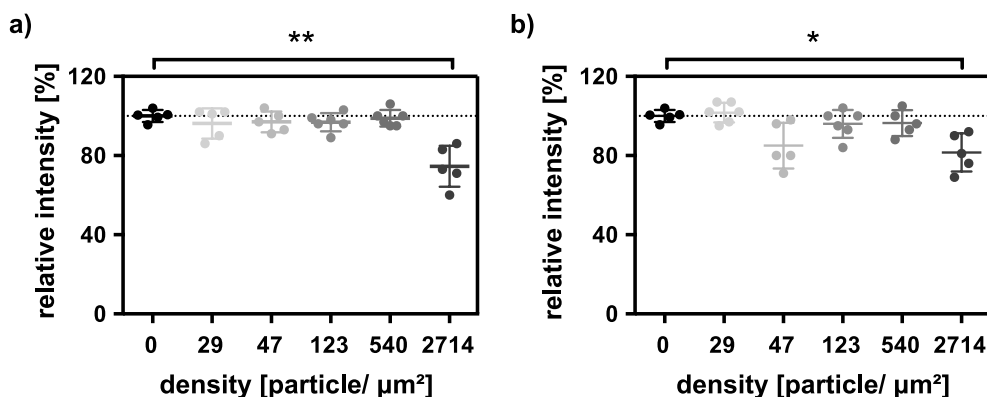
Figure 4.23.: Results of AlamarBlue®assay of immobilised, end-thiolated HA with LECs in a 12-well plate on nanostructured glass surfaces, functionalised with click-PEG: a) for enzymatically digested HA and b) short HA. The performed Kruskal-Wallis test followed by the Dunn's multiple comparison shows a significant difference between the control surface without HA and a particle density of 2714 particle/cm^2. The difference is larger in case of the digested HA (**) than the short HA (*). The results are baseline corrected and normalised to the average of the surfaces without HA.
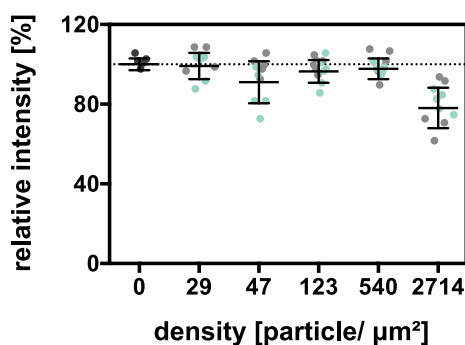
Figure 4.24.: The comparison of both used HA species show no difference in their influence. To compare the used HA species all data is plotted in one figure, where black represents the control, grey the enzymatically digested HA and light blue the short HA. The performance of the Kruskal-Wallis-test followed by the Dunn's multiple comparison shows no significant difference between the two HA species (Anhang)

Determination of the Relative Metabolic Activity

The results of these experiments show that it is important to take the attachment capability of the cells to the used surface into account when investigating the metabolic activity of the cells. As well for the digested HA as the short HA a decrease in the metabolic activity for a high particle density is found. But the results of the CyQuant® assay show, that the amount of cells is decreasing

as well with rising particle density. In the case of the short HA in a significant manner. Due to this, the results of the AlamarBlue® assay are normalised to the relative amount of DNA on the corresponding surface, to enable a comparison between the different surfaces and experiments. After normalising the
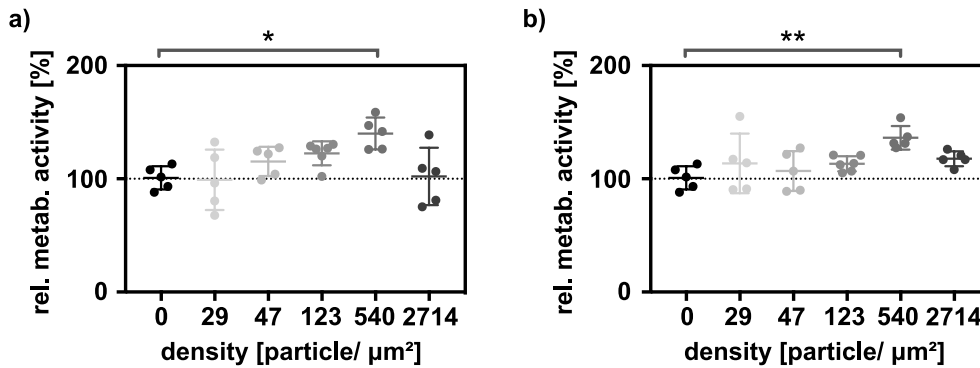
Figure 4.25.: Presentation of the relative metabolic activity of LECs (based on AlamarBlue®assay) normalised to the relative amount of DNA on the surface (based on CyQuant®assay) for a) the enzymatically digested HA and b) the short HA. To analyse the significance of the results a Kruskal-Wallis test followed by the Dunn's multiple comparison (p < 0.05, Appendix E).

metabolic activity to the amount of DNA the picture changes. Instead of a decreasing trend, now a biphasic development is found (fig. 4.25). The relative metabolic activity increases for both HA-species with increasing particle respectively HA density up to 540 particles/cm^2. Afterwards it decreases again. Only the difference between the point of inflexion and the control is found to be significant different (Kruskal-Wallis test followed by the Dunn's multiple comparison, p < 0.05, Appendix E). The level of significance is identified higher in case of the short HA than the enzymatically digested HA.

Summary of the analysis of the influence of short HA on human primary lymphendothelial cells

Compared is the influence of a digested and short HA species which are applied to LECs in different concentrations and densities. Between the different species no difference in the cell behaviour is found. In the case of the application of HA in solution no difference in the relative metabolic activity is found. For the immobilised HA species a reduced ability to adhere to the surface is found for the rising nanoparticle density. Here for both HA species a biphasic effect in relative metabolic activity is found with maxima for a particle density of 540 /μm^2.

4.4.4. Influence of Immobilised sHA on the Clustering and Adhesion of LECs

The previous experiments show the largest impact of immobilised, short HA on the cells, when it is immobilised on a nanostructured surface with a particle density of $540\,particles/\mu m^2$. To investigate other effects than the metabolic activity, a closer look is taken at the cells themselves. Therefore cells are seeded again on a surface passivated with a mixture of PEG_{2000}−silane (**8**) and PEG_{3000}−alkyne (**9**, ratio 1:100) functionalised with cRGD with no nanoparticles and $540\,particles/\mu m^2$. After 48 h the cells are fixed and several proteins, which are part of the adhesion complex, the actin cytoskeleton and the nuclei are stained. The proteins talin, paxillin and vinculin are chosen to enable the investigation of a difference in adhesion between both surfaces. Additionally, the main HA receptor in lymphendothelial cells LYVE-1 is analysed. To achieve a good staining, different antibodies and concentrations are applied (section 2.11). The evaluation of the staining shows no staining for neither talin, paxillin, vinculin nor LYVE-1. So no suitable antibody could be found for an ICC staining of LECs.
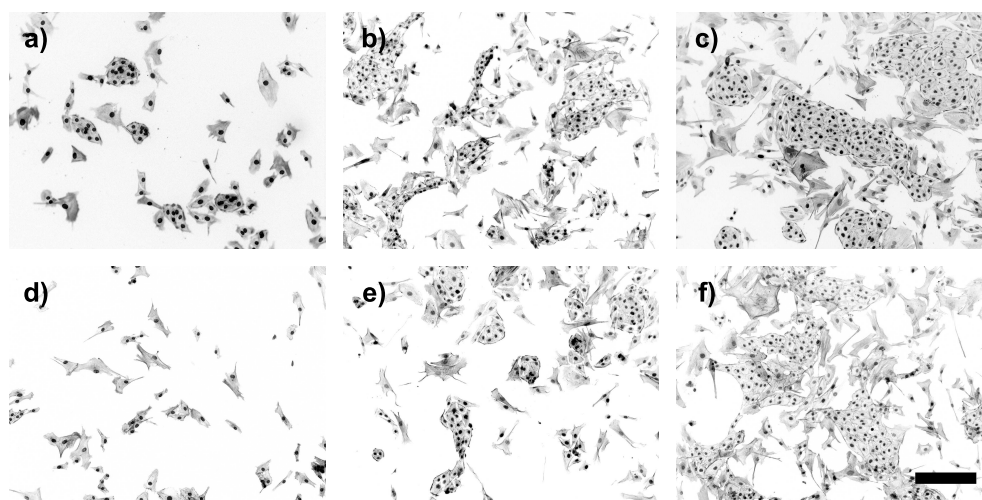
Figure 4.26.: To analyse the influence of immobilised HA on LECs the actin cytoskeleton (grey) and nuclei (black) are stained. Compared are the appearance of cells on a surface with a particle density of $540\,particles/\mu m^2$ (a) - c)) and without immobilised HA (d) - f)). All pictures have the same scaling (scale bar: $200\,\mu m$).

In figure 4.26 examples are shown for the actin and nuclei staining on surfaces with and without hyaluronan. No difference can be seen between both surface species. To analyse if more or less cells adhere on one surface type, the number of nuclei is counted on each surface using ImageJ. Because of a semi-automatic analysis the results are compared to a manual counting for 5

surfaces (tab. 4.2).

Table 4.2.: Evaluation of the used semi-automatic counting of nuclei on a surface using ImageJ.

counting	I	II	III	IV	V
manual	85	84	143	150	148
automatic	85	84	132	145	149
difference	0	0	11	5	-1
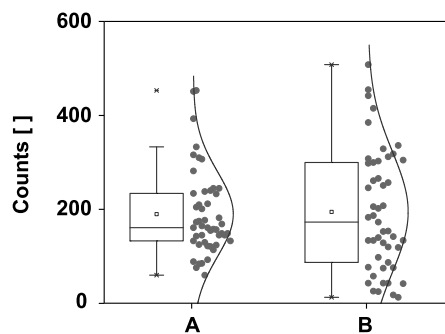
Figure 4.27.: The analysis of the number of LECs on surfaces with (A) and without (B) immobilised HA show no difference in the number of cells.

Also the analysis of cell number per surface shows no difference between the surfaces with and without immobilised HA (fig. 4.27). Although a larger distribution for the surface without HA is found. The clear decrease in number of cells on the surface which is found in the CyQuant® assay is not observed here.

Because it is not possible to use a scratch assay or a physical barrier the observation of the migration of the cells is difficult. The comparison of HA-free surface and a nanostructured surface with a particle density of $540\,/\mathrm{\mu m^2}$ shows no difference in the number and the appearances of the cells.

4.5. Influencing Collective Cell Migration

The aim of the second part is to study the influence of the cell adhesion on their migration behaviour. Therefor nanostructured surfaces with different interparticle distances are used, which were functionalised with an adhesive background. The used surfaces are prepared according to the protocol in section 2.8. Afterwards the surfaces are passivated using $\mathrm{PEG_{2000}}$−silane (**8**). The adhesive molecule is immobilised on the gold nanoparticles via a thiol function.

To create a defined collective of cells a photocleavable molecule is used to im-
mobilise on the gold nanoparticles. After partial irradiation with UV light, the
cells are able to adhere on cleaved molecules (fig. 4.28). After the cells become
confluent, the migration starts with a second irradiation step, which makes the
whole surface adhesive. Therefore two novel linker molecules are developed to
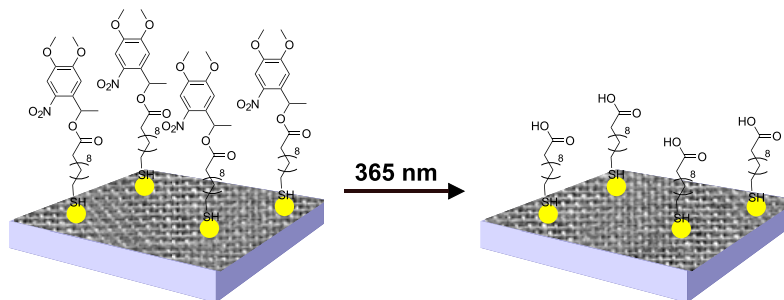
Figure 4.28.: Scheme of the surface applied in the study to investigate the
influence of the density of an adhesive background on MDCK II cells. The
glass surfaces is decorated with gold nanoparticles with different particle
densities and passivated with **8**. The nanoparticles are functionalised with **1**,
which can be cleaved using UV light to enable the adhesion of cells.

analyse unspecific as well as specific surface-integrin interactions (fig. 4.29). To
achieve an unspecific interaction 11-mercaptoundecanoic acid (**7**) is used where
the carboxy-group caged with the photolabile ligand 4,5-Dimethoxy-2-nitroace-
tophenone (DMNPE, **2**, a). To aim a specific interaction between surface and
cells, the artificial antagonist (*S*)-3-(4-(3-(6-(3-mercaptopropanamido)hexan-
amido)propoxy)benzamido)-4-(4-(3-((4-methoxypyridin-2-yl)amino)propoxy)
phenyl)butanoic acid (**13**) to the integrin $\alpha_5\beta_1$ is used.[21, 22] Here as well the
carboxy-group is caged with DMNPE (**2**) to prevent the specific interaction
with integrins (b).

4.5.1. Synthesis of 1-(4,5-dimethoxy-2-nitrophenyl)ethyl 11-mercaptoundecanoate (1)

The synthesis is started with a nitration of 3,4-dimethoxyacetophenone per-
formed in fuming nitric acid and glacial acetic acid (ratio 1:10; scheme 4.6).
This mild condition for the nitration can be used due to the directing effects
of the carbonyl- (-M and -I effect) and the methoxy-groups (+M and -I effect),
which enable the further substitution of the already highly substituted ben-
zene. The yellow product is crystallised by pouring the reaction solution on
ice. Because the solid is very fine the ice is kept at 4 °C to allow the crystals
to grow. After recrystallisation from acetone and filtration over silica gel the
yellow 4,5-dimethoxy-2-nitroacetophenone (**10**) can be isolated with a yield of
67 %. The NMR-spectra shows that no further purification is required.
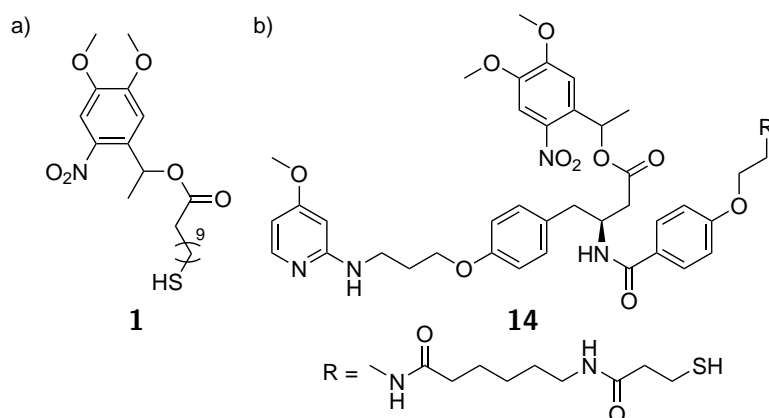
Figure 4.29.: Noval photolabile linker for the a) unspecific (1-(4,5-dimethoxy-2-nitrophenyl)ethyl 11-mercaptoundecanoate **1**) and b) specific (1-(4,5-dimethoxy-2-nitrophenyl)ethyl ($3(S)$)-3-(4-(3-(6-(3-mercaptopropan-amido)hexanamido)propoxy)benzamido)-4-(4-(3-((4-methoxypyridin-2-yl)amino)propoxy)phenyl)butanoate **14**) interaction with the integrin $\alpha_5\beta_1$.
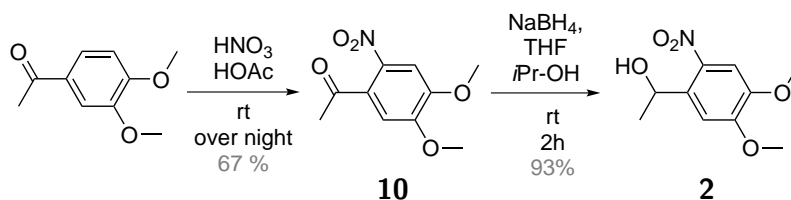
Scheme 4.6.: Schematic representation of the synthetic route to 1-(4,5-di-methoxy-2-nitrophenyl)ethan-1-ol (**2**) starting from 3,4-dimethoxyacetophe-none via 1-(4,5-dimethoxy-2-nitrophenyl)ethan-1-one (**10**).

In a second step the carbonyl-group of the acetophenone-body is hydro-genated using sodium borohydride. Because of this rigorous washing and re-crystallisation of **10** is required to remove the acid and prevent the reaction of acid and borohydride. The hydrogenation is performed in a mixture of 1-propanol and THF (ratio 2:1). During the reaction the colour of the reaction solution changes from yellow to red, which indicates the end of the reaction. After column chromatography the product is isolated with a yield of 93 % (scheme 4.6).

Before 11-mercapto-undecanoic acid (**7**) can be coupled to DMNPE (**2**) the thiol-group needs to be protected using a trityl-group (scheme 4.7). Therefor **7** is stirred with trityl chloride according to a protocol of Ryan *et al.*[75] The purification via column chromatography proves to be difficult due to the very similar R$_f$-values in various eluents (table 4.3). Additionally the NMR shows
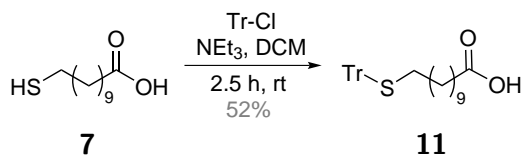
Scheme 4.7.: Protection of the thiol-group of 11-mercaptoundecanoic acid (**7**) with trityl chloride.

the presence of the side product trityl 11-mercaptoundecanoate (**11**), which is the trityl-protection at the carboxy-terminus of the molecule. The retention times of the two trityl protected species seems to be very similar. Due to the difficulty of the purification, the raw product is filter over silica to remove the unreacted acid. After removing the solvent, the resulting mixture is used for the next step. The yield of **11** is calculated from the NMR with 52 %.

Table 4.3.: Summary of the retention times (R_f) for the tested eluents for column chromatography of **11**. Compared are the values for the two educts 11-mercaptoundecanoic acid (**7**) and trityl chloride (Tr−Cl) with the product **11**.

#	eluent	R_f		
		Tr−Cl	7	11
1	DCM/ MeOH 95:5	0.79	-	0.79
2	DCM/ MeOH 6:1	0.75	0.53	0.77/ 0.84
3	DCM/ MeOH 5:1	0.76	0.54	0.77/ 0.82
4	hexane/ EtOAc 3:1	0.44	0.21	0.15
5	hexane/ EtOAc 2:1	0.43	0.20	0.43/ 0.49
6	hexane/ EtOAc/ MeOH 3:1:0.04	0.32	0.03	0.38/ 0.45

Finally **2** is coupled to **11** via Steglich esterification (scheme 4.8).[67] The carboxylic acid is activated using DCC. Because of the minor reactivity of the hydroxy group compared to amines a catalyst is necessary for the final ester formation. 4-*N*,*N'*-dimethylaminopyridine (DMAP) is used as a catalyst in this reaction. The carboxy group is transferred to the catalyst, which enables the formation of the ester bond. As a side reaction an acyl migration is found, which leads to the formation of *N*-aceylureas. This reaction is slow and can be minimised with an excess of nucleophile.[129] After extracting the product with CHCl$_3$, the raw product is purified via column chromatography. The yellow, crystalline product can be isolated with a yield of 33 %.

After the esterification, the thiol-group is deprotected using a mixture of trifluoroacetic acid (TFA), ddH$_2$O and triisopropylsilane (TIPS) in a ratio of 95.0:2.5:2.5.[21, 22] The reaction is quenched with ddH$_2$O and the product
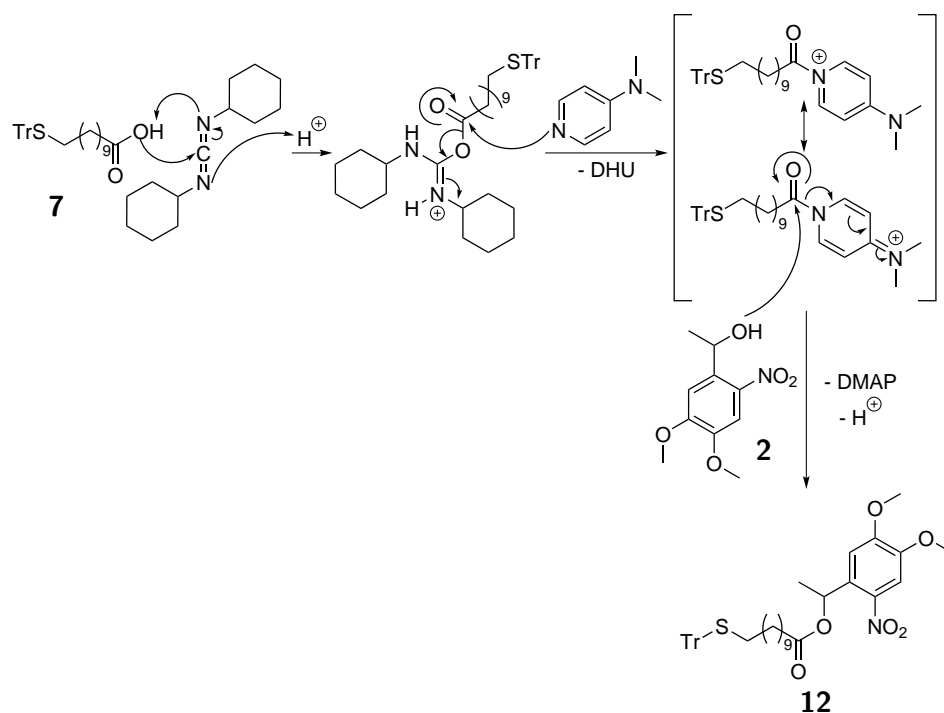
Scheme 4.8.: Reaction scheme of the Steglich esterification: The carboxy group of 11-mercaptoundecaonic acid (**7**) is activated using DCC. Afterwards the acid is transfered to the catalyst DMAP under the release of 1,3-dicyclohexylurea (DHU), which enables the coupling to the hydroxy group of **2**.

extracted with $CHCl_3$. The raw product is purified via column chromatography. The yellow 1-(4,5-dimethoxy-2-nitrophenyl)ethyl-11-mercaptoundecanoate (**1**) can be isolated with a yield of 89 %.

4.5.2. Characterisation of 1-(4,5-dimethoxy-2-nitrophenyl)ethyl 11-mercaptoundecanoate (1)

To analyse the cleavage behaviour of the 1-(4,5-dimethoxy-2-nitrophenyl)ethyl-11-mercaptoundecanoate (**1**), the change in UV-VIS spectra during irradiation is determined. Additional the absorption, cleavage and passivation properties are observed using QCM-D.

Observation of the Cleavage of 1-(4,5-dimethoxy-2-nitrophenyl)ethyl 11-mercaptoundecanoate via UV VIS Spectroscopy

To analyse the cleavage behaviour of **1**, a 1 mM solution in acetonitrile is prepared. The solution is irradiated with a laser (375 nm, 800 µW) in a black,

Scheme 4.9.: Scheme of the coupling of 1-(4,5-dimethoxy-2-nitrophenyl)ethan-1-ol (**2**) with 11-(tritylthio)undecanoic acid (**11**) followed by the deprotecting to 1-(4,5-dimethoxy-2-nitrophenyl)ethyl 11-mercaptoundecanoate (**1**).

closed quartz cuvette. Compared are **1** and uncoupled **2**. The adsorption spectra of both compounds are recorded from 250 to 500 nm, starting before irradiation and then after every 10 min interval up to 70 min of irradiation. All spectra are corrected to the background, in this case the cuvette with pure acetonitrile. The observation of the cleavage of **2** shows a rapid red shift of the the maxima from 347 nm to a plateau at 375 ± 5 nm (fig. 4.30). The largest

Figure 4.30.: The cleavage of a 1 mM solution of uncoupled **2** in acetonitrile shows a red shift in the UV VIS spectra over time. The first measurement was obtained before the irradiation (t_0, black) with a 375 nm laser (800 μW). Afterwards the spectra is obtained in intervals of 10 min over 30 min. An isobestic point is localised at 319 nm (green dotted line).

change in the absorbance spectrum is found after the first irradiation step. This indicates, that the cleavage process is fast and almost complete. After 20 min no further conversion is observed. This proves, that the cleavage is finished

within the first 20 min. Additionally, an isobestic point is observed at 319 nm. This shows, that only a two compound mixture takes part in the cleavage. In
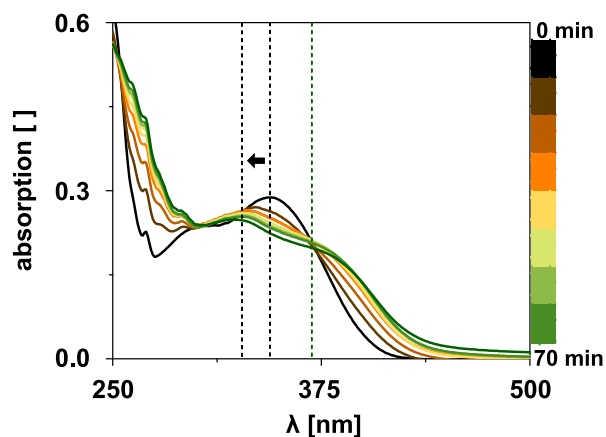
Figure 4.31.: The cleavage of a 1 mM solution of **1** in acetonitrile shows a blue shift in the UV VIS spectra over time. The first measurement was obtained before the irradiation (t$_0$, black) with a 375 nm laser (800 μW). Afterwards the spectra is obtained in intervals of 10 min over 70 min. An isobestic point is localised at 370 nm (green dotted line).

contrast, the irradiation of the **1** shows a blue shift in the absorbance maxima from 345 nm towards 322 nm(fig. 4.31). Here still a change in the absorbance maxima is found after 20 min. The cleavage is complete after 60 min, because no further difference in the last spectra is found. In this case an isobestic point is localised at 370 nm, which underlines that only a two component mixture takes part in the cleavage. This correlates to the postulated mechanism of the cleavage.

The change in the observed spectra of **2** is due to a photo-induced reaction (scheme 4.10). Bochet *et al.* postulate that the irradiation leads to the formation of a diradical, which can be quickley delocalised, and a rearrangement, which results in an isoxazolidin-derivative.[59] This molecule can decay spontaneously under the elimination of H$_2$O respectively **7**, to 1-(4,5-dimethoxy-2-nitrosophenyl)ethan-1-one. This leads to the change in the adsorption spectra. This also indicates a slower photoreaction for the **1** linker, because the increase in size enhances the steric hindrance of the rearrangement. This observation also proves that a cleavage is possible even though no functionality is attached to the **2** and only H$_2$O is eliminated. In case of the **1**, R' corresponds to **7**, which will remain on the surface after cleavage in further experiments on a surface.

The major difference is found for the time frame, which is needed to cleave the molecule. For **2** the reaction takes about 20 min, the reaction of **1** is finished after 60 min. Due to the observed isobestic point a direct equilibrium between
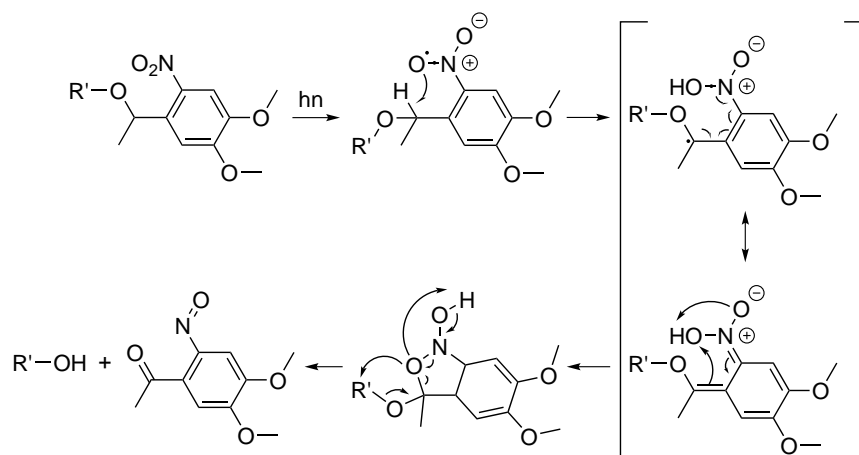
Scheme 4.10.: Postulated mechanism of the cleavage process of DMNP-derivative for the example of DMNPE (R': H, HS$-$(CH$_2$)$_9$$-C=$O). The mechanism shows the formation of a diradical due to the irradiation and the rearrangement to isoxazolidin-derivative. This can spontaneously decay to H$_2$O and the acid and **2**.[59]

educt and product is observed, which fits to the postulated mechanism.

Observation of the Adsorption and Cleavage of 1-(4,5-dimethoxy-2-nitrophenyl)ethyl 11-mercaptoundecanoate (1) via QCM-D

In the QCM-D experiment the adsorption of the 1-(4,5-dimethoxy-2-nitrophenyl)ethyl 11-mercaptoundecanoate (**1**) is compared to the adsorption of 11-mercaptoundecanoic acid (**7**) and DMNPE (**2**). Therefore, a gold coated quartz crystal is equilibrated in PBS with 1 % EtOH and 100 µM solution of the different tested compounds are added. The EtOH is added because the **1** is not soluble in water. The pure **2** shows no interaction with the surface as expected because **2** shows no functional group which would bind strongly to the gold surface. In case of the adsorption of **7** a $\Delta(\Delta f_7)$ of 44 Hz is determined (fig. 4.32 a). The adsorption of the complete **1** linker leads to a change in frequency of 161 Hz (fig. 4.32 a). It is noticeable that the time, which is necessary to form the monolayer on the surface varies significant between 11-mercaptoundecanoic acid (**7**) and 1-(4,5-dimethoxy-2-nitrophenyl)ethyl 11-mercaptoundecanoate (**1**). The adsorption of the free acid takes 10 min and the adsorption of the linker seems still not complete after 24 h. Because the adsorption takes over night a large drift is found. Even though the open module is closed with a lid to prevent evaporation of the solvent, the volume of the solvent on the crystal decreases slightly over night. To correct the effect of the drift, the results of the control surface can be subtracted from the other

Figure 4.32.: Observation of the successful adsorption and cleavage of **1**. In this study the adsorption a) of **1** (Δf: light green; ΔD: orange) is compared to the adsorption of **7** (Δf: green; ΔD: light brown) and a pure gold surface (Δf: dark green; ΔD: dark brown) and b) the behaviour under UV irradiation (365 nm). The QCM-D experiments is performed in PBS with 1 % EtOH. Shown is the 7th overtone.

samples. After changing the PBS/EtOH mixture after 24 h, the system equilibrates again and a good baseline is found for the control surface (fig. 4.32 b) Afterwards, the crystal is irradiated with UV light (365 nm) to perform the cleavage. Therefor, a UV hand-lamp is placed over the open modules, which are covered with a quartz glass slide to prevent evaporation of the solvent. In case of the acid no change in frequency can be observed, so no cleavage occurs. In contrast, an in increases of frequency of $\Delta(\Delta f_7) = (68.7 \pm 7.6)$ Hz is observed for the cleavage of **1**. After cleavage, the change in frequency on this surface is still larger than on the surfaces with **7**. This can be explained trough an incomplete cleavage or a difference in the formation of the SAM on the surface due to the aromatic ring, which can disturb the packing.[122] The last point is reflected in the extremely different adsorption times.

Characterisation of the Adsorption Process of 1-(4,5-dimethoxy-2-nitrophenyl)ethyl 11-mercaptoundecanoate (1)

QCM-D based analysis of the adsorption of 1-(4,5-dimethoxy-2-nitrophenyl)-ethyl 11-mercaptoundecanoate (**1**, c = 100 µM, 21 °C; fig. 4.33 a) takes much longer compared to the SAM formation of the OEG-layer on a gold surface in the previous QCM-D experiments (c = 100 µM, 24 °C; section 4.1).[54] In literature a time frame between 12 to 18 h is found for the SAM formation of alkanethiols (c = 1 to 10 mM) on gold in ethanol at room temperature. [122] Because of this difference in the adsorption time, it is analysed if the process takes several steps to form the SAM. Due to the poor solubility of the linker in water, a stock solution in ethanol is prepared and diluted into water.

Thus, the formation of micelles of the linker after diluting is conceivable. This micelles would descend to the surface, which would lead to a first change in frequency, burst and form a SAM comparable to the formation of a supported lipid bilayer (SLB), which would lead to another change in frequency. Because both layers on the surface show different viscous properties two changes in dissipation are expected as well. To analyse this correlation the change in dissipation (ΔD) is plotted against the change in frequency (Δf; fig. 4.33 b). The figure shows a linear correlation between dissipation and frequency, which proves the single-step SAM formation.

Figure 4.33.: To verify a single step absorption of **1** the change in frequency and dissipation in a QCM-D experiment is used. Due to a drift, which occurs over night, the adsorption process is corrected to the control surfaces (a). The plotting of the change in dissipation (ΔD) against the change in frequency (Δf_n) shows a linear correlation between the two parameters and so a single-step process (b). The linear fit (Pearson R = -0.997 88) is shown in grey.

To characterise the adsorption in a timely manner, the adsorption is corrected to the control, due to the drift, which occurs over night (fig. 4.33 a). After the correction a plateau is observed after 24 h and so a kinetic analysis is possible. Additionally the adsorption is observed and compared at 21 °C and 37 °C (table 4.4). The found results show a change in the adsorption de-

Table 4.4.: The adsorption of 1-(4,5-dimethoxy-2-nitrophenyl)ethyl 11-mer-captoundecanoate (**15**) observed during a QCM-D experiment is fitted with $y = y_0 + A_1 exp\left[-\frac{x}{t_1}\right] + A_2 exp\left[-\frac{x}{t_2}\right] + \cdots$. The decay times and the ratio of the amplitudes A are summarised below.

Temperature	t_1 [min]	t_2 [min]	ratio A_1 [%]
21 °C	83.03±68.17	1899.00±776.3	20.6±15.7
37 °C	320.88±58.36		98.6±2.0

pending on the temperature like expected.[122] The first thing that is apparent is the difference in the fitting function (Appendix G). Therefore, the decay in-between two pipetting steps (liquid exchange) is fitted with an exponential decay function. The decay at 21 °C could be fitted with a bi-exponential decay, while at 37 °C, only a mono exponential fit was sufficient. The comparison of the specific decay times show a fast and a slow process for 21 °C. The amplitude of the fast component A_1 of 20.6 % means that this component is only of minor importance to describe the decay and can be neglected. Therefore, only the main decay components can be compared. The decay time for 37 °C is roughly 6-fold shorter than the decay time for 21 °C.

Characterisation of the Cleavage Properties of
1-(4,5-dimethoxy-2-nitrophenyl)ethyl 11-mercaptoundecanoate (1)

Figure 4.34.: To verify a single step cleavage of **1** the change in frequency and dissipation in a QCM-D experiment is used. To reduce drift effects the cleavage process is corrected to the control surfaces (a). The plotting of the change in dissipation (ΔD) against the change in frequency (Δf_n) shows a linear correlation between the two parameters and so a single-step process (b). The linear fit (Pearson R = -0.999 61) is shown in grey.

To analyse the specific decay time of the cleavage the data is corrected to the control to reduce drift effects during the measurement (fig. 4.34 a)). Additionally, to ensure a single-step process, which is already forecast through the UV VIS analysis, the dissipation is plotted against the frequency change (b). As expected a linear correlation is found between dissipation and frequency which points to a single-step process. The cleavage is performed at 21 °C and shows like the adsorption a exponential correlation with two components (Appendix G). Here the increase in frequency can be described best with equation 4.1. Again, the decay is fitted in-between two exchange steps of the solvent. For the evaluation of the change in frequency in the QCM-D experiment a plateau of at least 5 min is used, so in some circumstances a long linear segment is

part of the otherwise exponential progression, which complicates the fitting.

$$y = y_0 + A_1 exp\left[-\frac{x - x_0}{t_1}\right] + A_2 exp\left[-\frac{x - x_0}{t_2}\right] \qquad (4.1)$$

Again a very fast process with $t_1 = (2.52 \pm 0.64)$ min and a slow process with t_2 = (23.55 ± 7.38) min are found. The ratio between the two amplitudes shows a large impact of the first process to the curve shape $(\bar{x}(\frac{A_1}{A_1+A_2}) = 76.4 \pm 2.7$ %). The slower process might be due to the plateau formation, which is necessary for the evaluation of the data as described above and the fast process the actual cleavage.

Analysis of the Passivation Properties of
1-(4,5-dimethoxy-2-nitrophenyl)ethyl 11-mercaptoundecanoate (1)

To ensure that the surface decorated with 1-(4,5-dimethoxy-2-nitrophenyl)-ethyl 11-mercaptoundecanoate (**1**) is passivated against unspecific interaction in the first place and changes this behaviour after the cleavage, the surface is incubated with BSA. Compared is a pure gold surface, a surface with 11-mercaptoundecanoic acid (**7**) and two surfaces with **1** (table 4.5). After the adsorption phase, the surfaces are rinsed with 0.4 % BSA in PBS. A large change in frequency is observed for the control surface $(\Delta(\Delta f_7) = -31$ Hz; # 4), whereas only a small change is found for the acid and DMNPE (**2**) surface (# 5,6). The irradiation leads only to a desorption in case of the **1** $(\Delta(\Delta f_7) =$ 38 Hz, #9). The second incubation step with 0.4 % BSA causes a $\Delta(\Delta f_7)$ of -15 Hz (# 12) for the now adhesive **1** surface. For the other surfaces only a small decrease is observed, which is due to the adsorption of BSA onto the BSA layer or the replacement of destroyed BSA after the UV irradiation.

The analysis of the passivation properties of **1** show a small adsorption of BSA on top of the SAM $(\Delta(\Delta f) = -8$ Hz; # 6). After cleavage a $\Delta(\Delta f)$ of -15 Hz (# 12) is observed. The change in frequency for **7** is in total about -13 Hz (# 5, 11) in two steps. So the BSA can adhere better on the cleaved **1** surface.

Characterisation of the Hydrophilicity of a
1-(4,5-dimethoxy-2-nitrophenyl)ethyl 11-mercaptoundecanoate (1)
Decorated Surface

To characterise the hydrophilicity of a gold surface functionalised with 1-(4,5-dimethoxy-2-nitrophenyl)ethyl 11-mercaptoundecanoate (**1**) before and after cleavage of the linker the water contact angle (Θ_w) is measured. Therefore, a glass surface is coated with a thin layer of titanium (3 nm) and of gold (30 nm). Afterwards, the surface is incubated for 2 h with a 100 µM solution of **1**. The surface is washed with water, dried under a stream of nitrogen and the contact angle is measured with a drop of 1 µL water. Compared are the angles on pure

Table 4.5.: Shown are the change in frequency $(\Delta(\Delta f_7))$ for the interaction of BSA with an unfunctionalised (control), an 11-mercaptoundecanoic acid (**7**) and an 1-(4,5-dimethoxy-2-nitrophenyl)ethyl 11-mercaptoundecanoate (**1**) functionalised gold surface before and after irradiation with UV light (365 nm), as well as the change due to the irradiation.

#	phase	sample	$\Delta(\Delta\mathbf{f_7})$ [Hz]
1		control	-31
2	BSA	**7**	-5
3		**1**	$-8/\ -9$
4		control	1
5	cleavage	**7**	-2
6		**1**	$31/\ 46$
7		control	-4
8	BSA	**7**	-8
9		**1**	$-15/\ -14$

gold and on the SAM formed by **1**. Then the surface is irradiated with UV light (365 nm) for 60 min and the contact angle determined again.
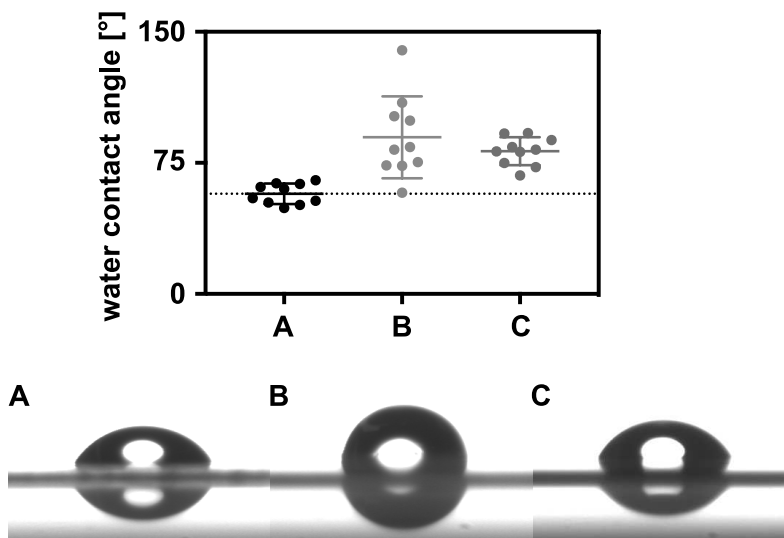
Figure 4.35.: Change in water contact angle of a gold coated surface (A) functionalised with 1-(4,5-dimethoxy-2-nitrophenyl)ethyl 11-mercaptoundecanoate (**1**) before (B) and after the irradiation with UV light (365 nm, C). Measured are 5 points on two surfaces with 1 µL water.

The measured contact angles show an increase in Θ_w after the functionalisation with **1** (fig. 4.35). After the irradiation the contact angle decreases again.

This is due to the end group of the SAM which changes from the aromatic ring, which is hydrophobic, to an carboxy group, which is more hydrophilic than the aromatic ring.

4.5.3. Toxicity Study

Before the cell experiments are performed, the set up is screened for possible risks for the cells. Problematic are on the one hand the irradiation with UV light and on the other hand the contact with chemicals with unknown characteristics. Even though the surfaces are washed after the irradiation, the cells get in contact with the cleavage products. To investigate a possible influence of this on the cell behaviour, the metabolic activity is determined by using the AlamarBlue® assay.

Establishment of the AlamarBlue® assay with MDCK II Cells

Before using the AlamarBlue® assay with MDCK II cells, the settings need to be optimised. Therefore 1000, 5000, 10000, 20000, 30000 and 40000 cells were seeded in a 96-well plate. After 18 h incubation at 37 °C and 5 % CO_2, the AlamarBlue® kit is added to each well with 100 μL medium. The absorbance is measured at 570 nm and 600 nm. The relative reduction of resazurin is calculated using equation 2.6 (section 2.10.1) and the results shown in figure 4.36. The data indicates a linear range between 0 to 4 h for a cell number below 20 000 cells per well (a). The absorbance plotted against the incubation time depending on the cell number shows a optimal incubation time between 1 to 2 h and a number of cells between 1000 to 10 000 (b), which is in good agreement with the first estimated parameters. For the following experiments an incubation time of one hour and a number of 5000 cells per well (156 cells/mm^2) is chosen.

Analysis of Toxicity of UV light

For the cleavage of the linker the surface needs to be irradiated with UV light, which can damage the cells. The influence of UV-irradiation on MDCK II cells is analysed. Therefor, 5000 cells are seeded in a 96 well plate. After 18 h the cells are irradiated using a X-cite UV-lamp, a microscope with a BFP-filter set (Excitation: 377/28 nm; Beamsplitter: 403 nm; Emission: 464/100 nm) and a 20x magnification. The samples are irradiated for 0, 15, 30 and 60 s. Afterwards, 100 μL media are removed and 10 μL AlamarBlue® kit are added. Then, the absorbance is measured at 570 and 600 nm. Because Sauer *et al.* report that the influence of irradiation on cells can even occur after several hours after the irradiation,[90] the absorbance is measured after 1, 2 and 3 h. The relative reduction of resazurin is calculated according to equation 2.6 (section 2.10.1). The comparison of the different time points, represented by the different colours in the scatter plot (fig. 4.37), do not show a significant
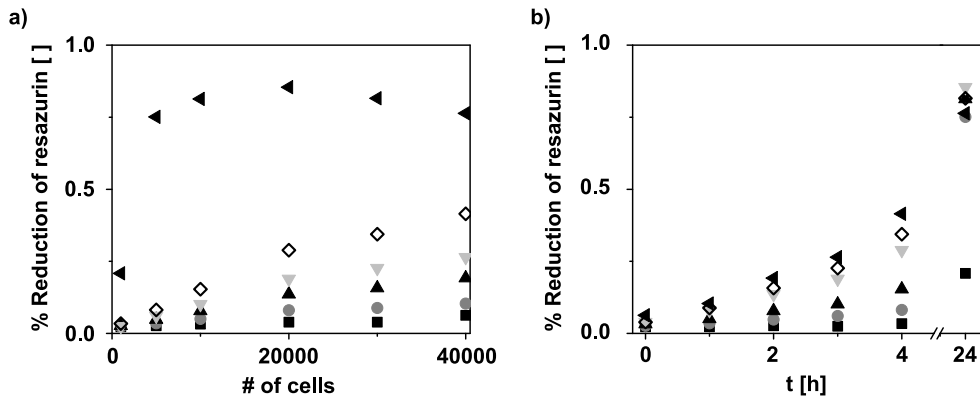
Figure 4.36.: Determination of optimal incubation time and cell number for using the Alamar Blue®assay with MDCK II cells. The relative absorbance is calculated with equation 2.6 using absorbance measurements at 570 nm and 600 nm, The results are plotted a) against number of cells for different incubation times (□ 0 h ∘ 1 h Δ 2 h ∇ 3 h ◊ 4 h ◁ 24 h) and b) against the incubation time for different cell numbers (□ 1000 ∘ 5000 Δ 10000 ∇ 20000 ◊ 30000 ◁ 40000).
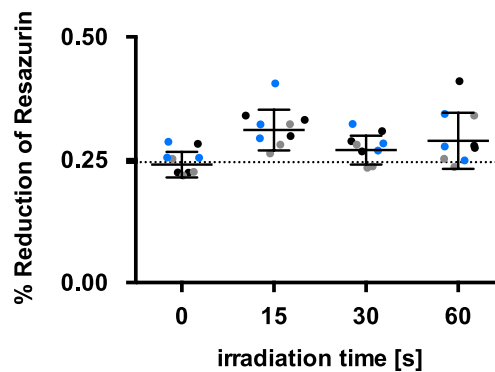
Figure 4.37.: The analysis of the toxicity of UV irradiation applied to MDCK II cells shows no difference between the applied irradiation time. The different colours represent the time between irradiation and adsorption measurements (black: 1 h; grey: 2 h; blue: 3 h). For the statistical analysis between irradiation time as well as the incubation time a Kruskal-Wallis test followed by the Dunn's multiple comparison (p < 0.05) is performed and shows no significant difference.

difference for each irradiation time. Also, no significant difference is found for the increasing irradiation time. If the cells would have been damaged or killed, a decrease in metabolic activity is expected. Because this is not observed, the irradiation conditions are applicable for the following experiments and the subsequent observation time frame of the cell experiments of two hours.

**Analysis of the Toxicity of 1-(4,5-dimethoxy-2-nitrophenyl)ethyl
11-mercaptoundecanoate (1)**

Besides the testing of the toxicity of the UV light, which is needed for the cell
experiment, the toxicity of the applied 1-(4,5-dimethoxy-2-nitrophenyl)ethyl
11-mercaptoundecanoate (**1**) is investigated. Therefore the thiol is added with
final concentrations of 5, 50 and 500 μM with 5000 cells in a 96-well plate.
Because the linker is not soluble in water an organic solvent needs to be used.
In literature, drugs are often dissolved in DMSO, when they are used in cell
experiments.[79] So DMSO is used as solvent in a first try (Appendix H fig.
H.1 a). But the test with the AlamarBlue® kit without cells (A) shows already
a higher reduction potential than the positive control (B). The sample with
DMSO and cells also show a higher reduction of the resazurin. Because of the
influence of DMSO itself on the assay ethanol is tested as solvent, which is
also used in the QCM-D experiments. The comparison of the positive control
(Appendix H fig. H.1 b, A), the control with ethanol and the AlamarBlue® kit
without (B) and with (C) cells show no difference. For this reason, ethanol is
chosen as solvent for the assay.

From a stock solution of **1** and **2** (10 mM) the final concentrations are di-
luted. Ethanol is added in a manner that all samples contain 5 % ethanol. No
ethanol is added of course to the positive control. The cells are incubated for
18 h with the compounds, before 100 μL media are removed and 10 % of the
kit are added. After incubation of 1 h the absorbance is measured at 570 nm
and 600 nm and the reduction of the resazurin calculated with equation 2.6
(section 2.10.1). The results are shown in figure 4.38. A small increase in the re-
duction is found especially for **2**. The performed Kruskal-Wallis test followed
by the Dunn's multiple comparison shows no significant difference between
the positive control and any other sample (Appendix E). So an insignificantly
increased cell activity is found. Due to this it will be necessary to change the
media in a cell experiment after the irradiation to remove the soluble cleavage
products. A closer look at the samples shows a crystal formation after 18 h
probably of **1** due to its bad water solubility. Because of the incubation of the
cells at 37 °C it is possible, that part of the ethanol evaporates over night and
the remaining amount is not enough to dissolve the complete linker. So the
results of the toxicity analysis of the high concentration are unclear. Besides
this, the cells look similar on all compared surfaces (fig. 4.39).

The toxicity test indicates that contact of the cleavage product and the
cells do not have a negative influence on cell behaviour. Although, the time
the cells get in contact with the **2** is much shorter than 18 h because the
medium is exchanged right after the cleavage. So the linker can be used for
the modification of the gold nanoparticles in cell experiments without having
a negative influence on cell behaviour.
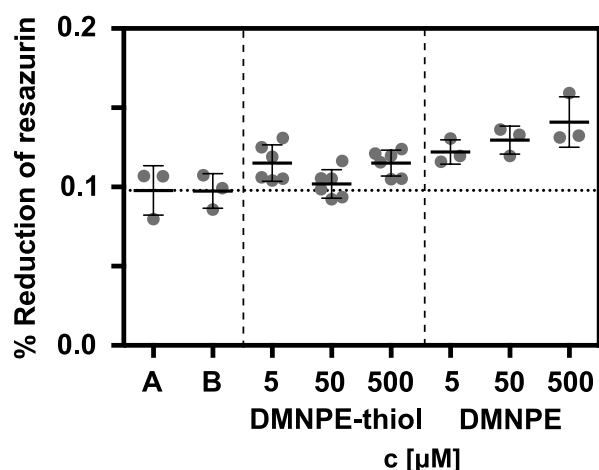
Figure 4.38.: An increasing metabolic activity is found for MDCK II cells incubated with DMNPE (**2**). For the toxicity assay of MDCK II cells with **1** or **2** different concentration of both compounds are applied and compared with the positive control (A) without additives and with only adding the solvent ethanol (B).

4.5.4. Migration of MDCK II Cells on Photopatterned Surfaces

After the characterisation of 1-(4,5-dimethoxy-2-nitrophenyl)ethyl 11-mercaptoundecanoate (**1**) the linker is tested in cell experiments. Aim of this study is to analyse the influence of the adhesion properties of MDCK II cells on their migration behaviour. Therefore the linker is immobilised on nanostructured glass surfaces with interparticle spacings of 30, 60 and 90 nm. The glass surfaces are nanostructured using the BCML method (section 2.6) and afterwards passivated using PEG_{2000}−silane (**8**). To functionalise the gold nanoparticles, the surfaces are glued to Teflon rings using Twinsil and incubated for 24 h with a solution of 100 µM **1** in PBS containing 1 % EtOH. After washing, the surfaces are irradiated using a microscope with a 5x magnification objective at the *Zeiss* "Observer" (BFP filter set (Excitation: 377/28 nm; Beamsplitter: 403 nm; Emission: 464/100 nm)) and a X-cite UV lamp. Parts of the surface are covered during the irradiation using a rectangular aperture. Afterwards the surfaces are washed with sterile PBS and 200 000 cells are seeded on each surface. After 18 h the surfaces are evaluated at the microscope. To ensure, that the surface stays intact during the UV irradiation and the passivation is working, additional glass slides (22 x 22 mm) are passivated and some are also irradiated with UV light before seeding 200 000 cells on top. The passivation controls shows almost no cells on top and the found cells look dead, so the passivation is working (fig. 4.40 B). But on the unfunctionalised, passivated surface as well as on the photopattered surface cells are found on the whole surface (A). This strongly indicates the possibility to remove the PEG passiva-
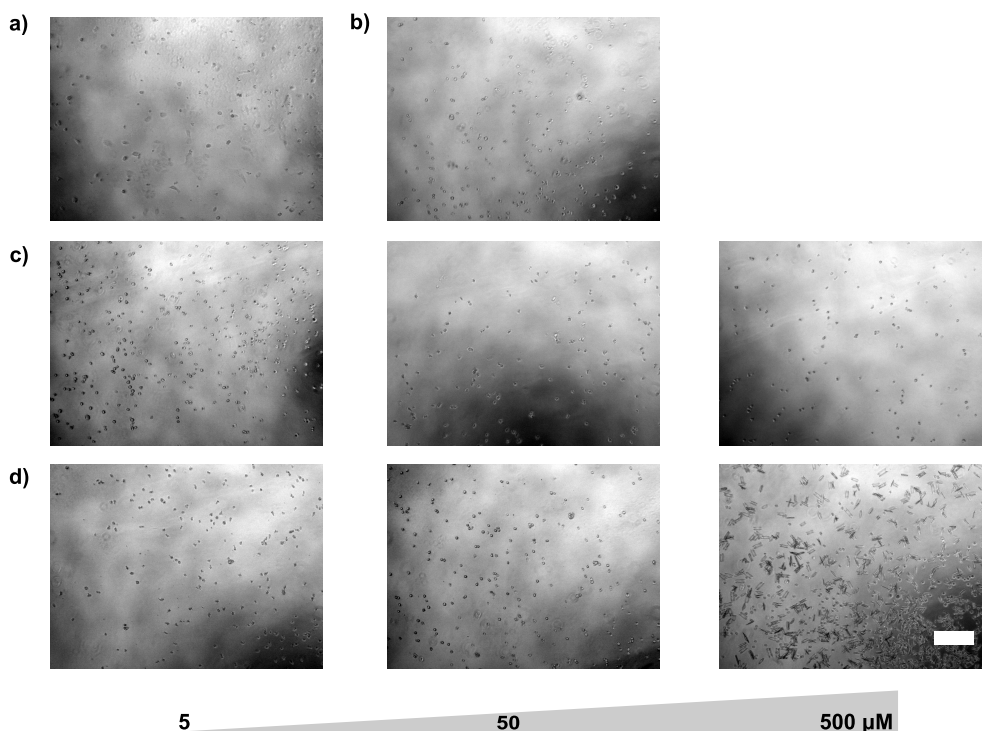
Figure 4.39.: The closer look at the cells of the positive control (a), the control with ethanol (b) and samples with the application of **2** show no major difference of the cells on the surface. This is also found for the cells incubated with 5 or 50 µM solutions of **1**. On the last surface large crystals are found on the surfaces (scale bar 200 µm).

tion with UV light. The surfaces are washed with PBS and the cells fixed with a 4 % PFA solution. The nuclei are stained with DAPI, using the protocol in section 2.11. Compared is the number of cells on three surfaces, which were irradiated with UV light, and three control surfaces. Therefore, the number of cells respectively the number of nuclei are determined at five positions on each surface. The counting is operated using *ImageJ* with the same procedure described for the LECs (section 4.4.4).

4.5.5. Modification of $\alpha_5\beta_1$-specific Antagonist

To enable the analysis of the influence of the specific interaction of the artificial antagonist of the integrine $\alpha_5\beta 1$ ((S))-3-(4-(3-(6-(3-mercaptopropanamido)-hexanamido)propoxy)benzamido)-4-(4-(3-((4-methoxypyridin-2-yl)amino)pro-poxy)phenyl)butanoic acid (**13**) with the integrin $\alpha_5\beta_1$, the antagonist is caged with DMNPE (**2**). Therefore the **2** is coupled in a Steglich esterification to the carboxy-group of the antagonist **13** (scheme 4.11). As described in the synthesis of 1-(4,5-dimethoxy-2-nitrophenyl)ethyl 11-mercaptoundecanoate (**1**), the
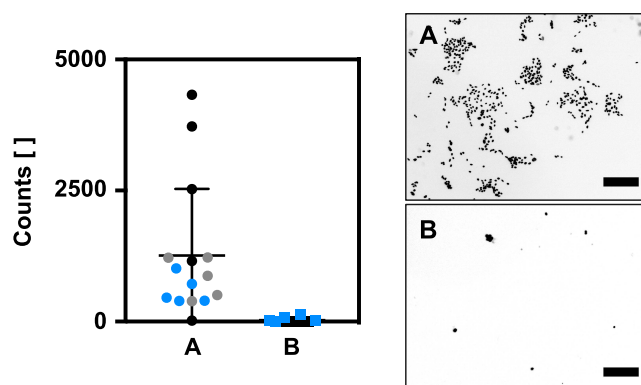
Figure 4.40.: The analysis of the PEG$-_{2000}-$silane (**8**) coating before and after UV irradiation with MDCK II cells shows the instability of PEG. Three surfaces are irradiated with UV light (365 nm) for 60 s (A), whereas two are kept in the dark before (B) the cells are seeded on top (scale bar: 250 μm). After 18 h the nuclei are stained and the number of cells on the surfaces determined

carboxy-group is activated using DCC. Because of the slow reaction between the acid and the alcohol, DMAP is used as catalyst, which enables the coupling between carboxy and hydroxy group. The raw product is purified using HPLC. The analysis of the isolated product shows the deprotection of the thiol function during the purification step. This is possible because the eluent contains TFA, which is used for the deprotection of the thiol group. So no additional deprotection must be performed. Because the batch size is to small, it is not possible to determine the yield, but successful coupling is obtained as seen by the NMR analysis.

Summary of Influencing Collective Cell Migration

1-(4,5-dimethoxy-2-nitrophenyl)ethyl 11-mercaptoundecanoate (**1**) can be synthesised with a yield of 18 %. In QCM-D experiments, the adsorption happens with a specific decay time of (320.88 ± 58.36) min at 37 °C and (1899.00 ± 776.30) min at 21 °C, while the cleavage after UV irradiation takes (2.52 ± 0.64) min (21 °C). The absorption spectrum of the molecule shows a band at 345 nm, which is blue shifted to 322 nm upon irradiation with UV light. Also, an isobestic point can be observed at 370 nm. An analysis of the toxicity of **2** shows an increasing of metabolic activity of the cells for **2**, but no effect for **1** is found. Because the passivation with PEG does not withstand the irradiation with UV light, no migration experiments can be performed.

Additionally it is possible to synthesis a caged specific antagonist of the integrin $\alpha_5\beta_1$ (**14**).
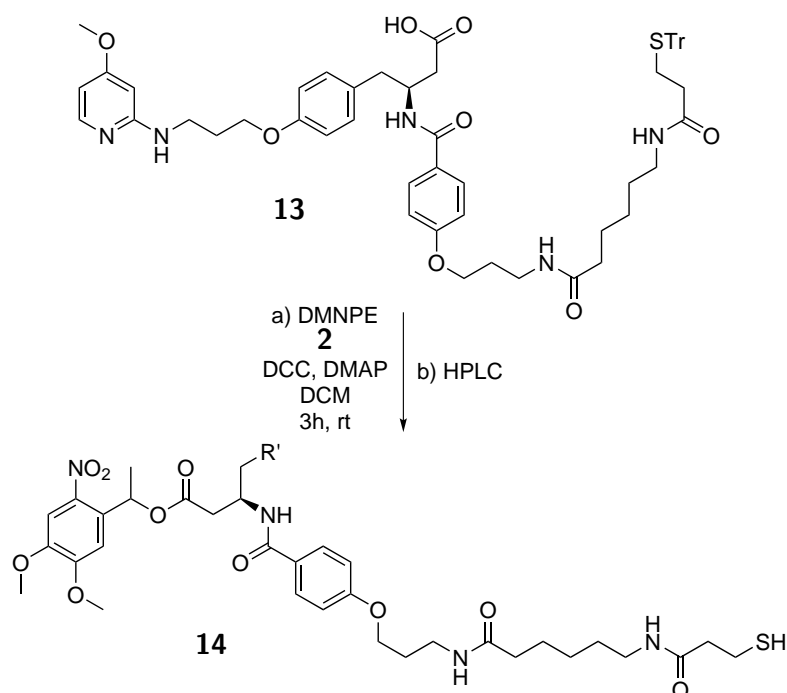
Scheme 4.11.: 13 is protected with DMNPE (**2**) via Steglich esterification. The thiol group is deprotected during the purification and results in **14**.

Part IV.

Discussion, Summary and Outlook

Chapter 5.

Discussion

In this thesis chemical synthesis and material science is combined to address biological questions in a biological chemistry approach. This enables the analysis of the influence of different extracellular matrix modules on cell behaviour. On the one hand a concentration and density depending effect of short hyaluronan is analysed. On the other hand a novel specific and unspecific binding model for the extracellular matrix is developed.

5.1. Chemical Modification of Hyaluronan

It is important to have a high control over the concentration of HA during experiments which deal with the influence of HA concentrations on these cells. So the first step is to find a suitable method to immobilise HA molecules on a surface.

The results in the previous section show several strategies to chemically modify HA to immobilise it on a surface. One the one hand modifications at the reducing-end are performed using cysteamine hydrochloride, propargylamine and dibenzocyclooctyne-amine. On the other hand the propargylamine is introduced at the carboxy groups within the chain (fig. 5.1). In case of the end-thiolated HA a degree of thiolation of below 4.0 ± 0.5 % (Appendix B) and of the functionalisation within the chain a degree of alkynation of 16 % is determined. All syntheses are performed successfully and enable the immobilisation of the HA-species.

In literature different approaches are found to functionalise HA (chapter 1.4.2). The easiest modification is the functionalisation at the carboxy-group within the HA chain.[45–48, 50, 51] Because short HA is used, a terminal modification is preferred to ensure the bioactivity of the HA, because the HA receptors address multiple disaccharide units.[15, 39] Here the modification at the reducing-end described by Lee *et al.* is performed.[49]

5.2. Bioactivity of Chemical Modified Hyaluronan

After the chemical modification to immobilise HA, the bioactivity is verified via the analysis of the interaction between the HA species and the hyaladerine
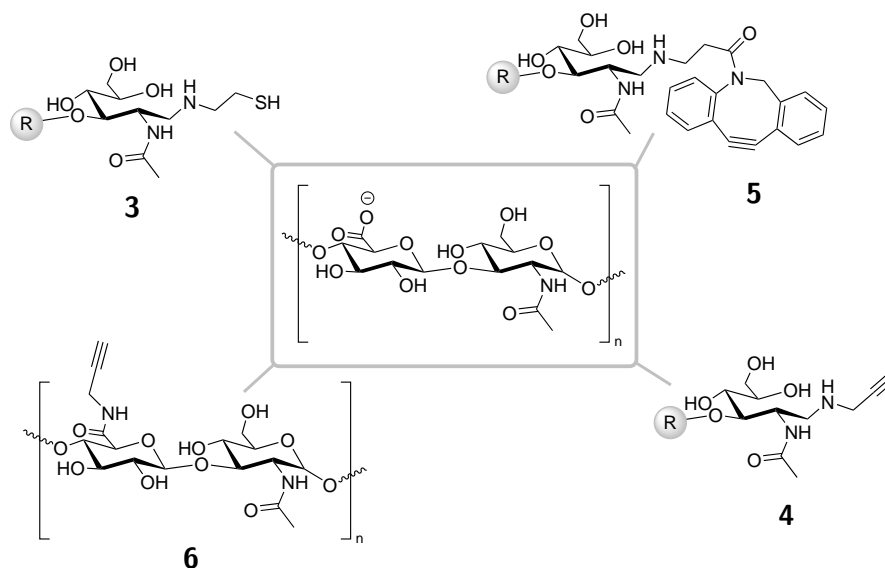
Figure 5.1.: Overview of the successfully synthesised HA species: the end-
modified thiol, DBCO and alkyne species as well as the alkyne function
within the chain.

aggrecan as well as LYVE-1. Especially the interaction between aggrecan and
HA proves the conservation of the bioactivity during the modification.

To verify the bioactivity a modification within the chain is compared to the
modification at the reducing-end. Via introduced thiol groups it is possible to
immobilise the HA directly to gold surfaces like gold coated QCM-D crystals
or gold nanoparticles. The usage of orthogonal functionalised gold nanostruc-
tured surfaces with the copresentation of cRGD enables the application in cell
experiments.[120]

On the other hand a two layer system is established, where alkyne function-
alised HA is immobilised on a previous formed OEG-SAM which bears azide
groups as we published in [54] (fig. 5.2). The immobilisation is based on the
copper catalysed azide-alkyne cycloaddition (CuAAC). Therefore, two oligo-
ethylene glycol species with a thiol terminus are used. To enable the CuAAC,
a mixture of $HS-(CH_2)_6-EG_3$ and $HS-(CH_2)_6-EG_6-N_3$ (ratio 2:1) is used.
Additionally to the possibility to immobilise HA , the OEG-SAM provides a
passivating background against unspecific interactions.[45,53] Because the use
of copper in biological samples bears the risk of incorporation of copper ions
into the surface layer, it is possible to use the strain promoted azide-alkyne cy-
cloaddition (SPAAC) reaction which also clicks an azide to an aklyne group.[50]
In this case the driving force is the strained alkyne in the cyclooctenyl-ring.

Having two different strategies, respectively two positions to immobilise the
HA, is of great advantage. This enables also the possibility to analyse, if the
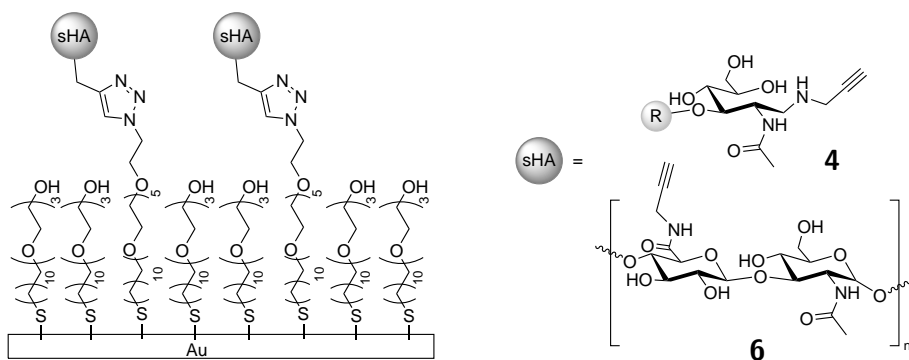
Figure 5.2.: A gold surface can be modified with an OEG-SAM decorated with azid groups, which enables the immobilisation of alkyne functionalised HA either at the reducing end or within the chain. By varying the azide ratio the concentration of HA on the surface can be tuned.

position of the modification influences the bioactivity of HA. So it can give evidences to the mechanism of the recognition of HA. Furthermore the usage of an azide bearing OEG-SAM and alkyne functionalised HA enables a well-controlled way to vary the density of HA on a surface (fig. 5.2). Because
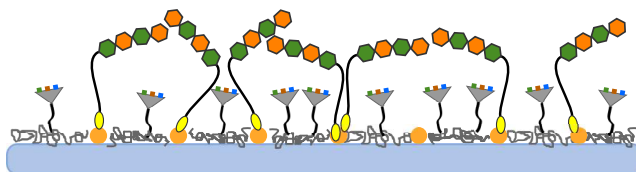
Figure 5.3.: The thiol-modification at the reducing end of HA enables the immobilisation of HA (hexagons) on a glass surface decorated with gold nanoparticles (dots). The surface can be orthogonal functionalised with an adhesive background using click-PEG (black lines) with cRGD (triangles).

QCM-D is used as technique to ensure the bioactivity of the HA after the chemical modification, it is also used to verify the success of the modification itself. The end-thiolated HA species can be immobilised directly onto the gold coated quartz crystal, whereas the alkyne functionalised species are immobilised via CuAAC to an azide bearing OEG-SAM. Because it is possible to immobilise all modified species on the corresponding surfaces, the modification was successful in each case (tab. 5.1). However, a problem occurs during the click reaction. The observed change in frequency indicates the incorporation of the used copper species into the OEG-SAM (fig. 4.3). The effect cannot be undone by washing the surfaces with an EDTA solution, which would complex divalent ions, the Cu^I-species, the actual catalyst of the CuAAC, which is incorporated into the SAM. To overcome this problem a complex of Cu^I with

tris(3-hydroxypropyltriazolylmethyl)amine (THPTA) is used.[128] But the performed QCM-D experiment shows no reaction between azide and alkyne when the complex is used as catalyst. The sterical hinderance of the ligand seems to prevent the reaction which is proven to be possible in solution.[126–128] An-

Table 5.1.: Summary of the changes in frequency due to the immobilisation of the different HA species to a gold surface respectively conjugated to $HS-(CH_2)_{11}-EG_6-N_3$. The QCM-D experiments are performed in PBS. For the analysis the 7th overtone is used (n = 2).[54]

#	sample	$\Delta\Delta f_7$ [Hz]
1	sHA-end-thiol (**3**)	50.5 ± 12.1
2	OEG	52.4 ± 10.1
3	OEG/ sHA-end-alkyne (**4**)	41.9 ± 0.1
4	OEG/ sHA-side-alkyne (**6**)	49.5 ± 0.1
5	sHA-end-DBCO (**5**)	50.0 ± 5.7

other option to ensure that no copper remains on the surface is using the strain-promoted alkyne-azide cycloaddition (SPAAC). As described before a ring strained triple bond can be used as driving force to couple an azide to an alkyne function. [50, 55, 56] The HA is again modified at the reducing end modifying the protocol by Lee *et al.*[49] Because of this the commercially available dibenzocyclooctyne-amine is chosen. The QCM-D experiment shows as well this successful modification and immobilisation. Disadvantage of this method is the prolonged reaction time. To improve the reaction kinetics another ring strained system needs to be tested because the reactivity depends strongly on the substitution of the cyclooctine. Otherwise a different biocompatible reaction can be tested to immobilise the HA.[130] Thinkable is the immobilisation via NHS chemistry. Therefore an active ester OEG needs to be immobilised on the surface and an amine function introduced to the HA. The amine is interesting because the reaction speed in this reaction is highest between active ester and amine compared to hydroxy- or thiol groups.

To analyse the bioactivity of the chemical modified HA species the different prepared surfaces are rinsed with a solution of either BSA, aggrecan or LYVE-1. QCM-D is used to observe this interaction.

HA forms a layer which prevents unspecific interactions with proteins. To analyse if this behaviour is still intact after the modification, the HA layer is incubated with a solution of BSA. Analysed are the homogeneous HA surfaces with the end-thiolated HA, as well as the two layer system of OEG-SAM with the two propargylamine bearing HA species. For none of these surfaces a binding of BSA is observed. This shows that the passivation properties of the HA are still intact after the chemical modification. To analyse also specific interactions with HA, the HA binding proteins aggrecan and LYVE-1 are chosen for further experiments.

Table 5.2.: Summary of the changes in frequency of the interaction of aggrecan or LYVE-1 with surfaces with different immobilised sHA. The used immobilisation strategies are the end-thiolation, end-alkynation and side-alkynation of sHA.[54] For the analysis the 7th overtone is used.

#	sample	$\Delta\Delta f_7$ [Hz]	
		Aggrecan	LYVE-1
1	EG_3-OH/EG_6-N_3	0.6	1.66
2	sHA-end-thiol (**3**)	3.9 ± 1.2	-
3	OEG/sHA-end-alkyne (**4**)	2.8 ± 2.3	0.02 ± 0.41
4	OEG/sHA-side-alkyne (**6**)	0.3 ± 0.6	0.48 ± 0.40

Aggrecan is a cartilage-specific proteoglycan core protein with a weight over 2500 kDA. It forms a hydrated gel structure in combination with HA and the link protein.[36] It is known that aggrecan needs at least 10-mers of HA to form strong binding. But between 4 and 8-mers still a weak interaction can be found.[37] The used HA has an average weight of 20 kDa, which correspond to a 50-mer. Because of this a good, strong interaction should be observable. The summary of the observed changes in frequency (tab. 5.2) shows the binding of aggrecan to each HA-species. Only a weak interaction is found for **6**, which is due to the relative high density of alkyne groups at the chain. A degree of alkynation of 16 % corresponds to a modification at every 8th unit. To improve the recognisability of this species, the synthesis needs to be repeated with an higher excess of HA compared to the used propargylamine to decrease the alkyne groups attached to the chain.

The used LYVE-1 is a homologous to the HA-receptor CD44, which is characteristic for lymphendothelial cells. For CD44 it is known that 6 to 10-mers of HA are necessary for an interaction.[131] Because both receptors show a very similar binding domain it is obvious that LYVE-1 needs as well 6 to 10-mers of HA.[39, 40] In the QCM-D experiment only the ectodomain with the binding domain of the receptor is used. Because it is rather light in weight (30 kDa)[39] its weight is increased by creating a conjugate with an antibody. Nevertheless the QCM-D experiment shows only a very weak interaction between LYVE-1 and the different surfaces. Possible explanations for this are high off-rates of the interaction as well as missing so far unknown co-factors which are needed for the binding. Also a needed clustering of the LYVE-1 receptors as it is reported for CD44 is thinkable. Therefore the intracellular part of the receptor is necessary.[132]

Although only a weak interaction between LYVE-1 and the HA modified surface is found the interaction with aggrecan proves the bioactivity of the chemical modified HA. The experiments show also that the modification at the reducing end does not interfere with the bioactivity. This indicates, that the reducing end is not the key player in the recognition of HA. In case of

the functionalisation within the chain a weaker interaction is found, which correlates to a dense functionalisation within the chain. But the HA is still bioactive.[54]

5.3. Influence of Short Hyaluronan on LECs

To determine the influence of short HA on LECs the performance of the AlamarBlue® and CyQuant® assay are established. A cell density of $131\,/\text{mm}^2$, an incubation time of $2\,\text{h}$ (AlamarBlue® assay) and $5\,\text{min}$ (CyQuant® assay) are established.

After showing that the immobilisation of hyaluronan is possible and the bioactivity stays intact, the HA is used in cell experiments. In the cell experiments two different HA species - on the one hand the short HA with an average weight of 20 kDa (50-mer) and on the other hand the digested HA with an average weight of 10 kDa (20-mer) - are compared. Both species are thiolated to enable the immobilisation of the HA on a nanostructured glass surface (fig. 5.3). Additionally, both species are added to the cells in solution in their functionalised and unfunctionalised version to analyse if any inhibition occurs due to the functionalisation at the reducing end. These experiments are performed, although the QCM-D experiments prove the bioactivity of the functionalised HA species. Besides the influence of the HA species the impact of the surface is compared as well. Therefore cells are seeded in a 96 well plate and on click PEG with and without gold nanoparticles. The analysed parameters are the toxicity of the HA species, the influence on the metabolic activity and the adhesion of the cells to the different concentrations either applied in solution or immobilised on the surface.

Toxicity Analysis of Short Hyaluronan

The determination of the toxic impact of digested and short HA species applied in different concentrations or different densities shows no negative effect to the metabolic activity.

The toxic effect of the different HA species is analysed (fig. 5.4). The comparison of the two end-thiolated HA species (fig. 5.4 a) shows no change in the activity of the cells, so the immobilised HA does not damage the cells. Figure 5.4 b) shows the influence of the end-thiolated and unfunctionalised species, which are incubated in solution. Here as well no difference between the species and concentrations is found. This shows that no toxic effect occurs through the thiolation of the HA and the HA itself on the LECs.

The Relative Metabolic Activity

Compared is the influence of a digested and short HA species which are applied to LECs in different concentrations and densities. Between the different species
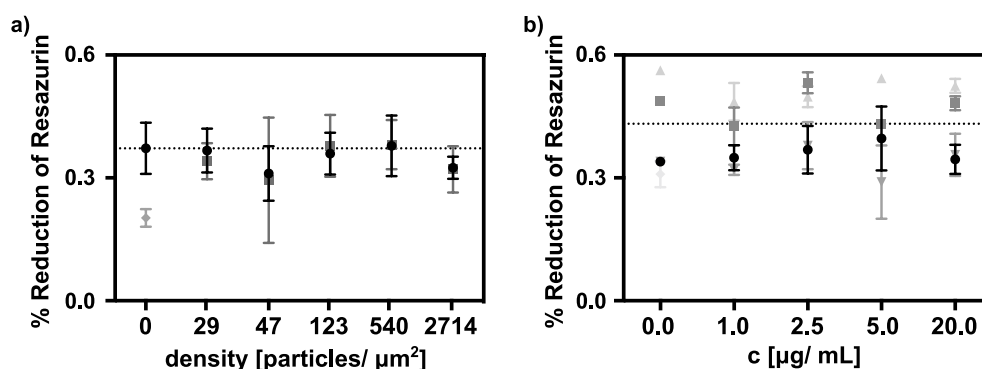
Figure 5.4.: Toxic effect of different HA species on LEC on nanostructured surfaces (a) and with HA in solution (b). Shown are mean and standard deviation for the incubation with the end-thiolated, short (black ●) and end-thiolated, digested HA (grey □), short (light grey △) and digested HA (grey ▽) and the passivation control (light grey).

no difference in the cell behaviour is found. In the case of the application of HA in solution no difference in the relative metabolic activity is found. For the immobilised HA species a reduced ability to adhere to the surface is found for the increasing nanoparticle density. Here for both HA species a biphasic effect in relative metabolic activity is found with maxima for a particle density of $540 \,/\mu m^2$.

The analysis of the amount of DNA per surface (CyQuant® assay) shows an effect on the cell adhesion for the immobilised HA species. This is due to the sterical hindrance of the cell adhesion. Especially for high HA densities the large HA molecules (50 disaccharide units) will cover some cRGD molecules on the surface and so less cells are able to adhere to the surface. To enable the comparison of the different surfaces after all, the results of the relative metabolic activity (AlamarBlue® assay (AB); $I(AB_c)/\overline{I(AB_0)}$) are normalised to the relative amount of DNA (CyQuant® assay (CQ); $I(CQ_c)\overline{I(CQ_0)}$) on the same surface. The comparison of the digested and short HA species shows no significant difference so the results of the analysis of short HA on the normalised metabolic activity of LECs (fig. 5.5). The comparison between the experiments performed on cell culture plastic (a) to the experiments performed on click PEG (b) shows no significant difference due to the different surface types with the same concentration of HA. As well no significant difference is found for the different applied HA concentrations on the same surface type.

This finding is contrary to discoveries described in literature. So Wu *et al.* describe a biphasic effect of low molecular weight (2.5 kDa, 3-10 mer) on lymphendothelial cells.[44] They use a stable cell line of mouse lymphendothelial cell, which is postulated to behave in the same way LECs do. Due to the applied HA in solution a biphasic effect is shown with a maximum at a con-
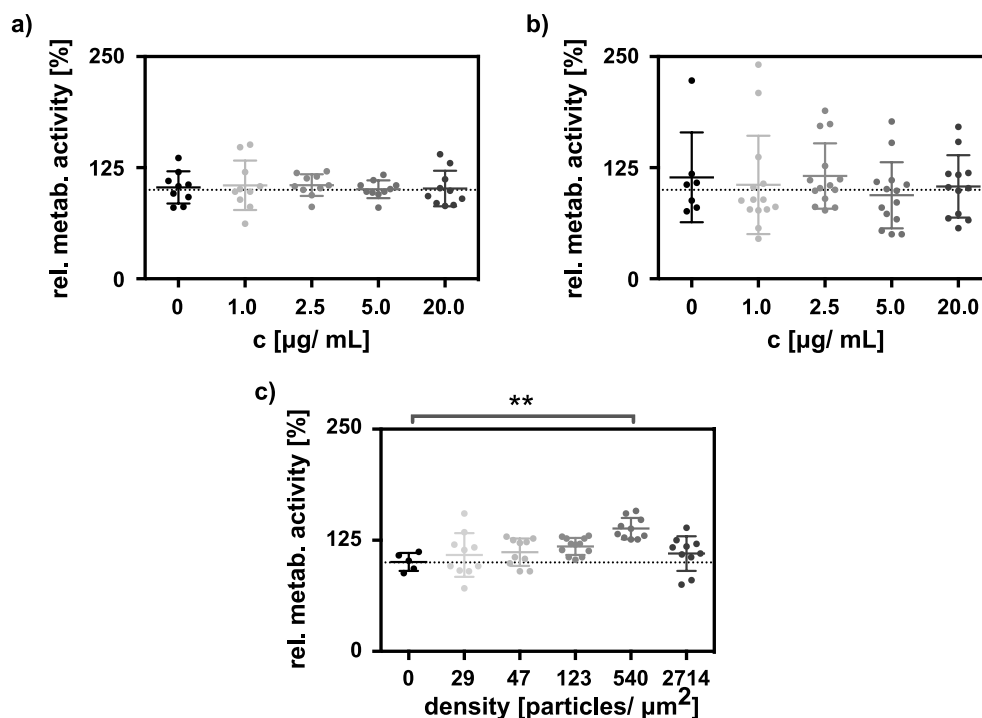
Figure 5.5.: Results of the influence of HA on the relative metabolic activity
of LECs (based on the AlamarBlue®assay) normalised to the relative amount
of DNA (based on the CyQuant®assay) on a) cell culture plastic in a 96-well
plate with HA in solution, b) on a click-PEG surfaces with HA in solution and
c) on nanostuctured, click-PEG surfaces with immobilised HA. To analyse
the significance of the samples a Kruskal-Wallis test (p < 0.05 with Dunn's
comparison is performed, Appendix E).

centration of $3.13\,\mu g/mL$ which decreases even under the level of untreated
cells for concentrations above $25.0\,\mu g/mL$. Additionally a scratch assay is per-
formed to analyse the effect on the migration velocity and an increase in the
migration ability is found. In the study presented here a biphasic effect is found
for the immobilised HA only. Up to a particle density of $540\,\text{particles}/\mu m^2$ the
relative metabolic activity increases. For the application of a higher density
of HA on the surface the activity decreases again. So there is a critical sur-
face density which leads to a higher activity level of the cells compared to
untreated cells (positive control). The different results of our study compared
to the results by Wu *et al.* are possibly due to the use of the different cells
respectively because primary cells are used, which can show variations in their
behaviour depending on the cell batch. To verify and strengthen the findings
the experiments can be repeated with different batches of cells or cells from
different donors. Additionally this indicates a different effect of the orientation
of the cells to the HA. For the immobilised HA the cells have only contact to

the HA at the basal side. Seeding the cells with diluted HA enables the contact from all sides until the cells adhere to the surface. Afterwards the HA can only interfere at the apical side with the cells. It is also reported, that HA supports the adhesion of cells to a substrate, because the interaction between HA and HA receptors is faster than the interaction between integrin and their corresponding binding domains on the surface.[133] This can also effect the response of the cells to the HA.

5.4. Influence of Immobilised, Short HA on Cell Migration

Due to the nanostructured surfaces to immobilise the HA in these experiments it is not possible to perform a scratch assay to analyse the migration behaviour of the cells. The passivation and functionalised nanoparticles would be removed with the cells during the assay. Due to this another method needs to be found. Unfortunately also the usage of a physical barrier like a PDMS-stencil,[79] other PDMS-blocks,[80] or commercially available masks[83] to create a collective is not possible because these barriers do not stick to the passivated glass surface and so no defined border can be created.

So cells are seeded to surfaces without the application of HA and on nanostructured surfaces with a particle density of $540\,/\mu m^2$, which should result in the highest effect on the cells. But the results indicate no change due to the HA application (fig. 4.26). Also various antibodies are tested to enable the determination of an effect on the adhesion via staining the focal complex and of the interaction between HA and LYVE-1. In case of the staining for the focal complex the proteins talin, paxillin and vinculin are chosen, but it is not possible to achieve an appropriate staining of any of these proteins. Likewise no antibody is found which can be used for ICC staining of LYVE-1. Stainings of LYVE-1 which are found in literature are mainly performed in micro sections.[14, 19, 134] A possibility to overcome this problem could be to use indirect labelling of the receptor by using a fluorescent labelled HA species or to stain a protein that colocalises with the receptor. To create a fluorescent labelled HA it would be possible to combine modification within the chain with a modification at the reducing end. To have a high accessibility of the HA on the nanostructured surface end-thiolation is still the best choice. So a dye could be introduced via CuAAC to alkyne groups within the chain. Therefore the degree of alkynation should be decreased so that the bioactivity is ensured. The disadvantage of using a labelled HA is, that due to the addition of a dye the sterical demand of the HA is increased which has an negative effect on the accessibility of the cRGD and so the adhesion of the cells. The problem with staining of a colocalised protein of LYVE-1 is that so far it is unclear which proteins would be suitable. To allow this, further investigations are necessary.

5.5. Summary of the Influence of Short Hyaluronan on LECs

In summary the analysis of immobilised short HA showed that it is possible to perform a chemical modification of HA within the chain or the reducing end while the bioactivity is conserved. The incubation of different concentrations of HA with LECs on either cell culture plastic or click-PEG shows no significant difference in the relative metabolic activity of the cells. Contrary the variation of the HA density on a surface leads to a biphasic effect in relative metabolic activity with a maximum at a density of $540 \, \text{particle}/\mu\text{m}^2$. This shows a higher response to the application of HA on the basal side. Further studies to investigate the influence of immobilised, short HA on cell migration or the binding mechanism of HA to its receptors are difficult. On the one hand no scratch or migration assays with a physical barrier can be performed due to the nanostructured surface. On the other hand no antibodies are found which enable the staining of the HA receptor LYVE-1.

5.6. Synthesis and Characterisation of Noval Photocleavable Ligands to Study Cell Migration

To study collective cell migration on nanostructured surfaces two novel photocleavable ligands are developed. Synthesised are an unspecific ligand 1-(4,5-dimethoxy-2-nitrophenyl)ethyl 11-mercaptoundecanoate (**1**) and the specific, caged antagonist of the intergrine $\alpha_5\beta_1$ 1-(4,5-dimethoxy-2-nitrophenyl)-ethyl $(3(S))$-3-(4-(3-(6-(3-mercaptopropanamido)hexanamido)propoxy)benzamido)-4-(4-(3-((4-methoxypyridin-2-yl)amino)propoxy)phenyl)butanoate (**14**).

To analyse the migration of cells on a substrate, various methods are reported (chapter 1). Several methods accept that cells get damaged and so additional unknown signals influence the migration. Aim of this study is to enable the comparison of the influence of the surface density of adhesion motives on collective migration. Therefore the well-established nanostructured glass surfaces are used.[24, 25, 27, 135, 136] Via BCML, gold nanostructures on glass surfaces with different interparticle distances are produced.[24] To prevent unspecific interactions of the cells with the surface, the glass is passivated with PEG_{2000}−silane (**8**) via silanisation reaction.[25] The gold nanoparticles are either decorated with an unspecific, caged adhesion molecule a) or an artificial, caged, specific intergrine antagonist b), fig. 5.6).[21]

1-(4,5-dimethoxy-2-nitrophenyl)ethyl 11-mercaptoundecanoate (1)

1-(4,5-dimethoxy-2-nitrophenyl)ethyl 11-mercaptoundecanoate (**1**) can be synthesised with a yield of $18\,\%$. In QCM-D experiments, the adsorption happens with a specific decay time of (320.88 ± 58.36) min at $37\,°\text{C}$ and $(1899.00 \pm$
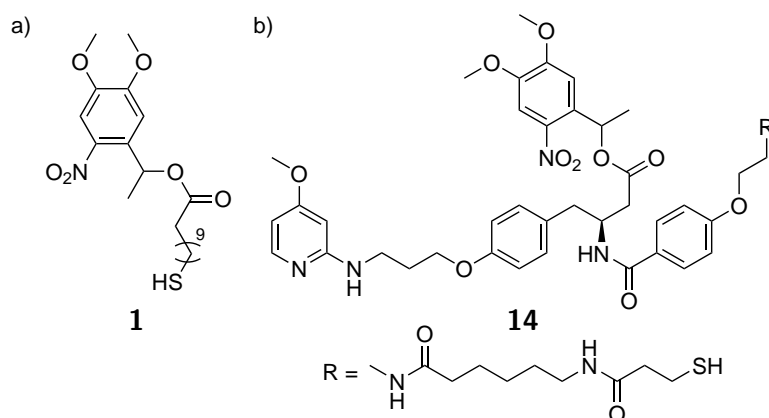
Figure 5.6.: Shown are the a) unspecific, caged adhesion molecule (**1**) and b) the artificial, caged, adhesion ligand **14**.

776.30) min at 21 °C, while the cleavage after UV irradiation takes (2.52 ± 0.64) min (21 °C). The absorption spectrum of the molecule shows a band at 345 nm, which is blue shifted to 322 nm upon irradiation with UV light. Also, an isobestic point can be observed at 370 nm. An analysis of the toxicity of DMNPE shows an increasing of metabolic activity of the cells for **2**, but no effect for **1** is found. Because the passivation with PEG does not withstand the irradiation with UV light, no migration experiments can be performed.

To establish all parameters for further cell experiments a simplified ligand is synthesised, which interacts unspecifically with integrins. Therefore 4,5-dimethoxy-2-nitrophenyl ethanol (**2**) is synthesised and its photochemistry characterised. It is known from studies with caged RGD that this molecule is sufficient to prevent cell adhesion. So this is also the targeted group in case of the artificial antagonist. The ligand to study the unspecific interaction is a minimalistic model for this. 11-mercaptoundecanoic acid (**7**) was chosen as a model compound, as it combines both necessary functions - a thiol and a carboxy group. In the beginning the **2** is synthesised with a yield of 62 % regarding acetophenone. This is successful coupled via Steglich esterification to 11--(tritylthio)undecanoic acid (**11**). After the deprotection of 1-(4,5-dimethoxy-2-nitrophenyl)ethyl-11-mercaptoundecanoate (**1**) could be achieved with a yield of 18 % regarding acetophenone.

The comparison of the adhesion of the unspecific ligand at 21 °C and 37 °C shows a 6-fold faster adsorption at the higher temperature. The cleavage analysis via QCM-D indicates a single-step process what corresponds to the postulated mechanism. The determined specific decay time is $t_1 = (2.52 \pm 0.64)$ min. The observation of the cleavage using the UV VIS spectra is in good agreement with this finding. The isobestic point at 370 nm proves also the single-step process of the cleavage. The analysis of the spectra before irradiation shows also a

maximum at 345 nm which is the optimal cleavage wavelength of the molecule. The comparison of the irradiation of **2** and **1** shows much faster process for DMNPE which might be due to the faster rearrangement of the molecule because no substitutent with sterical demand is attached. Because the ligand is
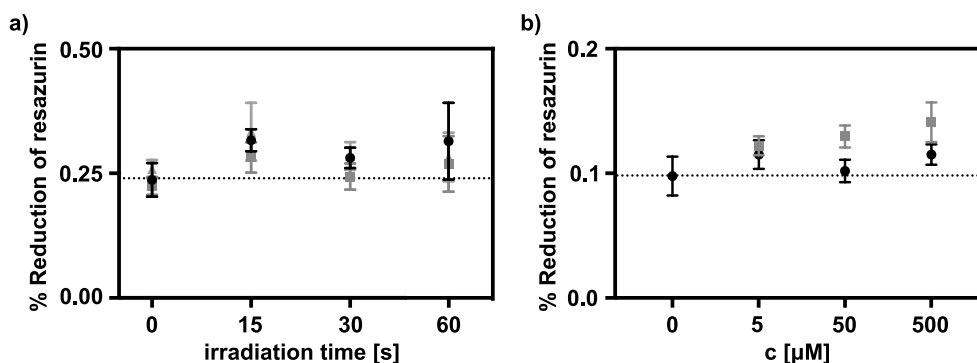
Figure 5.7.: The results of the toxicity assays for the cell assays with 1-(4,5-dimethoxy-2-nitrophenyl)ethyl 11-mercaptoundecanoate (**1**) are summarised. In a) the influence of the irradiation time on MDCK II cells is evaluated after different incubations times (1 h: black circles; 2 h: dark grey squares; 3 h: grey triangles). The effect of the incubation with DMNPE (**2**, grey squares) and **1** (black circles) is shown in b).

used in cell experiments and UV light is needed to cleave the molecule, which can damage the cells, the toxicity of the ligand as well as the UV light is determined. The performed toxicity assay analyses the influence of the irradiation time of 15, 30 and 60 s and without irradiation after 1, 2 and 3 h. This long observation time is meaningful because it is found that it is possible to fix cells with UV light, so that the cells still appear healthy, or to damage the cells formatively. This effects can still appear several hours after the actual irradiation.[90]

The irradiation times which are used for the toxicity assay show no difference in the metabolic activity (fig. 5.7 a). As well no significant difference is found for the application of **2** or **1** although an increase in the reduction is found which correlates to an higher metabolic activity (b).

Cell Experiments on Nanostructured Surfaces Decorated with 1-(4,5-dimethoxy-2-nitrophenyl)ethyl 11-mercaptoundecanoate (1)

For cell experiments nanostructured surfaces with interparticle distances of 30, 60 and 90 nm are passivated with PEG_{2000}−silane (**8**). Afterwards the surfaces are incubated with the ligand. Additionally surfaces are prepared without nanostructures to ensure on the one hand a successful passivation and that the ligand does not stick to the PEG. On the other hand it is tested if the passivation withstands the UV irradiation. To create a pattern on the

surface a rectangular aperture is used during the irradiation, which leads to a rectangular area in middle of the surface where the cells can adhere and so four edges which can be observed for the migration assay. While the negative control shows no cell adhesion and so demonstrates the the passivation worked out, the passivated surfaces which are irradiated with UV light show cell adhesion. This strongly indicates, that the PEG is removed during the irradiation with UV light. So it is unclear if the cells adhere on the nanostructured surfaces due to the cleaved ligand or because the PEG is removed. To perform the migration assay it is necessary to find a passivation which is stable against the irradiation with UV light. For the synthesis of the **8**, which is used in this study, a PEG−amine is coupled to 3-triethoxysilylpropyl isocyanate under the formation of a urea group. **8** used in this study has an urea bridge (fig. 5.8
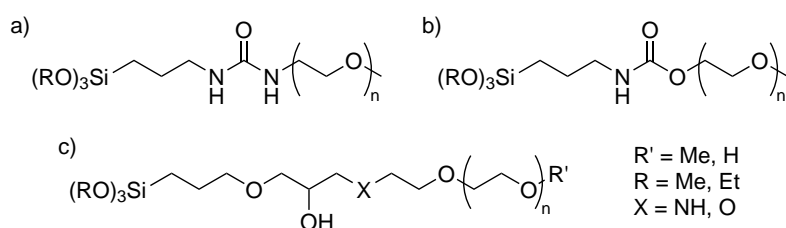
Figure 5.8.: Overview of different PEG-species which can be used as passivating background in cell experiments. In case of a) in two steps a silane is immobilised on the surface and afterwards coupled to a PEG species resulting in a carbamate. The urea species (b) and the urethane species (c) are immobilised as whole molecule.[25]

a). Known are also species with an internal urethane function and a two-step passivation resulting in a carbamate. Disadvantage of this two systems are worse passivating properties.[25] Nevertheless, both species can be tested, if they withstand the UV light. Other used photocleavable ligands, which are found in literature, are also immobilised via silanisation on a glass surface. [73,85,88,137] So it is unlikely, that the silane function is responsible for the instability.

1-(4,5-dimethoxy-2-nitrophenyl)ethyl (3-(*S*))-3-(4-(3-(6-(3-mercaptopropanamido)hexanamido)propoxy)benzamido)-4-(4-(3-((4-methoxypyridin-2-yl)amino)propoxy)phenyl)butanoate

Beside the unspecific ligand, the specific antagonist **13**[1] is coupled to DM-NPE (**2**) via Steglich esterification. Here the determination of the yield is not possible because the batch size was to low. Because of the unstable passiva-

---

[1]The artificial, specific anatagonist is synthesised by Dr. Stefanie Neubauer, Institute for Advanced Study at the Department of Chemistry, Group of Prof. Dr. H. Kessler, Technische Universitaet Muenchen (Germany).

tion on the nanostructured surfaces, no further cell experiments with **14** are performed.

Chapter 6.

Outlook

Various strategies are found to immobilised HA on a surface. To overcome the problematic application of the CuAAC the usage of the SPAAC needs further investigation. So other ring strained species can be tested to increase the reaction speed. Possible alternatives are the use of bicyclo[6.1.0]non-4-yne- or 3,3-difluoro-6-methylcyclooct-1-yne-derivatives (fig. 6.1).[55,57]
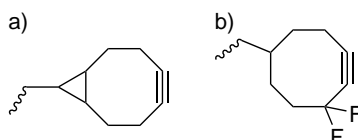
Figure 6.1.: Strained ring species which can be used for the SPAAC: a) bicyclo-[6.1.0]non-4-yne- and b) 3,3-difluoro-6-methylcyclooct-1-yne-derivatives.

Primary cells are used in the experiments to analyse the influence of immobilised HA. The behaviour of these cells can vary form batch to batch. To see, if the biphasic effect in the metabolic activity for the incubation of the cells with immobilised HA is only found for this batch other cell batches would have to be tested. Also a concentration depended effect in the activity is found for lymphatic cells which are incubated with diluted HA.[44] This enables the further investigation if cells react different when HA is applied in an immobilised (basal) density depending or diluted (apical) concentration depending way. Therefore it is also interesting to investigate if the immobilised HA interacts differently with the cells at different concentrations. For this study an orthogonal modified HA is of interest. In the synthesis two immobilisation strategies can be combined. On the one hand HA can be immobilised on gold nanoparticles by introducing a thiol group at the reducing end. On the other hand the alkynation within the chain can be used to click a dye to the HA chain using CuAAC. Therefor a lower degree of alkynation should be used than in this study to ensure the bioactivity. The interaction between the modified HA within the chain with a functionalisation degree of 16 % and aggrecan is found to be weak, which indicates that the degree of alkynation is too high for an effective interaction between receptor and HA. Additionally a possibility needs to be found to stain the HA receptor LYVE-1 to investigate the colocalisation

between HA and receptor. Instead of directly staining the receptor itself, it is possible to detect proteins which bind to the receptor on the intracellular domain. Because it is not well studied which proteins bind to LYVE-1 so far, this needs to be tested first. Due to the similarity between CD44 and LYVE-1 proteins which bind to CD44 can be tested first. Interesting candidates are ezrin and merlin which are also know to be important in migration.[17, 30]

In literature the terms short HA or small HA fragments contains a wide range of chain length from 2500 to 40 000 kDA.[2, 43, 44] In this study the impact of HA with an average size of 10 kDa is compared to a HA with an average size of 20 kDa and no difference is determined. The effective size of HA fragments that influence cell behaviour remains unknown. To investigate this, different sizes between 2.5 and 40 kDa can be tested. Important here is to use HA with a good defined size to ensure that the right size is tested. Besides it is interesting how small the fragments can get to increase the relative metabolic activity. To degrade HA three different methods can be used which lead to a different fragmentation of the HA. The usage of hyaluronan synthase (HAS) leads to a cleavage of the β-(1→3) glycosidic bond and a *N*-acetyl-D-glucosamine at the reducing end. The usage of lyases leads to a β-elimination at the β-(1→4) glycosidic bond with D-glucoronic acid at the reducing end. The third method is the application of reactive oxygen species (ROS) which lead to an uncontrollable fragmentation of the HA. Because all three methods are found in natural conditions it would be interesting to study the effect of the different cleavage methods with the different end-groups.
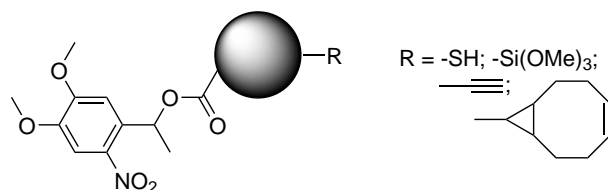
Figure 6.2.: To enable the use of the two DMNPE (**2**) caged molecules on different surfaces, the terminus can be varied. Besides the thiol function (-SH), it could be interesting to immobilise them directly to a glass surface via a −Si(OMe)$_3$ group. For applying a orthogonal functionalised surface with click-PEG either an alkyne (CuAAC) or a strained alkyne species (SPAAC) can be introduced or the molecule can be immobilised via NHS chemistry.

To enable the chemical barrier method to study collective cell migration, a working passivation needs to be found. Tested can be PEG-derivatives which are attached to the silane group under the formation of a carbamate or urethane group. After solving the passivation problem, the migration of cells can be analysed depending on the density of a adhesive background on the surface. It will be possible to compare an unspecific interaction of the cells with 11-mercaptoundecanoic acid (**7**) and the specific interaction with the integrin

$\alpha_5\beta_1$ via **13**. To enable the use of an orthogonal functionalised surfaces with this biological chemistry approach, different motifs can be used to immobilise the ligand to a surface. Thinkable are a silane group to immobilise the ligands directly to a glass surface or silicon wafer or either an alkyne group or a strained ring octenyl derivative to enable the CuAAC respectively the SPAAC (fig. 6.2).
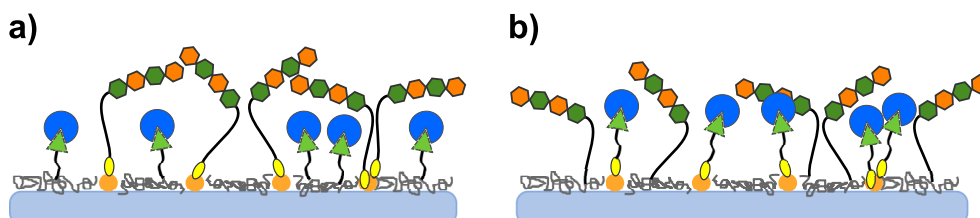
Figure 6.3.: Scheme of orthogonal functionalised surfaces which combine both strategies developed in this study: a) The density of immobilised HA can be varied by using surfaces with different particle densities in the presence of a photocleavable adhesive background. b) The density of the photocleavable, adhesive ligand can be varied by using surfaces with different particle densities in the presence of short HA.

Finally both developments of this study can be combined. Therefore a gold nanostructured surface can be created with a passivating PEG-background with either the photocleavable ligand attached to the gold particles via a thiol group and short HA is immobilised via CuAAC/ SPAAC to the PEG or vice versa. These strategies enable the determination of density depending effects on cell behaviour especially migration. The surface can be decorated either with varying HA density in the presence of a photocleavable adhesive background or by varying the density of the adhesive ligands in the presence of short HA fragments (fig. 6.3).

Part V.

Appendix

Appendix A.

Abbreviations and Synthesised Compounds

A.1. Abbreviations

$\Delta(\Delta f_n)$	change in frequency in QCM-D experiments for overtone n
BCML	block copolymer nanolithography
BSA	bovine serum albumin
CCD	charge coupled device
CD44	cell-surface glycoprotein involved in cell-HA interactions
CLEC-2	c-type lectin-like receptor
COSY	correlation spectroscopy (NMR method)
cRGD	cyclic RGD
CuAAC	copper catalysed azide alkyne cycloaddition
DAPI	$4'$,6-diamidino-2-phenylindole
DART	direct analysis in real time (MS method)
DBCO	dibenzocyclooctin
DCC	N,N'-dicyclohexylcarbodiimide
DCM	dichloromethane
DIPEA	diisopropylethylamine
DMF	dimethylformamide
DMNPE	4,5-dimethoxy-2-nitrophenyl)ethanol
DMSO	dimethylsulfoxide
DNA	deoxyribonucleic acid
DTNB	$5,5'$-dithio-bis-2-nitrobenzoic acid
ECM	extracellular matrix
EDC	1-ethyl-3-(3-dimethylaminopropyl)carbodiimide
EDTA	ethylenediaminetetraacetic acid
EG	ethylenglycol
EGM-2 MV	microvascular endothelial cell growth medium
ESI	electron spray ionisation
EtOH	ethanol
FADH2	flavin adenine dinucleotide
FAK	focal adhesion kinase

FBS	fetal bovine serum
FITC	fluorescein isothiocyanate
FMNH	Flavin mononucleotide
GAG	glycosaminoglycans
HA	hyaluronic acid
HAS	hyaluronan synthase
HPLC.	high performance liquid chromatography
HSQC	heteronuclear single quantum coherence (NMR method)
ICC	Immunocytochemistry
IgG	Immunoglobulin G
LEC	lymphendothelial cells
LYVE-1	lymphatic vessel endothelial hyaluronic acid receptor 1
MALDI MS	matrix-assisted laser desorption ionisation mass spectrometry
MDCK II	Madin-Darby canine kidney strain II cell line
MEM	minimum essential medium eagle with phenolred
MS	mass spectrometry
MTT	3-(4,5-dimethylthiazol-2-yl)-2,5-diphenyltetrazolium bromide
MWCO	molecular weight cut off
NAD(P)H	nicotinamide adenine dinucleotide (phosphate)
NHS	N-hydroxysuccinimide
NMR	nuclear magnetic resonance spectroscopy
OEG	oligoethylenglycol
PBS	phosphate buffered saline
PDMS	polydimethylsiloxane
PEG	polyethylenglycol
PFA	paraformaldehyde
QCM-D	quartz crystal microbalance with dissipation monitoring
RGD	amino acid sequence arginine-glycine-aspartic acid
RHAMM	receptor for hyaluronan mediated motility
RNA	ribonucleic acid
ROS	reactive oxygen species
SAM	self-assembled monolayer
SDS	sodium dodecyl sulphate
sHA	short HA
SPAAC	cooper-free strain-promoted azide-alkyne cycloaddition
Src	tyrosine-protein kinase
TEAA	triethylammonium acetate
TFA	trifluoroacetic acid
THF	tetrahydrofuran
THPTA	tris(3-hydroxypropyltriazolylmethyl)amine
TIPS	triisopropylsilane
TLC	thin layer chromatography

TRIS	tris(hydroxymethyl)aminomethane
UV	ultraviolet
UV VIS	absorption spectroscopy at the ultraviolet/visible range of electromagnetic spectrum
VEGF(R)	vascular endothelial growth factor (receptor)
Θ_w	water contact angle
$\epsilon_{\lambda_{max}}$	attenuation coefficient at the wavelength of the absorption maximum
λ_{max}	wavelength of the absorption maximum
HUPLEC	human primary lymphendothelial cells
$\lambda_{ex/em}$	excitation/ emission wavelength
SLB	supported lipid bilayer

A.2. Synthesised Compounds
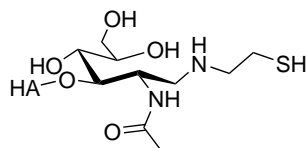
3
HA-end-thiol
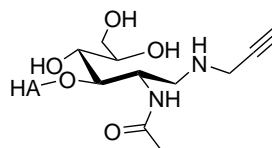
4
HA-end-alkyne
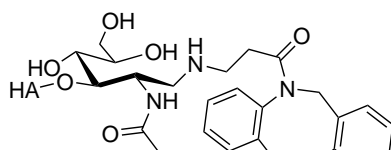
5
HA-end-DBCO
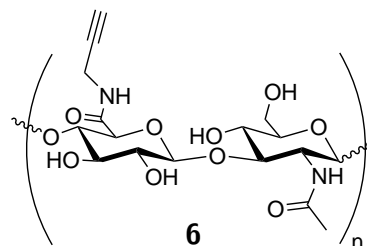
6
HA-side-alkyne
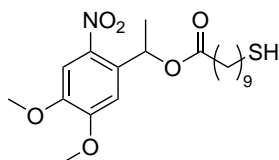
1
1-(4,5-dimethoxy-2-nitrophenyl)ethyl
11-mercaptoundecanoate
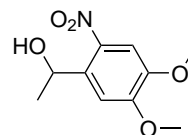
2
1-(4,5-dimethoxy-2-nitrophenyl)-
ethan-1-ol
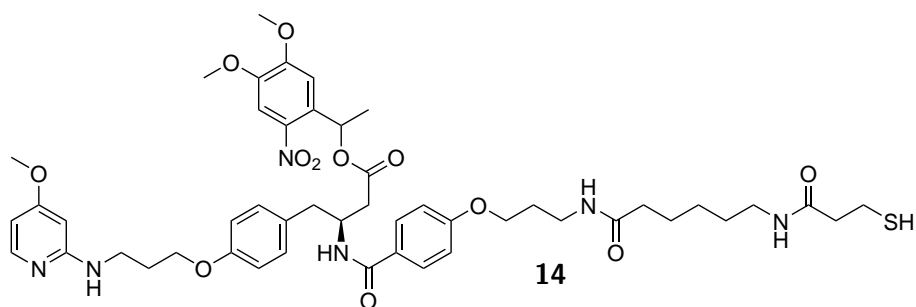
14

1-(4,5-dimethoxy-2-nitrophenyl)ethyl (3S)-3-(4-(3-(6-(3-mercaptopropanamido)-
hexanamido)propoxy)benzamido)-4-(4-(3-((4-methoxypyridin-2-yl)-
amino)propoxy)phenyl)butanoate

Appendix B.

Ellman's Assay

The degree of thiolation of a sample is determined according to the protocol in section 2.10.4. An example for a calibration curve with its linear fit equation is shown in fig. B.1. The calculated degree of thiolation for three different batches is summarised in table B.1 (4).
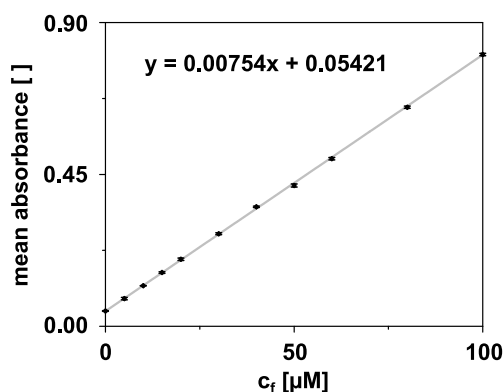
Figure B.1.: Example of a calibration curve for determining the degree of thiolation using the Ellman's assay. The measured absorbance at $420\,\mathrm{nm}$ is plotted versus the concentration of cysteamine hydrochloride and the linear equation determined.

Table B.1.: Summary of the results of the determination of the degree of thiolation (%) for three batches of short, end-thiolated HA with the according linear fit equations.

| # | ratio | mean absorbance (st.dev) | | |
		batch A[1]	batch B[2]	batch C[3]
1	1:41.5	0.0659 ± 0.0007	0.0685 ± 0.0059	0.0616 ± 0.0215
2	1:16.0	0.1016 ± 0.0008	0.0924 ± 0.0038	0.0871 ± 0.0567
3	1:9.6	0.1372 ± 0.0021	0.1215 ± 0.0081	0.0861 ± 0.0340
4	d.o.t.	4.47	3.33	4.12

[1] $y = 0.007542x + 0.05421$; [2] $y = 0.008138x + 0.0572$; [3] $y = 0.01075x + 0.03055$

Appendix C.

Determination of the Optimal Azide Concentration for Performing a CuAAC in the QCM-D

To enable the adhesion of alkyne functionalised HA for a QCM-D experiment a SAM of OEGs is formed, which also bears azide groups. A pure surface coating with $HS-(CH_2)_{11}-EG_6-N_3$ is not appropriate so the linker is mixed with $HS-(CH_2)_{11}-EG_3-OH$. To find the optimal ratio between the two compounds, the ratio is systematically varied and the HA clicked to it (fig. C.1). The change
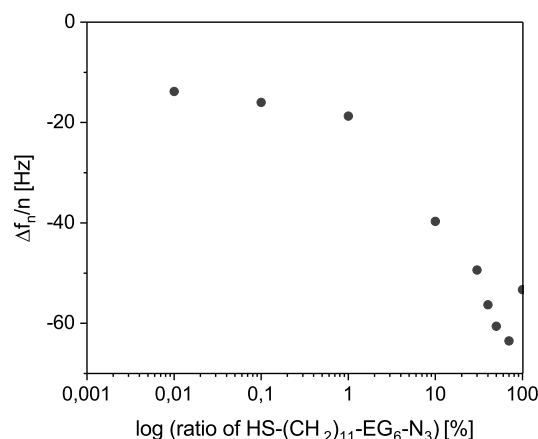
Figure C.1.: To determine the optimal azide concentration on the surface for performing the CuAAC in the QCM-D the ratio between $HS-(CH_2)_{11}-EG_3-OH$ and $HS-(CH_2)_{11}-EG_6-N_3$ is varied and the change in frequency of the reaction measured.

in frequency is determined after performing the click reaction and the Δf is plotted against the logarithm of the azide concentration. For concentrations between 1 to 40% a good response is observed. With concnetrations higher than 40% no further change in frequency is observed, which corresponds to no further immobilisation of HA to the surface.

143

Appendix D.

Control Experiments for the Analysis of the Influence of Hyaluronan on LECs

For performing the AlamarBlue[®] and CyQuant[®] assay additionally to the applied different concentrations several controls are performed as well. For the experiments on cell culture plastic the controls are the measurement of the background (cell culture plastic) and the positive control without adding HA.

For the experiments on click-PEG either with HA in solution or immobilised HA a passivation control is necessary (tab. D.1 #1) as well as a wash control for the cRGD (#2), where the surface is functionalised via CuAAC without adding copper sulfate. On these two no cell adhesion should be observed. Additionally the background is determined with a sample on a passivated surface decorated with cRGD, media and kit, but without cells (#3). To check if the cells are okay, cells are also seeded on cell culture plastic (# 4). The positive control is the passivated glass surface decorated with cRGD and cells but without adding HA (# 5). All shown data is normalised to the background.

Table D.1.: Summary of the composition of the different performed control experiments for the Alamar[®] and CyQuant[®]assay

#	type	cRGD	cells	HA
1	pass. control	+	+	+
2	wash cRGD	+[a]	+	-
3	background	+	-	-
4	plastic control	-	+	-
5	positiv control	+	+	-

a) click reaction without adding $CuSO_4$

As expected for the AlamarBlue[®] assay, a large difference in the relative intensities is found between the samples without an with cells. Even though the performed Kruskal-Wallis test with Dunn's comparison indicates a significant difference between them and the positive control only for the experiments with HA in solution (fig. D.1). A similar result is found for the CyQuant[®]
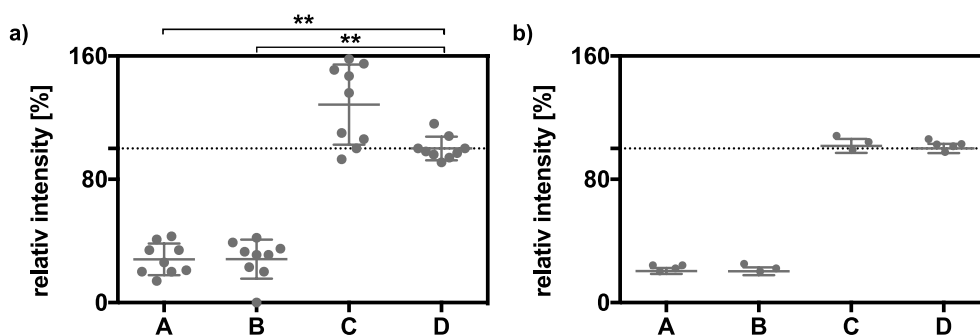
Figure D.1.: Summarised are the control experiments performed for the AlamarBlue® assay: A passivation control; B cRGD wash control; C cell culture plastic; D positive control for the experiments with HA in solution a) and immobilised on the gold nanoparticles b).

assay. The relative intensity is much smaller for the two control experiments without cells. The results found for the control on cell culture plastic and the positive control are similar to each other so the cells behave similar on both surfaces. In the end the results of the AlamarBlue® of each surface are
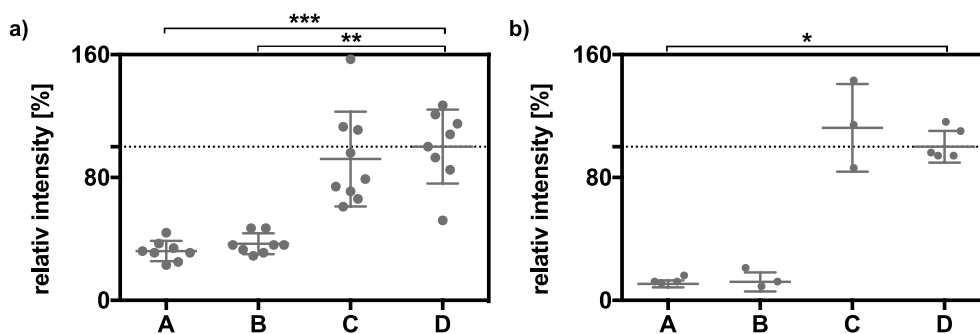
Figure D.2.: Summarised are the control experiments performed for the CyQuant® assay: A passivation control; B cRGD wash control; C cell culture plastic; D positive control for the experiments with HA in solution a) and immobilised on the gold nanoparticles b).

normalised to the results of the CyQuant® assay on the same surface. For the experiments with diluted HA no significant difference between the samples is found (fig. D.3 a), Kruskal-Wallis test with Dunn's comparison, Appendix E). The relative metabolic activity found for the cell culture plastic control is higher than for the positive control. In case of the immobilised HA species the relative metabolic activity for the controls without cells is higher than the positive control, which is due to the normalisation of the result of the AlamarBlue® to a very low amount of DNA. The comparison of the positive and plastic control show similar results, so that the cell are not damaged on

the click-PEG surface.
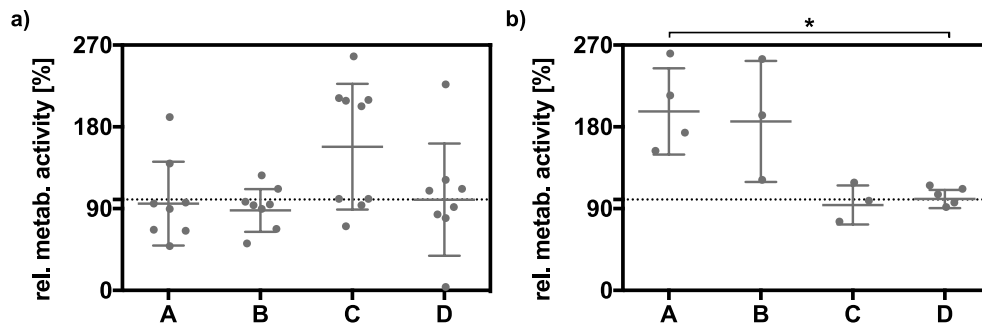
Figure D.3.: Summarised are the control experiments for the relativ metabolic activity of the LECs. Therefore the results of the AlamarBlue® are normalised to the results of the CyQuant® assay: A passivation control; B cRGD wash control; C cell culture plastic; D positive control for the experiments with HA in solution a) and immobilised on the gold nanoparticles b).

Appendix E.

Statistical Analysis

The Kruskal-Wallis-test (one-way Anova test) is a non-parametric method to analyse if samples belong to the same distribution. The statistical analysis is based on a rank which is called *H test*.[138]

$$H = \frac{\frac{12}{N(N-1)} \sum_{i=1}^{C} \frac{R_i^2}{n_i} - 3(N+1)}{1 - \sum \frac{T}{(N^3-N)}} \tag{E.1}$$

It is possible to describe the the mean rank for the cases with and without ties (equation E.1), where C represents the number of samples, n_i the number of observations in the ith sample, N the the number of observations in all samples, R_i the sum of the ranks in the ith sample and T the expression of ties with $\sum T = 0$, if no ties exist.[138]

For the comparison of different samples all values are ranked independent of there origin. The p-value is estimated using $Pr(\chi_{g-1}^2 \geq H)$. To enable the identification of the differing sample the Kruskal-Wallis test is followed by the Dunn's multiple comparison test.[139] The first step is the calculation of the value of the contrasts (y_m) for the rank sums (T_i) (equation E.2).

$$y_m = \frac{\sum_i T_i}{\sum_i n_i} - \frac{\sum_{i'} T_{i'}}{\sum_{i'} n_{i'}} \ (with \ m = 1, \dots, p) \tag{E.2}$$

The standard deviation for each value is calculated using equation E.3 considering possible ties (t_s). The comparison of the values for $\frac{y_m}{\sigma_m}$ are compared to the standard normal distribution and so vote as different or not.

$$\sigma_m^2 = \left[\frac{N(N+1)}{12} - \frac{\sum_{s=1}^{s}(t_s^3 - t_s)}{12(N-1)} \right] \left[\frac{1}{\sum_i n_i} + \frac{1}{\sum_{i'} n_{i'}} \right] \tag{E.3}$$

The calculation for both tests is performed using "GraphPad Prism" (version 6.0e/ 7.0c, *GraphPad Software Inc, USA*).

Statistical Analysis of the Toxicity of the Different HA Species

Influence of Applied HA Concentrations on Assay

Table E.1.: Kruskal-Wallis-Test with Dunn's multiple comparison

P value	0.5460
Exact or approximate P value?	Exact
P value summary	ns
Do the medians vary signif. (P < 0.05)?	No
Number of groups	4
Kruskal-Wallis statistic	2.333
Number of treatments (columns)	4
Number of values (total)	12

Dunn's comparisons	Mean rank diff.	Significant	Summary	P
1 vs. 2.5	2	No	ns	>0.9999
1 vs. 5	-0.6667	No	ns	>0.9999
1 vs. 20	3.333	No	ns	>0.9999
2.5 vs. 5	-2.667	No	ns	>0.9999
2.5 vs. 20	1.333	No	ns	>0.9999
5 vs. 20	4	No	ns	>0.9999

Test details	Mean rank 1	rank 2	rank diff	n1	n2
1 vs. 2.5	7.667	5.667	2	3	3
1 vs. 5	7.667	8.333	-0.6667	3	3
1 vs. 20	7.667	4.333	3.333	3	3
2.5 vs. 5	5.667	8.333	-2.667	3	3
2.5 vs. 20	5.667	4.333	1.333	3	3
5 vs. 20	8.333	4.333	4	3	3

Influence of Applied HA on Assay Depending on the Incubation Time

Table E.2.: Kruskal-Wallis-Test with Dunn's multiple comparison

P value	0.4636
Exact or approximate P value?	Approximate
P value summary	ns
Do the medians vary signif. (P < 0.05)?	No
Number of groups	3
Kruskal-Wallis statistic	1.538
Number of treatments (columns)	3
Number of values (total)	36

Dunn's comparisons	Mean rank diff.	Significant	Summary
0 vs. 1	5.333	No	ns
0 vs. 2	2.667	No	ns
1 vs. 2	-2.667	No	ns

Test details	rank 1	Mean rank 2	rank diff	n1	n2
0 vs. 1	21.17	15.83	5.333	12	12
0 vs. 2	21.17	18.5	2.667	12	12
1 vs. 2	15.83	18.5	-2.667	12	12

Comparison of different immobilised HA species

Table E.3.: Kruskal-Wallis-Test with Dunn's multiple comparison

P value	0.0061
Exact or approximate P value?	Approximate
P value summary	**
Do the medians vary signif. (P < 0.05)?	Yes
Number of groups	14
Kruskal-Wallis statistic	29.2
Number of treatments (columns)	14
Number of values (total)	77

Dunn's comparisons	Mean rank diff.	Significant	Summary	P_{adj}
0 µg/mL vs. 0 µg/mL	0	No	ns	>0.9999
20 µg/mL vs. 20 µg/mL	4.4	No	ns	>0.9999
50 µg/mL vs. 50 µg/mL	0.3333	No	ns	>0.9999
100 µg/mL vs. 100 µg/mL	-5.667	No	ns	>0.9999
150 µg/mL vs. 150 µg/mL	-0.6667	No	ns	>0.9999
190 µg/mL vs. 190 µg/mL	10.17	No	ns	>0.9999
Pass. control vs. Pass. control	0	No	ns	>0.9999

Test details	Mean rank 1	Mean rank 2	Mean rank diff.	n1	n2
0 µg/mL vs. 0 µg/mL	48	48	0	6	6
20 µg/mL vs. 20 µg/mL	33	28.6	4.4	5	5
50 µg/mL vs. 50 µg/mL	52.83	52.5	0.3333	6	6
100 µg/mL vs. 100 µg/mL	45	50.67	-5.667	6	6
150 µg/mL vs. 100 µg/mL	32	32.67	-0.6667	5	6
190 µg/mL vs. 100 µg/mL	47.4	37.33	10.17	4	4
Pass. con. vs. Pass. con.	6	6	0	4	4

Toxicity Comparison of different applied concentrations of unfunctionalised HA species in solution

Table E.4.: Kruskal-Wallis-Test with Dunn's multiple comparison

P value	0.1771
Exact or approximate P value?	Approximate
P value summary	ns
Do the medians vary signif. (P < 0.05)?	No
Number of groups	6
Kruskal-Wallis statistic	7.643
Number of treatments (columns)	6
Number of values (total)	36

Dunn's comparisons	Mean rank diff.	Significant	Summary	P_{adj}
0 µg/mL vs. 1 µg/mL	8.333	No	ns	0.8534
0 µg/mL vs. 2.5 µg/mL	2.5	No	ns	>0.9999
0 µg/mL vs. 5 µg/mL	3.5	No	ns	>0.9999
0 µg/mL vs. 20 µg/mL	3	No	ns	>0.9999
0 µg/mL vs. Pass. control	14.67	No	ns	0.0795

Test details	Mean rank 1	Mean rank 2	Mean rank diff.	n1	n2
0 µg/mL vs. 1 µg/mL	23.83	15.5	8.333	6	6
0 µg/mL vs. 2.5 µg/mL	23.83	21.33	2.5	6	6
0 µg/mL vs. 5 µg/mL	23.83	20.33	3.5	6	6
0 µg/mL vs. 20 µg/mL	23.83	20.83	3	6	6
0 µg/mL vs. Pass. control	23.83	9.167	14.67	6	6

Toxicity Comparison of the concentrations of different applied thiolated HA in solution

Table E.5.: Kruskal-Wallis-Test with Dunn's multiple comparison

P value	0.0620
Exact or approximate P value?	Approximate
P value summary	ns
Do the medians vary signif. (P < 0.05)?	No
Number of groups	6
Kruskal-Wallis statistic	10.51
Number of treatments (columns)	6
Number of values (total)	36

Dunn's comparisons	Mean rank diff.	Significant	Summary	P_{adj}
0 µg/mL vs. 1 µg/mL	2.833	No	ns	>0.9999
0 µg/mL vs. 2.5 µg/mL	-2.833	No	ns	>0.9999
0 µg/mL vs. 5 µg/mL	-0.8333	No	ns	>0.9999
0 µg/mL vs. 20 µg/mL	0.3333	No	ns	>0.9999
0 µg/mL vs. Pass. control	14.5	No	ns	0.0857

Test details	Mean rank 1	Mean rank 2	Mean rank diff.	n1	n2
0 µg/mL vs. 1 µg/mL	20.83	18	2.833	6	6
0 µg/mL vs. 2.5 µg/mL	20.83	23.67	-2.833	6	6
0 µg/mL vs. 5 µg/mL	20.83	21.67	-0.8333	6	6
0 µg/mL vs. 20 µg/mL	20.83	20.5	0.3333	6	6
0 µg/mL vs. Pass. control	20.83	6.333	14.5	6	6

Toxicity Comparison of different concentrations of immobilised HA

Table E.6.: Kruskal-Wallis-Test with Dunn's multiple comparison test

P value	<0.0001
Exact or approximate P value?	Approximate
P value summary	* * **
Do the medians vary signif. (P < 0.05)?	Yes
Number of groups	7
Kruskal-Wallis statistic	28.29
Number of treatments (columns)	7
Number of values (total)	77

Dunn's comparisons	Mean rank diff.	Significant	Summary	P_{adj}
0 nm vs. 20 nm	17.2	No	ns	0.4353
0 nm vs. 50 nm	-4.667	No	ns	>0.9999
0 nm vs. 100 nm	0.1667	No	ns	>0.9999
0 nm vs. 150 nm	15.64	No	ns	0.5642
0 nm vs. 190 nm	5.583	No	ns	>0.9999
0 nm vs. Pass. control	42	Yes	* * *	0.0002

Test details	Mean rank 1	Mean rank 2	Mean rank diff.	n1	n2
0 nm vs. 20 nm	48	30.8	17.2	12	10
0 nm vs. 50 nm	48	52.67	-4.667	12	12
0 nm vs. 100 nm	48	47.83	0.1667	12	12
0 nm vs. 150 nm	48	32.36	15.64	12	11
0 nm vs. 190 nm	48	42.42	5.583	12	12
0 nm vs. Pass. control	48	6	42	12	8

E.1. Statistical Analysis of Samples with short HA in Solution on Cell Culture Plastic

CyQuant® Assay for digested HA

Table E.7.: Kruskal-Wallis-Test with Dunn's multiple comparison

P value	0.5718
Exact or approximate P value?	Exact
P value summary	ns
Do the medians vary signif. (P < 0.05)?	No
Number of groups	5
Kruskal-Wallis statistic	3.233
Number of treatments (columns)	5
Number of values (total)	15

Dunn's comparisons	Mean rank diff.	Significant	Summary
0 vs. 1	-0.6667	No	ns
0 vs. 2.5	4.333	No	ns
0 vs. 5	1.333	No	ns
0 vs. 20	-1.667	No	ns
1 vs. 2.5	5	No	ns
1 vs. 5	2	No	ns
1 vs. 20	-1	No	ns
2.5 vs. 5	-3	No	ns
2.5 vs. 20	-6	No	ns
5 vs. 20	-3	No	ns

Test details	Mean rank 1	Mean rank 2	Mean rank diff.	n1	n2
0 vs. 1	8.667	9.333	-0.6667	3	3
0 vs. 2.5	8.667	4.333	4.333	3	3
0 vs. 5	8.667	7.333	1.333	3	3
0 vs. 20	8.667	10.33	-1.667	3	3
1 vs. 2.5	9.333	4.333	5	3	3
1 vs. 5	9.333	7.333	2	3	3
1 vs. 20	9.333	10.33	-1	3	3
2.5 vs. 5	4.333	7.333	-3	3	3
2.5 vs. 20	4.333	10.33	-6	3	3
5 vs. 20	7.333	10.33	-3	3	3

CyQuant® Assay for short HA

Table E.8.: Kruskal-Wallis-Test with Dunn's multiple comparison

P value	0.6441
Exact or approximate P value?	Approximate
P value summary	ns
Do the medians vary signif. (P < 0.05)?	No
Number of groups	5
Kruskal-Wallis statistic	2.503
Number of treatments (columns)	5
Number of values (total)	34

Dunn's comparisons	Mean rank diff.	Significant	Summary
0 vs. 1	8.143	No	ns
0 vs. 2.5	5.571	No	ns
0 vs. 5	5.357	No	ns
0 vs. 20	2.786	No	ns
1 vs. 2.5	-2.571	No	ns
1 vs. 5	-2.786	No	ns
1 vs. 20	-5.357	No	ns
2.5 vs. 5	-0.2143	No	ns
2.5 vs. 20	-2.786	No	ns
5 vs. 20	-2.571	No	ns

Test details	Mean rank 1	Mean rank 2	Mean rank diff.	n1	n2
0 vs. 1	22	13.86	8.143	6	7
0 vs. 2.5	22	16.43	5.571	6	7
0 vs. 5	22	16.64	5.357	6	7
0 vs. 20	22	19.21	2.786	6	7
1 vs. 2.5	13.86	16.43	-2.571	7	7
1 vs. 5	13.86	16.64	-2.786	7	7
1 vs. 20	13.86	19.21	-5.357	7	7
2.5 vs. 5	16.43	16.64	-0.2143	7	7
2.5 vs. 20	16.43	19.21	-2.786	7	7
5 vs. 20	16.64	19.21	-2.571	7	7

AlamarBlue® Assay for digested HA

Table E.9.: Kruskal-Wallis-Test with Dunn's multiple comparison

P value	0.0368
Exact or approximate P value?	Exact
P value summary	*
Do the medians vary signif. (P < 0.05)?	Yes
Number of groups	5
Kruskal-Wallis statistic	8.733
Number of treatments (columns)	5
Number of values (total)	15

Dunn's comparisons	Mean rank diff.	Significant	Summary
0 vs. 1	7	No	ns
0 vs. 2.5	7.333	No	ns
0 vs. 5	10	No	ns
0 vs. 20	4	No	ns
1 vs. 2.5	0.3333	No	ns
1 vs. 5	3	No	ns
1 vs. 20	-3	No	ns
2.5 vs. 5	2.667	No	ns
2.5 vs. 20	-3.333	No	ns
5 vs. 20	-6	No	ns

Test details	Mean rank 1	Mean rank 2	Mean rank diff.	n1	n2
0 vs. 1	13.67	6.667	7	3	3
0 vs. 2.5	13.67	6.333	7.333	3	3
0 vs. 5	13.67	3.667	10	3	3
0 vs. 20	13.67	9.667	4	3	3
1 vs. 2.5	6.667	6.333	0.3333	3	3
1 vs. 5	6.667	3.667	3	3	3
1 vs. 20	6.667	9.667	-3	3	3
2.5 vs. 5	6.333	3.667	2.667	3	3
2.5 vs. 20	6.333	9.667	-3.333	3	3
5 vs. 20	3.667	9.667	-6	3	3

AlamarBlue® Assay for short HA

Table E.10.: Kruskal-Wallis-Test with Dunn's multiple comparison

P value	0.7760
Exact or approximate P value?	Approximate
P value summary	ns
Do the medians vary signif. (P < 0.05)?	No
Number of groups	5
Kruskal-Wallis statistic	1.781
Number of treatments (columns)	5
Number of values (total)	34

Dunn's comparisons	Mean rank diff.	Significant	Summary
0 vs. 1	5.667	No	ns
0 vs. 2.5	3.524	No	ns
0 vs. 5	1.81	No	ns
0 vs. 20	-0.4762	No	ns
1 vs. 2.5	-2.143	No	ns
1 vs. 5	-3.857	No	ns
1 vs. 20	-6.143	No	ns
2.5 vs. 5	-1.714	No	ns
2.5 vs. 20	-4	No	ns
5 vs. 20	-2.286	No	ns

Test details	Mean rank 1	Mean rank 2	Mean rank diff.	n1	n2
0 vs. 1	19.67	14	5.667	6	7
0 vs. 2.5	19.67	16.14	3.524	6	7
0 vs. 5	19.67	17.86	1.81	6	7
0 vs. 20	19.67	20.14	-0.4762	6	7
1 vs. 2.5	14	16.14	-2.143	7	7
1 vs. 5	14	17.86	-3.857	7	7
1 vs. 20	14	20.14	-6.143	7	7
2.5 vs. 5	16.14	17.86/-1.714	7	7	
2.5 vs. 20	16.14	20.14	-4	7	7
5 vs. 20	17.86	20.14	-2.286	7	7

Comparison of the results for the AlamarBlue® assay for digested and short HA

Table E.11.: Kruskal-Wallis-Test with Dunn's multiple comparison

P value	0.0773
Exact or approximate P value?	Approximate
P value summary	ns
Do the medians vary signif. (P < 0.05)?	No
Number of groups	9
Kruskal-Wallis statistic	14.18
Number of treatments (columns)	9
Number of values (total)	49

Dunn's comparisons	Mean rank diff.	Significant	Summary
0 vs. 1.0	18.78	No	ns
0 vs. 2.5	17.44	No	ns
0 vs. 5.0	22.44	No	ns
0 vs. 20.0	9.611	No	ns
0 vs. 1_2	21.18	No	ns
0 vs. 2.5_2	15.83	No	ns
0 vs. 5_2	13.25	No	ns
0 vs. 20_2	5.254	No	ns
1.0 vs. 2.5	-1.333	No	ns
1.0 vs. 5.0	3.667	No	ns
1.0 vs. 20.0	-9.167	No	ns
1.0 vs. 1_2	2.405	No	ns
1.0 vs. 2.5_2	-2.952	No	ns
1.0 vs. 5_2	-5.524	No	ns
1.0 vs. 20_2	-13.52	No	ns
2.5 vs. 5.0	5	No	ns
2.5 vs. 20.0	-7.833	No	ns
2.5 vs. 1_2	3.738	No	ns
2.5 vs. 2.5_2	-1.619	No	ns
2.5 vs. 5_2	-4.19	No	ns
2.5 vs. 20_2	-12.19	No	ns
5.0 vs. 20.0	-12.83	No	ns
5.0 vs. 1_2	-1.262	No	ns
5.0 vs. 2.5_2	-6.619	No	ns
5.0 vs. 5_2	-9.19	No	ns
5.0 vs. 20_2	-17.19	No	ns
20.0 vs. 1_2	11.57	No	ns
20.0 vs. 2.5_2	6.214	No	ns
20.0 vs. 5_2	3.643	No	ns
20.0 vs. 20_2	-4.357	No	ns
1_2 vs. 2.5_2	-5.357	No	ns
1_2 vs. 5_2	-7.929	No	ns
1_2 vs. 20_2	-15.93	No	ns
2.5_2 vs. 5_2	-2.571	No	ns
2.5_2 vs. 20_2	-10.57	No	ns
5_2 vs. 20_2	-8	No	ns

Test details	Mean rank 1	Mean rank 2	Mean rank diff.	n1	n2
0 vs. 1.0	37.11	18.33	18.78	9	3
0 vs. 2.5	37.11	19.67	17.44	9	3
0 vs. 5.0	37.11	14.67	22.44	9	3
0 vs. 20.0	37.11	27.5	9.611	9	3
0 vs. 1_2	37.11	15.93	21.18	9	7
0 vs. 2.5_2	37.11	21.29	15.83	9	7
0 vs. 5_2	37.11	23.86	13.25	9	7
0 vs. 20_2	37.11	31.86	5.254	9	7
1.0 vs. 2.5	18.33	19.67	-1.333	3	3
1.0 vs. 5.0	18.33	14.67	3.667	3	3
1.0 vs. 20.0	18.33	27.5	-9.167	3	3
1.0 vs. 1_2	18.33	15.93	2.405	3	7
1.0 vs. 2.5_2	18.33	21.29	-2.952	3	7
1.0 vs. 5_2	18.33	23.86	-5.524	3	7
1.0 vs. 20_2	18.33	31.86	-13.52	3	7
2.5 vs. 5.0	19.67	14.67	5	3	3
2.5 vs. 20.0	19.67	27.5	-7.833	3	3
2.5 vs. 1_2	19.67	15.93	3.738	3	7
2.5 vs. 2.5_2	19.67	21.29	-1.619	3	7
2.5 vs. 5_2	19.67	23.86	-4.19	3	7
2.5 vs. 20_2	19.67	31.86	-12.19	3	7
5.0 vs. 20.0	14.67	27.5	-12.83	3	3
5.0 vs. 1_2	14.67	15.93	-1.262	3	7
5.0 vs. 2.5_2	14.67	21.29	-6.619	3	7
5.0 vs. 5_2	14.67	23.86	-9.19	3	7
5.0 vs. 20_2	14.67	31.86	-17.19	3	7
20.0 vs. 1_2	27.5	15.93	11.57	3	7
20.0 vs. 2.5_2	27.5	21.29	6.214	3	7
20.0 vs. 5_2	27.5	23.86	3.643	3	7
20.0 vs. 20_2	27.5	31.86	-4.357	3	7
1_2 vs. 2.5_2	15.93	21.29	-5.357	7	7
1_2 vs. 5_2	15.93	23.86	-7.929	7	7
1_2 vs. 20_2	15.93	31.86	-15.93	7	7
2.5_2 vs. 5_2	21.29	23.86	-2.571	7	7
2.5_2 vs. 20_2	21.29	31.86	-10.57	7	7
5_2 vs. 20_2	23.86	31.86	-8	7	7

Results for relative metabolic activity digested HA

Table E.12.: Kruskal-Wallis-Test with Dunn's multiple comparison

P value	0.5493
Exact or approximate P value?	Exact
P value summary	ns
Do the medians vary signif. (P < 0.05)?	No
Number of groups	5
Kruskal-Wallis statistic	3.345
Number of treatments (columns)	5
Number of values (total)	15

Dunn's comparisons	Mean rank diff.	Significant	Summary	P
0 vs. 1.0	5	No	ns	>0.9999
0 vs. 2.5	0	No	ns	>0.9999
0 vs. 5.0	4.167	No	ns	>0.9999
0 vs. 20.0	3.333	No	ns	>0.9999
1.0 vs. 2.5	-5	No	ns	>0.9999
1.0 vs. 5.0	-0.8333	No	ns	>0.9999
1.0 vs. 20.0	-1.667	No	ns	>0.9999
2.5 vs. 5.0	4.167	No	ns	>0.9999
2.5 vs. 20.0	3.333	No	ns	>0.9999
5.0 vs. 20.0	-0.8333	No	ns	>0.9999

Test details	Mean rank 1	Mean rank 2	Mean rank diff.	n1	n2
0 vs. 1.0	10.5	5.5	5	3	3
0 vs. 2.5	10.5	10.5	0	3	3
0 vs. 5.0	10.5	6.333	4.167	3	3
0 vs. 20.0	10.5	7.167	3.333	3	3
1.0 vs. 2.5	5.5	10.5	-5	3	3
1.0 vs. 5.0	5.5	6.333	-0.8333	3	3
1.0 vs. 20.0	5.5	7.167	-1.667	3	3
2.5 vs. 5.0	10.5	6.333	4.167	3	3
2.5 vs. 20.0	10.5	7.167	3.333	3	3
5.0 vs. 20.0	6.333	7.167	-0.8333	3	3

Results for relative metabolic activity short HA

Table E.13.: Kruskal-Wallis-Test with Dunn's multiple comparison

P value	0.8102
Exact or approximate P value?	Approximate
P value summary	ns
Do the medians vary signif. (P < 0.05)?	No
Number of groups	5
Kruskal-Wallis statistic	1.592
Number of treatments (columns)	5
Number of values (total)	34

Dunn's comparisons	Mean rank diff.	Significant	Summary	P
0 vs. 1.0	-5.69	No	ns	>0.9999
0 vs. 2.5	-5.69	No	ns	>0.9999
0 vs. 5.0	-2.69	No	ns	>0.9999
0 vs. 20.0	-2.119	No	ns	>0.9999
1.0 vs. 2.5	0	No	ns	>0.9999
1.0 vs. 5.0	3	No	ns	>0.9999
1.0 vs. 20.0	3.571	No	ns	>0.9999
2.5 vs. 5.0	3	No	ns	>0.9999
2.5 vs. 20.0	3.571	No	ns	>0.9999
5.0 vs. 20.0	0.5714	No	ns	>0.9999

Test details	Mean rank 1	Mean rank 2	Mean rank diff.	n1	n2
0 vs. 1.0	14.17	19.86	-5.69	6	7
0 vs. 2.5	14.17	19.86	-5.69	6	7
0 vs. 5.0	14.17	16.86	-2.69	6	7
0 vs. 20.0	14.17	16.29	-2.119	6	7
1.0 vs. 2.5	19.86	19.86	0	7	7
1.0 vs. 5.0	19.86	16.86	3	7	7
1.0 vs. 20.0	19.86	16.29	3.571	7	7
2.5 vs. 5.0	19.86	16.86	3	7	7
2.5 vs. 20.0	19.86	16.29	3.571	7	7
5.0 vs. 20.0	16.86	16.29	0.5714	7	7

Results for relative metabolic activity for digested HA

Table E.14.: Kruskal-Wallis-Test with Dunn's multiple comparison

P value	0.5493
Exact or approximate P value?	Exact
P value summary	ns
Do the medians vary signif. (P < 0.05)?	No
Number of groups	5
Kruskal-Wallis statistic	3.345
Number of treatments (columns)	5
Number of values (total)	15

Dunn's comparisons	Mean rank diff.	Significant	Summary
0 vs. 1.0	5	No	ns
0 vs. 2.5	0	No	ns
0 vs. 5.0	4.167	No	ns
0 vs. 20.0	3.333	No	ns
1.0 vs. 2.5	-5	No	ns
1.0 vs. 5.0	-0.8333	No	ns
1.0 vs. 20.0	-1.667	No	ns
2.5 vs. 5.0	4.167	No	ns
2.5 vs. 20.0	3.333	No	ns
5.0 vs. 20.0	-0.8333	No	ns

Test details	Mean rank 2	Mean rank diff.	n1	n2
0 vs. 1.0	5.5	5	3	3
0 vs. 2.5	10.5	06	3	3
0 vs. 5.0	6.333	4.167	3	3
0 vs. 20.0	7.167	3.333	3	3
1.0 vs. 2.5	10.5	-5	3	3
1.0 vs. 5.0	6.333	-0.8333	3	3
1.0 vs. 20.0	7.167	-1.667	3	3
2.5 vs. 5.0	6.333	4.167	3	3
2.5 vs. 20.0	7.167	3.333	3	3
5.0 vs. 20.0	7.167	-0.8333	3	3

Results for the relative metabolic activity for short HA

Table E.15.: Kruskal-Wallis-Test with Dunn's multiple comparison

P value	0.8102
Exact or approximate P value?	Approximate
P value summary	ns
Do the medians vary signif. (P < 0.05)?	No
Number of groups	5
Kruskal-Wallis statistic	1.592
Number of treatments (columns)	5
Number of values (total)	34

Dunn's comparisons	Mean rank diff.	Significant	Summary
0 vs. 1.0	-5.69	No	ns
0 vs. 2.5	-5.69	No	ns
0 vs. 5.0	-2.69	No	ns
0 vs. 20.0	-2.119	No	ns
1.0 vs. 2.5	0	No	ns
1.0 vs. 5.0	3	No	ns
1.0 vs. 20.0	3.571	No	ns
2.5 vs. 5.0	3	No	ns
2.5 vs. 20.0	3.571	No	ns
5.0 vs. 20.0	0.5714	No	ns

Test details	Mean rank 1	Mean rank 2	Mean rank diff.	n1	n2
0 vs. 1.0	14.17	19.86	-5.69	6	7
0 vs. 2.5	14.17	19.86	-5.69	6	7
0 vs. 5.0	14.17	16.86	-2.69	6	7
0 vs. 20.0	14.17	16.29	-2.119	6	7
1.0 vs. 2.5	19.86	19.86	0	7	7
1.0 vs. 5.0	19.86	16.86	3	7	7
1.0 vs. 20.0	19.86	16.29	3.571	7	7
2.5 vs. 5.0	19.86	16.86	3	7	7
2.5 vs. 20.0	19.86	16.29	3.571	7	7
5.0 vs. 20.0	19.86	16.29	0.5714	7	7

Results for relative metabolic activity

Table E.16.: Kruskal-Wallis-Test with Dunn's multiple comparison

P value	0.8754
Exact or approximate P value?	Approximate
P value summary	ns
Do the medians vary signif. (P < 0.05)?	No
Number of groups	5
Kruskal-Wallis statistic	1.217
Number of treatments (columns)	5
Number of values (total)	49

Dunn's comparisons	Mean rank diff.	Significant	Summary	P
0 vs. 1.0	-0.1333	No	ns	>0.9999
0 vs. 2.5	-4.483	No	ns	>0.9999
0 vs. 5.0	0.8667	No	ns	>0.9999
0 vs. 20.0	2.117	No	ns	>0.9999
1.0 vs. 2.5	-4.35	No	ns	>0.9999
1.0 vs. 5.0	1	No	ns	>0.9999
1.0 vs. 20.0	2.25	No	ns	>0.9999
2.5 vs. 5.0	5.35	No	ns	>0.9999
2.5 vs. 20.0	6.6	No	ns	>0.9999
5.0 vs. 20.0	1.25	No	ns	>0.9999

Test details	Mean rank 1	Mean rank 2	Mean rank diff.	n1	n2
0 vs. 1.0	24.67	24.8	-0.1333	9	10
0 vs. 2.5	24.67	29.15	-4.483	9	10
0 vs. 5.0	24.67	23.8	0.8667	9	10
0 vs. 20.0	24.67	22.55	2.117	9	10
1.0 vs. 2.5	24.8	29.15	-4.35	10	10
1.0 vs. 5.0	24.8	23.8	1	10	10
1.0 vs. 20.0	24.8	22.55	2.25	10	10
2.5 vs. 5.0	29.15	23.8	5.35	10	10
2.5 vs. 20.0	29.15	22.55	6.6	10	10
5.0 vs. 20.0	23.8	22.55	1.25	10	10

Results for relative metabolic activity for the controls

Table E.17.: Kruskal-Wallis-Test with Dunn's multiple comparison

P value	0.1243
Exact or approximate P value?	Approximate
P value summary	ns
Do the medians vary signif. (P < 0.05)?	No
Number of groups	4
Kruskal-Wallis statistic	5.752
Number of treatments (columns)	4
Number of values (total)	33

Dunn's comparisons	Mean rank diff.	Significant	Summary
A vs. B	-0.75	No	ns
A vs. C	-9.951	No	ns
A vs. D	-2.75	No	ns
B vs. C	-9.201	No	ns
B vs. D	-2	No	ns
C vs. D	7.201	No	ns

Test details	Mean rank 1	Mean rank 2	Mean rank diff.	n1	n2
A vs. B	13.44	14.19	-0.75	8	8
A vs. C	13.44	23.39	-9.951	8	9
A vs. D	13.44	16.19	-2.75	8	8
B vs. C	14.19	23.39	-9.201	8	9
B vs. D	14.19	16.19	-2	8	8
C vs. D	23.39	16.19	7.201	9	8

E.2. Statistical Analysis of Samples with short HA in Solution in Presence of cRGD

CyQuant® Assay for digested, unfunctionalised HA

Table E.18.: Kruskal-Wallis-Test with Dunn's multiple comparison

P value	0.4598
Exact or approximate P value?	Exact
P value summary	ns
Do the medians vary signif. (P < 0.05)?	No
Number of groups	5
Kruskal-Wallis statistic	3.919
Number of treatments (columns)	5
Number of values (total)	15

Dunn's comparisons	Mean rank diff.	Significant	Summary
0 vs. 1.0	-0.1667	No	ns
0 vs. 2.5	0.1667	No	ns
0 vs. 5.0	-1.667	No	ns
0 vs. 20.0	5	No	ns
1.0 vs. 2.5	0.3333	No	ns
1.0 vs. 5.0	-1.5	No	ns
1.0 vs. 20.0	5.167	No	ns
2.5 vs. 5.0	-1.833	No	ns
2.5 vs. 20.0	4.833	No	ns
5.0 vs. 20.0	6.667	No	ns

Test details	Mean rank 1	Mean rank 2	Mean rank diff.	n1	n2
0 vs. 1.0	8.667	8.833	-0.1667	3	3
0 vs. 2.5	8.667	8.5	0.1667	3	3
0 vs. 5.0	8.667	10.33	-1.667	3	3
0 vs. 20.0	8.667	3.667	5	3	3
1.0 vs. 2.5	8.833	8.5	0.3333	3	3
1.0 vs. 5.0	8.833	10.33	-1.5	3	3
1.0 vs. 20.0	8.833	3.667	5.167	3	3
2.5 vs. 5.0	8.5	10.33	-1.833	3	3
2.5 vs. 20.0	8.5	3.667	4.833	3	3
5.0 vs. 20.0	10.33	3.667	6.667	3	3

CyQuant® Assay for short, unfunctionalised HA

Table E.19.: Kruskal-Wallis-Test with Dunn's multiple comparison

P value	0.0828
Exact or approximate P value?	Approximate
P value summary	ns
Do the medians vary signif. (P < 0.05)?	No
Number of groups	5
Kruskal-Wallis statistic	8.25
Number of treatments (columns)	5
Number of values (total)	32

Dunn's comparisons	Mean rank diff.	Significant	Summary
0 vs. 1.0	3.257	No	ns
0 vs. 2.5	7.043	No	ns
0 vs. 5.0	-6.433	No	ns
0 vs. 20.0	-2.957	No	ns
1.0 vs. 2.5	3.786	No	ns
1.0 vs. 5.0	-9.69	No	ns
1.0 vs. 20.0	-6.214	No	ns
2.5 vs. 5.0	-13.48	No	ns
2.5 vs. 20.0	-10	No	ns
5.0 vs. 20.0	3.476	No	ns

Test details	Mean rank 1	Mean rank 2	Mean rank diff.	n1	n2
0 vs. 1.0	16.9	13.64	3.257	5	7
0 vs. 2.5	16.9	9.857	7.043	5	7
0 vs. 5.0	16.9	23.33	-6.433	5	6
0 vs. 20.0	16.9	19.86	-2.957	5	7
1.0 vs. 2.5	13.64	9.857	3.786	7	7
1.0 vs. 5.0	13.64	23.33	-9.69	7	6
1.0 vs. 20.0	13.64	19.86	-6.214	7	7
2.5 vs. 5.0	9.857	23.33	-13.48	7	6
2.5 vs. 20.0	9.857	19.86	-10	7	7
5.0 vs. 20.0	23.33	19.86	3.476	6	7

CyQuant® Assay for digested, end-thiolated HA

Table E.20.: Kruskal-Wallis-Test with Dunn's multiple comparison

P value	0.4275
Exact or approximate P value?	Exact
P value summary	ns
Do the medians vary signif. (P < 0.05)?	No
Number of groups	5
Kruskal-Wallis statistic	4.136
Number of treatments (columns)	5
Number of values (total)	15

Dunn's comparisons	Mean rank diff.	Significant	Summary
0 vs. 1.0	-2.5	No	ns
0 vs. 2.5	-0.6667	No	ns
0 vs. 5.0	2.333	No	ns
0 vs. 20.0	4.167	No	ns
1.0 vs. 2.5	1.833	No	ns
1.0 vs. 5.0	4.833	No	ns
1.0 vs. 20.0	6.667	No	ns
2.5 vs. 5.0	3	No	ns
2.5 vs. 20.0	4.833	No	ns
5.0 vs. 20.0	1.833	No	ns

Test details	Mean rank 1	Mean rank 2	Mean rank diff.	n1	n2
0 vs. 1.0	8.667	11.17	-2.5	3	3
0 vs. 2.5	8.667	9.333	-0.6667	3	3
0 vs. 5.0	8.667	6.333	2.333	3	3
0 vs. 20.0	8.667	4.5	4.167	3	3
1.0 vs. 2.5	11.17	9.333	1.833	3	3
1.0 vs. 5.0	11.17	6.333	4.833	3	3
1.0 vs. 20.0	11.17	4.5	6.667	3	3
2.5 vs. 5.0	9.333	6.333	3	3	3
2.5 vs. 20.0	9.333	4.5	4.833	3	3
5.0 vs. 20.0	6.333	4.5	1.833	3	3

CyQuant® Assay for short, end-thiolated HA

Table E.21.: Kruskal-Wallis-Test with Dunn's multiple comparison

P value	0.6272
Exact or approximate P value?	Exact
P value summary	ns
Do the medians vary signif. (P < 0.05)?	No
Number of groups	4
Kruskal-Wallis statistic	2.026
Number of treatments (columns)	4
Number of values (total)	12

Dunn's comparisons	Mean rank diff.	Significant	Summary
0 vs. 1.0	3	No	ns
0 vs. 2.5	1	No	ns
0 vs. 5.0	3.333	No	ns
1.0 vs. 2.5	-2	No	ns
1.0 vs. 5.0	0.3333	No	ns
2.5 vs. 5.0	2.333	No	ns

Test details	Mean rank 1	Mean rank 2	Mean rank diff.	n1	n2
0 vs. 1.0	8	5	3	5	2
0 vs. 2.5	8	7	1	5	2
0 vs. 5.0	8	4.667	3.333	5	3
1.0 vs. 2.5	5	7	-2	2	2
1.0 vs. 5.0	5	4.667	0.3333	2	3
2.5 vs. 5.0	7	4.667	2.333	2	3

AlamarBlue® Assay for digested, unfunctionalised HA

Table E.22.: Kruskal-Wallis-Test with Dunn's multiple comparison

P value	0.2128
Exact or approximate P value?	Exact
P value summary	ns
Do the medians vary signif. ($P < 0.05$)?	No
Number of groups	5
Kruskal-Wallis statistic	5.864
Number of treatments (columns)	5
Number of values (total)	14

Dunn's comparisons	Mean rank diff.	Significant	Summary
0 vs. 1.0	3.333	No	ns
0 vs. 2.5	7.333	No	ns
0 vs. 5.0	4.833	No	ns
0 vs. 20.0	1.167	No	ns
1.0 vs. 2.5	4	No	ns
1.0 vs. 5.0	1.5	No	ns
1.0 vs. 20.0	-2.167	No	ns
2.5 vs. 5.0	-2.5	No	ns
2.5 vs. 20.0	-6.167	No	ns
5.0 vs. 20.0	-3.667	No	ns

Test details	Mean rank 1	Mean rank 2	Mean rank diff.	n1	n2
0 vs. 1.0	10.83	7.5	3.333	3	2
0 vs. 2.5	10.83	3.5	7.333	3	3
0 vs. 5.0	10.83	6	4.833	3	3
0 vs. 20.0	10.83	9.667	1.167	3	3
1.0 vs. 2.5	7.5	3.5	4	2	3
1.0 vs. 5.0	7.5	6	1.5	2	3
1.0 vs. 20.0	7.5	9.667	-2.167	2	3
2.5 vs. 5.0	3.5	6	-2.5	3	3
2.5 vs. 20.0	3.5	9.667	-6.167	3	3
5.0 vs. 20.0	6	9.667	-3.667	3	3

AlamarBlue® Assay for short, unfunctionalised HA

Table E.23.: Kruskal-Wallis-Test with Dunn's multiple comparison

P value	0.1959
Exact or approximate P value?	Approximate
P value summary	ns
Do the medians vary signif. (P < 0.05)?	No
Number of groups	5
Kruskal-Wallis statistic	6.043
Number of treatments (columns)	5
Number of values (total)	31

Dunn's comparisons	Mean rank diff.	Significant	Summary
0 vs. 1.0	7.524	No	ns
0 vs. 2.5	11.58	No	ns
0 vs. 5.0	3.75	No	ns
0 vs. 20.0	2.583	No	ns
1.0 vs. 2.5	4.06	No	ns
1.0 vs. 5.0	-3.774	No	ns
1.0 vs. 20.0	-4.94	No	ns
2.5 vs. 5.0	-7.833	No	ns
2.5 vs. 20.0	-9	No	ns
5.0 vs. 20.0	-1.167	No	ns

Test details	Mean rank 1	Mean rank 2	Mean rank diff.	n1	n2
0 vs. 1.0	21.17	13.64	7.524	6	7
0 vs. 2.5	21.17	9.583	11.58	6	6
0 vs. 5.0	21.17	17.42	3.75	6	6
0 vs. 20.0	21.17	18.58	2.583	6	6
1.0 vs. 2.5	13.64	9.583	4.06	7	6
1.0 vs. 5.0	13.64	17.42	-3.774	7	6
1.0 vs. 20.0	13.64	18.58	-4.94	7	6
2.5 vs. 5.0	9.583	17.42	-7.833	6	6
2.5 vs. 20.0	9.583	18.58	-9	6	6
5.0 vs. 20.0	17.42	18.58	-1.167	6	6

AlamarBlue® Assay for digested, end-thiolated HA

Table E.24.: Kruskal-Wallis-Test with Dunn's multiple comparison

P value	0.1411
Exact or approximate P value?	Exact
P value summary	ns
Do the medians vary signif. (P < 0.05)?	No
Number of groups	5
Kruskal-Wallis statistic	6.653
Number of treatments (columns)	5
Number of values (total)	14

Dunn's comparisons	Mean rank diff.	Significant	Summary
0 vs. 1.0	4.833	No	ns
0 vs. 2.5	0	No	ns
0 vs. 5.0	-4	No	ns
0 vs. 20.0	-2.167	No	ns
1.0 vs. 2.5	-4.833	No	ns
1.0 vs. 5.0	-8.833	No	ns
1.0 vs. 20.0	-7	No	ns
2.5 vs. 5.0	-4	No	ns
2.5 vs. 20.0	-2.167	No	ns
5.0 vs. 20.0	1.833	No	ns

Test details	Mean rank 1	Mean rank 2	Mean rank diff.	n1	n2
0 vs. 1.0	7.5	2.667	4.833	3	3
0 vs. 2.5	7.5	7.5	0	3	3
0 vs. 5.0	7.5	11.5	-4	3	2
0 vs. 20.0	7.5	9.667	-2.167	3	3
1.0 vs. 2.5	2.667	7.5	-4.833	3	3
1.0 vs. 5.0	2.667	11.5	-8.833	3	2
1.0 vs. 20.0	2.667	9.667	-7	3	3
2.5 vs. 5.0	7.5	11.5	-4	3	2
2.5 vs. 20.0	7.5	9.667	-2.167	3	3
5.0 vs. 20.0	11.5	9.667	1.833	2	3

AlamarBlue® Assay for short, end-thiolated HA

Table E.25.: Kruskal-Wallis-Test with Dunn's multiple comparison

P value	0.1442
Exact or approximate P value?	Exact
P value summary	ns
Do the medians vary signif. (P < 0.05)?	No
Number of groups	5
Kruskal-Wallis statistic	6.541
Number of treatments (columns)	5
Number of values (total)	13

Dunn's comparisons	Mean rank diff.	Significant	Summary
0 vs. 1.0	3.833	No	ns
0 vs. 2.5	2.667	No	ns
0 vs. 5.0	-2	No	ns
0 vs. 20.0	-3.5	No	ns
1.0 vs. 2.5	-1.167	No	ns
1.0 vs. 5.0	-5.833	No	ns
1.0 vs. 20.0	-7.333	No	ns
2.5 vs. 5.0	-4.667	No	ns
2.5 vs. 20.0	-6.167	No	ns
5.0 vs. 20.0	-1.5	No	ns

Test details	Mean rank 1	Mean rank 2	Mean rank diff.	n1	n2
0 vs. 1.0	7.5	3.667	3.833	2	3
0 vs. 2.5	7.5	4.833	2.667	2	3
0 vs. 5.0	7.5	9.5	-2	2	3
0 vs. 20.0	7.5	11	-3.5	2	2
1.0 vs. 2.5	3.667	4.833	-1.167	3	3
1.0 vs. 5.0	3.667	9.5	-5.833	3	3
1.0 vs. 20.0	3.667	11	-7.333	3	2
2.5 vs. 5.0	4.833	9.5	-4.667	3	3
2.5 vs. 20.0	4.833	11	-6.167	3	2
5.0 vs. 20.0	9.5	11	-1.5	3	2

Comparison of different applied unfunctionalised HA species in solution

Table E.26.: Kruskal-Wallis-Test with Dunn's multiple comparison

P value	0.2887
Exact or approximate P value?	Approximate
P value summary	ns
Do the medians vary signif. (P < 0.05)?	No
Number of groups	10
Kruskal-Wallis statistic	10.81
Number of treatments (columns)	10
Number of values (total)	45

Dunn's comparisons	Mean rank diff.	Significant	Summary
0 vs. 1	9.333	No	ns
0 vs. 2.5	18.83	No	ns
0 vs. 5	10.83	No	ns
0 vs. 20	2.167	No	ns
0 vs. 0_2	-0.4167	No	ns
0 vs. 1_2	11.4	No	ns
0 vs. 2.5_2	17.5	No	ns
0 vs. 5_2	5.417	No	ns
0 vs. 20_2	3.917	No	ns
1 vs. 2.5	9.5	No	ns
1 vs. 5	1.5	No	ns
1 vs. 20	-7.167	No	ns
1 vs. 0_2	-9.75	No	ns
1 vs. 1_2	2.071	No	ns
1 vs. 2.5_2	8.167	No	ns
1 vs. 5_2	-3.917	No	ns
1 vs. 20_2	-5.417	No	ns
2.5 vs. 5	-8	No	ns
2.5 vs. 20	-16.67	No	ns
2.5 vs. 0_2	-19.25	No	ns
2.5 vs. 1_2	-7.429	No	ns
2.5 vs. 2.5_2	-1.333	No	ns
2.5 vs. 5_2	-13.42	No	ns
2.5 vs. 20_2	-14.92	No	ns
5 vs. 20	-8.667	No	ns
5 vs. 0_2	-11.25	No	ns
5 vs. 1_2	0.5714	No	ns
5 vs. 2.5_2	6.667	No	ns
5 vs. 5_2	-5.417	No	ns
5 vs. 20_2	-6.917	No	ns
20 vs. 0_2	-2.583	No	ns
20 vs. 1_2	9.238	No	ns
20 vs. 2.5_2	15.33	No	ns
20 vs. 5_2	3.25	No	ns
20 vs. 20_2	1.75	No	ns
0_2 vs. 1_2	11.82	No	ns
0_2 vs. 2.5_2	17.92	No	ns
0_2 vs. 5_2	5.833	No	ns
0_2 vs. 20_2	4.333	No	ns
1_2 vs. 2.5_2	6.095	No	ns
1_2 vs. 5_2	-5.988	No	ns
1_2 vs. 20_2	-7.488	No	ns
2.5_2 vs. 5_2	-12.08	No	ns
2.5_2 vs. 20_2	-13.58	No	ns
5_2 vs. 20_2	-1.5	No	ns

Test details	Mean rank 1	Mean rank 2	Mean rank diff.	n1	n2
0 vs. 1	30.83	21.5	9.333	3	2
0 vs. 2.5	30.83	12	18.83	3	3
0 vs. 5	30.83	20	10.83	3	3
0 vs. 20	30.83	28.67	2.167	3	3
0 vs. 0_2	30.83	31.25	-0.4167	3	6
0 vs. 1_2	30.83	19.43	11.4	3	7
0 vs. 2.5_2	30.83	13.33	17.5	3	6
0 vs. 5_2	30.83	25.42	5.417	3	6
0 vs. 20_2	30.83	26.92	3.917	3	6
1 vs. 2.5	21.5	12	9.5	2	3
1 vs. 5	21.5	20 1.5	2	3	
1 vs. 20	21.5	28.67	-7.167	2	3
1 vs. 0_2	21.5	31.25	-9.75	2	6
1 vs. 1_2	21.5	19.43	2.071	2	7
1 vs. 2.5_2	21.5	13.33	8.167	2	6
1 vs. 5_2	21.5	25.42	-3.917	2	6
1 vs. 20_2	21.5	26.92	-5.417	2	6
2.5 vs. 5	12	20	-8	3	3
2.5 vs. 20	12	28.67	-16.67	3	3
2.5 vs. 0_2	12	31.25	-19.25	3	6
2.5 vs. 1_2	12	19.43	-7.429	3	7
2.5 vs. 2.5_2	12	13.33	-1.333	3	6
2.5 vs. 5_2	12	25.42	-13.42	3	6
2.5 vs. 20_2	12	26.92	-14.92	3	6
5 vs. 20	20	28.67	-8.667	3	3
5 vs. 0_2	20	31.25	-11.25	3	6
5 vs. 1_2	20	19.43	0.5714	3	7
5 vs. 2.5_2	20	13.33	6.667	3	6
5 vs. 5_2	20	25.42	-5.417	3	6
5 vs. 20_2	20	26.92	-6.917	3	6
20 vs. 0_2	28.67	31.25	-2.583	3	6
20 vs. 1_2	28.67	19.43	9.238	3	7
20 vs. 2.5_2	28.67	13.33	15.33	3	6
20 vs. 5_2	28.67	25.42	3.25	3	6
20 vs. 20_2	28.67	26.92	1.75	3	6
0_2 vs. 1_2	31.25	19.43	11.82 6	7	
0_2 vs. 2.5_2	31.25	13.33	17.92	6	6
0_2 vs. 5_2	31.25	25.42	5.833	6	6
0_2 vs. 20_2	31.25	26.92	4.333	6	6
1_2 vs. 2.5_2	19.43	13.33	6.095	7	6
1_2 vs. 5_2	19.43	25.42	-5.988	7	6
1_2 vs. 20_2	19.43	26.92	-7.488	7	6
2.5_2 vs. 5_2	13.33	25.42	-12.08	6	6
2.5_2 vs. 20_2	13.33	26.92	-13.58	6	6
5_2 vs. 20_2	25.42	26.92	-1.5	6	6

Comparison of different applied thiolated HA species in solution

Table E.27.: Kruskal-Wallis-Test with Dunn's multiple comparison

P value	0.1023
Exact or approximate P value?	Approximate
P value summary	ns
Do the medians vary signif. (P < 0.05)?	No
Number of groups	10
Kruskal-Wallis statistic	14.61
Number of treatments (columns)	10
Number of values (total)	27

Dunn's comparisons	Mean rank diff.	Significant	Summary
0 vs. 1	10.17	No	ns
0 vs. 2.5	-0.1667	No	ns
0 vs. 5	-7.083	No	ns
0 vs. 20	-3.333	No	ns
0 vs. 0_2	-0.8333	No	ns
0 vs. 1_2	7	No	ns
0 vs. 2.5_2	4.833	No	ns
0 vs. 5_2	-6	No	ns
0 vs. 20_2	-8.583	No	ns
1 vs. 2.5	-10.33	No	ns
1 vs. 5	-17.25	No	ns
1 vs. 20	-13.5	No	ns
1 vs. 0_2	-11	No	ns
1 vs. 1_2	-3.167	No	ns
1 vs. 2.5_2	-5.333	No	ns
1 vs. 5_2	-16.17	No	ns
1 vs. 20_2	-18.75	No	ns
2.5 vs. 5	-6.917	No	ns
2.5 vs. 20	-3.167	No	ns
2.5 vs. 0_2	-0.6667	No	ns
2.5 vs. 1_2	7.167	No	ns
2.5 vs. 2.5_2	5	No	ns
2.5 vs. 5_2	-5.833	No	ns
2.5 vs. 20_2	-8.417	No	ns
5 vs. 20	3.75	No	ns
5 vs. 0_2	6.25	No	ns
5 vs. 1_2	14.08	No	ns
5 vs. 2.5_2	11.92	No	ns
5 vs. 5_2	1.083	No	ns
5 vs. 20_2	-1.5	No	ns
20 vs. 0_2	2.5	No	ns
20 vs. 1_2	10.33	No	ns
20 vs. 2.5_2	8.167	No	ns
20 vs. 5_2	-2.667	No	ns
20 vs. 20_2	-5.25	No	ns
0_2 vs. 1_2	7.833	No	ns
0_2 vs. 2.5_2	5.667	No	ns
0_2 vs. 5_2	-5.167	No	ns
0_2 vs. 20_2	-7.75	No	ns
1_2 vs. 2.5_2	-2.167	No	ns
1_2 vs. 5_2	-13	No	ns
1_2 vs. 20_2	-15.58	No	ns
2.5_2 vs. 5_2	-10.83	No	ns
2.5_2 vs. 20_2	-13.42	No	ns
5_2 vs. 20_2	-2.583	No	ns

Test details	Mean rank 1	Mean rank 2	Mean rank diff.	n1	n2
0 vs. 1	14.17	4	10.17	3	3
0 vs. 2.5	14.17	14.33	-0.1667	3	3
0 vs. 5	14.17	21.25	-7.083	3	2
0 vs. 20	14.17	17.5	-3.333	3	3
0 vs. 0_2	14.17	15	-0.8333	3	2
0 vs. 1_2	14.17	7.167	7	3	3
0 vs. 2.5_2	14.17	9.333	4.833	3	3
0 vs. 5_2	14.17	20.17	-6	3	3
0 vs. 20_2	14.17	22.75	-8.583	3	2
1 vs. 2.5	4	14.33	-10.33	3	3
1 vs. 5	4	21.25	-17.25	3	2
1 vs. 20	4	17.5	-13.5	3	3
1 vs. 0_2	4	15	-11	3	2
1 vs. 1_2	4	7.167	-3.167	3	3
1 vs. 2.5_2	4	9.333	-5.333	3	3
1 vs. 5_2	4	20.17	-16.17	3	3
1 vs. 20_2	4	22.75	-18.75	3	2
2.5 vs. 5	14.33	21.25	-6.917	3	2
2.5 vs. 20	14.33	17.5	-3.167	3	3
2.5 vs. 0_2	14.33	15	-0.6667	3	2
2.5 vs. 1_2	14.33	7.167	7.167	3	3
2.5 vs. 2.5_2	14.33	9.333	5	3	3
2.5 vs. 5_2	14.33	20.17	-5.833	3	3
2.5 vs. 20_2	14.33	22.75	-8.417	3	2
5 vs. 20	21.25	17.5	3.75	2	3
5 vs. 0_2	21.25	15	6.25	2	2
5 vs. 1_2	21.25	7.167	14.08	2	3
5 vs. 2.5_2	21.25	9.333	11.92	2	3
5 vs. 5_2	21.25	20.17	1.083	2	3
5 vs. 20_2	21.25	22.75	-1.5	2	2
20 vs. 0_2	17.5	15	2.5	3	2
20 vs. 1_2	17.5	7.167	10.33	3	3
20 vs. 2.5_2	17.5	9.333	8.167	3	3
20 vs. 5_2	17.5	20.17	-2.667	3	3
20 vs. 20_2	17.5	22.75	-5.25	3	2
0_2 vs. 1_2	15	7.167	7.833	2	3
0_2 vs. 2.5_2	15	9.333	5.667	2	3
0_2 vs. 5_2	15	20.17	-5.167	2	3
0_2 vs. 20_2	15	22.75	-7.75	2	2
1_2 vs. 2.5_2	7.167	9.333	-2.167	3	3
1_2 vs. 5_2	7.167	20.17	-13	3	3
1_2 vs. 20_2	7.167	22.75	-15.58	3	2
2.5_2 vs. 5_2	9.333	20.17	-10.83	3	3
2.5_2 vs. 20_2	9.333	22.75	-13.42	3	2
5_2 vs. 20_2	20.17	22.75	-2.583	3	2

Comparison of unfunctionalised and functionalised HA species in solution

Table E.28.: Kruskal-Wallis-Test with Dunn's multiple comparison

P value	0.0054
Exact or approximate P value?	Approximate
P value summary	**
Do the medians vary signif. (P < 0.05)?	Yes
Number of groups	5
Kruskal-Wallis statistic	14.71
Number of treatments (columns)	5
Number of values (total)	67

Dunn's comparisons	Mean rank diff.	Significant	Summary
0 vs. 1	19.34	No	ns
0 vs. 2.5	18.38	No	ns
0 vs. 5	1.992	No	ns
0 vs. 20	-0.4008	No	ns
1 vs. 2.5	-0.9667	No	ns
1 vs. 5	-17.35	No	ns
1 vs. 20	-19.75	No	ns
2.5 vs. 5	-16.39	No	ns
2.5 vs. 20	-18.78	No	ns
5 vs. 20	-2.393	No	ns

Test details	Mean rank 1	Mean rank 2	Mean rank diff.	n1	n2
0 vs. 1	42.78	23.43	19.34	9	15
0 vs. 2.5	42.78	24.4	18.38	9	15
0 vs. 5	42.78	40.79	1.992	9	14
0 vs. 20	42.78	43.18	-0.4008	9	14
1 vs. 2.5	23.43	24.4	-0.9667	15	15
1 vs. 5	23.43	40.79	-17.35	15	14
1 vs. 20	23.43	43.18	-19.75	15	14
2.5 vs. 5	24.4	40.79	-16.39	15	14
2.5 vs. 20	24.4	43.18	-18.78	15	14
5 vs. 20	40.79	43.18	-2.393	14	14

Table E.29.: Kruskal-Wallis-Test with Dunn's multiple comparison

P value	0.0042
Exact or approximate P value?	Approximate
P value summary	**
Do the medians vary signif. (P < 0.05)?	Yes
Number of groups	9
Kruskal-Wallis statistic	22.4
Number of treatments (columns)	9
Number of values (total)	67

Dunn's comparisons	Mean rank diff.	Significant	Summary
0 vs. 1	15.06	No	ns
0 vs. 2.5	24.39	No	ns
0 vs. 5	8.556	No	ns
0 vs. 20	4.5	No	ns
0 vs. 1_2	25.78	No	ns
0 vs. 2.5_2	9.361	No	ns
0 vs. 5_2	-9.822	No	ns
0 vs. 20_2	-9.222	No	ns
1 vs. 2.5	9.333	No	ns
1 vs. 5	-6.5	No	ns
1 vs. 20	-10.56	No	ns
1 vs. 1_2	10.72	No	ns
1 vs. 2.5_2	-5.694	No	ns
1 vs. 5_2	-24.88	No	ns
1 vs. 20_2	-24.28	No	ns
2.5 vs. 5	-15.83	No	ns
2.5 vs. 20	-19.89	No	ns
2.5 vs. 1_2	1.389	No	ns
2.5 vs. 2.5_2	-15.03	No	ns
2.5 vs. 5_2	-34.21	No	ns
2.5 vs. 20_2	-33.61	No	ns
5 vs. 20	-4.056	No	ns
5 vs. 1_2	17.22	No	ns
5 vs. 2.5_2	0.8056	No	ns
5 vs. 5_2	-18.38	No	ns
5 vs. 20_2	-17.78	No	ns
20 vs. 1_2	21.28	No	ns
20 vs. 2.5_2	4.861	No	ns
20 vs. 5_2	-14.32	No	ns
20 vs. 20_2	-13.72	No	ns
1_2 vs. 2.5_2	-16.42	No	ns
1_2 vs. 5_2	-35.6	No	ns
1_2 vs. 20_2	-35	No	ns
2.5_2 vs. 5_2	-19.18	No	ns
2.5_2 vs. 20_2	-18.58	No	ns
5_2 vs. 20_2	0.6	No	ns

Test details	Mean rank 1	Mean rank 2	Mean rank diff.	n1	n2
0 vs. 1	42.78	27.72	15.06	9	9
0 vs. 2.5	42.78	18.39	24.39	9	9
0 vs. 5	42.78	34.22	8.556	9	9
0 vs. 20	42.78	38.28	4.5	9	9
0 vs. 1_2	42.78	17	25.78	9	6
0 vs. 2.5_2	42.78	33.42	9.361	9	6
0 vs. 5_2	42.78	52.6	-9.822	9	5
0 vs. 20_2	42.78	52	-9.222	9	5
1 vs. 2.5	27.72	18.39	9.333	9	9
1 vs. 5	27.72	34.22	-6.5	9	9
1 vs. 20	27.72	38.28	-10.56	9	9
1 vs. 1_2	27.72	17	10.72	9	6
1 vs. 2.5_2	27.72	33.42	-5.694	9	6
1 vs. 5_2	27.72	52.6	-24.88	9	5
1 vs. 20_2	27.72	52	-24.28	9	5
2.5 vs. 5	18.39	34.22	-15.83	9	9
2.5 vs. 20	18.39	38.28	-19.89	9	9
2.5 vs. 1_2	18.39	17	1.389	9	6
2.5 vs. 2.5_2	18.39	33.42	-15.03	9	6
2.5 vs. 5_2	18.39	52.6	-34.21	9	5
2.5 vs. 20_2	18.39	52	-33.61	9	5
5 vs. 20	34.22	38.28	-4.056	9	9
5 vs. 1_2	34.22	17	17.22	9	6
5 vs. 2.5_2	34.22	33.42	0.8056	9	6
5 vs. 5_2	34.22	52.6	-18.38	9	5
5 vs. 20_2	34.22	52	-17.78	9	5
20 vs. 1_2	38.28	17	21.28	9	6
20 vs. 2.5_2	38.28	33.42	4.861	9	6
20 vs. 5_2	38.28	52.6	-14.32	9	5
20 vs. 20_2	38.28	52	-13.72	9	5
1_2 vs. 2.5_2	17	33.42	-16.42	6	6
1_2 vs. 5_2	17	52.6	-35.6	6	5
1_2 vs. 20_2	17	52	-35	6	5
2.5_2 vs. 5_2	33.42	52.6	-19.18	6	5
2.5_2 vs. 20_2	33.42	52	-18.58	6	5
5_2 vs. 20_2	52.6	52	0.6	5	5

Results for relative metabolic activity of unfunctionalised HA

Table E.30.: Kruskal-Wallis-Test with Dunn's multiple comparison

P value	0.0738
Exact or approximate P value?	Approximate
P value summary	ns
Do the medians vary signif. (P < 0.05)?	No
Number of groups	5
Kruskal-Wallis statistic	8.537
Number of treatments (columns)	5
Number of values (total)	43

Dunn's comparisons	Mean rank diff.	Significant	Summary
0 vs. 1.0	2.508	No	ns
0 vs. 2.5	-2.992	No	ns
0 vs. 5.0	13.17	No	ns
0 vs. 20.0	5.397	No	ns
1.0 vs. 2.5	-5.5	No	ns
1.0 vs. 5.0	10.67	No	ns
1.0 vs. 20.0	2.889	No	ns
2.5 vs. 5.0	16.17	No	ns
2.5 vs. 20.0	8.389	No	ns
5.0 vs. 20.0	-7.778	No	ns

Test details	Mean rank 1	Mean rank 2	Mean rank diff.	n1	n2
0 vs. 1.0	25.79	23.28	2.508	7	9
0 vs. 2.5	25.79	28.78	-2.992	7	9
0 vs. 5.0	25.79	12.61	13.17	7	9
0 vs. 20.0	25.79	20.39	5.397	7	9
1.0 vs. 2.5	23.28	28.78	-5.5	9	9
1.0 vs. 5.0	23.28	12.61	10.67	9	9
1.0 vs. 20.0	23.28	20.39	2.889	9	9
2.5 vs. 5.0	28.78	12.61	16.17	9	9
2.5 vs. 20.0	28.78	20.39	8.389	9	9
5.0 vs. 20.0	12.61	20.39	-7.778	9	9

Results for relative metabolic activity for functionalised HA

Table E.31.: Kruskal-Wallis-Test with Dunn's multiple comparison

P value	0.2392
Exact or approximate P value?	Approximate
P value summary	ns
Do the medians vary signif. (P < 0.05)?	No
Number of groups	5
Kruskal-Wallis statistic	5.506
Number of treatments (columns)	5
Number of values (total)	25

Dunn's comparisons	Mean rank diff.	Significant	Summary
0 vs. 1.0	4.471	No	ns
0 vs. 2.5	1.271	No	ns
0 vs. 5.0	-4.929	No	ns
0 vs. 20.0	-4.929	No	ns
1.0 vs. 2.5	-3.2	No	ns
1.0 vs. 5.0	-9.4	No	ns
1.0 vs. 20.0	-9.4	No	ns
2.5 vs. 5.0	-6.2	No	ns
2.5 vs. 20.0	-6.2	No	ns
5.0 vs. 20.0	0	No	ns

Test details	Mean rank 1	Mean rank 2	Mean rank diff.	n1	n2
0 vs. 1.0	12.57	8.1	4.471	7	5
0 vs. 2.5	12.57	11.3	1.271	7	5
0 vs. 5.0	12.57	17.5	-4.929	7	5
0 vs. 20.0	12.57	17.5	-4.929	7	3
1.0 vs. 2.5	8.1	11.3	-3.2	5	5
1.0 vs. 5.0	8.1	17.5	-9.4	5	5
1.0 vs. 20.0	8.1	17.5	-9.4	5	3
2.5 vs. 5.0	11.3	17.5	-6.2	5	5
2.5 vs. 20.0	11.3	17.5	-6.2	5	3
5.0 vs. 20.0	17.5	17.5	0	5	3

Results for relative metabolic activity

Table E.32.: Kruskal-Wallis-Test with Dunn's multiple comparison

P value	0.4917
Exact or approximate P value?	Approximate
P value summary	ns
Do the medians vary signif. (P < 0.05)?	No
Number of groups	5
Kruskal-Wallis statistic	3.41
Number of treatments (columns)	5
Number of values (total)	61

Dunn's comparisons	Mean rank diff.	Significant	Summary	P
0 vs. 1.0	6.321	No	ns	>0.9999
0 vs. 2.5	-2.571	No	ns	>0.9999
0 vs. 5.0	8.536	No	ns	>0.9999
0 vs. 20.0	2.732	No	ns	>0.9999
1.0 vs. 2.5	-8.893	No	ns	>0.9999
1.0 vs. 5.0	2.214	No	ns	>0.9999
1.0 vs. 20.0	-3.589	No	ns	>0.9999
2.5 vs. 5.0	11.11	No	ns	0.9777
2.5 vs. 20.0	5.304	No	ns	>0.9999
5.0 vs. 20.0	-5.804	No	ns	>0.9999

Test details	Mean rank 1	Mean rank 2	Mean rank diff.	n1	n2
0 vs. 1.0	34.36	28.04	6.321	7	14
0 vs. 2.5	34.36	36.93	-2.571	7	14
0 vs. 5.0	34.36	25.82	8.536	7	14
0 vs. 20.0	34.36	31.63	2.732	7	12
1.0 vs. 2.5	28.04	36.93	-8.893	14	14
1.0 vs. 5.0	28.04	25.82	2.214	14	14
1.0 vs. 20.0	28.04	31.63	-3.589	14	12
2.5 vs. 5.0	36.93	25.82	11.11	14	14
2.5 vs. 20.0	36.93	31.63	5.304	14	12
5.0 vs. 20.0	25.82	31.63	-5.804	14	12

,E.3. Statistical Analysis of Samples with Immobilised HA in the presence of cRGD

CyQuant® assay for immobilised, digested HA

Table E.33.: Kruskal-Wallis-Test with Dunn's multiple comparison

P value	0.0141
Exact or approximate P value?	Approximate
P value summary	*
Do the medians vary signif. (P < 0.05)?	Yes
Number of groups	6
Kruskal-Wallis statistic	14.25
Number of treatments (columns)	6
Number of values (total)	31

Dunn's comparisons	Mean rank diff.	Significant	Summary
0 vs. 2714	14.6	No	ns
0 vs. 540	16.7	No	ns
0 vs. 123	10.77	No	ns
0 vs. 47	7.8	No	ns
0 vs. 29	1.3	No	ns
2714 vs. 540	2.1	No	ns
2714 vs. 123	-3.833	No	ns
2714 vs. 47	-6.8	No	ns
2714 vs. 29	-13.3	No	ns
540 vs. 123	-5.933	No	ns
540 vs. 47	-8.9	No	ns
540 vs. 29	-15.4	No	ns
123 vs. 47	-2.967	No	ns
123 vs. 29	-9.467	No	ns
47 vs. 29	-6.5	No	ns

Test details	Mean rank 1	Mean rank 2	Mean rank diff.	n1	n2
0 vs. 2714	24.6	10	14.6	5	5
0 vs. 540	24.6	7.9	16.7	5	5
0 vs. 123	24.6	13.83	10.77	5	6
0 vs. 47	24.6	16.8	7.8	5	5
0 vs. 29	24.6	23.3	1.3	5	5
2714 vs. 540	10	7.9	2.1	5	5
2714 vs. 123	10	13.83	-3.833	5	6
2714 vs. 47	10	16.8	-6.8	5	5
2714 vs. 29	10	23.3	-13.3	5	5
540 vs. 123	7.9	13.83	-5.933	5	6
540 vs. 47	7.9	16.8	-8.9	5	5
540 vs. 29	7.9	23.3	-15.4	5	5
123 vs. 47	13.83	16.8	-2.967	6	5
123 vs. 29	13.83	23.3	-9.467	6	5
47 vs. 29	16.8	23.3	-6.5	5	5

CyQuant® assay for immobilised, short HA

Table E.34.: Kruskal-Wallis-Test with Dunn's multiple comparison

P value	0.0025
Exact or approximate P value?	Approximate
P value summary	**
Do the medians vary signif. (P < 0.05)?	Yes
Number of groups	6
Kruskal-Wallis statistic	18.38
Number of treatments (columns)	6
Number of values (total)	31

Dunn's comparisons	Mean rank diff.	Significant	Summary
0 vs. 2714	20.2	Yes	**
0 vs. 540	19.5	Yes	*
0 vs. 123	8.5	No	ns
0 vs. 47	11.5	No	ns
0 vs. 29	6.8	No	ns
2714 vs. 540	-0.7	No	ns
2714 vs. 123	-11.7	No	ns
2714 vs. 47	-8.7	No	ns
2714 vs. 29	-13.4	No	ns
540 vs. 123	-11	No	ns
540 vs. 47	-8	No	ns
540 vs. 29	-12.7	No	ns
123 vs. 47	3	No	ns
123 vs. 29	-1.7	No	ns
47 vs. 29	-4.7	No	ns

Test details	Mean rank 1	Mean rank 2	Mean rank diff.	n1	n2
0 vs. 2714	27	6.8	20.2	5	5
0 vs. 540	27	7.5	19.5	5	5
0 vs. 123	27	18.5	8.5	5	6
0 vs. 47	27	15.5	11.5	5	5
0 vs. 29	27	20.2	6.8	5	5
2714 vs. 540	6.8	7.5	-0.7	5	5
2714 vs. 123	6.8	18.5	-11.7	5	6
2714 vs. 47	6.8	15.5	-8.7	5	5
2714 vs. 29	6.8	20.2	-13.4	5	5
540 vs. 123	7.5	18.5	-11	5	6
540 vs. 47	7.5	15.5	-8	5	5
540 vs. 29	7.5	20.2	-12.7	5	5
123 vs. 47	18.5	15.5	3	6	5
123 vs. 29	18.5	20.2	-1.7	6	5
47 vs. 29	15.5	20.2	-4.7	5	5

CyQuant® assay – Controls

Table E.35.: Kruskal-Wallis-Test with Dunn's multiple comparison

P value	0.0018
Exact or approximate P value?	Exact
P value summary	**
Do the medians vary signif. (P < 0.05)?	Yes
Number of groups	4
Kruskal-Wallis statistic	10.54
Number of treatments (columns)	4
Number of values (total)	15

Dunn's comparisons	Mean rank diff.	Significant	Summary
A vs. B	-0.5833	No	ns
A vs. C	-7.917	No	ns
A vs. D	-7.65	No	ns
B vs. C	-8	No	ns
B vs. D	-7.333	No	ns
C vs. D	0.2667	No	ns

Test details	Mean rank 1	Mean rank 2	Mean rank diff.	n1	n2
A vs. B	3.75	4.333	-0.5833	4	3
A vs. C	3.75	11.67	-7.917	4	3
A vs. D	3.75	11.4	-7.65	4	5
B vs. C	4.333	11.67	-7.333	3	3
B vs. D	4.333	11.4	-7.067	3	5
C vs. D	11.67	11.4	0.2667	3	5

AlamarBlue® assay for immobilised, digested HA

Table E.36.: Kruskal-Wallis-Test with Dunn's multiple comparison

P value	0.0221
Exact or approximate P value?	Approximate
P value summary	*
Do the medians vary signif. (P < 0.05)?	Yes
Number of groups	6
Kruskal-Wallis statistic	13.14
Number of treatments (columns)	6
Number of values (total)	32

Dunn's comparisons	Mean rank diff.	Significant	Summary
0 vs. 2714	19.3	Yes	*
0 vs. 540	3.15	No	ns
0 vs. 123	5.4	No	ns
0 vs. 47	4.7	No	ns
0 vs. 29	3.5	No	ns
2714 vs. 540	-16.15	No	ns
2714 vs. 123	-13.9	No	ns
2714 vs. 47	-14.6	No	ns
2714 vs. 29	-15.8	No	ns
540 vs. 123	2.25	No	ns
540 vs. 47	1.55	No	ns
540 vs. 29	0.35	No	ns
123 vs. 47	-0.7	No	ns
123 vs. 29	-1.9	No	ns
47 vs. 29	-1.2	No	ns

Test details	Mean rank 1	Mean rank 2	Mean rank diff.	n1	n2
0 vs. 2714	22.4	3.1	19.3	5	5
0 vs. 540	22.4	19.25	3.15	5	6
0 vs. 123	22.4	17	5.4	5	6
0 vs. 47	22.4	17.7	4.7	5	5
0 vs. 29	22.4	18.9	3.5	5	5
2714 vs. 540	3.1	19.25	-16.15	5	6
2714 vs. 123	3.1	17	-13.9	5	6
2714 vs. 47	3.1	17.7	-14.6	5	5
2714 vs. 29	3.1	18.9	-15.8	5	5
540 vs. 123	19.25	17	2.25	6	6
540 vs. 47	19.25	17.7	1.55	6	5
540 vs. 29	19.25	18.9	0.35	6	5
123 vs. 47	17	17.7	-0.7	6	5
123 vs. 29	17	18.9	-1.9	6	5
47 vs. 29	17.7	18.9	−1.23	5	5

AlamarBlue® assay for immobilised, short HA

Table E.37.: Kruskal-Wallis-Test with Dunn's multiple comparison

P value	0.0067
Exact or approximate P value?	Approximate
P value summary	**
Do the medians vary signif. (P < 0.05)?	Yes
Number of groups	6
Kruskal-Wallis statistic	16.05
Number of treatments (columns)	6
Number of values (total)	32

Dunn's comparisons	Mean rank diff.	Significant	Summary
0 vs. 2714	16.6	No	ns
0 vs. 540	4.8	No	ns
0 vs. 123	4.9	No	ns
0 vs. 47	13.1	No	ns
0 vs. 29	-2.183	No	ns
2714 vs. 540	-11.8	No	ns
2714 vs. 123	-11.7	No	ns
2714 vs. 47	-3.5	No	ns
2714 vs. 29	-18.78	Yes	*
540 vs. 123	0.1	No	ns
540 vs. 47	8.3	No	ns
540 vs. 29	-6.983	No	ns
123 vs. 47	8.2	No	ns
123 vs. 29	-7.083	No	ns
47 vs. 29	-15.28	No	ns

Test details	Mean rank 1	Mean rank 2	Mean rank diff.	n1	n2
0 vs. 2714	22.4	5.8	16.6	5	5
0 vs. 540	22.4	17.6	4.8	5	5
0 vs. 123	22.4	17.5	4.9	5	6
0 vs. 47	22.4	9.3	13.1	5	5
0 vs. 29	22.4	24.58	-2.183	5	6
2714 vs. 540	5.8	17.6	-11.8	5	5
2714 vs. 123	5.8	17.5	-11.7	5	6
2714 vs. 47	5.8	9.3	-3.5	5	5
2714 vs. 29	5.8	24.58	-18.78	5	6
540 vs. 123	17.6	17.5	0.1	5	6
540 vs. 47	17.6	9.3	8.3	5	5
540 vs. 29	17.6	24.58	-6.983	5	6
123 vs. 47	17.5	9.3	8.2	6	5
123 vs. 29	17.5	24.58	-7.083	6	6
47 vs. 29	9.3	24.58	-15.28	5	6

AlamarBlue® assay - **Controls**

Table E.38.: Kruskal-Wallis-Test with Dunn's multiple comparison

P value	0.0018
Exact or approximate P value?	Exact
P value summary	**
Do the medians vary signif. (P < 0.05)?	Yes
Number of groups	4
Kruskal-Wallis statistic	10.54
Number of treatments (columns)	4
Number of values (total)	15

Dunn's comparisons	Mean rank diff.	Significant	Summary
A vs. B	0.5833	No	ns
A vs. C	-7.417	No	ns
A vs. D	-7.15	No	ns
B vs. C	-8	No	ns
B vs. D	-7.733	No	ns
C vs. D	0.2667	No	ns

Test details	Mean rank 1	Mean rank 2	Mean rank diff.	n1	n2
A vs. B	4.25	3.667	0.5833	4	3
A vs. C	4.25	11.67	-7.417	4	3
A vs. D	4.25	11.4	-7.15	4	5
B vs. C	3.667	11.67	-8	3	3
B vs. D	3.667	11.4	-7.733	3	5
C vs. D	11.67	11.4	0.2667	3	5

Comparison between different HA species

Table E.39.: Kruskal-Wallis-Test with Dunn's multiple comparison

P value	0.0002
Exact or approximate P value?	Approximate
P value summary	* * *
Do the medians vary signif. (P < 0.05)?	Yes
Number of groups	6
Kruskal-Wallis statistic	24.52
Number of treatments (columns)	6
Number of values (total)	59

Dunn's comparisons	Mean rank diff.	Significant	Summary
0 vs. 2714	33.35	Yes	**
0 vs. 540	6.8	No	ns
0 vs. 123	9.092	No	ns
0 vs. 47	16.7	No	ns
0 vs. 29	1.073	No	ns
2714 vs. 540	-26.55	Yes	**
2714 vs. 123	-24.26	Yes	*
2714 vs. 47	-16.65	No	ns
2714 vs. 29	-32.28	Yes	* * *
540 vs. 123	2.292	No	ns
540 vs. 47	9.9	No	ns
540 vs. 29	-5.727	No	ns
123 vs. 47	7.608	No	ns
123 vs. 29	-8.019	No	ns
47 vs. 29	-15.63	No	ns

Test details	Mean rank 1	Mean rank 2	Mean rank diff.	n1	n2
0 vs. 2714	41.8	8.45	33.35	5	10
0 vs. 540	41.8	35	6.8	5	11
0 vs. 123	41.8	32.71	9.092	5	12
0 vs. 47	41.8	25.1	16.7	5	10
0 vs. 29	41.8	40.73	1.073	5	11
2714 vs. 540	8.45	35	-26.55	10	11
2714 vs. 123	8.45	32.71	-24.26	10	12
2714 vs. 47	8.45	25.1	-16.65	10	10
2714 vs. 29	8.45	40.73	-32.28	10	11
540 vs. 123	35	32.71	2.292	11	12
540 vs. 47	35	25.1	9.9	11	10
540 vs. 29	35	40.73	-5.727	11	11
123 vs. 47	32.71	25.1	7.608	12	10
123 vs. 29	32.71	40.73	-8.019	12	11
47 vs. 29	25.1	40.73	-15.63	10	11

Results of the relative metabolic activity for digested, immobilised HA

Table E.40.: Kruskal-Wallis-Test with Dunn's multiple comparison

P value	0.0249
Exact or approximate P value?	Approximate
P value summary	*
Do the medians vary signif. (P < 0.05)?	Yes
Number of groups	6
Kruskal-Wallis statistic	12.84
Number of treatments (columns)	6
Number of values (total)	31

Dunn's comparisons	Mean rank diff.	Significant	Summary	P
0 vs. 2714	-2.4	No	ns	>0.9999
0 vs. 540	-16.6	No	ns	0.0584
0 vs. 123	-10.9	No	ns	0.7159
0 vs. 47	-6.4	No	ns	>0.9999
0 vs. 29	-1.2	No	ns	>0.9999
2714 vs. 540	-14.2	No	ns	0.2030
2714 vs. 123	-8.5	No	ns	>0.9999
2714 vs. 47	-4	No	ns	>0.9999
2714 vs. 29	1.2	No	ns	>0.9999
540 vs. 123	5.7	No	ns	>0.9999
540 vs. 47	10.2	No	ns	>0.9999
540 vs. 29	15.4	No	ns	0.1111
123 vs. 47	4.5	No	ns	>0.9999
123 vs. 29	9.7	No	ns	>0.9999
47 vs. 29	5.2	No	ns	>0.9999

Test details	Mean rank 1	Mean rank 2	Mean rank diff.	n1	n2
0 vs. 2714	9.6	12	-2.4	5	5
0 vs. 540	9.6	26.2	-16.6	5	5
0 vs. 123	9.6	20.5	-10.9	5	6
0 vs. 47	9.6	16	-6.4	5	5
0 vs. 29	9.6	10.8	-1.2	5	5
2714 vs. 540	12	26.2	-14.2	5	5
2714 vs. 123	12	20.5	-8.5	5	6
2714 vs. 47	12	16	-4	5	5
2714 vs. 29	12	10.8	1.2	5	5
540 vs. 123	26.2	20.5	5.7	5	6
540 vs. 47	26.2	16	10.2	5	5
540 vs. 29	26.2	10.8	15.4	5	5
123 vs. 47	20.5	16	4.5	6	5
123 vs. 29	20.5	10.8	9.7	6	5
47 vs. 29	16	10.8	5.2	5	5

Results of the relative metabolic activity for short, immobilised HA

Table E.41.: Kruskal-Wallis-Test with Dunn's multiple comparison

P value	0.0155
Exact or approximate P value?	Approximate
P value summary	*
Do the medians vary signif. (P < 0.05)?	Yes
Number of groups	6
Kruskal-Wallis statistic	14.01
Number of treatments (columns)	6
Number of values (total)	31

Dunn's comparisons	Mean rank diff.	Significant	Summary	P
0 vs. 2714	-10.4	No	ns	>0.9999
0 vs. 540	-20.2	Yes	**	0.0067
0 vs. 123	-7.033	No	ns	>0.9999
0 vs. 47	-4.6	No	ns	>0.9999
0 vs. 29	-7.2	No	ns	>0.9999
2714 vs. 540	-9.8	No	ns	>0.9999
2714 vs. 123	3.367	No	ns	>0.9999
2714 vs. 47	5.8	No	ns	>0.9999
2714 vs. 29	3.2	No	ns	>0.9999
540 vs. 123	13.17	No	ns	0.2517
540 vs. 47	15.6	No	ns	0.1001
540 vs. 29	13	No	ns	0.3566
123 vs. 47	2.433	No	ns	>0.9999
123 vs. 29	-0.1667	No	ns	>0.9999
47 vs. 29	-2.6	No	ns	>0.9999

Test details	Mean rank 1	Mean rank 2	Mean rank diff.	n1	n2
0 vs. 2714	7.8	18.2	-10.4	5	5
0 vs. 540	7.8	28	-20.2	5	5
0 vs. 123	7.8	14.83	-7.033	5	6
0 vs. 47	7.8	12.4	-4.6	5	5
0 vs. 29	7.8	15	-7.2	5	5
2714 vs. 540	18.2	28	-9.8	5	5
2714 vs. 123	18.2	14.83	3.367	5	6
2714 vs. 47	18.2	12.4	5.8	5	5
2714 vs. 29	18.2	15	3.2	5	5
540 vs. 123	28	14.83	13.17	5	6
540 vs. 47	28	12.4	15.6	5	5
540 vs. 29	28	15	13	5	5
123 vs. 47	14.83	12.4	2.433	6	5
123 vs. 29	14.83	15	-0.1667	6	5
47 vs. 29	12.4	15	-2.6	5	5

Results of the relative metabolic activity

Table E.42.: Kruskal-Wallis-Test with Dunn's multiple comparison

P value	0.0002
Exact or approximate P value?	Approximate
P value summary	* * *
Do the medians vary signif. (P < 0.05)?	Yes
Number of groups	6
Kruskal-Wallis statistic	24.39
Number of treatments (columns)	6
Number of values (total)	62

Dunn's comparisons	Mean rank diff.	Significant	Summary	P
0 vs. 2714	-11.1	No	ns	>0.9999
0 vs. 540	-37.05	Yes	* * **	<0.0001
0 vs. 123	-18.43	No	ns	0.2552
0 vs. 47	-11.95	No	ns	>0.9999
0 vs. 29	-8.3	No	ns	>0.9999
2714 vs. 540	-25.95	Yes	*	0.0195
2714 vs. 123	-7.333	No	ns	>0.9999
2714 vs. 47	-0.85	No	ns	>0.9999
2714 vs. 29	2.8	No	ns	>0.9999
540 vs. 123	18.62	No	ns	0.2392
540 vs. 47	25.1	Yes	*	0.0280
540 vs. 29	28.75	Yes	**	0.0055
123 vs. 47	6.483	No	ns	>0.9999
123 vs. 29	10.13	No	ns	>0.9999
47 vs. 29	3.65	No	ns	>0.9999

Test details	Mean rank 1	Mean rank 2	Mean rank diff.	n1	n2
0 vs. 2714	7.8	18.2	-10.4	5	5
0 vs. 540	7.8	28	-20.2	5	5
0 vs. 123	7.8	14.83	-7.033	5	6
0 vs. 47	7.8	12.4	-4.6	5	5
0 vs. 29	7.8	15	-7.2	5	5
2714 vs. 540	18.2	28	-9.8	5	5
2714 vs. 123	18.2	14.83	3.367	5	6
2714 vs. 47	18.2	12.4	5.8	5	5
2714 vs. 29	18.2	15	3.2	5	5
540 vs. 123	28	14.83	13.17	5	6
540 vs. 47	28	12.4	15.6	5	5
540 vs. 29	28	15	13	5	5
123 vs. 47	14.83	12.4	2.433	6	5
123 vs. 29	14.83	15	-0.1667	6	5
47 vs. 29	12.4	15	-2.6	5	5

Results of the relative metabolic activity for immobilised HA – Controls

Table E.43.: Kruskal-Wallis-Test with Dunn's multiple comparison

P value	0.0018
Exact or approximate P value?	Exact
P value summary	**
Do the medians vary signif. (P < 0.05)?	Yes
Number of groups	4
Kruskal-Wallis statistic	10.54
Number of treatments (columns)	4
Number of values (total)	15

Dunn's comparisons	Mean rank diff.	Significant	Summary
A vs. B	0.5833	No	ns
A vs. C	7.917	No	ns
A vs. D	7.65	No	ns
B vs. C	7.333	No	ns
B vs. D	7.067	No	ns
C vs. D	-0.2667	No	ns

Test details	Mean rank 1	Mean rank 2	Mean rank diff.	n1	n2
A vs. B	12.25	11.67	0.5833	4	3
A vs. C	12.25	4.333	7.917	4	3
A vs. D	12.25	4.6	7.65	4	5
B vs. C	11.67	4.333	7.333	3	3
B vs. D	11.67	4.6	7.067	3	5
C vs. D	4.333	4.6	-0.2667	3	5

E.4. Toxicity Assays of Photocleavabel Ligand

Toxicity Assay of UV-light

Comparison of Irradiation Time after One Hour

Table E.44.: Kruskal-Wallis-Test with Dunn's multiple comparison

P value	0.1606
Exact or approximate P value?	Exact
P value summary	ns
Do the medians vary signif. (P < 0.05)?	No
Number of groups	4
Kruskal-Wallis statistic	5.205
Number of treatments (columns)	4
Number of values (total)	12

Dunn's comparisons	Mean rank diff.	Significant	Summary	P_{adj}
positiv control vs. 60 s	-4	No	ns	0.5227
positiv control vs. 30 s	-3.333	No	ns	0.7726
positiv control vs. 15 s	-6.667	No	ns	0.0706

Test details	Mean rank 1	Mean rank 2	Mean rank diff.	n1	n2
positiv control vs. 60 s	3	7	-4	3	3
positiv control vs. 30 s	3	6.333	-3.333	3	3
positiv control vs. 15 s	3	9.667	-6.667	3	3

Comparison of Irradiation Time after Two Hours

Table E.45.: Kruskal-Wallis-Test with Dunn's multiple comparison

P value	0.1748
Exact or approximate P value?	Exct
P value summary	ns
Do the medians vary signif. (P < 0.05)?	No
Number of groups	4
Kruskal-Wallis statistic	5.051
Number of treatments (columns)	4
Number of values (total)	12

Dunn's comparisons	Mean rank diff.	Significant	Summary	P
positiv control vs. 60 s	-4.667	No	ns	0.3388
positiv control vs. 30 s	-3	No	ns	0.9245
positiv control vs. 15 s	-6.333	No	ns	0.0944

Test details	Mean rank 1	Mean rank 2	Mean rank diff.	n1	n2
positiv control vs. 60 s	3	7.667	-4.667	3	3
positiv control vs. 30 s	3	6	-3	3	3
positiv control vs. 15 s	3	9.333	-6.333	3	3

Comparison of Irradiation Time after Three Hours

Table E.46.: Kruskal-Wallis-Test with Dunn's multiple comparison

P value	0.3040
Exact or approximate P value?	Exact
P value summary	ns
Do the medians vary signif. (P < 0.05)?	No
Number of groups	4
Kruskal-Wallis statistic	3.923
Number of treatments (columns)	4
Number of values (total)	12

Dunn's comparisons	Mean rank diff.	Significant	Summary	P
positiv control vs. 60 s	-1.667	No	ns	>0.9999
positiv control vs. 30 s	-2.667	No	ns	>0.9999
positiv control vs. 15 s	-5.667	No	ns	0.1627

Test details	Mean rank 1	Mean rank 2	Mean rank diff.	n1	n2
positiv control vs. 60 s	4	5.667	-1.667	3	3
positiv control vs. 30 s	4	6.667	-2.667	3	3
positiv control vs. 15 s	4	9.667	-5.667	3	3

Comparison of Irradiation Time of 60 Seconds

Table E.47.: Kruskal-Wallis-Test with Dunn's multiple comparison

P value	0.2483
Exact or approximate P value?	Exact
P value summary	ns
Do the medians vary signif. (P < 0.05)?	No
Number of groups	4
Kruskal-Wallis statistic	4.267
Number of treatments (columns)	4
Number of values (total)	18

Dunn's comparisons	Mean rank diff.	Significant	Summary	P
positiv control vs. 60 s_1h	-6.778	No	ns	0.1706
positiv control vs. 60 s_2h	-2.444	No	ns	>0.9999
positiv control vs. 60 s_3h	-4.444	No	ns	0.6352

Test details	Mean rank 1	Mean rank 2	Mean rank diff.	n1	n2
positiv control vs. 60 s_1h	7.222	14	-6.778	9	3
positiv control vs. 60 s_2h	7.222	9.667	-2.444	9	3
positiv control vs. 60 s_3h	7.222	11.67	-4.444	9	3

Comparison of Irradiation Time of 30 Seconds

Table E.48.: Kruskal-Wallis-Test with Dunn's multiple comparison

P value	0.0394
Exact or approximate P value?	Exact
P value summary	*
Do the medians vary signif. (P < 0.05)?	Yes
Number of groups	4
Kruskal-Wallis statistic	7.425
Number of treatments (columns)	4
Number of values (total)	18

Dunn's comparisons	Mean rank diff.	Significant	Summary	P
positiv control vs. 30 s_1h	-7.444	No	ns	0.1094
positiv control vs. 30 s_2h	-0.7778	No	ns	>0.9999
positiv control vs. 30 s_3h	-7.444	No	ns	0.1094

Test details	Mean rank 1	Mean rank 2	Mean rank diff.	n1	n2
positiv control vs. 30 s_1h	6.889	14.33	-7.444	9	3
positiv control vs. 30 s_2h	6.889	7.667	-0.7778	9	3
positiv control vs. 30 s_3h	6.889	14.33	-7.444	9	3

Comparison of Irradiation Time of 15 Seconds

Table E.49.: Kruskal-Wallis-Test with Dunn's multiple comparison

P value	0.0006
Exact or approximate P value?	Exact
P value summary	$* * *$
Do the medians vary signif. (P < 0.05)?	Yes
Number of groups	4
Kruskal-Wallis statistic	11.73
Number of treatments (columns)	4
Number of values (total)	18

Dunn's comparisons	Mean rank diff.	Significant	Summary	P
positiv control vs. 15 s_1h	-9.889	Yes	$*$	0.0164
positiv control vs. 15 s_2h	-5.222	No	ns	0.4269
positiv control vs. 15 s_3h	-9.222	Yes	$*$	0.0287

Test details	Mean rank 1	Mean rank 2	Mean rank diff.	n1	n2
positiv control vs. 15 s_1h	5.444	15.33	-9.889	9	3
positiv control vs. 15 s_2h	5.444	10.67	-5.222	9	3
positiv control vs. 15 s_3h	5.444	14.67	-9.222	9	3

Toxicity Assay of DMNPE in DMSO

Table E.50.: Kruskal-Wallis-Test with Dunn's multiple comparison

P value	0.1591
Exact or approximate P value?	Approximate
P value summary	ns
Do the medians vary signif. (P < 0.05)?	No
Number of groups	9
Kruskal-Wallis statistic	11.83
Number of treatments (columns)	9
Number of values (total)	27

Dunn's comparisons	Mean rank diff.	Significant	Summary
Positive control vs. DMSO control	7.667	No	ns
Positive control vs. 5 µM 143	-12	No	ns
Positive control vs. 50 µM 143	-16.83	No	ns
Positive control vs. 500 µM 143	-17.83	No	ns
Positive control vs. 5 µM 133	-11.33	No	ns
Positive control vs. 50 µM 133	-13.33	No	ns
Positive control vs. 500 µM 133	-15.33	No	ns
Positive control vs. DMSO without cells	2	No	ns

Test details	Mean rank 1	rank 2	rank diff	n1	n2
Pos. con. vs. DMSO control	2.667	10.33	-7.667	3	3
Pos. con. vs. 5 µM 143	2.667	14.67	-12	3	3
Pos. con. vs. 50 µM 143	2.667	19.5	-16.83	3	3
Pos. con. vs. 500 µM 143	2.667	20.5	-17.83	3	3
Pos. con. vs. 5 µM 133	2.667	14	-11.33	3	3
Pos. con. vs. 50 µM 133	2.667	16	-13.33	3	3
Pos. con. vs. 500 µM 133	2.667	18	-15.33	3	3
Pos. con. vs. DMSO w/o cells	2.667	10.33	-7.667	3	3

Toxicity assay of DMNPE in EtOH

Table E.51.: Kruskal-Wallis-Test with Dunn's multiple comparison

P value	0.0074
Exact or approximate P value?	Approximate
P value summary	**
Do the medians vary signif. (P < 0.05)?	Yes
Number of groups	8
Kruskal-Wallis statistic	19.28
Number of treatments (columns)	8
Number of values (total)	33

Dunn's comparisons	Mean rank diff.	Significant	Summary
Positive control vs. EtOH control	2	No	ns
Positive control vs. 5 μM 127	-7.167	No	ns
Positive control vs. 50 μM 127	1.083	No	ns
Positive control vs. 500 μM 127	-7.917	No	ns
Positive control vs. 5 μM 132	-12.17	No	ns
Positive control vs. 50 μM 132	-18.17	No	ns
Positive control vs. 500 μM 132	-20.67	No	ns

Test details	Mean rank 1	Mean rank 2	Mean rank diff.	n1	n2
Pos. con. vs. EtOH control	10	8	2	3	3
Pos. con. vs. 5 μM 127	10	17.17	-7.167	3	6
Pos. con. vs. 50 μM 127	10	8.917	1.083	3	6
Pos. con. vs. 500 μM 127	10	17.92	-7.917	3	6
Pos. con. vs. 5 μM 132	10	22.17	-12.17	3	3
Pos. con. vs. 50 μM 132	10	28.17	-18.17	3	3
Pos. con. vs. 500 μM 132	10	30.67	-20.67	3	3

Appendix F.

NMR Spectra
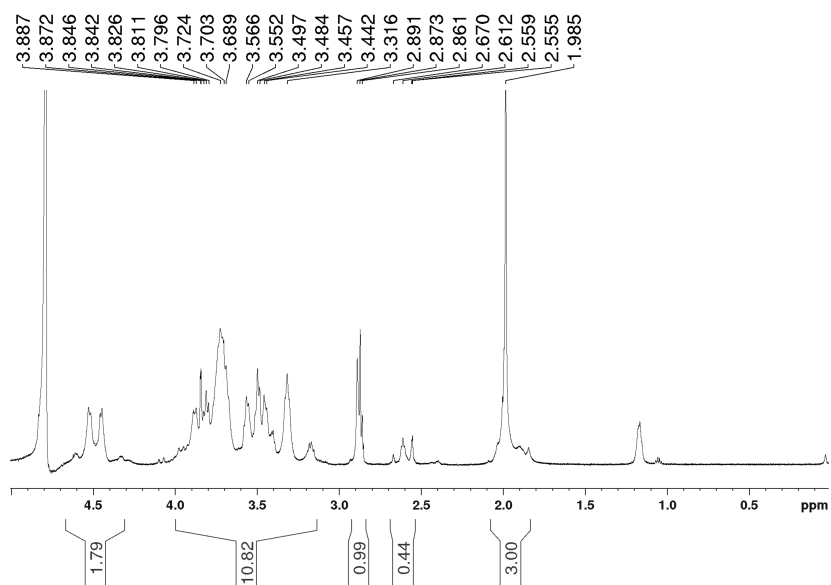
Figure F.1.: ^{1}H-NMR of the alkyne-functionalised HA within the chain (**6**) in D$_2$O (600 MHz)
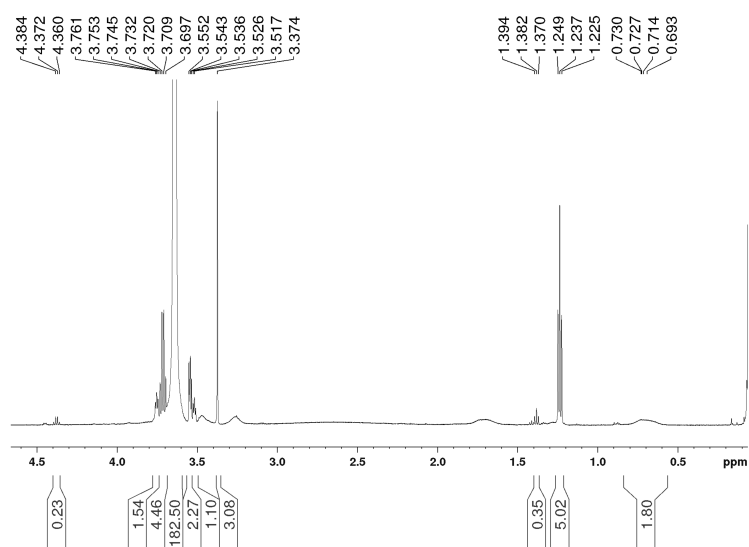
Figure F.2.: ^{1}H-NMR of PEG$_{2000}$−silane (**8**) in CDCl$_3$ (600 MHz)
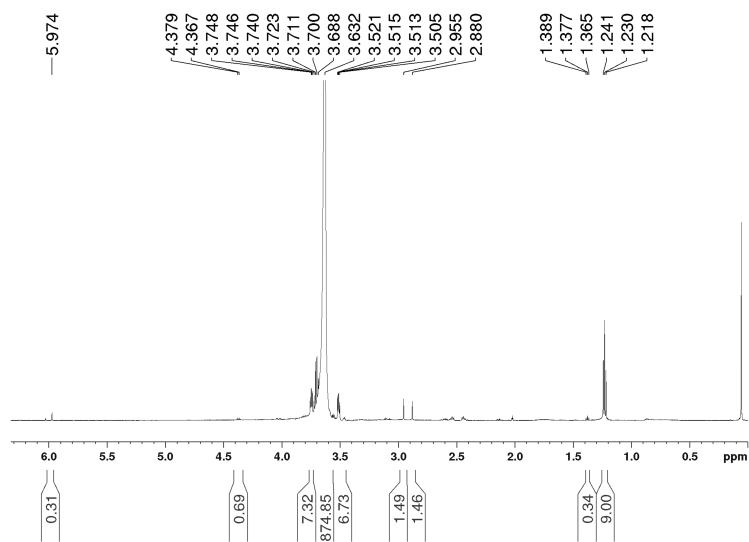
Figure F.3.: ^{1}H-NMR of PEG$_{3000}$−alkyne (**9**) in CDCl$_3$ (600 MHz)

—7.618
—6.760
—3.985
—2.502

7.5 7.0 6.5 6.0 5.5 5.0 4.5 4.0 3.5 3.0 2.5 2.0 1.5 1.0 0.5 ppm

1.00   1.01   6.75   3.03
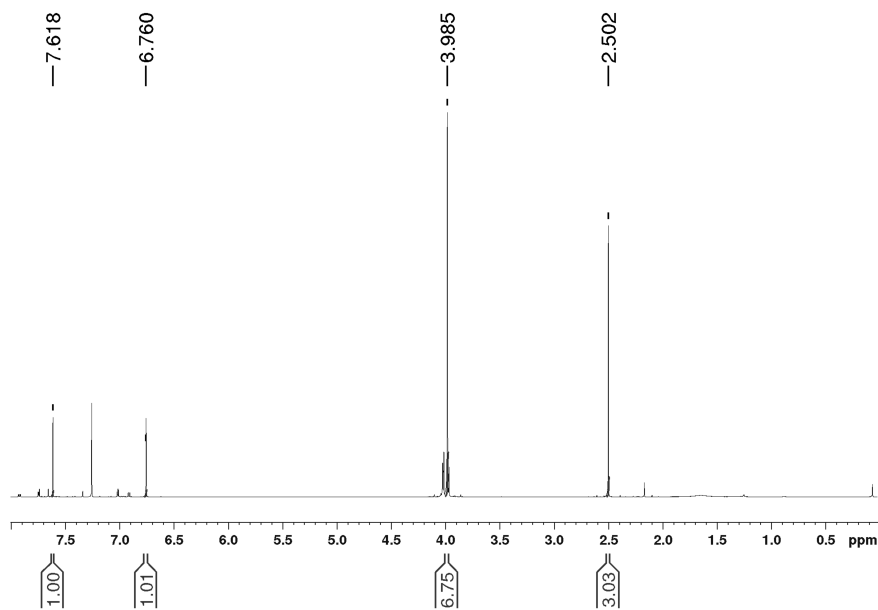
Figure F.4.: ^{1}H-NMR of 4,5-Dimethoxy-2-nitroacetophenone (**10**) in CDCl$_3$ (600 MHz)

—200.13
\153.99
/149.60
—132.88
\108.59
/106.81
\56.72
/56.61
—30.45

210 200 190 180 170 160 150 140 130 120 110 100 90 80 70 60 50 40 30 20 10 0 ppm
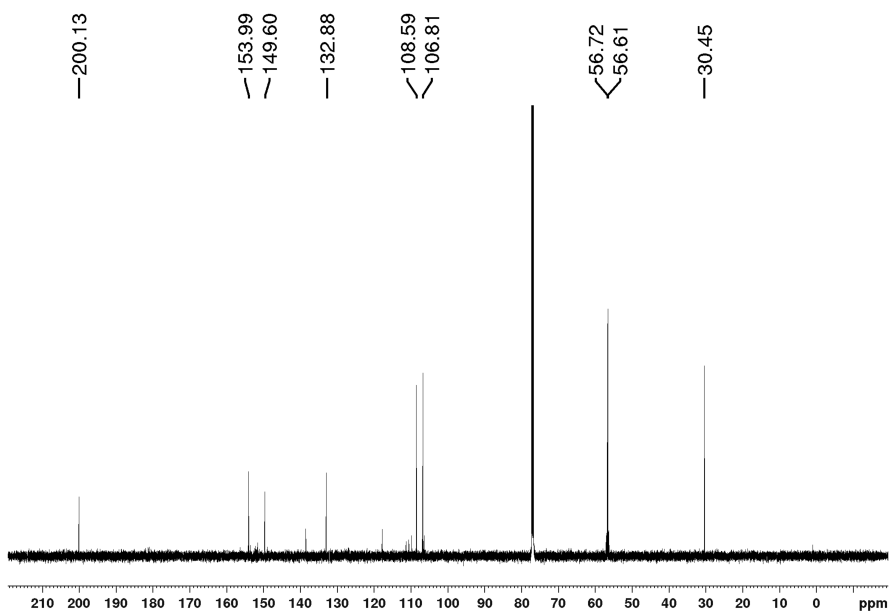
Figure F.5.: ^{13}C-NMR of 4,5-Dimethoxy-2-nitroacetophenone (**10**) in CDCl$_3$ (150 MHz)
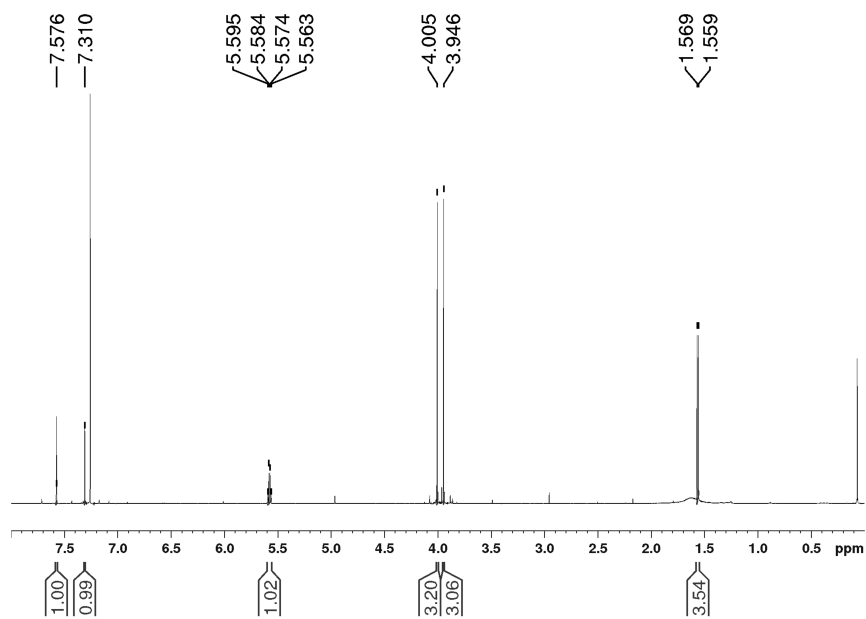
Figure F.6.: ^{1}H-NMR of 4,5-dimethoxy-2-nitrophenyl ethanol (**2**) in CDCl$_3$ (600 MHz)
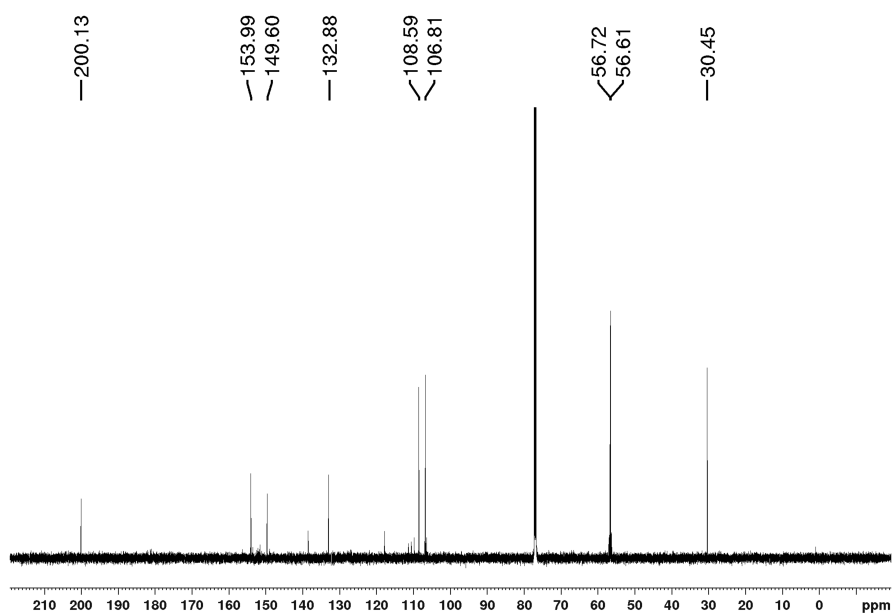
Figure F.7.: ^{13}C-NMR of 4,5-dimethoxy-2-nitrophenyl ethanol (**2**) in CDCl$_3$ (150 MHz)
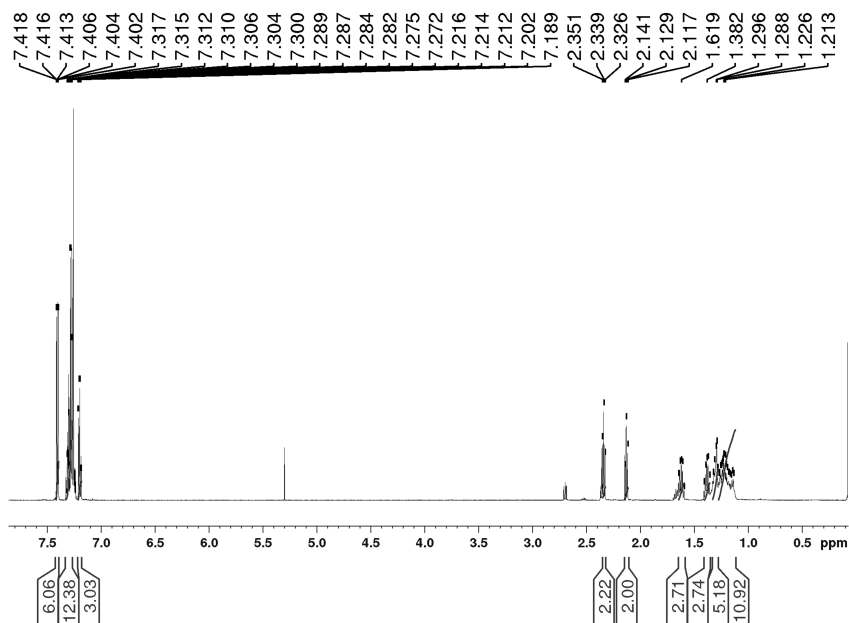
Figure F.8.: ^{1}H-NMR of 11-(tritylthio)undecanoic acid (**11**) in CDCl$_3$ (600 MHz)
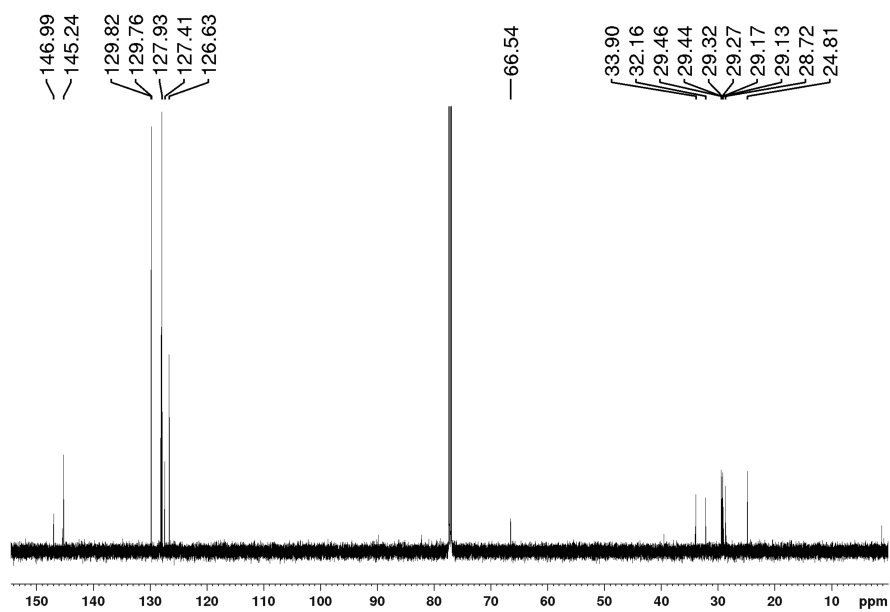
Figure F.9.: ^{13}C-NMR of 11-(tritylthio)undecanoic acid (**11**) in CDCl$_3$ (150 MHz)
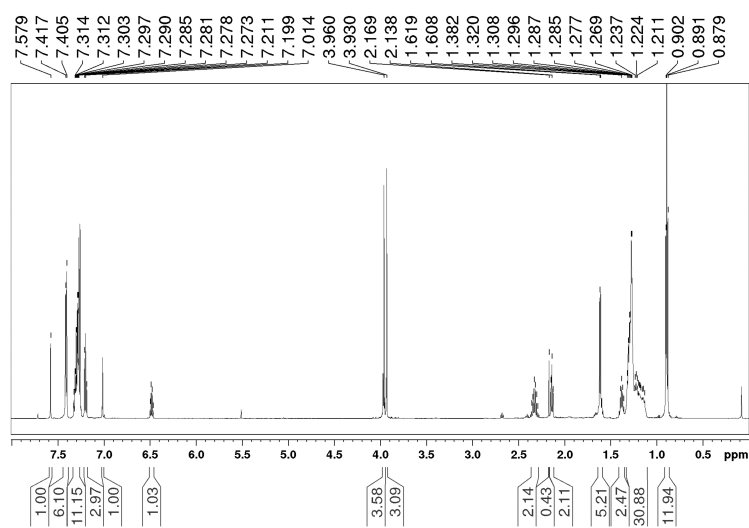
Figure F.10.: ¹H-NMR of 1-(4,5-dimethoxy-2-nitrophenyl)ethyl 11--(tritylthio)undecanoate (**12**) in CDCl₃ (600 MHz)
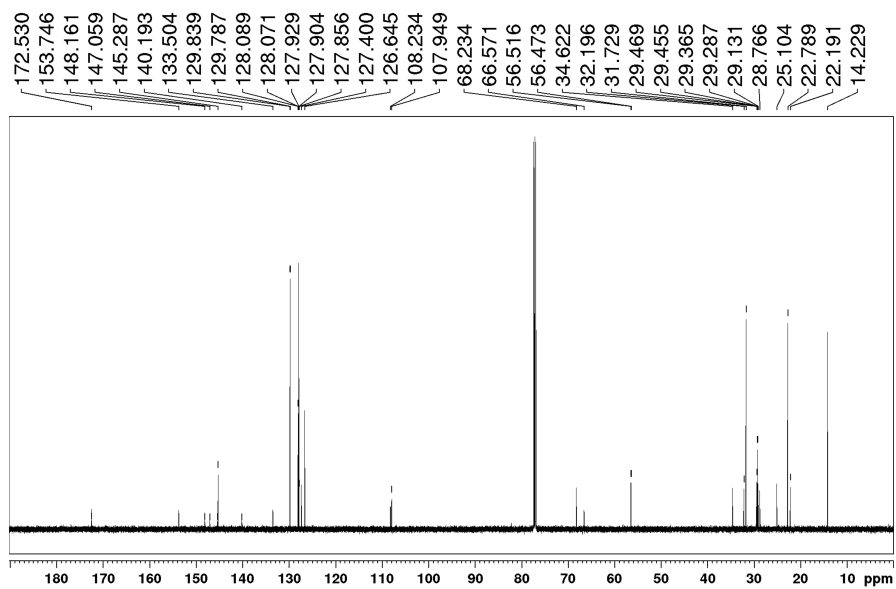
Figure F.11.: ¹³C-NMR of 1-(4,5-dimethoxy-2-nitrophenyl)ethyl 11--(tritylthio)undecanoate (**12**) in CDCl₃ (150 MHz)
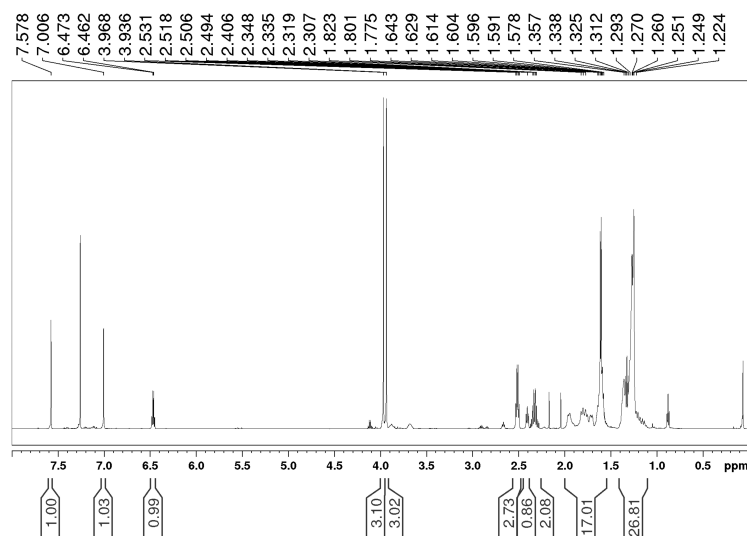
Figure F.12.: ¹H-NMR of 1-(4,5-dimethoxy-2-nitrophenyl)ethyl 11-mercaptoundecanoate (**1**) in CDCl₃ (600 MHz)
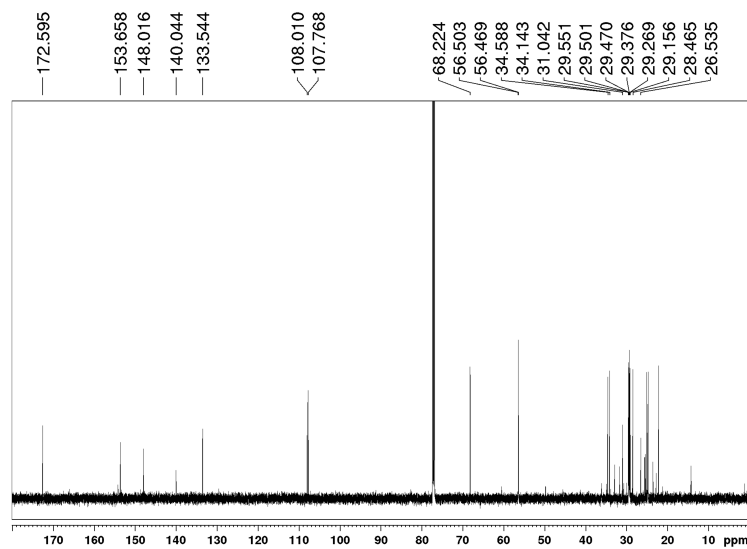
Figure F.13.: ¹³C-NMR of 1-(4,5-dimethoxy-2-nitrophenyl)ethyl 11-mercaptoundecanoate (**1**) in CDCl₃ (150 MHz)
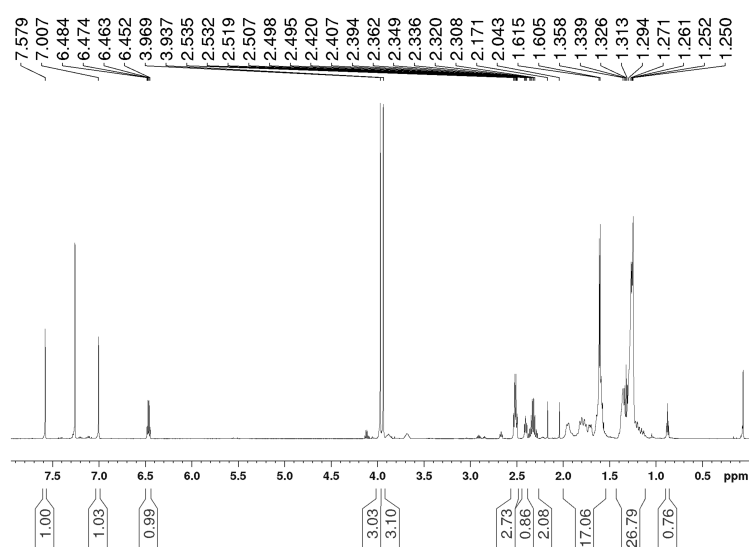
Figure F.14.: ^1H-NMR of 1-(4,5-dimethoxy-2-nitrophenyl)ethyl (3(*S*))-3-(4-(3-(6-(3-mercaptopropanamido)hexanamido)propoxy)benzamido)-4-(4-(3--((4-methoxypyridin-2-yl)amino)propoxy)phenyl)butanoate (**14**) in CDCl$_3$ (600 MHz)

Appendix G.

Kinetic Analysis of the Adsorption and Cleavage Process of DMNPE-thiol in the QCM-D

G.1. Adsorption of DMNPE-thiol at Different Temperatures

To develop the effect of temperature to the adsorption of DMNPE-thiol (**1**) to a gold surface, the curve of the adsorption process observed via QCM-D is fitted with equation G.1 using OriginPro (2017G, version b9.4.0.220, OriginLab Corporation).

$$y = y_0 + A_1 exp\left[-\frac{x}{t_1}\right] + A_2 exp\left[-\frac{x}{t_2}\right] \tag{G.1}$$

The results for the amplitude (A) and time (t) as well as the ratio of A_1 of the adsorption at $21\,°C$ are summarised in table G.1 and for $37\,°C$ in table G.2. For the adsorption at $37\,°C$ the equation can be simplified in two cases because A_2 is zero.

Table G.1.: Results of the fit to the adsorption curve of DMNPE-thiol (**1**) at $21\,°C$

sample	A1	t1	A2	t2	ratio A1 [%]
20160711 S3	120.70688	190.82759	78.60308	1353.69153	60.6
20161026 S2	44.04875	181.01587	149.96145	2330.31123	22.7
20161026 S3	21.17302	38.8034	140.28505	783.26099	13.1
20160711 S4	49.09925	138.12911	267.69231	1884.56792	15.5
20170306 S2	14.87394	42.37014	189.04852	1701.68984	7.3
20170306 S3	14.60207	72.69469	108.18859	3094.05399	11.9
20170309 S2	18.93493	25.39529	113.66793	2870.44861	14.3
20170309 S3	10.68453	24.05499	40.40023	2000.59515	20.9
20170309 S4	17.89268	33.96057	75.56981	1079.55234	19.1

Table G.2.: Results of the fit to the adsorption curve of DMNPE-thiol (**1**) at 37 °C

sample	A1	t1	A2	t2	ratio A1 [%]
CA143b 1	309.17678	285.80784			100.0
CA143b 2	279.79702	288.58841	12.65282	2439.81225	95.7
CA143b 3	312.80638	388.24584			100.0

G.2. Cleavage of DMNPE-thiol in the QCM-D

To analyse the kinetic of the cleavage of DMNPE-thiol on a gold surface, the curve of the cleavage process observed via QCM-D is fitted with equation G.2 using OriginPro (2017G, version b9.4.0.220, OriginLab Corporation).

$$y = y_0 + A_1 exp\left[-\frac{x - x_0}{t_1}\right] + A_2 exp\left[-\frac{x - x_0}{t_2}\right] \tag{G.2}$$

The results for the amplitude (A) and time (t) as well as the ratio of A_1 are summarised in table G.3.

Table G.3.: Results of the fit to the cleavgae curve of DMNPE-thiol (**1**) at 21 °C

sample	A1	t1	A2	t2	ratio A1 [%]
20160711 S3	-65.58113	3.04432	-20.28466	27.30017	76.4
20160711 S4	-86.31253	1.90945	-20.13366	24.39251	81.1
20160818 S2	-34.10663	2.45226	-8.89505	18.82567	79.3
20160818 S3	-14.81195	3.29734	-4.95054	14.87633	74.9
20161026 S2	-37.87714	2.88499	-12.54958	31.91942	75.1
20161026 S3	-49.11138	3.03432	-15.2357	31.47667	76.3
20170306 S2	-40.56384	1.99573	-12.86521	27.17474	75.9
20170306 S3	-25.16336	1.56184	-9.63555	12.45457	72.3

Appendix H.

Selection of the Solvent for the Toxicity Assay of 1-(4,5-dimethoxy-2-nitrophenyl)ethyl 11-mercaptoundecanoate

To analyse the toxic effect of 1-(4,5-dimethoxy-2-nitrophenyl)ethyl 11-mercaptoundecanoate (**1**) and 4,5-dimethoxy-2-nitrophenyl ethanol (**2**) on MDCK II cells a solvent is necessary, because these compounds are not soluble in water respectively media. In the beginning DMSO is tested, which is also used for the application of drugs in cell experiments. [79] The toxicity is determined with the AlamarBlue® assay. The results for the reduction of resazurin is shown in figure H.1 a). The comparison of the controls (A-C) shows a large effect due to mixing DMSO with the AlamarBlue® kit and media (A) even without cells. The comparison of the positive control (B) and the control with DMSO and cells shows more reduction when DMSO is added. Because of this, it stays unclear which effect in the following samples is due to the applied compounds and which due to the DMSO. Nevertheless an increase in the reduction potential with increasing concentration of the chemicals is found. This is significant in case of the applied $500\,\mu\mathrm{M}$ solution of 1-(4,5-dimethoxy-2-nitrophenyl)ethyl 11-mercaptoundecanoate. But possibly here the crystallisation of the linker takes place as described for the experiment in ethanol (section 4.5.3). So additionally ethanol is tested as solvent, which is also used in the QCM-D experiments. Here the determined reduction of resazurin of the positive control (A), control with ethanol without (B) and with (C) cells is shown in figure H.1 b). In this case no effect on the toxicity due to the solvent is found. Because of this ethanol seems to be the more appropriate solvent for using in the toxicity assay.
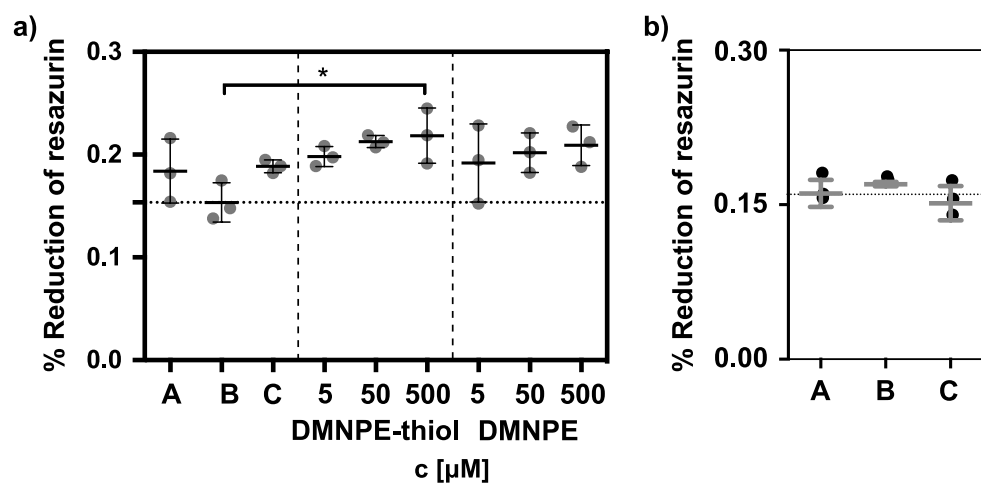
Figure H.1.: a) For the toxicity assay 1-(4,5-dimethoxy-2-nitrophenyl)ethyl 11-mercaptoundecanoate or 4,5-dimethoxy-2-nitrophenyl ethanol are added in different concentration to MDCK II cells in DMSO and media. This samples are compared with the positive control (B) without additives, a mixture of kit, media and DMSO (A) and a positiv control with DMSO(C). b) shows the control surfaces for ethanol as solvent in A the positive control, B kit with media and solvent and C the positive control with adding solvent. For the statistical analysis a Kruskal-Wallis test with Dunn's comparison is performed.

Bibliography

[1] Rørth, P. *Annual Review of Cell and Developmental Biology* **2009,** *25,* 407–429.

[2] Tolg, C.; Telmer, P.; Turley, E. *PloS ne* **2014,** *9,* e88479.

[3] Maquart, F. X.; Monboisse, J. C. *Pathologie-biologie* **2014,** *62,* 91–95.

[4] Alitalo, K.; Tammela, T.; Petrova, T. V. *Nature* **2005,** *438,* 946–953.

[5] Hirakawa, S.; Detmar, M.; Karaman, S. *Advanced Drug Delivery Reviews* **2014,** *74,* 12–18.

[6] Gailit, J.; Welch, M. P.; Clark, R. A. F. *The Journal of Investigative Dermatology* **1994,** 221–227.

[7] Kenny, F. N.; Connelly, J. T. *Cell and Tissue Research* **2014,** *360,* 571–582.

[8] Alberts, B.; Schäfer, U.; Häcker, B., Eds.; *Molekularbiologie der Zelle;* Wiley-VCH: Weinheim, 5. Aufl. ed.; 2011.

[9] Al-Rawi, M. A. A.; Mansel, R. E.; Jiang, W. G. *European Journal of Surgical Oncology : the Journal of the European Society of Surgical Oncology and the British Association of Surgical Oncology* **2005,** *31,* 117–121.

[10] Du, Y.; Liu, H.; He, Y.; Liu, Y.; Yang, C.; Zhou, M.; Wang, W.; Cui, L.; Hu, J.; Gao, F. *PloS One* **2013,** *8,* e63463.

[11] Betterman, K.; Harvey, N. *Immunological Reviews* **2016,** *271,* 276–292.

[12] Avraamides, C. J.; Garmy-Susini, B.; Varner, J. A. *Nature Reviews. Cancer* **2008,** *8,* 604–617.

[13] Astarita, J. L.; Acton, S. E.; Turley, S. J. *Frontiers in Immunology* **2012,** *3,* 283.

[14] Jackson, D. G.; Prevo, R.; Clasper, S. *Trends in Immunology* **2001,** *22,* 317–321.

[15] Jackson, D. G. *Immunological Reviews* **2009,** 216–231.

[16] Breiteneder-Geleff, S.; Matsui, K.; Soleiman, A.; Meraner, P.; Poczewski, H.; Kalt, R.; Schaffner, G.; Kerjaschki, D. *The American Journal of Pathology* **1997,** *151,* 1141–1152.

[17] Bai, Y.; Liu, Y.-J.; Wang, H.; Xu, Y.; Stamenkovic, I.; Yu, Q. *Oncogene* **2007,** *26,* 836–850.

[18] Bertozzi, C. C. *et al. Blood* **2010,** *116,* 661–670.

[19] Prevo, R.; Banerji, S.; Ferguson, D. J.; Clasper, S.; Jackson, D. G. *The Journal of Biological Chemistry* **2001,** *276,* 19420–19430.

[20] Ross, R. S.; Borg, T. K. *Circulation Research* **2001,** *88,* 1112–1119.

[21] Rechenmacher, F.; Neubauer, S.; Polleux, J.; Mas-Moruno, C.; de Simone, M.; Cavalcanti-Adam, E. A.; Spatz, J. P.; Fassler, R.; Kessler, H. *Angewandte Chemie (International ed. in English)* **2013,** *52,* 1572–1575.

[22] Heckmann, D.; Meyer, A.; Laufer, B.; Zahn, G.; Stragies, R.; Kessler, H. *Chembiochem : a European Journal of Chemical Biology* **2008,** *9,* 1397–1407.

[23] Heckmann, D.; Meyer, A.; Marinelli, L.; Zahn, G.; Stragies, R.; Kessler, H. *Angewandte Chemie (International ed. in English)* **2007,** *46,* 3571–3574.

[24] Lohmuller, T.; Aydin, D.; Schwieder, M.; Morhard, C.; Louban, I.; Pacholski, C.; Spatz, J. P. *Biointerphases* **2011,** *6,* MR1-12.

[25] Blummel, J.; Perschmann, N.; Aydin, D.; Drinjakovic, J.; Surrey, T.; Lopez-Garcia, M.; Kessler, H.; Spatz, J. P. *Biomaterials* **2007,** *28,* 4739–4747.

[26] Cavalcanti-Adam, E. A.; Micoulet, A.; Blummel, J.; Auernheimer, J.; Kessler, H.; Spatz, J. P. *European Journal of Cell Biology* **2006,** *85,* 219–224.

[27] Cavalcanti-Adam, E. A.; Volberg, T.; Micoulet, A.; Kessler, H.; Geiger, B.; Spatz, J. P. *Biophysical Journal* **2007,** *92,* 2964–2974.

[28] Mecham, R. P. *The Extracellular Matrix: an Overview;* Springer Berlin Heidelberg: Berlin, Heidelberg, 2011.

[29] Maytin, E. V. *Glycobiology* **2016,** *26,* 553–559.

[30] Anderegg, U.; Simon, J. C.; Averbeck, M. *Experimental Dermatology* **2014,** *23,* 295–303.

[31] Bharti Mangla, Suresh Kumar Joshi, Kushagra Khanna, Prakhar Kapoor, Ipsita Kukreja, *Biopharm Journal* **2015,** *1,* 64–70.

[32] Winter, W. T.; Arnott, S. *Journal of Molecular Biology* **1977,** *117,* 761–784.

[33] Scott, J. E.; Heatley, F.; Moorcroft, D.; Olavesen, A. H. *Biochemical Journal* **1981,** *199,* 829–832.

[34] Winter, W.; Smith, P.; Arnott, S. *Journal of Molecular Biology* **1975,** *99,* 219-235.

[35] Scott, J. E.; Cummings, C.; Brass, A.; Chen, Y. *Biochemistry Journal* **1991,** *274,* 699-705.

[36] Kiani, C.; Chen, L.; Wu, Y. J.; Yee, A. J.; Yang, B. B. *Cell Research* **2002,** *12,* 19–32.

[37] Hascall, V. C.; Heingård, D. *The Journal of Biological Chemistry* **1974,** *13,* 4232–4241.

[38] Knudson, C. B.; Knudson, W. *FASEB Journal* **1993,** *7,* 1233-1241.

[39] Banerji, S.; Ni, J.; Wang, S.-X.; Clasper, S.; Su, J.; Tammi, R.; Jones, M.; Jackson, D. G. *The Journal of Cell Biology* **1999,** *144,* 789–801.

[40] Banerji, S.; Hide, B. R. S.; James, J. R.; Noble, M. E. M.; Jackson, D. G. *The Journal of Biological Chemistry* **2010,** *285,* 10724–10735.

[41] Mo, W.; Yang, C.; Liu, Y.; He, Y.; Wang, Y.; Gao, F. *Acta Biochimica et Biophysica Sinica* **2011,** 930–939.

[42] Stern, R.; Asari, A. A.; Sugahara, K. N. *European Journal of Cell Biology* **2006,** *85,* 699–715.

[43] Ghazi, K.; Deng-Pichon, U.; Warnet, J.-M.; Rat, P. *PloS One* **2012,** *7,* e48351.

[44] Wu, M.; Du, Y.; Liu, Y.; He, Y.; Yang, C.; Wang, W.; Gao, F. *PloS One* **2014,** *9,* e92857.

[45] Dubacheva, G. V.; Curk, T.; Mognetti, B. M.; Auzely-Velty, R.; Frenkel, D.; Richter, R. P. *Journal of the American Chemical Society* **2014,** *136,* 1722–1725.

[46] Dubacheva, G. V.; Curk, T.; Auzely-Velty, R.; Frenkel, D.; Richter, R. P. *Proceedings of the National Academy of Sciences of the United States of America* **2015,** *112,* 5579–5584.

[47] Mergy, J.; Fournier, A.; Hachet, E.; Auzély-Velty, R. *Journal of Polymer Science Part A: Polymer Chemistry* **2012,** *50,* 4019–4028.

[48] Crescenzi, V.; Cornelio, L.; Di Meo, C.; Nardecchia, S.; Lamanna, R. *Biomacromolecules* **2007,** *8,* 1844–1850.

[49] Lee, H.; Lee, K.; Kim, I. K.; Park, T. G. *Biomaterials* **2008,** *29,* 4709–4718.

[50] Takahashi, A.; Suzuki, Y.; Suhara, T.; Omichi, K.; Shimizu, A.; Hasegawa, K.; Kokudo, N.; Ohta, S.; Ito, T. *Biomacromolecules* **2013,** *14,* 3581–3588.

[51] Shu, X. Z.; Liu, Y.; Luo, Y.; Roberts, M. C.; Prestwich, G. D. *Biomacromolecules* **2002,** *3,* 1304–1311.

[52] Martini, M.; Hegger, P.; Schädel, N.; Minsky, B.; Kirchhof, M.; Scholl, S.; Southan, A.; Tovar, G.; Boehm, H.; Laschat, S. *Materials* **2016,** *9,* 810.

[53] Herrwerth, S.; Eck, W.; Reinhardt, S.; Grunze, M. *Journal of the American Chemical Society* **2003,** *125,* 9359–9366.

[54] Minsky, B. B.; Antoni, C. H.; Boehm, H. *Scientific reports* **2016,** *6,* 21608.

[55] Jewett, J. C.; Bertozzi, C. R. *Chemical Society Reviews* **2010,** *39,* 1272.

[56] Jewett, J. C.; Sletten, E. M.; Bertozzi, C. R. *Journal of the American Chemical Society* **2010,** *132,* 3688–3690.

[57] Lutz, J.-F. *Angewandte Chemie* **2008,** *120,* 2212–2214.

[58] Pillai, V. N. R. *Synthesis* **1980,** *1980,* 1–26.

[59] Bochet, C. G. *Journal of the Chemical Society, Perkin Transactions 1* **2002,** 125–142.

[60] Cui, J.; Miguel, V. S.; del Campo, A. *Macromolecular Rapid Communications* **2013,** *34,* 310–329.

[61] Hansen, M. J.; Velema, W. A.; Lerch, M. M.; Szymanski, W.; Feringa, B. L. *Chemical Society Reviews* **2015,** *44,* 3358–3377.

[62] Adams, S. R.; Tsien, R. Y. *Annual Review of Physiology* **1993,** *55,* 755-784.

[63] Hahner, S.; Olejnil, J.; Lüdemann, H.-C.; Krzymanska-Olejnik,; Hillenkamp, F.; Rothschild, K. J. *Biomolecular Engineering* **1999,** 127–133.

[64] Friedsam, C.; Bécares, A. D. C.; Jonas, U.; Seitz, M.; Gaub, H. E. *New Journal of Physics* **2004,** *6,* 9.

[65] Hwang, L.; Guardado-Alvarez, T. M.; Ayaz-Gunner, S.; Ge, Y.; Jin, S. *Langmuir : the ACS Journal of Surfaces and Colloids* **2016,** *32,* 3963–3969.

[66] Mathias, F.; Tahir, M. N.; Tremel, W.; Zentel, R. *Macromolecular Chemistry and Physics* **2014,** *215,* 604–613.

[67] Specht, A.; Thomann, J.-S.; Alarcon, K.; Wittayanan, W.; Ogden, D.; Furuta, T.; Kurakawa, Y.; Goeldner, M. *Chembiochem : a European Journal of Chemical Biology* **2006,** *7,* 1690–1695.

[68] Chandra, B.; Subramaniam, R.; Mallik, S.; Srivastava, D. K. *Organic & Biomolecular Chemistry* **2006,** *4,* 1730–1740.

[69] Mizuta, H.; Watanabe, S.; Sakurai, Y.; Nishiyama, K.; Furuta, T.; Kobayashi, Y.; Iwamura, M. *Bioorganic & Medicinal Chemistry* **2002,** *10,* 675–683.

[70] Lemke, E. A.; Summerer, D.; Geierstanger, B. H.; Brittain, S. M.; Schultz, P. G. *Nature Chemical Biology* **2007,** *3,* 769–772.

[71] Atta, S.; Ikbal, M.; Kumar, A.; Pradeep Singh, N. D. *Journal of Photochemistry and Photobiology. B, Biology* **2012,** *111,* 39–49.

[72] Alvarez, M.; Alonso, J. M.; Filevich, O.; Bhagawati, M.; Etchenique, R.; Piehler, J.; del Campo, A. *Langmuir : the ACS Journal of Surfaces and Colloids* **2011,** *27,* 2789–2795.

[73] Alonso, J. M.; Reichel, A.; Piehler, J.; del Campo, A. *Langmuir : the ACS Journal of Surfaces and Colloids* **2008,** *24,* 448–457.

[74] Goubko, C. A.; Majumdar, S.; Basak, A.; Cao, X. *Biomedical Microdevices* **2010,** *12,* 555–568.

[75] Ryan, D.; Parviz, B. A.; Linder, V.; Semetey, V.; Sia, S. K.; Su, J.; Mrksich, M.; Whitesides, G. M. *Langmuir : the ACS Journal of Surfaces and Colloids* **2004,** *20,* 9080–9088.

[76] Liang, C.-C.; Park, A. Y.; Guan, J.-L. *Nature Protocols* **2007,** *2,* 329–333.

[77] Miyake, Y.; Inoue, N.; Nishimura, K.; Kinoshita, N.; Hosoya, H.; Yonemura, S. *Experimental Cell Research* **2006,** *312,* 1637–1650.

[78] Keese, C. R.; Wegener, J.; Walker, S. R.; Giaever, I. *Proceedings of the National Academy of Sciences of the United States of America* **2004,** *101,* 1554–1559.

[79] Rausch, S.; Das, T.; Soine, J. R.; Hofmann, T. W.; Boehm, C. H.; Schwarz, U. S.; Boehm, H.; Spatz, J. P. *Biointerphases* **2013,** *32,* 8.

[80] Poujade, M.; Grasland-Mongrain, E.; Hertzog, A.; Jouanneau, J.; Chavrier, P.; Ladoux, B.; Buguin, A.; Silberzan, P. *Proceedings of the National Academy of Sciences of the United States of America* **2007,** *104,* 15988–15993.

[81] Riahi, R.; Yang, Y.; Zhang, D. D.; Wong, P. K. *Journal of Laboratory Automation* **2012,** *17,* 59–65.

[82] Vedula, S. R. K.; Leong, M. C.; Lai, T. L.; Hersen, P.; Kabla, A. J.; Lim, C. T.; Ladoux, B. *Proceedings of the National Academy of Sciences of the United States of America* **2012,** *109,* 12974–12979.

[83] ibidi GmbH, 01.05.2017.

[84] Rolli, C. G.; Nakayama, H.; Yamaguchi, K.; Spatz, J. P.; Kemkemer, R.; Nakanishi, J. *Biomaterials* **2012,** *33,* 2409–2418.

[85] Nakanishi, J.; Kikuchi, Y.; Inoue, S.; Yamaguchi, K.; Takarada, T.; Maeda, M. *Journal of the American Chemical Society* **2007,** *129,* 6694–6695.

[86] Stegmaier, P.; del Campo, A. *Chemphyschem : a European Journal of Chemical Physics and Physical Chemistry* **2009,** *10,* 357–369.

[87] Salierno, M. J.; García, A. J.; del Campo, A. *Advanced Functional Materials* **2013,** *23,* 5974–5980.

[88] Wirkner, M.; Weis, S.; San Miguel, V.; Alvarez, M.; Gropeanu, R. A.; Salierno, M.; Sartoris, A.; Unger, R. E.; Kirkpatrick, C. J.; del Campo, A. *Chembiochem : a European Journal of Chemical Biology* **2011,** *12,* 2623–2629.

[89] Weis, S.; Lee, T. T.; del Campo, A.; Garcia, A. J. *Acta Biomaterialia* **2013,** *9,* 8059–8066.

[90] Waldchen, S.; Lehmann, J.; Klein, T.; van de Linde, S.; Sauer, M. *Scientific reports* **2015,** *5,* 15348.

[91] Fulmer, G. R.; Miller, A. J. M.; Sherden, N. H.; Gottlieb, H. E.; Nudelman, A.; Stoltz, B. M.; Bercaw, J. E.; Goldberg, K. I. *Organometallics* **2010,** *29,* 2176–2179.

[92] August Köhler, *Zeitschrift für wissenschaftliche Mikroskopie und für Mikroskopische Technik* **1893,** *4,* 433–440.

[93] Michael W. Davidson, "Configurring a Microscope für Köhler Illumination", 27.02.2017.

[94] Matthew C. Dixon, *Journal of Biomolecular Techniques* **2008,** *19,* 151–158.

[95] C.K. O'Sullivan and G.G. Guilbault, *Biosensors and Bioelectronics* **1999,** 663–670.

[96] Günter Sauerbrey, *Zeitschrift für Physik* **1959,** 206–222.

[97] E. L. Decker, B. Frank, Y. Suo, S. Garoff, *Colloids and Surfaces A: Physicochemical and Engineering Aspects 1999,* 177–189.

[98] Yuan, Y.; Lee, T. R. Contact Angle and Wetting Properties. In *Surface Science Techniques*, Vol. 51; Bracco, G.; Holst, B., Eds.; Springer Berlin Heidelberg: Berlin, Heidelberg, 2013.

[99] Lamour, G.; Hamraoui, A.; Buvailo, A.; Xing, Y.; Keuleyan, S.; Prakash, V.; Eftekhari-Bafrooei, A.; Borguet, E. *Journal of Chemical Education* **2010,** *87,* 1403–1407.

[100] D.Y. Kwok, A. N. *Advances in Colloid and Interface Science* **1999,** 167–249.

[101] Cassie, A. B. D.; Baxter, S. *Transactions of the Faraday Society* **1944,** *40,* 546.

[102] Berridge, M. V.; Herst, P. M.; Tan, A. S. *Biotechnology Annual Review* **2005,** 127–152.

[103] Mosmann, T. *Journal of Immunological Methods* **1983,** *65,* 55–63.

[104] Berridge, M. V.; Tan, A. S. *Archives of Biochemistry and Biophysics* **1993,** *303,* 474–482.

[105] Hamid, R.; Rotshteyn, Y.; Rabadi, L.; Parikh, R.; Bullock, P. *Toxicology in Vitro : an International Journal published in association with BIBRA* **2004,** *18,* 703–710.

[106] O'Brien, J.; Wilson, I.; Orton, T.; Pognan, F. *European Journal of Biochemistry* **2000,** *267,* 5421–5426.

[107] Rampersad, S. N. *Sensors (Basel, Switzerland)* **2012,** *12,* 12347–12360.

[108] Quent, V. M. C.; Loessner, D.; Friis, T.; Reichert, J. C.; Hutmacher, D. W. *Journal of Cellular and Molecular Medicine* **2010,** *14,* 1003–1013.

[109] Goegan, P.; Johnson, G.; Vincent, R. *Toxicology in Vitro* **1995,** *9,* 257–266.

[110] R. S. Twigg, *Nature* **1945,** 401–402.

[111] DeBaun, R. M.; de Stevens, G. *Archives of Biochemistry and Biophysics* *1950,* 300–308.

[112] Eric M. Larson, Donald J. Doughman, Dale S. Gregerson, and Wesley F. Obritsch, *Investigative Ophthalmology and Visual Science* **1997,** 1929–1933.

[113] Thermoscientific, "alamarBlue Cell Viability Assay Reagant: Technical Datasheet", 28.02.2017.

[114] Laurie J. Jones, Matthew Gray, Stephen T. Yue, Richard P. Haugland, Victoria L. Singer, *Journal of Immunological Methods* **2001,** *254,* 85–98.

[115] Sriwilaijaroen, N.; Kelly, J. X.; Riscoe, M.; Wilairat, P. *The Southeast Asian Journal of Tropical Medicine and Public Health* **2004,** *35,* 840–844.

[116] Ellman, G. L. *Archives of Biochemistry and Biophysics* **1958,** *74,* 443–450.

[117] Ellman, G. L. *Archives of Biochemistry and Biophysics* **1959,** *82,* 70–77.

[118] Ellman, G. L.; Courtney, K. D.; Andres Jr., V.; Featherstone, R. M. *Biochemical Pharmacology* **1961,** 88–95.

[119] Jozef Sedlak and Raymond H. Lindsay, *Analytical Biochemistry* **1968,** *25,* 192–205.

[120] Schenk, F. C.; Boehm, H.; Spatz, J. P.; Wegner, S. V. *Langmuir : the ACS Journal of Surfaces and Colloids* **2014,** *30,* 6897–6905.

[121] Thakar, D.; Migliorini, E.; Coche-Guerente, L.; Sadir, R.; Lortat-Jacob, H.; Boturyn, D.; Renaudet, O.; Labbe, P.; Richter, R. P. *Chemical Communications (Cambridge, England)* **2014,** *50,* 15148–15151.

[122] Love, J. C.; Estroff, L. A.; Kriebel, J. K.; Nuzzo, R. G.; Whitesides, G. M. *Chemical reviews* **2005,** *105,* 1103–1169.

[123] Hudalla, G. A.; Murphy, W. L. *Langmuir : the ACS Journal of Surfaces and Colloids* **2009,** *25,* 5737–5746.

[124] Likhar, P. R.; Subhas, M. S.; Roy, S.; Kantam, M. L.; Sridhar, B.; Seth, R. K.; Biswas, S. *Organic & biomolecular chemistry* **2009,** *7,* 85–93.

[125] Brückner, R. *Reaktionsmechanismen: Organische Reaktionen, Stereo-chemie, moderne Synthesemethoden;* Spektrum Akad. Verl.: Berlin, 3. Aufl., aktualisiert und überarb., 2. korrigierter Nachdr ed.; 2009.

[126] Hong, V.; Presolski, S. I.; Ma, C.; Finn, M. G. *Angewandte Chemie (International ed. in English)* **2009,** *48,* 9879–9883.

[127] Hong, V.; Steinmetz, N. F.; Manchester, M.; Finn, M. G. *Bioconjugate Chemistry* **2010,** *21,* 1912–1916.

[128] Chan, T. R.; Hilgraf, R.; Sharpless, K. B.; Fokin, V. V. *Organic Letters* **2004,** *6,* 2853–2855.

[129] Neises, B.; Steglich, W. *Angewandte Chemie (International ed. in English)* **1978,** *17,* 522–524.

[130] Sapsford, K. E.; Algar, W. R.; Berti, L.; Gemmill, K. B.; Casey, B. J.; Oh, E.; Stewart, M. H.; Medintz, I. L. *Chemical Reviews* **2013,** *113,* 1904–2074.

[131] Tammi, R.; MacCallum, D.; Hascall, V. C.; Pienimaki, J.-P.; Hytti-nen, M.; Tammi, M. *Journal of Biological Chemistry* **1998,** *273,* 28878–28888.

[132] Banerji, S.; Lawrance, W.; Metcalfe, C.; Briggs, D. C.; Yamauchi, A.; Dushek, O.; van der Merwe, P. A.; Day, A. J.; Jackson, D. G. *The Journal of Biological Chemistry* **2016,** *291,* 25004–25018.

[133] Cohen, M.; Kam, Z.; Addadi, L.; Geiger, B. *The EMBO Journal* **2006,** *25,* 302–311.

[134] Mouta Carreira, C.; Nasser, S. M.; Di Tomaso, E.; Padera, T. P.; Boucher, Y.; Tomarev, S. I.; Jain, R. K. *Cancer Research* **2001,** *61,* 8079–8084.

[135] Arnold, M.; Cavalcanti-Adam, E. A.; Glass, R.; Blummel, J.; Eck, W.; Kantlehner, M.; Kessler, H.; Spatz, J. P. *Chemphyschem : a European Journal of Chemical Physics and Physical Chemistry* **2004,** *5,* 383–388.

[136] Missirlis, D.; Haraszti, T.; Scheele, C. v. C.; Wiegand, T.; Diaz, C.; Neubauer, S.; Rechenmacher, F.; Kessler, H.; Spatz, J. P. *Scientific reports* **2016,** *6,* 23258.

[137] del Campo, A.; Boos, D.; Spiess, H. W.; Jonas, U. *Angewandte Chemie (International ed. in English)* **2005,** *44,* 4707–4712.

[138] Kruskal, W. H.; Wallis, W. A. *Journal of the American Statistical Association* **1952,** *260,* 583–621.

[139] Dunn, O. J. *Technometrics* **1964,** *6,* 241–252.

Journal Articles and Poster Presentations

Peer-reviewed Journal Articles

- B.B. Minsky, **C.H. Antoni** and H. Boehm, "Controlled Immobilization Strategies to Probe Short Hyaluronan-Protein Interactions", *Sci. Rep.* **2016**, *6*, 21608. DOI: 10.1038/srep21608(2016).

- **Christiane H. Antoni**, Stefanie Neubauer, Horst Kessler, Joachim P. Spatz and Heike Boehm, "Light Triggered Cell Adhesion Specific to $\alpha_5\beta_1$ Integrin", *in preparation*.

- **Christiane H. Antoni**, Yvonne McDuffie, Melanie Rothley, Jonathan Sleeman and Heike Boehm, "Matrix model for lymphangiogenesis: co-presentation of short hyaluronan and adhesive ligands", *in preparation*.

Poster Presentations

- B.B. Minsky, **C.H. Antoni**, L. Rieble and H. Boehm, "Sweet Interfaces", Biomembrane Days 2016, Berlin, September 5-7, 2016.

- B.B. Minsky, **C.H. Antoni**, M. Frieling, D. Brüggemann, H. Boehm and J.P. Spatz, "Mimicking the sweet side of platelet adhesion", Biomembrane Days 2016, Berlin, September 5-7, 2016.

- B.B. Minsky, **C.H. Antoni** and H. Boehm, "Immobilisation of Short Hyaluronic Acid on Bioactive Hydrogels", Symposium on Active Hydrogels, Ringberg Castle, Kreutz, May 15-18, 2016.

- S. Rausch, **C.H. Antoni**, T. Das, J.R.D. Soiné, U.S. Schwarz, H. Boehm and J.P. Spatz, "Polarizing Cytoskeletal Tension to Induce Leader Cell Formation During Collective Cell Migration", IWH-workshop on Collective Cell Migration, Heidelberg, July 14-15, 2015

- B.B. Minsky, **C.H. Antoni**, S. Klein, M. Frieling and H. Boehm, "Tunable Immobilisation For Low Molecular Weight Hyaluronan to Probe Its Interactions with Macromolecules", ISHAS HA 2015, Florence, Italy, June 7-11, 2015

- **C.H. Antoni**, Y. McDuffie, S. Wegner, J.P. Spatz, J. Sleeman and H. Boehm, "Dual-functionalized Surfaces to Investigate Biological Effects of Hyaluronan Oligosaccharides", ISHAS HA 2015, Florence, Italy, June 7-11, 2015

- **C.H. Antoni**, S. Rausch, T. Mundinger, Y. Schön, T. Das, H. Boehm and J.P. Spatz, "Influence of functionalized biomaterials on collective cell migration", 547. WE-Heraeus Seminar on Physics and Biology of Directed Movements of Cells and Organisms, Bad Honnef, December 8-11, 2013

Danksagung/ Acknowledgements

Zuallererst möchte ich mich bei Prof. Joachim Spatz dafür bedanken, dass er mich in seiner Gruppe aufgenommen hat und die Erstellung dieser Arbeit ermöglicht hat.

Vielen Dank auch an Prof. Reiner Dahint für die Bereitschaft Teil meiner Prüfungskomission und Gutachter für diese Arbeit zu sein. Mein unendlicher Dank gebührt Dr. Heike Böhm für ihre unendliche Geduld, ihre Anleitung und all ihr Wissen, die dieses Projekt möglich gemacht haben. Darüberhinaus danke ich ihr für ihr Vertrauen in den vergangenen vier Jahren.

Großer Dank geht auch an Prof. Horst Kessler (TU München) und sein Team, insbesondere Dr. Stefanie Neubauer für die Bereitstellung der Vorstufe des $\alpha_5\beta_1$- Mimetikums und Diskussionen bezüglich der Synthese. Außerdem danke ich Prof. Jonathan Sleeman und seinem Team vor allem Dr. Wilko Thiele und Dr. Melanie Rothley für den Austausch zu Hyaluronsäure und einer Hyaluronsäurespezies mit kurzer Kettenlänge, die im Rahmen dieser Arbeit genutzt wurde. Prof. Dirk-Peter Herten danke ich für die Erlaubnis das UVVIS-Spektrometer und die HPLC seiner Arbeitsgruppe nutzen zu dürfen. Im Weiteren bedanke ich mich bei Prof. Ulrich Schwarz für seine hilfreichen Kommentare bezüglich kollektiver Zellmigration.

Ein großes Dankeschön an Klaus Schmitt und das Team in der Feinmechanischen Werkstatt, die es schaffen jede noch so seltsame Idee zu realisieren und so eine große Hilfe sind.

Mein besonderer Dank gilt Tabea Oswald, Yvonne McDuffie, Burcu Minsky, Patricia Hegger, Johanna Dickmann und Cornelia Zapp für die schöne Zeit im Labor in Guten wie in schlechten Zeiten und dafür, dass sie mir immer mit Rat und Tat zur Seite standen, vor allem in biologischen Fragestellungen. Yvonne McDuffie und Johannes Hirte danke ich darüberhinaus für die Einführung in die BCML-Technik.

Thanks to Tamal Das, Sebastian Rausch and Medhavi Vishvakarma for the introduction to the world of collective cell migration and its mysteries.

Außerdem möchte ich mich auch bei allen anderen Mitgliedern der AG Böhm für die schöne Zeit bedanken.

Im besonderen möchte ich mich bei Franziska Schenk bedanken für die Chemiediskussionen und dem gemeinsamen Kampf gegen das Chaos im Chemielabor und gegen den inneren Schweinehund beim Gang zum Unisport. Vielen Dank auch fürs Korrekturlesen.

Großen Dank auch an Rebecca Medda für ihr stets offenes Ohr und ihre Hilfe in Fragen zu Zellen und Mikroskopie und Tamas Haraszti für seine Un-

Eidesstattliche Versicherung

gemäß § 8 der Promotionsordnung der Naturwissenschaftlich- Mathematischen Gesamtfakultät der Universität Heidelberg

1. Bei der eingereichten Dissertation zu dem Thema **"Chemically Modified Substrates to Probe Cell Behaviour in Wound Healing"** handelt es sich um meine eigenständig erbrachte Leistung.

2. Ich habe nur die angegebenen Quellen und Hilfsmittel benutzt und mich keiner unzulässigen Hilfe Dritter bedient. Insbesondere habe ich wörtlich oder sinngemäß aus anderen Werken übernommene Inhalte als solche kenntlich gemacht.

3. Die Arbeit oder Teile davon habe ich bislang nicht an einer Hochschule des In- oder Auslands als Bestandteil einer Prüfungs- oder Qualifikationsleistung vorgelegt.

4. Die Richtigkeit der vorstehenden Erklärungen bestätige ich.

5. Die Bedeutung der eidesstattlichen Versicherung und die strafrechtlichen Folgen einer unrichtigen oder unvollständigen eidesstattlichen Versicherung sind mir bekannt.

Ich versichere an Eides statt, dass ich nach bestem Wissen die reine Wahrheit erklärt und nichts verschwiegen habe.

Heidelberg, den 8. Juni 2017

Christiane Antoni